PICOSECOND PHOTORESPONSE OF HIGH-T_C SUPERCONDUCTOR THIN FILMS

By

Frank A. Hegmann, B.Sc., M.Sc.

A Thesis

Submitted to the Faculty of Graduate Studies

in Partial Fulfillment of the Requirements

for the Degree

Doctor of Philosophy

McMaster University

November 1994

DOCTOR OF PHILOSOPHY (1994) **McMASTER UNIVERSITY**

(Physics) Hamilton, Ontario

TITLE: Picosecond Photoresponse of High-T_c Superconductor Thin Films

AUTHOR: Frank A. Hegmann, B.Sc. (Carleton University)
M.Sc. (McMaster University)

SUPERVISOR: Dr. John S. Preston

NUMBER OF PAGES: xiii, 150

PICOSECOND PHOTORESPONSE OF HIGH-T_C SUPERCONDUCTOR THIN FILMS

DEFINITION OF TERMS

Variables and Constants:

Parameter	Description	Typical units
l	length of bridge	μm
w	width of bridge	μm
d	thickness of bridge	μm
ω	frequency	s^{-1}
ω_P	plasma frequency	s^{-1}
ϵ	dielectric constant	F/m
ϵ_0	permittivity of free space	F/m
μ_0	permeability of free space	H/m
δ	optical penetration depth	nm
λ	penetration depth	nm
λ_L	London penetration depth	nm
ξ	coherence length	nm
Δ	superconducting energy gap or order parameter	meV
ψ	superconducting wave function	
σ	electrical conductivity	$\Omega^{-1}cm^{-1}$
ρ	electrical resistivity	Ω cm
n	carrier density	cm^{-3}
n_{SC}	superfluid carrier density	cm^{-3}
n_N	normal fluid carrier density	cm^{-3}
f_{SC}	superfluid fraction = n_{SC} / n	
f_N	normal fluid fraction = n_N / n	

T	temperature	K
T_C	critical temperature	K
T_{C0}	zero resistance critical temperature	K
t	reduced temperature = T / T_C	
t	time	s, ns, ps
C	heat capacity	$J / cm^3 K$
T_e	electron temperature	K
T_{ph}	phonon or lattice temperature	K
C_e	electronic specific heat capacity	J/cm^3K
C_{ph}	phonon or lattice specific heat capacity	J/cm^3K
κ	thermal conductivity	W / cm K
δ	optical penetration depth	nm
F	incident light fluence	$\mu J / cm^2$
R	reflectance	
R	electrical resistance	Ω
R_S	surface resistance	Ω/sq
L	inductance	H
L_{KIN}	kinetic inductance	H
V	voltage	V
V_{KIN}	voltage due to change in L_{KIN}	mV
$V_{KIN(NORM)}$	V_{KIN} with effect of normal fluid branch	mV
I	current	A
J	current density	A / cm^2
J_C	critical current density	A/cm^2
G	thermal conductance	W / K
G	laser source term	W/cm^3
P	incident radiation power	W, W/cm^2
R_{BD}	thermal boundary resistance	$K\ cm^2 / W$
Γ	relaxation rate	s^{-1}

τ	relaxation time = $1 / \Gamma$	s, ns, ps
τ	thermal time constant (C/G)	ms
τ_P	laser pulse width term	ns, ps, fs
τ_r	rise time	ns, ps
$\tau_{e\text{-}ph}$	electron-phonon relaxation time (energy)	ps
τ_S	electron-phonon scattering time (momentum)	ps
τ_R	recombination time	ns, ps
τ_γ	phonon escape time	ns
τ_B	phonon pair breaking time	ps
τ_Δ	order parameter relaxation time	μs, ns, ps
τ_J	supercurrent response time	ps
g	quasiparticle multiplication factor	
γ	Sommerfeld constant ($C_e = \gamma T_e$)	J/cm^3K^2
B	magnetic field	G, T
ϕ_0	flux quantum	Wb
η	viscosity for vortex flow	Kg/m s

Abbreviations:

YBCO	high-T_C superconductor $YBa_2Cu_3O_{7-\delta}$
HTSC	high-temperature superconductor
KIB	kinetic inductive bolometric
FWHM	full width at half maximum
SQUID	superconducting quantum interference device
NMR	nuclear magnetic resonance
SFFT	superconducting flux flow transistor
CMOS	complementary metal-oxide semiconductor
MCM	multi-chip module
NEP	noise equivalent power
MSM	metal-semiconductor-metal

FIR	far-infrared
QWIP	quantum well infrared photodetector
BCS	Bardeen, Cooper, and Schrieffer theory of superconductivity
DOS	density of states
FF	flux flow
TAFF	thermally-activated flux flow
BW	bandwidth of electrical measurement system
CW	continuous wave (constant laser source)
Nd:YAG	neodynium-doped yttrium aluminum garnet (laser)
HeNe	helium-neon (laser)

Useful conversions and definitions:

$\hbar\omega$ (eV) = 12400 / λ (Å)

$\hbar\omega$ (meV) = 0.124 x ν (cm^{-1})

k_B = 0.0862 meV/K

1 μm = 10^{-6} m

1 nm = 10 Å

1 ns = 10^{-9} s

1 ps = 10^{-12} s

1 fs = 10^{-15} s

0° C = 273.2 K

ϕ_0 = 2.07 x 10^{-15} Wb

1 G = 10^{-4} T

Boiling point of liquid nitrogen = 77.4 K

Boiling point of liquid helium = 4.2 K

light travels about 1 foot in 1 ns, or 0.3 mm/ps

ABSTRACT

The origin of the fast photoresponse observed below T_C from current-biased, epitaxial $YBa_2Cu_3O_{7-\delta}$ (YBCO) thin films has been a source of controversy for several years now. The photoresponse signals have been attributed to either bolometric (thermal or equilibrium) or nonbolometric (nonthermal or nonequilibrium) mechanisms. A variety of nonbolometric mechanisms have been proposed to explain the fast photoresponse transients, such as nonequilibrium electron heating and transient flux dynamics.

We have studied the fast photoresponse of epitaxial YBCO thin film bridge structures using 100 ps and 5 ps laser pulses. Both fast and slow voltage transients were observed. In the resistive transition region, a slow component was seen in the photoresponse wave form with a decay time of several nanoseconds which could be attributed to a resistive bolometric response. However, below the resistive transition region and well into the superconducting state, we have observed for the first time fast voltage transients with subnanosecond widths that were not followed by a slow resistive component. The fast transients cannot be explained by a simple resistive bolometric response.

We have developed what is called the kinetic inductive bolometric (KIB) model to explain the origin of the fast photoresponse signals. The KIB model assumes equilibrium heating of the film by the laser pulse, contrary to some of the nonbolometric mechanisms that have been proposed. We show that the KIB model provides excellent qualitative and reasonable quantitative agreement with the observed photoresponse using 100 ps and 5 ps laser pulses. With 5 ps laser pulses, we have observed voltage transients as fast as 16 ps wide from a 200 nm YBCO film. To our knowledge, this is the fastest photoresponse signal reported to date (September, 1994) from epitaxial YBCO thin films. The implications that the success of the KIB model has on the nature of superconductivity in the high-T_C materials is also discussed.

ACKNOWLEDGEMENTS

Probing solids with fast laser pulses is a fascinating topic, and to work with such interesting materials as the high-T_c superconductors has made my thesis work here at McMaster all the more exciting. For giving me the freedom I wanted in my experiments, for helping me when I got somewhat confused, for providing me with inspiration for new ideas, for allowing me to spend hoots of cash for new equipment, and for teaching me that sarcastic wit has no bounds, I sincerely thank John, my supervisor.

Timidly, I have approached Tom Timusk many times in his office, my head down and another stupid question in my hand, and yet every time he was very patient with my curiosity for the high-T_c superconductors. His answers have always been very thorough and clear, and he made me feel much better when he pretended not to know the full answer to my questions. (Hmmm.. maybe he was just tyring to get me out of his office ?!) Anyhow, for many valuable discussions, I am grateful. I also wish to thank Jules Carbotte for spending the time to explain to me some of the intricacies of superconductivity.

For their help around the lab and for keeping things really interesting, I extend a sincere thank you to my lab mates Bruce Takasaki (for crossing the line), Darcy Poulin (for that perma-smile), Steve Moffat (for forgiving me about 8 am), and Jean Lachapelle (ma vieille pieuvre, où est-ce que j'ai parké mon char ?). Thanks, Rob Hughes (Thunder Bay's finest), for supplying me with an abundance of excellent YBCO films, without which this project would never have succeeded. For helping me get started in the clean room, I gratefully acknowledge Mike Daly, Doug Bruce, and Ke Chang Song. Of course, patterning the films would have been impossible if Jon Showell hadn't introduced me to the ICeditor software used to make the masks for photolithography. I also wish to thank Adrian Kitai and Mike Clarke for their generosity in letting me use their gold evaporation systems. The technical assistance I received from Venice ("carry on"), Gino, and Yosh in the machine shops was always indispensable, and advice from Tadek ("what do you want") and Gord was always appreciated. Making purchases at Chemistry stores was always a pleasure with a

friendly smile from Christina. Finally, I wish to thank Wendy, Marg, Rose, and Charlene in the Physics office for always lending a helping hand. Elaine, Bobby, and Fran in the Engineering Physics department have also been quite helpful, and Marg in the IMR was always very nice despite what John said about me.

I have had the privilege of getting to know a lot of fun people during my stay at McMaster. This was usually achieved through the GSA soccer team (Hamiltonian Operators) and the softball team (Liquid State). Making bets for pitchers at the Phoenix or watching the Simpsons and playing pool at Fat Tuesday's (thanks Mike !) also helped. For some really good times on or off the field, I would like to say thanks again to John and the lab mates (sounds like a new band), and to Rob G. (Mr. P.E.I.), Rob, K. (stop poking me), Andy D. (is there a sport you don't play? ... or a beer you don't drink?), Frank and Carol (I am not a toaster), Jake V. (the best third baseman I know), Jason P. (master of all sports), Dave M. (quarterback extraordinaire), Pat D. (have another coke), Rachid O. (Pele would be jealous), Bill and Tammy (the corn calleth), Chuck C. (yup), Peter and Anita (made for each other), Abdallah^2 (sabotage 101), Kanan (Canoe) and Peter, Mike E. (Baggio on quaaludes), Dave J. (composer of the infamous budgie song), Rob B. (not a bad office mate after all), Jon S. (defensive wall), Wu (soccer animal), and Eugene T. (another wall). I'm sure I mistakingly forgot to mention several people. My memory improves with each pitcher (or donut) received. .... mmmm,... dooonuts....

Dave (not going down) and Brian (Wongly) have remained good friends over the years, proving that friendships made at McMaster do indeed last. My family has always supported me in my work, even if they didn't have a clue what I was doing (they still think I'm trying to improve the targeting efficiency of a satellite-based anti-missile laser system).

Most of all, I thank Claudia for her love and support. Claudia, you're the best !

PREFACE

For ease of readability, some of the experimental details and analysis have been omitted in the main text and placed in appendices and copies of journal publications included at the end of the thesis. The journal publications will be referred to often from within the main text as Papers A, B, C, and D. The main text is self contained; the papers are included only as a source of supplementary information on the experiments.

After quickly describing the type of experiments being done here, the first chapter provides a brief and by no means complete introduction to superconductivity from its discovery in 1911 to the excitement surrounding the new high-T_c superconductors. Some of the potential applications of these new materials are discussed, including the possibility of developing practical high speed photodetectors. In order to better understand nonequilibrium mechanisms in the high-T_c superconductors, Chapter 2 first provides an overview of some of the main equilibrium properties of these new materials. Following this is a brief summary of some of the nonequilibrium processes that are believed to occur in conventional superconductors. The mechanisms by which the high-T_c superconductors can detect light are discussed in Chapter 3. The study of the photoresponse from high-T_c superconductors is still very controversial, and I have attempted to classify the various photoresponse mechanisms believed to occur in epitaxial thin films as bolometric or nonbolometric. The kinetic inductive bolometric (KIB) response is presented in Chapter 4 as the mechanism we believe gives rise to the observed photoresponse in epitaxial YBaCuO thin films. Chapter 5 provides some of the main experimental results that support the KIB mechanism. Finally, Chapter 6 discusses some of the successes and limitations of the KIB model. In particular, the effect of nonequilibrium processes will be discussed. Suggestions for future experiments are also provided which might help further our understanding of the mechanism responsible for the observed photoresponse and perhaps even superconductivity in the high-T_c materials.

TABLE OF CONTENTS

LIST OF PAPERS INCLUDED AT THE END OF THE THESIS

A. F. A. Hegmann and J. S. Preston, "Identification of nonbolometric photoresponse in $YBa_2Cu_3O_{7-\delta}$ thin films based on magnetic field dependence", Appl. Phys. Lett. 62, 1158 (1993).

B. F. A. Hegmann and J. S. Preston, "Origin of the fast photoresponse of epitaxial $YBa_2Cu_3O_{7-\delta}$ thin films", Phys. Rev. B 48, 16023 (1993).

C. F. A. Hegmann, R. A. Hughes, and J. S. Preston, "High speed kinetic inductive bolometric photoresponse of epitaxial $YBa_2Cu_3O_{7-\delta}$ thin films", in *High-Temperature Superconducting Detectors: Bolometric and Nonbolometric*, eds. M. Nahum and J.-C. Villegier, Proc. SPIE 2159, 88 (1994). (Proceedings of the *OE/LASE '94* (SPIE) conference, Los Angeles, California, January 22-28, 1994.)

D. F. A. Hegmann, R. A. Hughes, and J. S. Preston, "Picosecond photoresponse of epitaxial $YBa_2Cu_3O_{7-\delta}$ thin films", Appl. Phys. Lett. 64, 3172 (1994).

For Claudia,

For my Mother,

And

In Memory of Omi

1. INTRODUCTION

1.1. Brief description of the photoresponse measurements

The response of superconductors to light has been extensively studied with a variety of different experiments for more than 30 years now. The experiments have ranged from probing the absorption as a function of wavelength in the microwave and far-infrared regions to using optical wavelength femtosecond laser pulses for studying transient changes in the transmission of thin films due to nonequilibrium effects. The type of photoresponse experiment described in this thesis is shown schematically in Fig. 1.1. In these experiments, a thin film (~ 200 nm thick) of the high-T_C superconductor $YBa_2Cu_3O_{7-\delta}$ (YBCO) grown

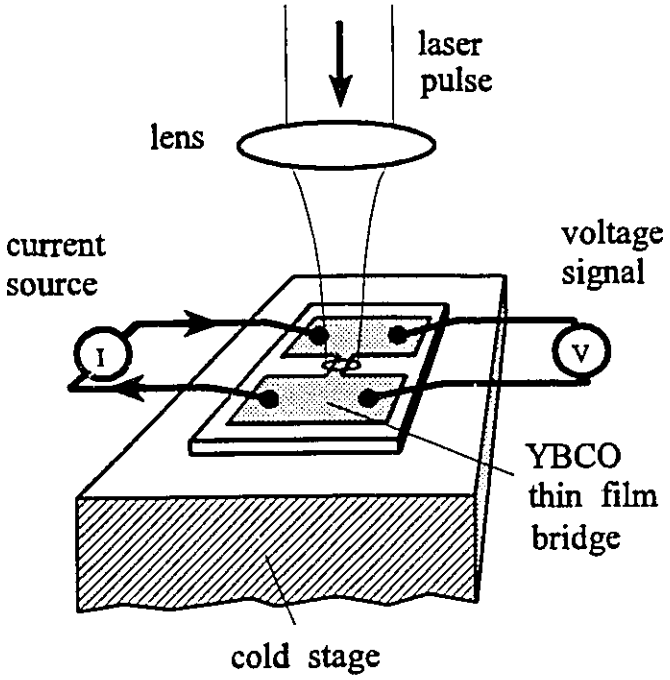

Fig. 1.1. Schematic of a typical setup used for photoresponse measurements.

epitaxially on a $LaAlO_3$ substrate is patterned using standard photolithographic techniques into a narrow bridge structure with a width of 10 to 20 μm and a length of 100 to 200 μm. The film is then mounted on a cold stage which cools the film from room temperature down to about 40 K (or 77 K if liquid nitrogen is used). A current source supplies a bias current

I to the bridge and a sensitive voltmeter measures the voltage V across the bridge. The resistance R of a typical bridge can be monitored as a function of temperature T as shown in Fig. 1.2. The critical transition temperature T_c for the bridge structures to become superconducting is typically around 90 K.

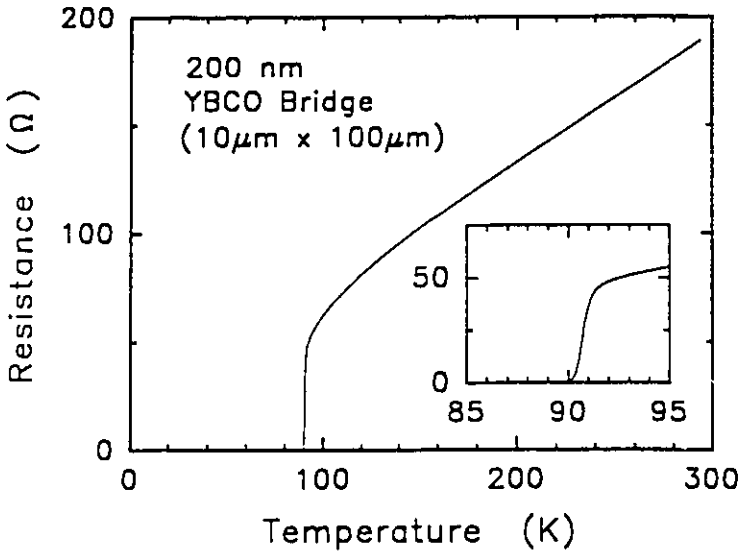

Fig. 1.2. Resistance as a function of temperature for a YBCO bridge with a width of 10 μm, a length of 100 μm, and a thickness of 200 nm. The transition region near 90 K is shown on an expanded scale in the inset.

Picosecond laser pulses from a mode-locked laser are then focused onto the bridge and any voltage transients induced by the laser pulses are recorded on a high speed digital sampling oscilloscope. The observed voltage transients are referred to as the photoresponse of the bridge. The photoresponse can be studied as a function of temperature, bias current, film thickness, laser pulse width, and laser fluence. Fast transients 16 ps wide and slower transients with nanosecond decay times have been observed. Figure 1.3 shows a 16 ps wide photoresponse signal from a 200 nm YBCO film using 5 ps laser pulses, which is the fastest voltage transient observed to date (September 1994) from YBCO thin films.

One of the interesting aspects of such measurements is that a voltage transient can be seen when the film is in the superconducting (zero resistance) state. The fast transient seen in Fig. 1.3 cannot be explained by the laser pulse simply heating the film into the resistive region. Studying the origin of such voltage transients has therefore been one of the

main motivations of this thesis. Another motivation has been in addressing a controversy which exists in this area of research as to whether these fast voltage transients are due to thermal or nonequilibrium mechanisms. There is also the possibility of developing a practical high speed photodetector with the high-T_c superconductors.

Understanding the origin of the fast photoresponse observed below T_c may also help provide clues for the superconducting mechanism in the high-T_c oxides. However, before discussing some of the photoresponse mechanisms, it is necessary to first look at what we already know about the high-T_c's and superconductivity in general.

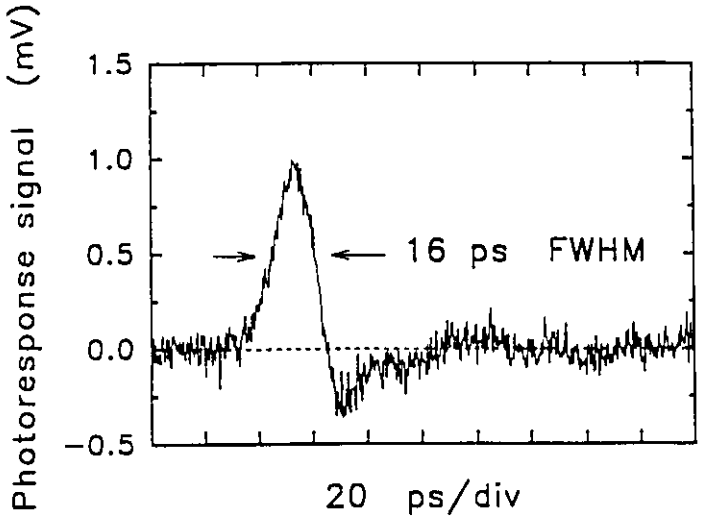

Fig. 1.3. Example of a photoresponse signal from a 200 nm YBCO thin film at 77 K using 5 ps laser pulses. The full width at half maximum (FWHM) of the transient is 16 ps.

1.2. Superconductivity: a brief history

In 1911, Kamerlingh Onnes[1] discovered that mercury lost its resistance below 4.2 K. Soon afterwards, superconductivity was discovered in many more elements such as Al, Sn, and Pb with the highest T_c being around 9.3 K for Nb. Since superconductors with higher transition temperatures meant that cooling requirements could be made less stringent, much of the work over the following decades was devoted to finding superconductors with higher T_c 's. As shown in Fig. 1.4, the highest T_c before 1985 was only 23.2 K in Nb_3Ge.[2]

However, in 1986 Bednorz and Müller[3] discovered the onset of superconductivity at 35 K in a LaBaCuO compound. This encouraged researchers to search for variations of this compound that might have even higher T_c's. In 1987, Wu *et al.*[4] made the landmark discovery of superconductivity at 90 K in a compound of YBaCuO, or more exactly, $YBa_2Cu_3O_{7-\delta}$ where $\delta \sim 0.1$. Even higher T_c's were discovered in BiSrCaCuO (110 K)[5], TlBaCaCuO (125 K)[6], and recently in HgBaCaCuO compounds[7] with the highest T_c reported to date of 164 K while under pressure.

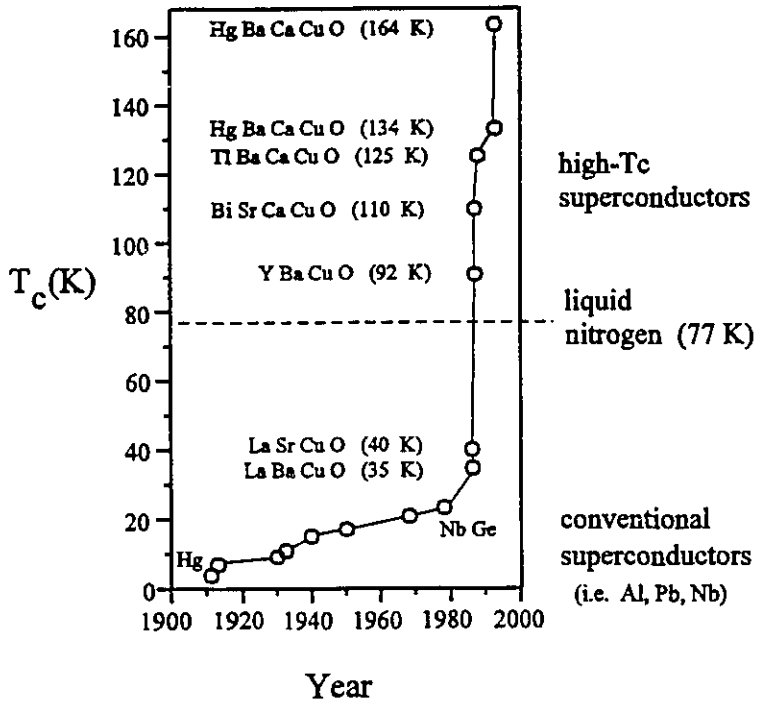

Fig. 1.4. Critical temperature T_c of various superconductors as a function of their year of discovery showing the sudden increase in T_c after 1986. The dashed line shows the boiling point of liquid nitrogen at 77 K.

A superconductor with T_c above the boiling point of liquid nitrogen caught the imagination of the world as, suddenly, superconducting technology developed before 1986 became more accessible with the lower cost and ease of cooling with liquid nitrogen. Unfortunately, the "superconducting revolution" that had been anticipated by so many has yet to materialize. Our cities have not, as predicted, been linked by magnetic levitation trains or high power transmission lines using the new high-T_c superconductors. The superconducting revolution was hampered by materials problems, such as their extreme

brittleness, and by a general lack of understanding of the mechanism of superconductivity in these new compounds. Nevertheless, several niche applications have been found, as discussed later in Section 1.3.

One of the common features with the high-T_c superconductors is the presence of one or more planes of Cu and O atoms. Because of this, the high-T_c superconductors (HTSCs) are referred to by several names such as the copper oxide superconductors, the oxide ceramic superconductors, or the high-T_c oxides. It is believed that the superconductivity in these compounds resides within the CuO planes, which gives the HTSCs a somewhat two dimensional character for carrier transport. Fig. 1.5 below shows the structure of YBCO and the location of the CuO planes. With such a complicated structure, it is not surprising that the nature of superconductivity in the HTSCs remains elusive.

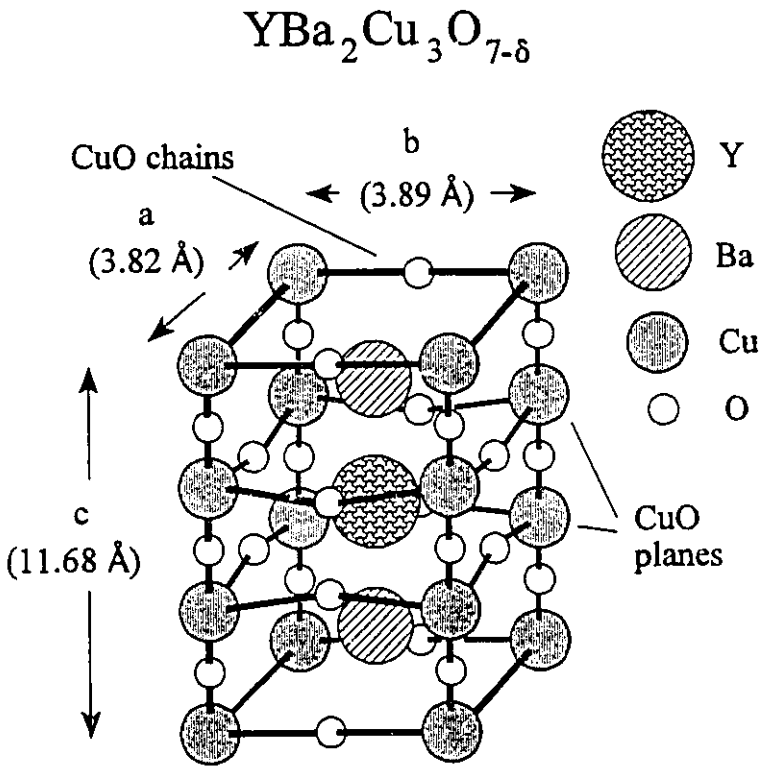

Fig. 1.5. Structure of $YBa_2Cu_3O_{7-\delta}$ (T_c = 90 K) showing location of the CuO planes and chains.

The superconducting elements and compounds discovered before 1986 are commonly referred to as the *conventional superconductors* since the nature of

superconductivity in these compounds is understood within the framework of BCS theory developed by Bardeen, Cooper, and Schrieffer in 1957.[3] The BCS theory of superconductivity is based on the idea that, despite their mutual repulsion, electrons will bind attractively to each other and form Cooper pairs in the superconducting state. The attractive interaction between pairs of electrons is mediated by phonons in conventional superconductors. In a crude picture, the interaction starts by one electron pulling ions in a lattice towards itself as it travels by. The inward movement of the ions creates a region of positive charge which can attract a second electron. The movement inward of the ions constitutes emission of a phonon by the first electron which is then "sensed" and then absorbed by the second electron. The Cooper pairs in the superconducting state, therefore, behave cooperatively by exchanging phonons and have a certain binding energy per electron designated by Δ. To break a Cooper pair, an energy of 2Δ is required since an electron excited out of the superconducting must also pull its partner out because an unpaired electron cannot exist in the superconducting state. This gives rise to the zero resistance property of superconductors since the Cooper pairs can only be broken if they are scattered by an excitation with an energy greater than 2Δ.

The superconducting state therefore has an energy gap between normal and superconducting electrons analogous to the energy gap seen between the valence and conduction bands in semiconductor materials, as illustrated in Fig. 1.6. In semiconductors, the gap has an energy E_G of the order of 1 eV, whereas BCS theory predicts a much smaller energy gap for excitations of 1 to 3 meV in conventional superconductors given by

$$2\Delta(0) = 3.52\ k_B\ T_C \qquad (1.1)$$

where k_B is Boltzmann's constant and Δ is taken at $T = 0$. In semiconductors, as shown in Fig. 1.6a, photons with energy $\hbar\omega \geq E_G$ will be able to excite electrons across the gap resulting in the creation of electron-hole pairs. A similar situation occurs in superconductors, as shown in Fig. 1.6b, where photons with $\hbar\omega \geq 2\Delta$ can break Cooper pairs and excite electrons into the normal state. These excitations in the normal state are often referred to as *quasiparticle* excitations since the electrons in these states can have both hole-like and

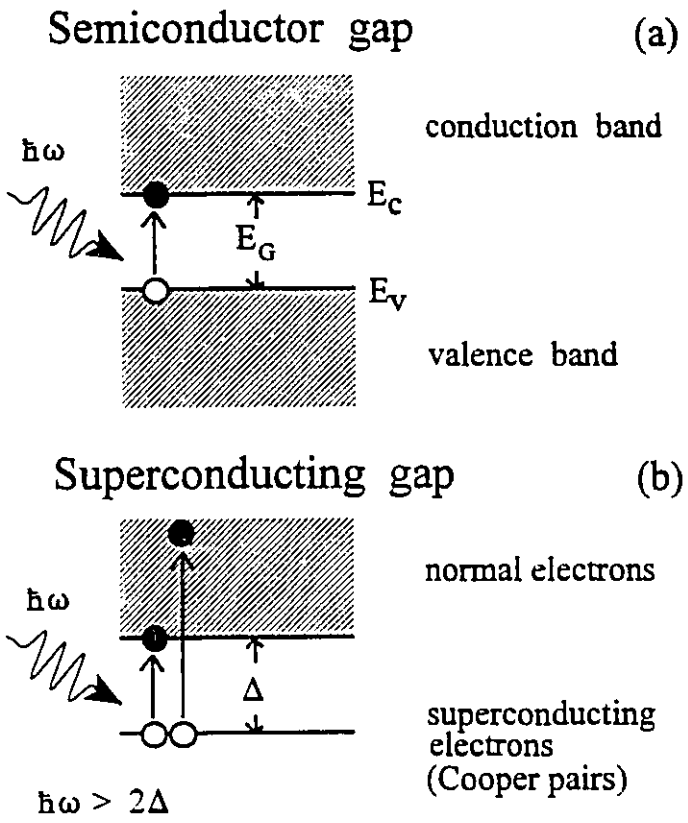

Fig. 1.6. Energy level diagrams showing energy gaps in (a) semiconductors and (b) superconductors. Photons or other excitations with energy $\hbar\omega \geq E_G$ can create electron-hole pairs in semiconductors, or break Cooper pairs in superconductors if $\hbar\omega \geq 2\Delta$. The normal state excitations produced in superconductors are commonly referred to as quasiparticle excitations.

electron-like properties.

If $\hbar\omega < 2\Delta$ for light incident on a conventional superconductor, then at T= 0 the reflectivity is unity. If $\hbar\omega > 2\Delta$, then some of the photons will be absorbed as they break Cooper pairs, and the reflectivity will be less than unity. This prediction was tested by Richards and Tinkham[9] in 1960 by studying the absorption as a function of wavelength in the far-infrared region of conventional superconductors such as Sn, Pb, and Nb. Their results showed that absorption of light occurred at energies above the gap value predicted by BCS theory in Eq. (1.1). Similar experiments were performed with the high-T_c materials after 1986, but no evidence for a BCS-like gap structure in the far infrared region has been found.[10]

In general, the energy gap is a maximum at T = 0 and decreases to zero at T_c, as shown in Fig. 1.7a. In the two-fluid model for superconductivity developed by Gorter and Casimir in 1934,[11] the carriers in a material below T_c are divided into a normal fluid component and a superfluid component. Above T_c, all the electrons are in the normal state. As the temperature is lowered below T_c, some of the carriers condense into the superconducting state while some remain in the normal state. At T = 0, all the carriers have condensed into the superconducting state. If the carrier density above T_c is n, then the superfluid and normal fluid fractions below T_c are denoted by $f_{sc} = n_{sc} / n$ and $f_N = n_N / n$, respectively, such that $f_{sc} + f_N = 1$. The temperature dependence of the superfluid and normal fluid fractions below T_c is shown in Figs. 1.7b and 1.7c. In the two-fluid model, the

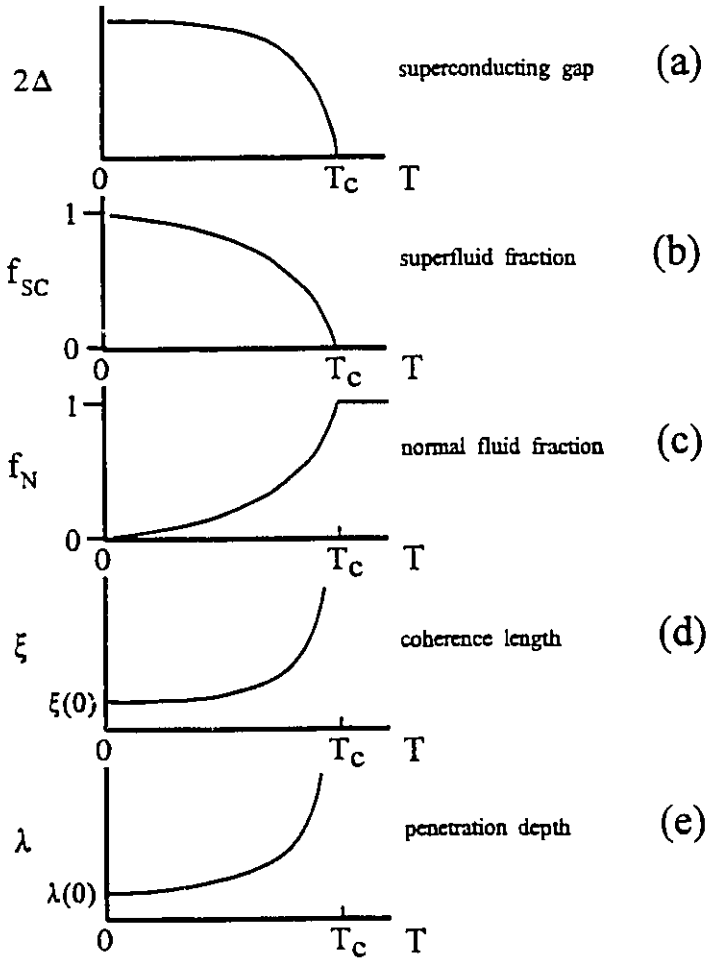

Fig. 1.7. Schematic of the temperature dependence of (a) the energy gap 2Δ, (b) the superfluid fraction f_{sc}, (c) the normal fluid fraction f_N, (d) the coherence length ξ, and (e) the penetration depth λ. Above T_c, all the carriers are in the normal state, whereas at T=0 all the carriers have condensed into the superconducting state.

temperature dependence of the superfluid fraction is given by $f_{SC} = 1 - t^4$, where $t = T/T_C$ is the reduced temperature. As will be discussed in Section 2.1, a good fit for the superfluid fraction in the HTSCs seems to follow a "t^2 law", or $f_{SC} = 1 - t^2$.

Table 1.1 gives experimentally observed values for the energy gap in some conventional superconductors. If YBCO were a conventional BCS superconductor with a T_C of 90 K, it would have an energy gap of about 27 meV (220 cm^{-1}), which would mean incident radiation with wavelengths less than 45 μm would be absorbed. It is also seen in Table 1.1 that the gap ratio $2\Delta/k_BT_C$ for elements such as Pb is larger than the BCS value of 3.52. This can be attributed to strong-coupling effects due to an enhanced electron-phonon interaction in these materials.[12] A stronger electron-phonon interaction results in shorter Drude relaxation times τ and therefore higher resistivities in the normal state. This leads to the general observation that poorer conductors make better superconductors. The HTSCs have resistivities much larger than most metals, and so one might expect the electron-phonon interaction to be quite large. It is believed, however, that the electron-phonon interaction in the HTSCs cannot account for the large T_C values observed in these materials, and new electronic mechanisms such as spin-fluctuation induced superconductivity have been proposed, as discussed later in Section 2.1.

Other important superconducting parameters such as the coherence length ξ and the penetration depth λ are compared in Table 1.1. The coherence length is a measure of the range of interaction between two electrons in a Cooper pair. It also determines the distance over which the gap function, or order parameter ψ (where $|\psi|^2 = |\Delta|^2 = n_{SC}$), falls to zero at a superconducting-normal interface. In the Meissner state, a superconductor will expel an external magnetic field from its interior, but will allow some penetration of the field near the surface. The distance over which the magnetic field can penetrate a superconductor in the Meissner state is given by λ. The shielding ability of a superconductor depends on the superfluid carrier density such that $\lambda^2 \sim 1/n_{SC}$. The values quoted for both ξ and λ are usually taken as the minimum values extrapolated to T=0. As T increases from T = 0 and approaches T_C, both ξ and λ increase and diverge.

In type II superconductors, such as Nb, Nb_3Ge, and the HTSCs, a magnetic field can penetrate into the interior in the form of quantized vortices. Each vortex contains a quantum

of magnetic flux $\phi_0 = h/2e = 2.07 \times 10^{-15}$ Wb, where h is Planck's constant and 2e is the charge of a Cooper pair. A vortex consists of a normal core of radius ξ surrounded by a supercurrent circulating around the core at a distance λ. The magnetic field of the vortex is also confined within a distance λ of the core, and so λ defines the size of the vortex. If a vortex moves in a superconductor it will cause dissipation which will appear as a resistance. A transport current will force vortices to move if they are not pinned by defect sites in the superconductor. It is therefore very important to understand pinning in superconductors for applications such as superconducting magnets. More information on these and other superconducting properties can be found in several excellent books on superconductivity[13-17] and solid state physics.[18,19]

Table 1.1. Typical values for various superconducting parameters in some conventional superconductors[15,18] and YBCO.[16,17] The values for the resistivity ρ and Drude scattering time τ were taken from Ref. (19) .

	Al	Sn	Pb	YBCO
T_C (K)	1.18	3.72	7.20	92
2Δ (meV)	0.34	1.15	2.73	28 (BCS)
$\nu_{2\Delta}$ (cm^{-1})	2.7	9.3	22	225 (BCS)
$\lambda_{2\Delta}$ (mm)	3.6	1.1	0.454	0.044 (BCS)
$f_{2\Delta}$ (THz)	0.082	0.28	0.66	6.7 (BCS)
$2\Delta/k_BT_C$	3.3	3.5	4.38	3.52 (BCS)
$\xi(0)$ (nm)	1600	230	83	(ab) ≈ 2 - 3 (c) ≈ 0.3
$\lambda(0)$ (nm)	16	36	37	(ab) ≈ 150 (c) ≈ 1200
n ($x10^{22}$ cm^{-3})	18.1	14.8	13.2	≈ 0.4
ρ ($\mu\Omega$ cm)	0.3 @ 77K	2.1 @ 77K	4.7 @ 77K	≈ 100 @ 100K
τ (ps)	0.065 @ 77K	0.011 @ 77K	0.0057 @ 77K	0.033 @ 100K

What is unique about the HTSCs is the rather small values for ξ and large values for λ in comparison with the conventional superconductors, and that these values are highly anisotropic depending on whether the parameter is measured in the ab-plane or along the c-axis. The large anisotropy of the HTSCs is also seen in resistivity measurements along the different crystal directions. For instance, ρ_c/ρ_{ab} in YBCO is about 10^2 to 10^3, and as high as 10^5 in the BiSrCaCuO compound.[20] On the other hand, the conventional superconductors are mostly isotropic in their properties. This makes it easier to make superconducting devices with conventional superconductors than with the HTSCs. Nevertheless, the ability to cool the HTSCs with liquid nitrogen is a major practical advantage over conventional superconductors. As discussed in the next section, there has been much effort in developing niche applications which incorporate the new high-T_C materials.

1.3. Applications of high-T_C thin films

The high-T_C superconductors can be made as single crystals, bulk polycrystalline material, or thin films on substrates. Single crystals are too small to be of practical importance, and much work is still needed to make flexible wires from polycrystalline HTSCs for use in superconducting magnets. However, some promising applications of these new materials have already been realized with thin films.[16,22] Most of these applications stem from technologies that were developed with conventional superconductors.[15,16]

High-T_C thin films have found niche applications primarily in the medical sector and in microwave communications. Active devices which have been made successfully from high-T_C thin films include SQUID (superconducting quantum interference device) magnetometers and SFFTs (superconducting flux-flow transistors). Conductus, a company in California working with the HTSCs, has recently started selling high-T_C SQUID magnetometers. Passive devices such as microwave filters and delay lines are already being sold by Superconducting Technologies, Inc. Another promising application of the HTSCs is their integration with CMOS (complementary metal-oxide semiconductor) technology in multi-chip module (MCM) packages.[22] These applications will be discussed in more detail after first describing how high-T_C thin films are made and patterned into device structures.

Thin film superconductors can be made by several techniques such as multisource

evaporation or sputtering, single-source off-axis sputtering, pulsed laser deposition by laser ablation, and metal organic chemical vapour deposition (MOCVD).[23-28] The two most commonly used techniques are sputtering and laser ablation. Laser ablation[24-26], which was the method used to deposit the films described in this work, produces the best quality films with the highest critical current densities J_C at 77 K of about 1 to 4 x 10^6 A/cm^2, the highest T_C's, and the lowest surface resistances R_S at microwave frequencies. The laser ablation process uses high power nanosecond laser pulses from an excimer laser which are focused onto a bulk polycrystalline superconducting target located inside a vacuum chamber. A substrate is mounted on a heater a few centimetres away, and material "blown" off the surface of the target by the laser pulse is deposited onto the substrate material. The deposition rate is relatively fast (~ 10 nm per minute), but the substrate area that can be covered without rastering the laser pulse across the target is about 1 cm^2. Sputtering[25-27], on the other hand, has a slower deposition rate but can cover much larger areas. Large substrates are important for device fabrication, and it has been shown that YBCO can be deposited uniformly on substrates with diameters of 5 cm.[27]

Good quality films can be grown epitaxially on substrates with lattice constants closely matched to those of the superconducting material. Examples of typical substrate materials are $LaAlO_3$, MgO, $NdGaAlO_3$, and $SrTiO_3$. $LaAlO_3$ and MgO are two of the most commonly used substrates, with $LaAlO_3$ providing better quality films. $SrTiO_3$ is an excellent substrate material, but its dielectric constant is much too large for high frequency applications. Sapphire (Al_2O_3) is an excellent substrate for high frequency applications, but is chemically incompatible with YBCO at the high temperatures required for processing. It is still possible to use sapphire, but a thin buffer layer of CeO or YSZ (yttrium stabilized zirconia) must be deposited before the YBCO.[29] Integrating YBCO devices on silicon chips would be ideal, but Si diffuses into YBCO and destroys the superconducting properties.[30] Again, a buffer layer is needed to deposit on silicon substrates.

To pattern the film into a useful device structure, several patterning and etching techniques can be used similar to the ones already used in the semiconductor industry. Wet chemical etching with dilute acids[31] is most common, but dry etching techniques such as reactive ion etching[32] and ion milling[33,34] have also been used to produce YBCO bridges only

200 nm wide. A laser writing technique[35] has recently been investigated which uses heating from a focused laser to remove oxygen from selected areas of a YBCO film. The removal of oxygen renders these areas semiconducting, and regions not exposed to the laser remain superconducting allowing transmission lines to be patterned into the film. It is also possible to remove parts of the film by laser ablation with an excimer laser, where linewidths down to 3.5 μm have been achieved without degradation in T_C or J_C.[36] Appendix A provides a detailed description of the growth and processing of the YBCO films used in the photoresponse experiments described in this work.

Processing of high-T_C thin film superconductors has advanced to the point where several layers of superconductor material separated by insulating layers can be deposited without affecting the superconducting properties. This is extremely important for device structures where crossovers are essential, such as SQUIDS. SQUIDS are devices which use Josephson junctions to sense very small magnetic fields.[14-16] In conventional superconductor Josephson junctions, two superconductors are separated by an insulating oxide with a thickness approximately equal to the coherence length. However, the small coherence length of the HTSCs has made the reproducible fabrication of these junctions difficult. Several special techniques have therefore been used to make these junctions. Step-edge junctions,[37] which are formed by depositing high-T_C material on 0.3 to 0.4 μm high steps on the substrate, have proven to be very successful.[38] Layers of nonsuperconducting $PrBa_2Cu_3O_7$ have also been used to form the insulating barrier in the junctions.[39] A four layer SQUID magnetometer was made recently using junctions formed at the twin boundary of a $SrTiO_3$ bicrystal.[40]

Even though conventional superconductor SQUIDs are can be extremely sensitive to magnetic fields, high-T_C SQUIDs operating at 77 K are intrinsically noisy due to movement of vortices in the film.[41] At low frequencies, where medical applications are most important, the noise is the highest and follows a 1/f behaviour.[41-43] Special chopping techniques have been used to significantly reduce this 1/f noise.[43] Noise levels have typically been just under 1 pT $Hz^{-1/2}$ at 1 Hz, which is the sensitivity required for medical applications.[44] Recently, a four channel YBCO SQUID magnetometer successfully monitored magnetocardiac signals from a patient.[44] The SQUIDs were cooled with liquid

nitrogen, which made it possible for the insulating gap between the patient and the SQUID devices to be only 2.5 cm. The patient and apparatus had to be placed in a magnetically shielded room to reduce noise pickup. The experiment was a first step to establishing high-T_c superconductor SQUID magnetometers as viable clinical diagnostic instruments. A YBCO thin film SQUID has also been used as a magnetic field microscope with a resolution of 80 μm.[45] Another potential application of the HTSCs in the medical industry is the use of YBCO thin film pickup coils in nuclear magnetic resonance (NMR) imaging machines to significantly improve sensitivity compared to liquid nitrogen cooled copper loops.[46] This is very important since the large magnetic fields used now, which may have possible health risks, can be reduced without lowering the sensitivity of the machine.

Another promising active device made with the high-T_c materials is the superconducting flux flow transistor, or SFFT.[47] The SFFT is a three terminal device consisting of two superconducting regions connected by a parallel array of weak links. A control line, or the "base" of the transistor, launches vortices into the weak links. The vortices travel at high speeds (~ 5 x 10^5 m/s) through the weak links and modulate the resistance of the device as measured between the two main terminals. Response times less than 200 ps have been measured,[48] and operation up to 30 GHz is predicted. The fabrication of the devices is very simple since only a single layer of high-T_c film is required. The SFFT offers high power gain, low input and output impedances, and can be easily matched to conventional circuitry. One application of these devices is for amplifying signals from cooled far-infrared array detectors.[48] However, one of the main applications of the SFFT will be in providing a suitable interface with CMOS electronics cooled to 77 K where it is believed that an increase in speed by a factor of 2 is possible.[49] It has already been demonstrated[49] that CMOS and SFFT devices can be made on the same substrate, and the readout of CMOS memory cells was recently achieved using SFFTs on a separate substrate.[50] High-T_c superconductors, therefore, have strong potential for use in hybrid semiconductor-superconductor circuits.

In passive microwave devices such as filters and delay lines, the HTSCs offer lower surface resistance R_s than metals such as copper. At 1 GHz, R_s for YBCO is roughly 1000 times less than for copper at 77 K.[51] However, for normal metals $R_s \sim \omega^{1/2}$ whereas $R_s \sim \omega^2$

for superconductors. Therefore R_S increases with frequency more rapidly for YBCO than for copper. At 10 GHz, R_S for YBCO is only 60 times less than that for copper, and at about 100 GHz the surface resistances of the two materials are equal. Fortunately, the range of frequencies for most microwave applications is from 1 to 10 GHz, and a lower value for R_S means less insertion loss for the device in a microwave circuit. Satellites currently use bulky and heavy waveguide structures for microwave telecommunications. The possibility for reducing the size and weight of these devices by using monolithic YBCO microwave structures is a very attractive prospect, and much research is being directed towards this goal.[22,51,52]

The use of the HTSCs as high speed electrical interconnects has also been considered.[53] However, for transmission of 1 ps wide electrical pulses, the HTSCs offer no advantage over gold transmission lines cooled to 77 K.[53] High-T_C thin films also have the potential of being used as infrared or high speed photodetectors, as discussed in the next section.

1.4. High-T_C photodetectors

The reflectivity of YBCO[54] is about 10 % from 1.5 eV to 3 eV, and starts to rise slowly below the plasma edge $\omega_P \approx 1.1$ eV.[55] The optical penetration depth for YBCO around 2 eV (620 nm, or red light) is $\delta \approx 90$ nm.[56] This is why YBCO films thicker than 200 nm appear black and opaque. These optical properties of low reflection and high absorption over a broad range of radiation frequencies make YBCO thin films well suited for broadband photodetectors, unlike semiconductor photodetectors which are usually limited in wavelength sensitivity by the size of their band gaps.

There are two general classes of photodetectors: thermal detectors and photon detectors.[57] In thermal detectors, electrons which are excited by the incident radiation relax to thermal equilibrium with the lattice at an elevated temperature in an absorbing element. The change in temperature of the absorber is then detected. Some examples of thermal detectors include thermoelectric detectors, Golay cells which sense a change in pressure due to heating of a gas, pyroelectric detectors which rely on a change in dielectric constant of the absorber, and bolometers which use changes in resistance of materials. In photon detectors,

or nonthermal detectors, electrons are excited by the incoming radiation and the resulting nonequilibrium distribution of electrons is detected before they have a chance to reach thermal equilibrium with the lattice. The best example of a photon detector is a semiconductor photodetector where electron-hole pairs are created across the band gap and are swept out of the material by an electric field and detected before they have a chance to recombine.

One of the first requirements for a sensitive bolometer is a large change in resistance with temperature. If the change in temperature induced in an absorbing element by incident light is ΔT, then the change in voltage that is detected, or the photoresponse, is

$$\Delta V = I \frac{dR}{dT} \Delta T \qquad (1.2)$$

where I is the bias current and dR / dT is the derivative of the resistance with respect to the temperature of the absorbing element at a given initial temperature T_0. If dR / dT is not constant, then Eq. (1.2) is valid only for small increments of ΔT. Both superconductors and semiconductors have been used to make bolometers. In a semiconductor bolometer, the resistance increases exponentially as the temperature is lowered, as shown in Fig. 1.8(a). In a superconductor, there is a sharp decrease in the resistance right at the transition temperature T_C, as shown in Fig. 1.8(b), which makes it ideal for use as a sensitive bolometer if the temperature of the detector is kept near T_C. A bolometer which uses a superconductor is often referred to as a transition-edge bolometer. Figure 1.8(c) shows how the response of a transition-edge bolometer is peaked right at T_C, as predicted by Eq. (1.2). The responsivity (or photoresponse) of a bolometer is usually given in units of V/W.

A simple thermal model for a bolometer (or any thermal detector) is shown schematically in Fig. 1.9. Incident radiation is converted to heat in an absorbing medium with heat capacity C and temperature T_B. The absorber is connected to a heat sink at temperature T_0 by a thermal conductance G. In the steady state with incident power P, the difference in temperature between the absorber and the heat sink is[57]

$$\Delta T = T_B - T_0 = \frac{P}{G} \qquad (1.3)$$

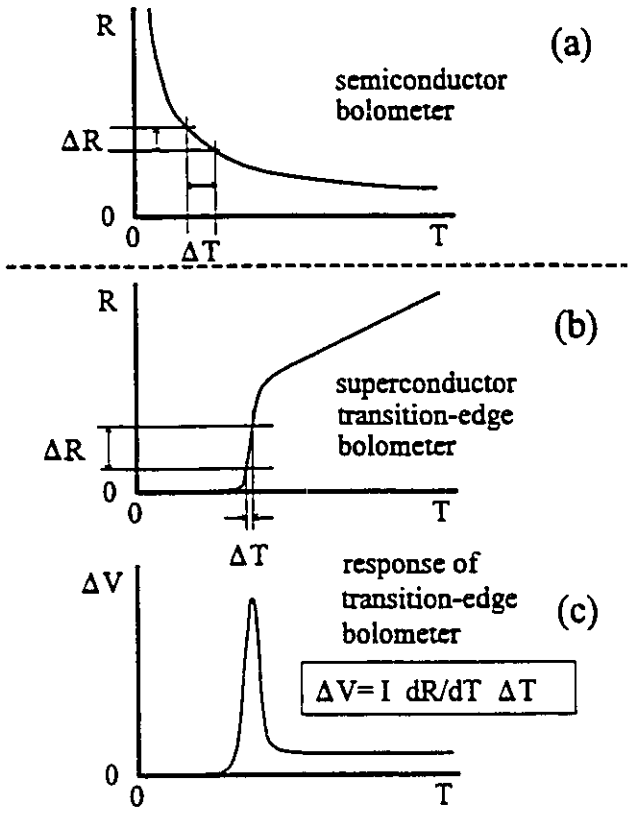

Fig. 1.8. Resistance R versus temperature T for (a) a semiconductor bolometer and (b) a superconductor transition edge bolometer. ΔR is the change in resistance produced as a result of a change in temperature ΔT in the detector. In (c), the derivative of the resistance with respect to temperature is shown for the curve in (b). Notice how the response of the superconducting bolometer is peaked at T_c.

and the time constant for excess heat escape out of the absorber and into the heat sink once the radiation has been switched off is

$$\tau = \frac{C}{G} \tag{1.4}$$

The thermal time constant τ determines the speed of the detector and the temperature transient ΔT from Eq. (1.3) determines the responsivity. To make a fast bolometer, the heat capacity of the absorber must be reduced or the thermal conductance to the heat sink must be increased. If G is increased, however, then the responsivity according to Eq. (1.3) goes down. There is a trade-off between speed and responsivity for bolometers, where increased speed is compensated by decreased responsivity. Usually, bolometers are required to be

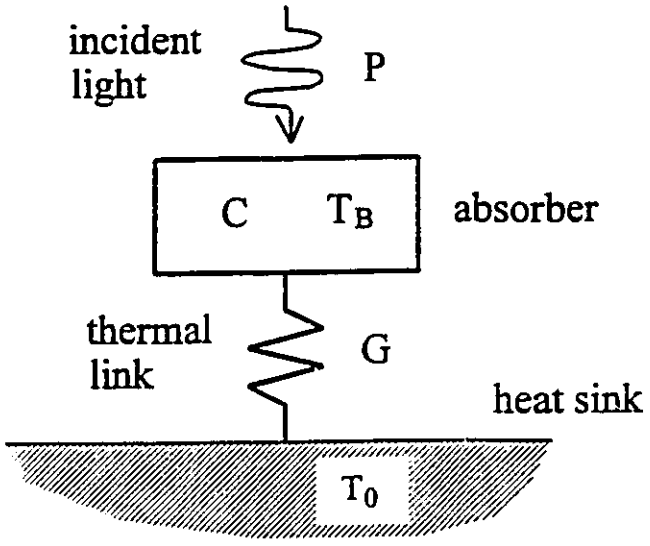

Fig. 1.9. Simplified thermal model for a bolometer. Incident radiation with power P (W) heats an absorbing element with heat capacity C (J/K) and temperature T_B. The heat can escape to a heat sink at temperature T_0 through a thermal link designated by a thermal conductance G (W/K).

sensitive rather than fast, so response times typically range from about 1 s to 1 ms.

The fundamental limit on the sensitivity of bolometers is determined by the amount of Johnson (thermal) noise. The thermal noise voltage is given by[57]

$$V_N = \sqrt{4\, k_B\, T\, R\, \Delta f} \qquad (1.5)$$

where R is the resistance of the detecting element and Δf is the frequency bandwidth over which the noise voltage is measured. The noise associated with bolometers is usually quoted as the noise equivalent power (NEP) of the detector within a 1 Hz wide bandwidth at a given frequency. The NEP, which has units of W $Hz^{-1/2}$, has a minimum value given by the amount of incident radiation power that would give a voltage from the detector equal to that given by Eq. (1.5) with Δf = 1 Hz. Clarke *et al.*[58] built an Al bolometer with an NEP of 1.7×10^{-15} W $Hz^{-1/2}$ at 2 Hz and cooled to a temperature of 1.2 K, which is within a factor of 2 of the theoretical thermal noise limit given by Eq. (1.5). The bolometer had a response time of about 80 ms and a responsivity of 7.4×10^4 V/W. However, no real advantage of superconductor over semiconductor (Ge) bolometers was found as far as performance was

concerned.[58,59]

Both semiconductor and conventional superconductor bolometers have to be cooled with liquid helium to temperatures of 4.2 K or less for best performance characteristics. The potential of using high-T_c superconductors as sensitive bolometers operating at 77 K with liquid nitrogen has generated much interest over the past few years.[57,60-62] One of the main goals has been to develop a HTSC bolometer that can compete with currently available HgCdTe photodetectors, which also operate at 77 K but have a cutoff wavelength from 10 to 50 μm,[63] by offering an extended range of sensitivity for wavelengths above 20 μm.[57] In 1989, Richards *et al.*[60] performed a feasibility study for YBCO thin film bolometers and found that NEPs of 1 to 20 x 10^{-12} W $Hz^{-½}$ could be achieved which compared favourably with other 77 K detectors for $\lambda > 20$ μm. In 1993, Verghese *et al.*[61] constructed a YBCO thin film bolometer on a sapphire substrate with a broadband responsivity of 19 V/W from 20 to 100 μm and an NEP of 2.4 x 10^{-11} W $Hz^{-½}$ at 10 Hz and 77 K. The response time of the detector was about 55 ms. The bolometer was shown to be more sensitive than commercially available room temperature detectors (i.e. pyroelectric) for wavelengths in the range of 20 to 300 μm. The bolometer was also used in an experiment to look at water absorption lines in the same wavelength region, and it was suggested that YBCO bolometers could be used commercially for FIR spectroscopy and space observation of bright sources. YBCO bolometers have recently been constructed on micromachined Si substrates[62] with responsivities of 1750 V/W, NEPs of about 7 x 10^{-10} W/$Hz^{-½}$, and response times as short as 0.5 ms. Similar detectors are now available commercially.[64]

The response of a bolometer to long and short light pulses is compared in Fig. 1.10. In Fig. 1.10(a), the duration of the light pulse is much larger than the thermal decay time given by Eq. (1.4). If the incident light pulse has power P, the maximum temperature change given by Eq. (1.3) is reached after a few thermal time constants. When the light pulse has ended, the temperature decays to the temperature of the heat sink over the same time period. However, if the duration of the light pulse is much less than the thermal time constant, as depicted in Fig. 1.10(b), it is better to describe the increase in temperature of the film by the amount of energy E absorbed in the film from the light pulse divided by the heat capacity of the absorbing film. The temperature will then decay back to its initial value according to the

thermal time constant of the system. The scenario shown in Fig. 1.10 must be considered when working with either chopped radiation sources or short laser pulses.

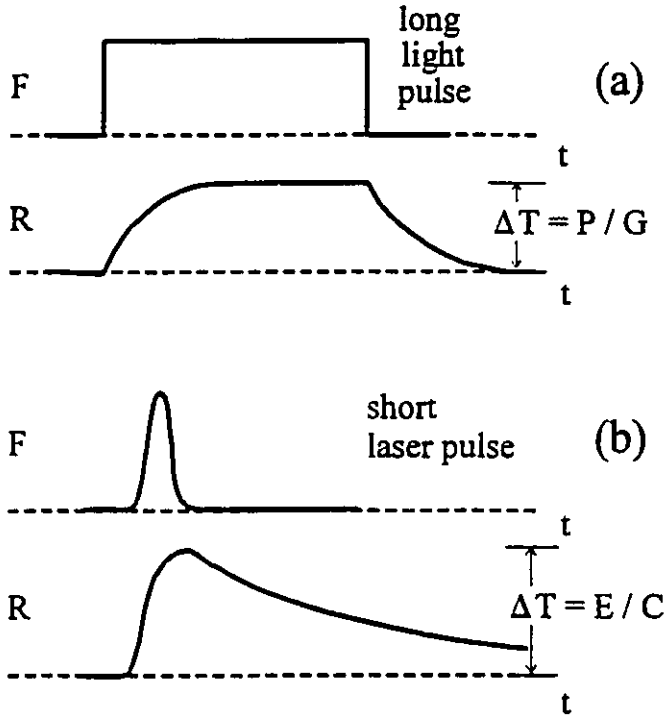

Fig. 1.10. Effect of long and short light pulses on the response of a bolometer. F represents the fluence or intensity of the incident light pulse, and R is the resulting response of the bolometer. In (a), the width τ_p of a long light pulse is much greater than the thermal time constant $\tau = C/G$. The maximum temperature change ΔT in the detector is shown, where P (W) is the power of the light pulse and G (W/K) is the thermal conductance. In (b), a short light pulse is used with $\tau_p << C/G$. The maximum temperature change in the absorbing material of the bolometer is then given by E/C, where E (J) is the absorbed energy and C (J/K) is the heat capacity of the absorbing medium. The decay time of the thermal transient is determined by the thermal time constant τ.

There may also be potential for high speed YBCO photodetectors with subnanosecond response times. Bolometers are inherently slow because the response time relies on how fast heat can escape from the detector element. The fastest thermal decay time would be of the order of a few nanoseconds for a very thin YBCO film (~ 30 nm). To achieve faster response times on the order of picoseconds for measuring fast laser pulses, a nonthermal detection mechanism in the HTSCs may be needed.

The big question is whether high speed HTSC photodetectors could compete with currently available semiconductor photodetectors. One commercially available GaAs photodiode[65] can produce 10 ps FWHM (full width at half maximum) voltage pulses directly

on an oscilloscope when excited with femtosecond laser pulses. Another semiconductor photodetector which recently came out on the market has produced 7 ps FWHM pulses on an oscilloscope.[66] Both detectors are sensitive to wavelengths from 400 to 900 nm (3.1 eV to 1.4 eV), and both use an optical fibre to bring the laser pulse directly to the detector element. The basic technique for performing such fast transient measurements with an oscilloscope is shown in Fig. 1.11(a). The time resolution in this case is usually limited by the speed of the oscilloscope, which is typically 7 ps for a 50 GHz bandwidth.

To measure faster response times, special techniques such as electro-optic sampling,[67-71] as shown in Fig. 1.11(b), or photoconductive sampling[72,73] are used. In electro-optic sampling, a short laser pulse is divided by a beam splitter into two pulses. One pulse is used to excite the detector, and the second pulse is used to probe the electric field within an electro-optic crystal arising from the voltage transient. The polarization of the probe beam will be rotated in proportion to the electric field in the crystal. By changing the delay of the probe pulse with respect to the excitation pulse, the voltage transient on a transmission line can be resolved temporally. The electro-optic effect[74] in commonly used crystals such as $LiTaO_3$ is very fast, and so the speed of the technique is usually limited by the duration of the laser pulse, or about 0.1 ps. Using these sampling techniques, MSM (metal-semiconductor-metal) photodiodes have been shown to have operating bandwidths up to 105 GHz,[72] with response times of about 5 ps FWHM.[71] Response times as short as 0.6 ps FWHM have been seen from GaAs photoconductive switches using electro-optic sampling techniques.[70] One of the considerations in such measurements is dispersion effects as the electrical transient travels down the transmission line. Short pulse propagation on YBCO transmission lines has already been studied be several groups.[75-77]

Even though semiconductors are already extremely fast, YBCO photodetectors might still be useful for their sensitivity to a broad range of wavelengths. However, fast semiconductor detectors have recently been developed which are sensitive to wavelengths from 5 to 20 μm.[78] These detectors, known as quantum well infrared detectors (QWIPs), are based on transitions from bound states in InGaAs/GaAs quantum wells to continuum states above the wells, which allows tuning of the wavelength sensitivity simply by varying the structure of the wells. So it seems as if the wavelength region spanned by most

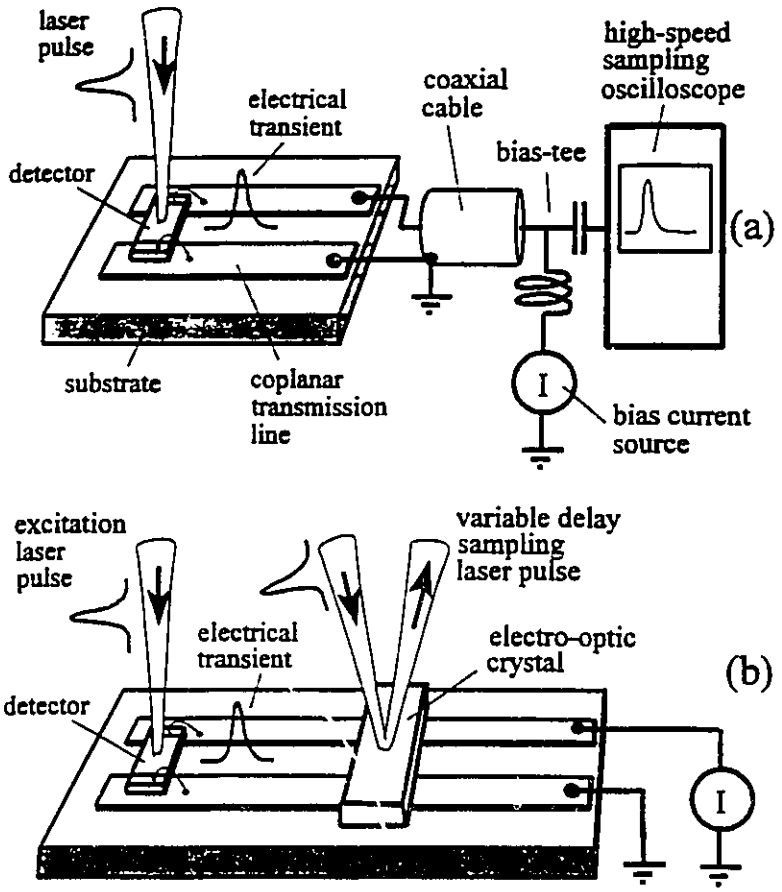

Fig. 1.11. Two commonly used techniques used to measure fast transient voltages from high speed photodetectors. The photodetector is usually mounted on a coplanar transmission line structure on a substrate. In (a), the voltage transient that is generated by an incident laser pulse is launched into a coaxial cable and measured directly by a high speed digital sampling oscilloscope. A bias-tee allows current bias I to be applied to the device under test. Faster time resolutions can be obtained with electro-optic sampling shown in (b). After a first laser pulse excites the device, a second laser pulse derived from the same source but with a variable time delay with respect to the first pulse is used to monitor the electric field within an electro-optic crystal due to the fast voltage transient. A bias-tee is not usually needed in this case, and so the current bias is applied directly to the transmission line.

picosecond and femtosecond laser sources is covered by various semiconductor photodetectors. The potential of using a single YBCO detector for the entire range may not be enough of an advantage considering that YBCO detectors need to be cooled and will probably be much less sensitive than optimized semiconductor detectors.

Even if picosecond YBCO photodetectors may not be competitive with existing semiconductor technology, studying the fast photoresponse from YBCO thin films may help reveal the nature of superconductivity in the HTSC materials. This alone may have important consequences for other high-T_c devices which have to operate at high speeds.

2. NONEQUILIBRIUM PROCESSES IN SUPERCONDUCTORS

2.1. Equilibrium properties of high-T_C superconductors

Before discussing nonequilibrium phenomena in high-T_C superconductors which may lead to nonthermal photoresponse mechanisms (Chapter 3), it is important to first understand some of the observed equilibrium properties of these complicated materials. Only after the nature of superconductivity in the conventional superconductors had been well established with BCS[8] and Eliashberg[12] theory did work with nonequilibrium superconductivity in the conventional materials experience significant progress. However, even today, theories describing the nonequilibrium properties of conventional superconductors are controversial and have had limited success. Without a clear understanding of how the HTSCs become superconducting,[17,79] the study of their nonequilibrium properties is made even more difficult. The following is a brief overview of some of the equilibrium properties of HTSCs most relevant to this work.

As seen earlier in Fig. 1.5, the structure of YBCO and the HTSCs in general is quite complex. In YBCO, the oxygen atoms in the CuO chains along the b-axis remove electrons from the CuO planes making them conducting. The oxygen atoms added to the CuO chains therefore act as "dopants" analogous to doping in semiconductors. The carriers added to the CuO planes are holes instead of electrons as in most metals and conventional superconductors. Figure 2.1 is a phase diagram[17,80] for $YBCO_x$ as a function of oxygen content x. Without any oxygen atoms in the CuO chains, $YBCO_6$ is an antiferromagnetic insulator with a Néel temperature T_N just above 400 K. As the oxygen content in the chains is increased, the long range antiferromagnetic order is diminished by doping the CuO planes with holes and T_N is reduced. At x = 0.4, the ordered antiferromagnetic state has been completely destroyed and the material goes from a tetragonal crystal structure in the insulating state to an orthorhombic structure with metallic behaviour. Increasing the oxygen doping further makes the material become a superconductor with a maximum T_C of about 93 K for $YBCO_{6.95}$. The fully doped material is $YBCO_7$ with a T_C slightly less than this maximum value. At high temperatures, the oxygen atoms in the chains are highly mobile and

can easily escape from the material. Therefore, any processing of YBCO films or crystals performed at high temperatures must be done in an oxygen atmosphere to ensure that superconducting properties are maintained.

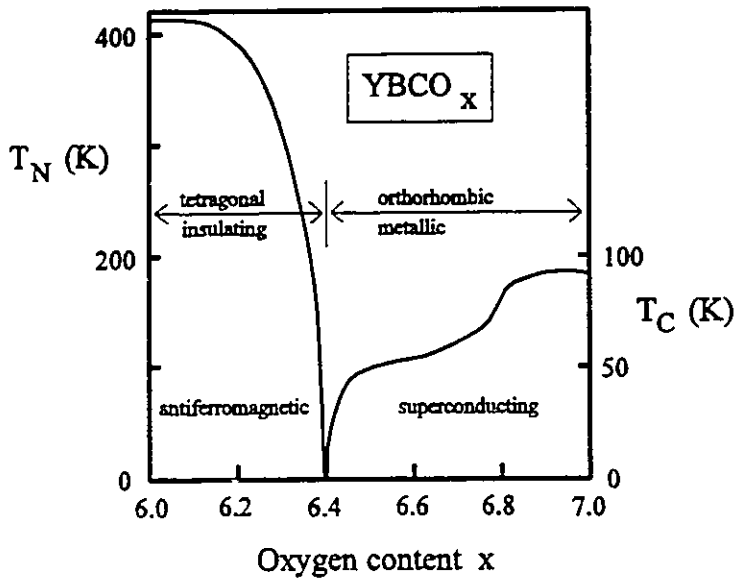

Fig. 2.1. Phase diagram for $YBCO_x$ as a function of oxygen content x (adapted from Ref. 80). T_N is the Néel temperature for the transition into the antiferromagnetic state, and T_C is the critical temperature of the superconducting state.

The fact that $YBCO_6$ exhibits antiferromagnetism has prompted several groups[81-84] to speculate that the origin of superconductivity in the HTSC materials arises from spin fluctuations, rather than phonons as with the conventional superconductors. It is also believed that the superconducting order parameter exhibits d-wave symmetry as opposed to s-wave symmetry in BCS theory. A comparison[85] between s and d wave symmetries is made in Fig. 2.2(a). An s-wave (BCS) superconductor has a gap function $\Delta(k)$, where k is a wavevector on the Fermi surface, which is isotropic on the Fermi surface with magnitude Δ. On the other hand, the gap function for a d-wave superconductor is not constant over the Fermi surface and contains points (or nodes) where the magnitude of the gap goes to zero. The density of states (DOS) for quasiparticle excitations out of the superconducting state is also quite different between the two types of symmetries,[85] as shown in Fig. 2.2(b). In an s-wave superconductor,[12-19] there are no allowed states for excitations within the gap. However, because a d-wave superconductor has nodes in the gap, excited states are allowed

below the maximum gap energy Δ. It has been proposed[83,84] that Δ in a d-wave scenario with spin fluctuation induced superconductivity opens up quite rapidly as the temperature is lowered below T_C, and that the gap ratio at low temperatures is $2\Delta(0)/k_BT_C \sim 10$. This gap ratio is quite large considering that a strong-coupling s-wave superconductor such as Pb has a gap ratio of only 4.38 (see Table 1.1), which means that spin fluctuation induced superconductivity would lead to very strong coupling between the electrons in Cooper pairs in the HTSCs.

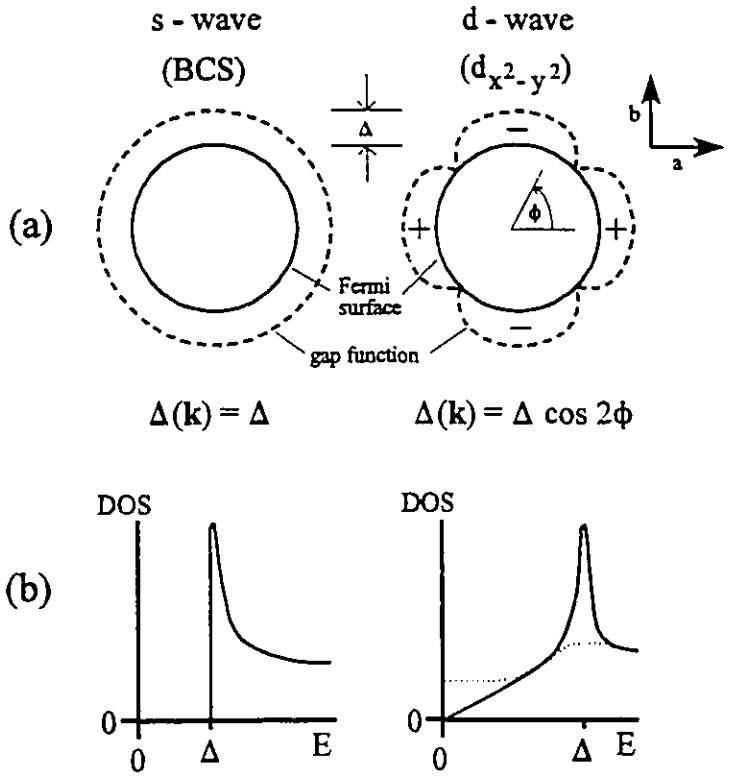

Fig. 2.2. (a) Symmetry of the gap parameter Δ(k) in k space and (b) the density of states (DOS) for quasiparticle excitations out of the superconducting state for s-wave and d-wave superconductors. The dotted line for the DOS in the d-wave picture in (b) represents the effect of impurity scatterers on the pure d-wave DOS, as discussed in the text.

Even though conventional superconductors are predominantly s-wave, there has recently been much experimental evidence to support the d-wave scenario in the HTSCs.[81] SQUID devices made from YBCO and Pb junctions[86] have shown d-wave behaviour in their electrical characteristics, and very recently YBCO rings made on a $SrTiO_3$ tricrystal and scanned with a SQUID microscope have generated half flux quanta (i.e. h/4e) as predicted

by a d-wave scenario.[87] The measurement of the low temperature dependence of the penetration depth in very pure YBCO single crystals[88] has provided some of the strongest evidence for d-wave symmetry in the HTSCs. The penetration depth $\lambda(T)$, which is usually measured using microwave resonator techniques, is an excellent probe for the symmetry of the gap and the temperature dependence of the superfluid fraction given by

$$f_{SC} = \left(\frac{\lambda(0)}{\lambda(T)} \right)^2 \qquad (2.1)$$

At low temperatures, $\lambda(T)$ falls exponentially as the temperature is lowered in a BCS superconductor, whereas $\lambda(T) \sim T$ in a d-wave superconductor.[88,89] In the YBCO single crystal experiments,[88] it was found that $\lambda(T)$ varied linearly at low T and therefore supported a d-wave picture for the gap. However, experiments with YBCO thin films[90-97] show $\lambda(T) \sim T^2$ at low T, and reveal a temperature dependence for the superfluid fraction over the entire temperature range below T_C described by

$$f_{SC} = 1 - t^2 \qquad (2.2)$$

where $t = T/T_C$ is the reduced temperature. Figure 2.3 compares the temperature dependence of the superfluid fraction for various types of superconductors. In this work, Eq. (2.2) will be used for the value of f_{SC} in thin films. It is also interesting that $\lambda(0)$ in pure single crystals is about 150 nm,[88] but can range from 160 to 270 nm in thin films[91-93] depending on the film quality.[92]

Since thin films contain more defects and impurities than good single crystals, it has been postulated that the presence of impurities in a d-wave superconductor will change the low temperature behaviour of $\lambda(T)$ from a T to a T^2 dependence as observed in thin films.[98] This has also been shown experimentally with YBCO single crystals where adding Zn impurities changed the temperature dependence of $\lambda(T)$ from a T to T^2 behaviour.[99]

Another interesting phenomena observed in the HTSCs is a sudden drop in the quasiparticle scattering rate τ_s^{-1} just below T_C.[94,95,99,100] This is shown in Fig. 2.4 for YBCO single crystals (Bonn *et al.*[95]) and thin films (Gao *et al.*[94]). In the data by Bonn *et al*,[95] the scattering rate τ_s^{-1} drops by a factor of 400 as the temperature is lowered from 84 K to 15 K,

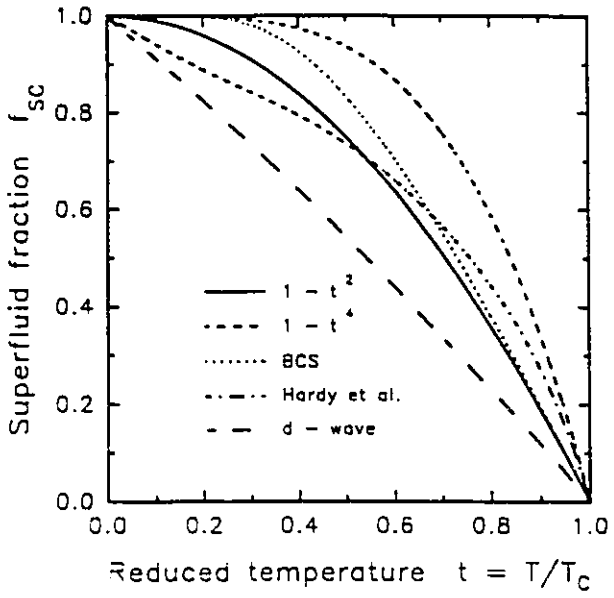

Fig. 2.3. Comparison of the superfluid fraction as a function of reduced temperature for a variety of models. The experimental result for the superfluid fraction measured by Hardy *et al.* (Ref. 88) in high quality YBCO single crystals is also shown.

and follows an exponential behaviour $\tau_s^{-1} \sim \exp(-T/T_0)$ where $T_0 \approx 12$ K. Such a dramatic drop in the scattering rate below T_c is not normally observed in conventional superconductors where the scattering rate for electrons depends on the phonon population in the material or may even be temperature independent if the scattering rate is limited by impurities. This has provided support for the idea that the pairing mechanism in the HTSCs may be electronic in origin rather than due to the electron-phonon interaction,[95] and that the mechanism responsible for scattering in the normal state is suddenly suppressed below T_c. It has been shown[101] that the scattering rate data from Bonn *et al.*[95] more closely follows the behaviour of spin fluctuation induced superconductivity in a d-wave rather than s-wave superconductor. The sudden suppression of the quasiparticle scattering rate below T_c has also been seen in NMR experiments.[102] Neutron inelastic scattering experiments,[80,103-105] which are excellent probes of the antiferromagnetic state as well as antiferromagnetic fluctuations in the superconducting state in the HTSCs, have revealed suppression below T_c of the low energy spin fluctuations below 28 meV in $YBCO_{6.92}$.[103] However, whether neutron experiments provide evidence for s-wave or d-wave superconductivity in the HTSCs is still controversial.[106]

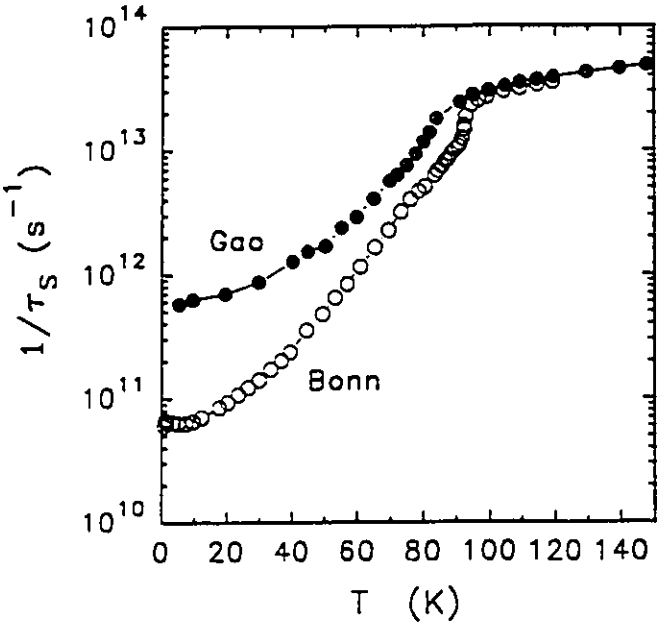

Fig. 2.4. Temperature dependence of the quasiparticle scattering rate τ_s^{-1} in YBCO single crystals (Bonn *et al.* Ref. 95) and YBCO thin films (Gao *et al.* Ref. 94) determined from microwave measurements. Notice the sudden drop in scattering rate just below T_c ~ 90 K for both samples. The scattering rate in the thin film is higher most likely due to a larger concentration of impurities and defect sites compared to the single crystal.

The debate over whether the HTSCs are s-wave or d-wave superconductors has not yet been settled, and much experimentation has been motivated by this controversy. Tunnelling experiments[107] do not show any evidence for an anisotropic gap and exhibit BCS behaviour in the temperature dependence of the gap. Although it was believed early on that the electron-phonon interaction could not possibly produce the high values for T_C observed in the new oxide superconductors,[108] other groups[109,110] have recently shown that the electron-phonon interaction can still explain the origin of the pairing mechanism due to large phononenergies in these materials extending out to 70 meV with strong coupling to some of these modes.[110] Even the interpretation of experiments supporting the d-wave scenario have been questioned, such as whether the linear temperature dependence of λ at low temperatures can be explained within an s-wave picture.[111]

Attempts at calculating the electronic band structure of YBCO have also been made,[112] but more work is needed before the band structure in these materials can be understood. Knowledge of the band structure is especially important in optical experiments where the origin of absorption mechanisms must be known in order to interpret experimental results. This has been the source of much controversy with the HTSCs, as discussed in

Section 2.3. Band structure effects are also important in photoinduced superconductivity experiments.[113-115] In these experiments, an underdoped YBCO superconducting sample is exposed for several minutes or hours to light from a HeNe (~ 1.95 eV) or Ar (~ 2.5 eV) laser. The resistivity of the sample is then observed to decrease and the T_C of the sample is enhanced (increases). The effect can last for up to a few days after the sample has been exposed. It is believed that the laser light generates long lived holes in the CuO planes which effectively enhance the superconductivity in the sample, but more work is needed to obtain a clearer understanding of the phenomena.

2.2. Nonequilibrium processes in superconductors

Despite a strong understanding of the equilibrium properties of conventional superconductors, their nonequilibrium properties are much less understood. Nonequilibrium conditions can be obtained by injecting excess quasiparticles through a tunnel junction into a superconductor or by breaking Cooper pairs with photons, light, electron beams, and phonons as long as the condition $\hbar\omega \geq 2\Delta$ is satisfied. The nonequilibrium state can be probed by tunnel junctions, voltage transients, and microwave or optical transmission and reflection. Excellent reviews of nonequilibrium superconductivity in conventional superconductors can be found in Refs. 116 to 118.

Figure 2.5 describes some of the processes that can occur in a superconductor thin film exposed to light with photon energy $\hbar\omega \geq 2\Delta$. In Fig. 2.5(a), Cooper pairs are broken by the incident photons and two quasiparticles are formed with excess energy $\hbar\omega - 2\Delta$. If the excess energy is greater than 2Δ, then these quasiparticles can lose their excess energy by breaking more Cooper pairs in an avalanche-like process, as shown in Fig. 2.5(b). This process is governed by the electron-electron scattering time $\tau_{e\text{-}e}$, which is usually quite fast. The excited quasiparticles can also lose their excess energy by emitting phonons at a rate determined by the electron-phonon scattering time $\tau_{e\text{-}ph}$ (or τ_S), as shown in Fig. 2.5(c). If the phonons that are emitted have energies larger than 2Δ, then they can break more Cooper pairs within a time τ_B, as seen in Fig. 2.5(d). Once excited quasiparticles have lost most of their excess energy, they can then recombine to form Cooper pairs again, as shown in Fig. 2.5(e). In this process, τ_R is the quasiparticle recombination time. For recombination to occur, a phonon must be emitted which has an energy larger or equal to 2Δ. This

recombination phonon can then break more Cooper pairs as in Fig. 2.5(d), or it can escape out of the film and into the substrate in a time τ_γ, as depicted in Fig. 2.5(f). In equilibrium, Cooper pair breaking and quasiparticle recombination are still taking place but the two rates are equal.

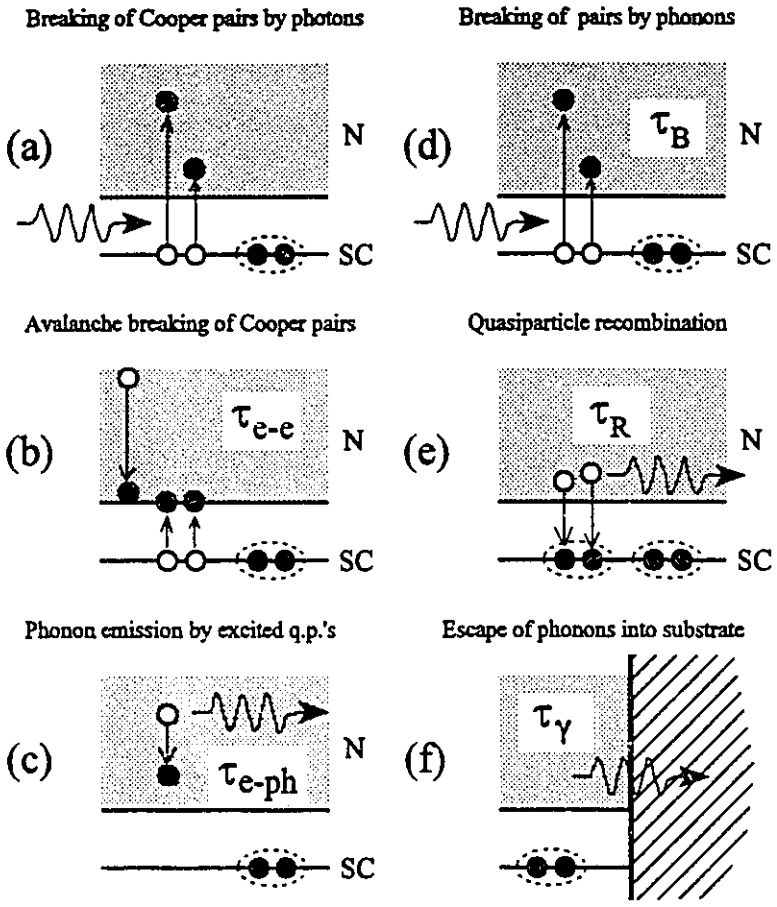

Fig. 2.5. Description of nonequilibrium processes in superconductors. The normal states (N) and the superconducting state (SC) are separated by the gap energy Δ. The relevant time constants for each process are also shown in the diagrams.

To find out exactly what these equilibrium rates are, one must first disturb the system and probe the evolution of the nonequilibrium state back to its equilibrium condition. The rate equations which govern these processes were developed by Rothwarf and Taylor[119] in 1967 to better interpret tunnel injection experiments, and were designed to consider the re-breaking of Cooper pairs by recombination phonons and the escape of phonons into thesubstrate. For small perturbations of excess quasiparticle density δN_{qp} injected at a rate I_0, the Rothwarf-Taylor equations can be linearized[120] in the form

$$\frac{d\ \delta N_{qp}}{dt} = I_0 + \frac{2\ \delta N_{ph}}{\tau_B} - \frac{\delta N_{qp}}{\tau_R} \qquad (2.3)$$

$$\frac{d\ \delta N_{ph}}{dt} = \frac{\delta N_{qp}}{2\ \tau_R} - \frac{\delta N_{ph}}{\tau_B} - \frac{\delta N_{ph}}{\tau_\gamma}$$

where δN_{ph} is the density of excess phonons with energies greater or equal to 2Δ. The factors of 2 come in because 2 quasiparticles are created by each phonon.

The intrinsic values for the equilibrium time constants τ_R, τ_B, and τ_S have been investigated theoretically by Kaplan *et al.*[121] and by Chang and Scalapino.[122] The phonon pair breaking time τ_B becomes shorter as the temperature is reduced and as the energy of the phonon increases. The electron-phonon scattering time τ_S depends on the excess energy of the quasiparticle. For large excess energies, τ_S is short since the quasiparticles can spontaneously emit phonons and lower their energy. However, once the quasiparticle reaches an energy just above the gap, it cannot lower its energy any further without recombining first with another quasiparticle and forming a pair. At this point, τ_S can be quite large since it will then depend on the phonon population at that temperature, and so τ_S increases as the temperature is lowered for quasiparticles near the gap edge. The recombination time τ_R depends on the presence of other quasiparticles in order to recombine. Since the normal fluid fraction decreases as the temperature is lowered, one expects that τ_R should increase almost exponentially at low temperatures. The recombination time also depends on the excess energy of the recombining quasiparticles, where quasiparticles with larger excess energies have shorter recombination times. For instance, τ_R for Pb at $T = 0.5T_C$ is about 100 ps at the gap edge but only 25 ps for quasiparticles at twice the gap energy.[121]

Experimentally, the intrinsic recombination time τ_R cannot be measured directly due to phonon trapping effects.[119,120] If the recombination phonons could escape before breaking more Cooper pairs (i.e. $\tau_B \to \infty$), then τ_R could be measured directly. However, τ_B is usually quite short, and the relaxation of quasiparticles back into the superconducting state is then determined by how long these phonons take in order to get out of the film so that the pair-

breaking process can end. This leads to an effective time constant[119]

$$\tau_{eff} = \tau_R \left(1 + \frac{\tau_\gamma}{2\,\tau_B} \right) \tag{2.4}$$

which is dominated by phonon trapping if $\tau_\gamma >> \tau_B$. The two bottlenecks which slow the recovery of a superconductor back to equilibrium are therefore the quasiparticle recombination time τ_R and phonon trapping determined by the phonon escape time τ_γ. The overall recovery time is determined by Eq. (2.4).

Recombination times have usually been measured in superconductors such as Al where τ_R can be of the order of microseconds and is therefore easier to measure. In 1977, Hu, Dynes, *et al.*[123] looked at quasiparticle relaxation times in Pb films using 5 ns laser pulses. They deduced that the observed relaxation time was an order of magnitude larger than the intrinsic recombination time τ_R due to recombination phonons re-breaking Cooper pairs within the excited volume. The first photoresponse experiments using picosecond laser pulses (20 to 50 ps) were performed by Chi *et al.*[124] on Pb films in 1981. The observed voltage transients had decay times of about 3 ns, which was found to be determined by the phonon escape time from the films. They concluded that in order to speed up the response, the energy from the laser pulse absorbed in the film would have to be carried away by quasiparticle diffusion rather than the escape of phonons. Using 300 fs laser pulses and a high speed scope, the intrinsic recombination time in Nb was measured recently by Johnson[125] to be as short as 22 ps at $T = 0.78\ T_C$. The actual voltage transient seen on the scope had a biexponential decay where the first decay time was the effective recombination time of about 230 ps and the second decay was due to thermal heat escape out of the film (2.6 ns). The intrinsic recombination time was extracted from the observed effective recombination time.

Very close to T_C, the relaxation of the order parameter begins to diverge as T approaches T_C instead of decreasing as predicted for τ_R. This divergence is due to the gap relaxation time τ_Δ which is different from τ_R. Normally, $\tau_R >> \tau_\Delta$ so that τ_R dominates. However, very close to T_C, the order parameter takes longer to adjust after recombination of quasiparticles has occurred, resulting in $\tau_\Delta >> \tau_R$. Experiments in which Al films were

illuminated by laser pulses and the resulting quasiparticle distribution probed by a tunnel junction on the back of the film[126] showed that for $0.98T_C > T > T_C$,

$$\tau_\Delta \sim \frac{\tau_E}{\Delta} \tag{2.5}$$

where τ_E is the electron-phonon inelastic scattering time (or $\tau_{e\text{-}ph}$). The effect of the gap relaxation time is also believed to be observed in the delay of the onset of a voltage transient across a superconducting bridge subjected to a supercritical current pulse.[127] Figure 2.6 describes the general behaviour of the relaxation of the order parameter determined by τ_R and τ_Δ as a function of temperature.

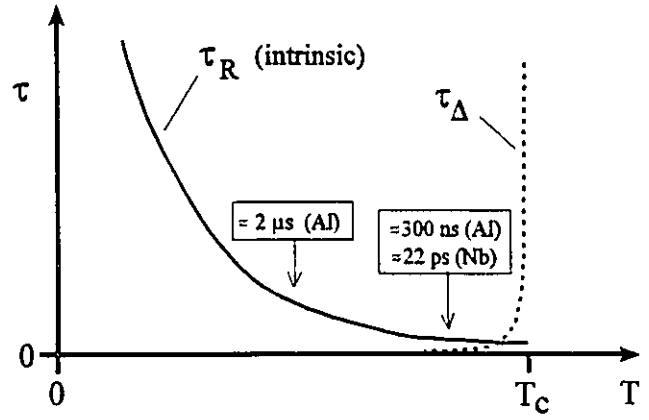

Fig. 2.6. General behaviour of the intrinsic quasiparticle recombination time τ_R and the order parameter relaxation time τ_Δ as a function of temperature. Experimental data for the recombination times observed in Al (Ref. 122) and Nb (Ref. 125) give an idea of the range of values for τ_R.

Creating nonequilibrium conditions in a superconductor by tunnel injection is different from optically breaking Cooper pairs in that tunnelling experiments inject low energy quasiparticles into the superconductor but optical experiments inject higher energy quasiparticles. In optical experiments, therefore, one has to consider the energy relaxation of quasiparticles by avalanche pair breaking or the electron-phonon interaction. The question also arises as to what happens at very high injection levels. Is it possible to destroy the superconductivity in a material with a light pulse ?

This last question was first addressed by Testardi[128] in 1971 with a paper entitled "Destruction of Superconductivity by Laser Light". Testardi found that voltage transients

from Pb films exposed to 40 μs laser pulses could not be explained by thermal heating of the films, and he estimated that the nonequilibrium electron temperature was 3 to 18 K above the lattice temperature. This prompted the development of several theories on nonequilibrium superconductivity.

In 1972, Owen and Scalapino[129] developed the μ^* model for nonequilibrium superconductors where the quasiparticles and Cooper pairs are both in thermal equilibrium with the lattice at a temperature T but are not in chemical equilibrium with each other. The quasiparticle distribution was determined by an effective quasiparticle chemical potential μ^* not equal to the Cooper pair chemical potential. One of the predictions of this model was that the gap would decrease as the quasiparticle injection increased. This was seen by Parker and Williams[130] soon afterwards using optically illuminated Sn and Pb tunnel junctions. The suppression of the gap for low quasiparticle injection densities was found to follow

$$\frac{\Delta(n)}{\Delta_0} \approx 1 - 2n \qquad (2.6)$$

where n was a parameter representing the normalized excess quasiparticle density injected into the system. The μ^* model also predicted a first order transition to the normal state once a certain injection level had been reached. However, this transition was not observed by Sai-Halasz *et al.*[131] who conducted transient microwave reflectivity experiments on Sn films illuminated by 60 to 90 ns optical pulses. Instead of a 1st order transition, a transition to a partially resistive state was observed above a certain injection threshold. This prompted Parker[132] to develop the T^* model for nonequilibrium superconductors in 1975. The T^* model assumes that the quasiparticles and Cooper pairs are not only in thermal and chemical equilibrium with each other, but also in thermal equilibrium with phonons with energies $\hbar\omega \geq 2\Delta$ at a temperature T^* greater than the temperature T of the bath. Phonons with $\hbar\omega < 2\Delta$ are in thermal equilibrium with the bath at temperature T. However, in 1977 Fuchs *et al.*[133] reconfirmed the predictions made by the μ^* model and showed the existence of a first order transition to the normal state at the predicted injection levels using a double junction technique (Sn-Sn-Pb structure). Figure 2.7 compares the amount of gap suppression predicted by both the μ^* and T^* models. The two models are very similar at low injection

densities, but differ significantly at higher levels of quasiparticle injection. The T* model predicts a 2nd order transition to the normal state at injection densities higher than those needed for the 1st order transition in the μ* model.

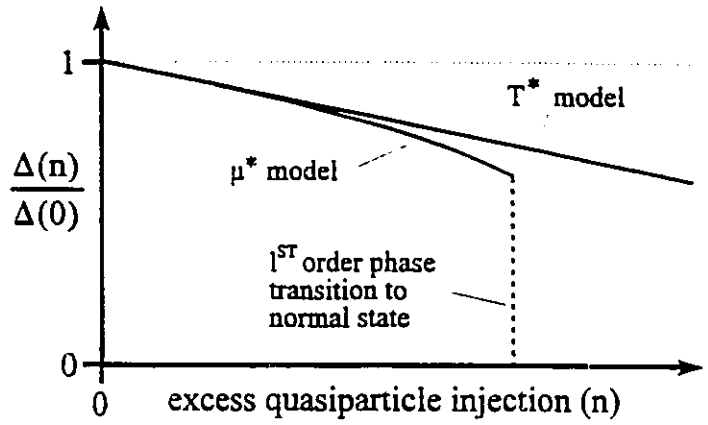

Fig. 2.7. Gap suppression as a function of excess quasiparticle injection n in the μ* and T* models (adapted from Ref. 133). In the μ* model, a first order transition to the normal state occurs above a certain critical injection density. At higher injection densities, the T*model predicts a second order transition to the normal state.

The limited success of both the μ* and T* models prompted Elesin *et al.*[134,135] to develop a new nonequilibrium theory which combined aspects from both models. One of the main predictions of Elesin's theory was the appearance of a resistive, spatially inhomogeneous state above a certain injection threshold that consisted of superconducting and normal regions similar to the intermediate state in Type I superconductors.[14] As the injection increased, the superconductor would eventually enter the normal state. This was soon confirmed by Sobolewski *et al.*[136] in 1986 by studying voltage transients from current-biased Pb films exposed to 30 ps wide laser pulses. Transients as fast as 100 ps FWHM were seen above a certain laser-fluence threshold consistent with Elesin's theory. Recently, Hu *et al.*[137] used electro-optic sampling to show that superconducting to normal transition in Pb films induced by picosecond laser pulses was faster than 1 ps. The results were interpreted in terms of Elesin's model for the appearance of an intermediate resistive state.

Even more theories have been developed to explain nonequilibrium phenomena in superconductors. A multiple gap state induced by tunnel injection has been predicted and examined,[138] and further modifications have been made to the μ* and T* models.[139] Very recently, quasiparticles were injected into a YBCO junction made on a bicrystal substrate and

it was shown that nonequilibrium processes were present. But whatever the theory used to describe nonequilibrium phenomena in a superconductor, it is vital to first thoroughly understand the nature of the superconducting mechanism or at least the nature of the gap. It is difficult to justify interpreting nonequilibrium phenomena in the HTSCs in terms of nonequilibrium theories for BCS superconductors because the HTSCs are so different in many ways from conventional superconductors. Nevertheless, nonequilibrium theories developed for conventional superconductors provide a starting point from which to analyze transient processes in the HTSCs, even if these theories still have limited success with conventional superconductors.

2.3. Nonequilibrium heating and pump-probe experiments

A thermal model for the absorption of light in a metal film is shown in Fig. 2.8. The case for a thin film on an insulating substrate is considered so that diffusion effects can be ignored. The thermal analysis is similar to that presented earlier in section 1.4 and Fig. 1.9, but the difference here is that the electrons and lattice phonons have been separated into two different heat absorbing systems. Incident light is absorbed by the electrons and heats the electron system to a temperature T_e. Through collisions with phonons, the electrons are thermally coupled to the lattice through $G_{e\text{-}ph}$, and heat transferred from the electron system to the phonon system raises the temperature T_{ph} of the phonon system (or lattice). Since the substrate is electrically insulating, only phonons can carry heat out of the film through the film-substrate thermal conductance G. If the two systems are in thermal equilibrium, then $T_e = T_{ph}$ and most of the heat energy is contained in the lattice since the lattice heat capacity C_{ph} is usually much greater than the electronic heat capacity C_e (as long as T_{ph} is not too low).

The thermal coupling between the electrons and lattice is characterized by the electron-phonon energy relaxation time $\tau_{e\text{-}ph}$, which is typically of the order of a picosecond in most metals. If a laser pulse with duration τ_p comparable to $\tau_{e\text{-}ph}$ is absorbed by the electron system, then it is possible for T_e to be brought out of equilibrium with T_{ph} by hundreds or even thousands of degrees before the heat energy even has a chance to dissipate into the phonon system. The time for T_e to come into equilibrium with T_{ph} is given by $\tau_{e\text{-}ph}$,

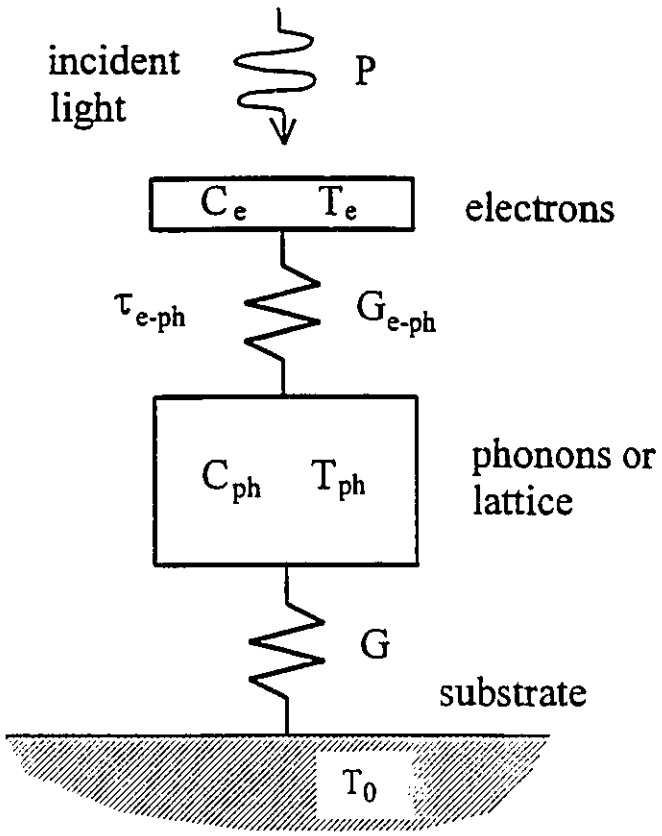

Fig. 2.8. Thermal model used to describe nonequilibrium electron heating in metals.

but since $C_{ph} >> C_e$ the final temperature of the lattice will have changed very little relative to the change in T_e. The relaxation time for Nb is about 360 fs, whereas for Cu it is a few picoseconds.[141] This is because the electron-phonon coupling is about 17 times greater in Nb than in Cu,[141] which results in thermal equilibrium between T_e and T_{ph} being attained more rapidly in Nb. Even though the electrons are excited by the laser pulse to energies well above the Fermi energy E_F, it is assumed that the electron temperature can be characterized by a Fermi-Dirac distribution at a temperature T_e. Such a thermal distribution is a good approximation only if the electron-electron thermalization time $\tau_{e\text{-}e}$ is much shorter than $\tau_{e\text{-}ph}$, which is usually the case in metals and semiconductors.

Nonequilibrium heating of the electron system in metal films was first described by Anisimov *et al.*[142] in 1974. The evolution of the electron and lattice temperatures is governed by the two coupled differential equations

$$C_e \frac{\partial T_e}{\partial t} = P - G_{e\text{-}ph} (T_e - T_{ph}) \tag{2.7}$$

$$C_{ph} \frac{\partial T_{ph}}{\partial t} = G_{e\text{-}ph} (T_e - T_{ph})$$

where P is the absorbed power from the light pulse in units of W/cm^3. Diffusion terms and the slow rate of heat escape into the substrate have been neglected for the case with thin films and picosecond laser pulses. It is important to keep in mind that both heat capacities C_e and C_{ph} and the electron-phonon coupling constant $G_{e\text{-}ph}$ are temperature dependent.[141]

The short time scales for energy relaxation in metals, semiconductors, and even superconductors can be measured directly by optical pump-probe techniques, as described in Fig. 2.9. In such experiments, the metal is first heated by a pump laser pulse. The transient nature of the energy relaxation process can then be monitored by a second probe pulse derived from the same laser source but delayed in time with respect to the pump pulse. The change in reflection $\Delta R/R$ or transmission $\Delta T/T$ of the probe pulse through the sample is measured and recorded as a function of delay time with respect to the pump pulse. The magnitude of the change in these parameters is not large, and in typical experiments is of the order of 10^{-4} with resolutions of 10^{-6} to 10^{-7}. This can then be related to the temperature of the electron and phonon systems in several ways. If the optical properties of the material are temperature dependent, then the change in lattice temperature can be extracted.[141] The rise time of this change will then provide a value for $\tau_{e\text{-}ph}$. The fall time of such a signal will be relatively much slower due to the slow rate of heat escape out of the probed region.

Another widely used technique is to probe the smearing of the hot electron distribution at the Fermi surface by measuring the change in absorption in the electronic transitions from d-bands in the material to the Fermi surface, as described in Fig. 2.10(a). The width of the smearing at the Fermi surface[18,19] will be of the order of $k_B T_e$. As T_e increases, smearing will reduce the electron distribution just below E_F and increase it just above E_F. If the probe energy $\hbar\omega$ is larger than $E_F - E_d$, then the smearing will reduce the

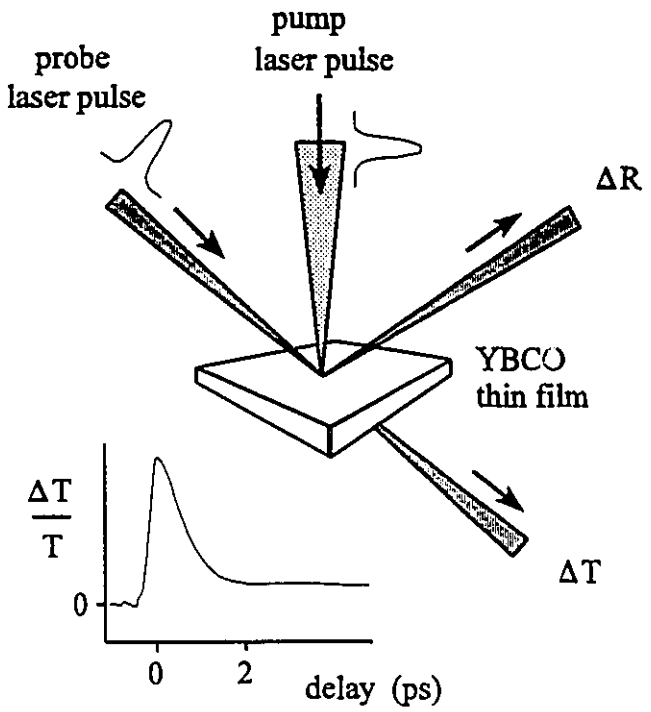

Fig. 2.9. Schematic of a typical pump-probe experiment using femtosecond laser pulses.

amount of states available for the probe pulse to induce a transition from the d-band. The absorption of the probe pulse will be reduced, and the reflection from the metal surface will increase, as shown in Fig. 2.10(c). If the perturbation in the electron distribution is small, then the change in reflectance can be directly related to T_e, as depicted in Fig. 2.10(d). If $\hbar\omega = E_F - E_d$, then there is no change in reflection since the occupation at E_F is approximately temperature independent. If $\hbar\omega < E_F - E_d$, then the reflection will decrease due to increased absorption as more states below E_F become available, which will result in $\Delta R < 0$. Significant changes in ΔR or ΔT will only be obtained for probe energies close to either side of the Fermi surface where the changes in occupation due to smearing are the largest. The d-bands for Cu lie 2.15 eV below the Fermi surface, which makes it an ideal transition to probe with laser sources tunable in the 2 eV range. The d-bands in Cu also give Cu its characteristic reddish colour by absorbing more strongly in the blue end of the optical spectrum. The d-bands in gold and silver are 2.4 and 4 eV below E_F, respectively.

The technique was first used by Eesley[143] to investigate electron-phonon thermalization times in Cu. Even though he couldn't resolve $\tau_{e\text{-}ph}$ with the 5 ps laser pulses he was using, he was still able to observe nonequilibrium effects by monitoring the sign of

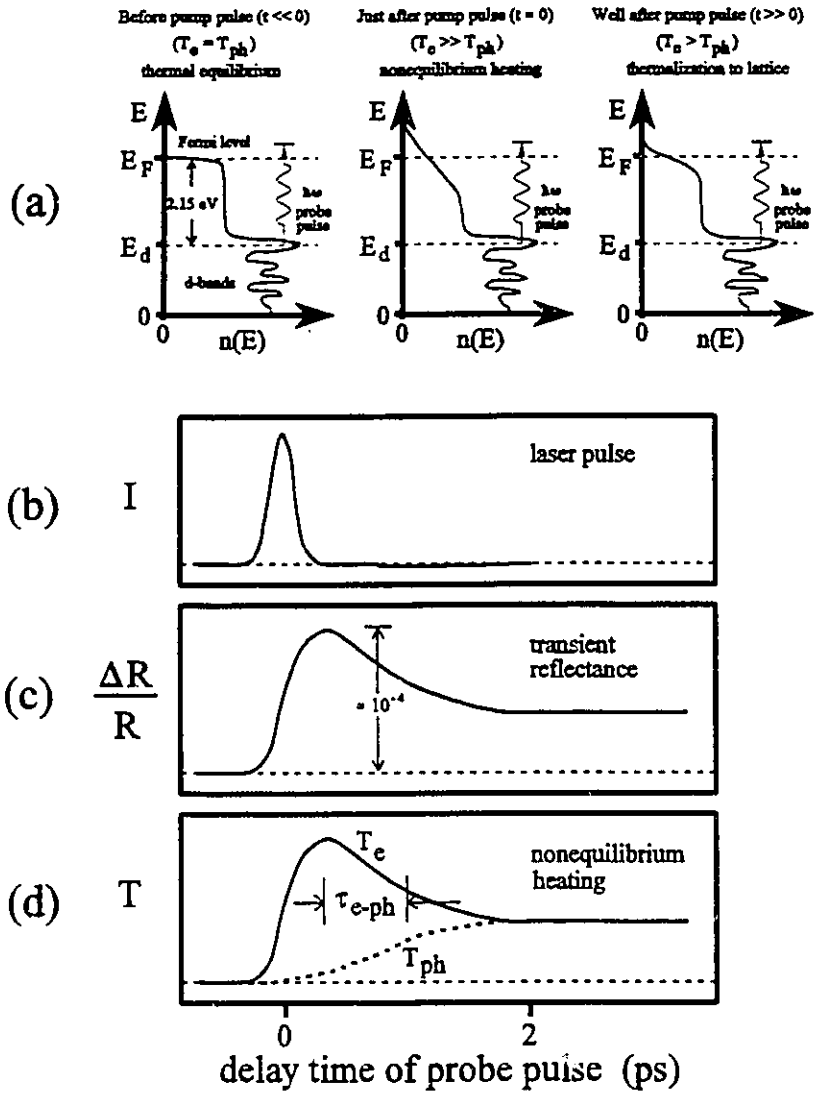

Fig. 2.10. Description of pump-probe experiments that use d-bands below the Fermi level in metals to probe Fermi smearing due to nonequilibrium electron heating. In (a), a simplified energy band diagram for copper is shown with the d-band energy levels positioned about 2.15 eV below the Fermi energy E_F. A probe pulse with energy $\hbar\omega$ greater than the transition energy from the d-band to the Fermi energy can probe the occupation of states just above E_F. Heating of the electrons by the laser pulse smears the distribution near the Fermi surface and changes the occupation of states probed by the probe pulse. If (b) is the pump pulse, then the change in reflection of the probe pulse is shown in (c). This can be directly related to the temperature of the electron distribution T_e as shown in (d). The temperature of the lattice T_{ph} is shown as a dashed line rising to equilibrium with the electron temperature in a time $\tau_{e\text{-}ph}$ in (d).

$\Delta R/R$ as the probe energy was tuned across the Fermi surface from 2.10 to 2.16 eV. The reflectance signals contained fast and slow components. The initial fast transient was due to Fermi smearing from nonequilibrium changes in T_e, whereas the slow component was attributed to temperature-dependent changes in the optical properties of the lattice which did not change the sign of $\Delta R/R$ as the probe energy was changed. In 1987, Elsayed-Ali *et al.*[144]

probed $\Delta T/T$ for Cu films with 150 to 300 fs laser pulses and found thermalization times of 1 to 4 ps and nonequilibrium temperature transients for T_e up to a few thousand degrees above T_{ph}. Probing Au films[145] gave similar electron-phonon thermalization times of 2 to 3 ps. It was later found[146] that $\tau_{e\text{-}ph}$ increased as the laser fluence increased and decreased as the temperature was lowered. In fact, $\tau_{e\text{-}ph}$ is ~ 1 ms in gold at 25 mK but decreases to a few picoseconds at temperatures around 10 K.[146] The use of thicker films resulted in smaller values for $\tau_{e\text{-}ph}$ due to fast diffusion of hot electrons out of the absorbing region.[147] One would also expect the electron-electron relaxation time to be very fast in metals, but screening reduces the rate of this process. For Au films, it was found that increased screening of the electron-electron interaction resulted in $\tau_{e\text{-}e} \approx 500$ fs, which was very close to the value for $\tau_{e\text{-}ph}$ of 1 ps.[147] With such long electron-electron thermalization times, the assumption of a well characterized thermal distribution must be questioned.

In semiconductors such as GaAs with a band gap of ~ 1.5 eV, nonequilibrium heating is monitored in pump-probe experiments where the probe pulse measures the change in absorption in transitions from the valence band to the conduction band. In one experiment,[148] carrier densities of 10^{17} to 10^{18} cm^{-3} were pumped into the conduction band with 35 fs, 2 eV laser pulses and the change in transmission to a broad range of probe pulse energies was monitored. It was observed that the electron-electron thermalization time was of the order of 20 fs while cooling of electrons to the lattice occurred over a few picoseconds. As the injection density increased, it was found that $\tau_{e\text{-}e}$ decreased from 30 fs to 13 fs. Saturation effects were also observed at high injection levels.

If d-bands are not situated at convenient energies below the Fermi surface, Fermi smearing due to nonequilibrium electron heating can also be examined by measuring the thermally enhanced photoelectric emission from materials. This probe technique was used on tungsten where electron-phonon thermalization times of several hundred femtoseconds were found using 75 fs laser pulses.[149] Time-resolved photoelectron spectroscopy has recently shown that the electron-phonon thermalization time in Si is less than 1 ps.[150]

The first systematic pump-probe study of conventional superconductor materials was performed by Brorson *et al.*[151] in 1990 using 60 fs, 2 eV laser pulses. Even though the transient reflectance measurements were performed at room temperature, important information about the strength of the electron-phonon coupling in materials such as Pb, Nb,

and NbN could be obtained. Since most of these materials did not have d-bands at the right energy below the Fermi level, a thin (40 Å) layer of Cu was deposited on the surface. It was assumed that the electron temperature in the Cu overlayer would be the same as T_e in the underlying material, and so the Fermi smearing induced in the Cu could be probed as discussed earlier. Most materials exhibited electron-phonon relaxation times less than 1 ps, with the relaxation time observed for NbN being one of the fastest and actually limited by the duration of the 60 fs laser pulse. The general trend observed was that the higher the value for T_c, the shorter the electron-phonon relaxation time. This is also seen in Table 1.1 where materials with higher T_c's such as Pb are strong-coupling superconductors with larger gap ratios. Visible pump and FIR probe of Pb films in the superconducting state was performed recently by Federici *et al.*[152]. The change in transmission of a 0.4 ps FIR pulses after a 100 fs visible pulse excited the film was found to occur over the time scale of a picosecond. It was concluded that the breaking of Cooper pairs by the visible pulse in the film occurred in less than 1 ps.

In the pump-probe experiments discussed above, it is necessary to have a detailed knowledge of the actual band structure of the material under investigation in order to properly interpret $\Delta R/R$ or $\Delta T/T$ in terms of a nonequilibrium electron temperature. The band structure in the HTSCs is far from being understood, and yet pump-probe techniques have been used by several groups to determine $\tau_{e\text{-}ph}$.[153-169] The belief is that experience gained from pump-probe experiments with metals can be used to interpret results from the HTSCs, and that the observed relaxation may be related to the pairing mechanism.

The Hubbard model[17,170,171] has had some success in explaining some of the properties of the insulating phase of the HTSCs. In the Hubbard model, a two-dimensional square lattice containing one electron per site is constructed. This would normally result in a half-filled band, as shown in Fig. 2.11(a), and therefore a conductor. However, if an on-site Coulomb repulsion U is added, then it becomes energetically favourable for the electrons to remain localized at their sites and the system becomes insulating. This is believed to be the case for the CuO planes in insulating $YBCO_6$. The effect of U on the band structure of $YBCO_6$ is seen in Fig. 2.11(b) where the Cu 3d orbitals of the CuO planes have been split apart by 8 to 10 eV into upper (UHB) and lower (LHB) Hubbard bands.[170] The O 2p orbitals remain filled making the material an insulator. Optical reflectivity studies on YBCO

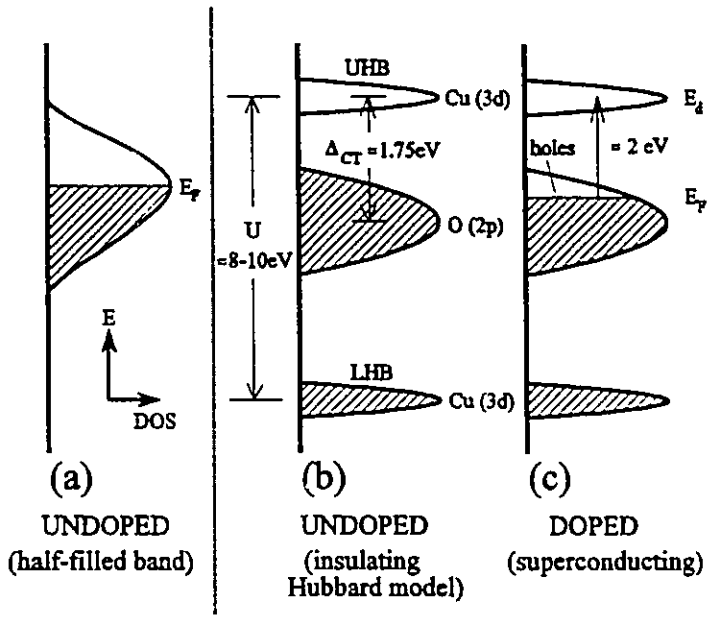

Fig. 2.11. Simplified diagram for the band structure of the CuO planes in YBCO according to the Hubbard model. For undoped $YBCO_6$, the expected band structure with no on-site repulsion is shown in (a) which results in half-filling of the band and a conducting state. With on-site repulsion U in (b), the Cu 3d bands split into the upper Hubbard band (UHB) and the lower Hubbard band (LHB) and the O 2p band becomes full resulting in an insulating state. As oxygen is added to the YBCO (c), the CuO planes become doped with holes. It is estimated that the Fermi level in the doped state is about 2 eV below the UHB. The values for U and the charge transfer gap Δ_{CT} were obtained from Ref. 170.

films as a function of oxygen doping[170] reveal an absorption edge at 1.75 eV for $YBCO_6$. This is believed to be the charge-transfer energy required to transfer a hole between the Cu and O atoms in the CuO planes, and is the amount of energy that separates the UHB from the O 2p orbital, as depicted in Fig. 2.11(b). The absorption edge seen at 1.75 eV in $YBCO_6$ disappears with increased oxygen doping.[170] In $YBCO_7$, the optical spectra are almost featureless from 1 to 2 eV and it is difficult to extract any band structure data. What is believed to happen in doped (superconducting) YBCO samples is shown in Fig. 2.11(c) where O atoms in the CuO chains remove electrons from the planes and leave holes behind. The separation between the UHB and the Fermi level is about 2 eV,[153-155,166-168] which is ideal for pump-probe experiments using d-band transitions to monitor nonequilibrium electron temperatures. The position of the Fermi level with respect to the UHB as a function of O doping[153,154,166-168] and Pr doping[155,164] has been studied by several groups using the sign change in $\Delta R/R$ as a guide. (Recall that a sign change in $\Delta R/R$ means that states close to the Fermi level are being probed.) As expected, the Fermi level moves towards the UHB as

the oxygen doping decreases or as the Pr content increases. However, the results have not been completely consistent between groups. The energy separation between E_F and the UHB was determined to be 2 eV in reduced-oxygen YBCO samples with T_C's of 60 K,[168] 70 K,[166] and 80 K.[163]

Figure 2.12 shows schematically typical $\Delta R/R$ pump-probe results seen from $YBCO_7$ above and below T_C.[165] In such experiments, laser fluences of 1 to 10 $\mu J/cm^2$ are used producing temperature transients in the lattice of 0.1 to 1 K. Since high repetition rate (~ 80 MHz) laser sources are usually used, average powers of about 10 mW at the sample can raise the average temperature of the probed area by ~ 10 K above the ambient temperature of the sample holder depending on the spot size of the pump laser pulse. Such experimental conditions are important to consider when interpreting data taken close to T_C. Above T_C, as in Fig. 2.12(b), there is a very fast transient less than 0.5 ps wide followed by a slowly decaying component. Similar data taken at room temperature or in the normal state just above T_C has been seen by several groups.[153-155,158,164,165,167,168] The fast transient has been interpreted in terms of the electron-lattice thermalization time whereas the slower component is due to heat escape out of the film. In one case,[154] the decay time of the fast transient at 300 K went from 60 fs in a superconducting sample to as long as 1 ps in a nonsuperconducting sample, and the sign of ΔR was opposite between the two samples. It was suggested that the increased relaxation rate for the superconducting sample (at 300 K) could be due to the same mechanism responsible for superconductivity in the HTSCs.[154] Other groups[156,158,166,167] have also noticed longer decay times in the normal state for oxygen-reduced YBCO samples. This is similar to the trend mentioned earlier with conventional superconductors at room temperature[152] where metals with lower T_C's had longer relaxation times.

In the superconducting state below T_C, $\Delta R/R$ suddenly changes sign with the onset of superconductivity and the decay time becomes longer, as shown in Fig. 2.12(c). The decay time is also the longest just below T_C, and then decreases as the temperature is lowered further. This peculiar characteristic has been seen by several groups.[156-159,164,165] Fig. 2.12(d) shows some of the observed decay times for the fast transients as a function of temperature. Han *et al.*[156,157] have interpreted their relaxation time data below T_C which ranged from 1 to 5 ps in terms of the quasiparticle recombination time τ_R. They also

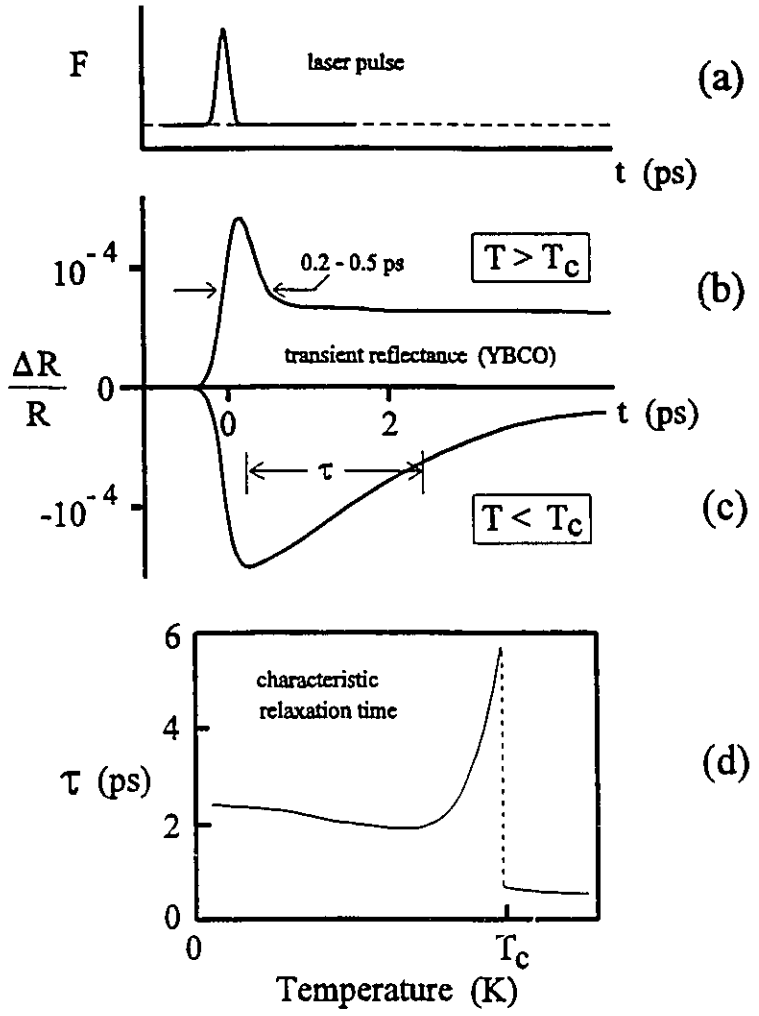

Fig. 2.12. Typical results for pump-probe experiments on YBCO (adapted from Ref. 165). In (a), a nominally 100 fs laser pulse is used as to induce nonequilibrium electron temperatures in the YBCO sample. Above T_c in the normal state (b), the relaxation of the nonequilibrium transient is quite fast and is usually less than 0.5 ps. Cooling below T_c in (c), the relaxation time increases to a few picoseconds. A plot of the typical temperature dependence of the relaxation time is shown in (d) showing a sudden rise in relaxation time close to T_c.

attributed the rise time of the fast $\Delta R/R$ transients as evidence for quasiparticle avalanche multiplication. The quasiparticle multiplication factor is given by

$$g = 2\frac{\hbar\omega}{2\Delta} \tag{2.8}$$

so that if $2\Delta = 5k_BT_c$ ($\approx$ 40 meV) and $\hbar\omega$ = 2 eV, then one photon would break about 50 Cooper pairs and produce 100 quasiparticles in such an avalanche process in YBCO. The rise in decay time just below T_c has been compared with the divergence of the gap parameter

relaxation time τ_Δ[158,159] as described earlier by Eq. (2.5) and Fig. 2.6. The decay times from Reitze *et al.*[164] also show a sudden increase just below T_C, but were not interpreted as an indication of the quasiparticle lifetime in YBCO. Instead, it was emphasized that more information on the band structure was needed in order to correctly interpret the results. Finally, the transmission data from Chwalek *et al.*[160] show an increase in decay time below T_C for a superconducting YBCO sample but not for a nonsuperconducting film.

Pump-probe experiments on the HTSCs have revealed some very interesting phenomena that are unique to the superconducting state. Until band theory has improved for the HTSCs, the interpretation of the pump-probe data will still be controversial. The sudden increase in decay time observed below T_C in pump-probe experiments is reminiscent of the sudden drop in scattering rate observed by Bonn *et al.*[95] in YBCO single crystals, but how does one interpret the corresponding change in sign for $\Delta R/R$? Nonequilibrium processes developed for conventional superconductors assumed an isotropic BCS gap. What happens to nonequilibrium processes when there are nodes in the gap as in the d-wave scenario ? In particular, how will relaxation processes such as quasiparticle recombination be affected by the presence of nodes in the gap ? What will the quasiparticle multiplication factor in Eq. (2.8) be if Δ is not constant over the Fermi surface or has nodes in some directions ? Above T_C in the normal state, the decay time is very fast and provides evidence for strong electron-lattice coupling. However, with all the uncertainty about band structure, perhaps the characteristic time constants in the superconducting state for the HTSCs can be probed more directly by looking at voltage transients produced across current-biased thin films exposed to picosecond laser pulses. The mechanisms that might produce such voltage transients are discussed in the next chapter.

3. PHOTORESPONSE MECHANISMS

3.1. The controversy: bolometric versus nonbolometric photoresponse

There has been considerable effort over the past few years studying the photoresponse of current-biased HTSC thin films.[173-250] Part of the motivation behind such work has been the development of high-T_C photodetectors operating at 77 K and sensitive to a broad range of wavelengths. However, much of the work has focused on the origin of the photoresponse mechanism in both granular and epitaxial thin films. A controversy has developed over whether claims of nonbolometric photoresponse voltage transients can be explained in terms of a bolometric response. A *bolometric* response is a thermal response due to heating of the film by the incident light or laser pulse with T_e in equilibrium with T_{ph}. It is usually associated with changes in resistance from heating of the film, as in bolometers, which is referred to in this work as the resistive bolometric response. A *nonbolometric* response is a nonthermal response which cannot be explained in terms of equilibrium heating of the film and is usually associated with nonequilibrium superconductivity (Section 2.2) or nonequilibrium electron heating with $T_e >> T_{ph}$ (Section 2.3). In epitaxial films, some groups have only seen a bolometric photoresponse,[197-202] while others have seen both bolometric *and* nonbolometric signals.[216-246] Amongst the groups claiming to have seen a nonbolometric response, there is little consensus even today on the origin of the nonbolometric mechanism. Our work,[247-250] which is described in Papers A, B, C, and D included at the end of the thesis, has led us to the conclusion that the fast photoresponse signals we observe from YBCO thin films, which would otherwise be labelled as nonbolometric by other groups, can be attributed to a thermal mechanism called the kinetic inductive bolometric (KIB) response. The KIB response is discussed in detail in Chapter 4. It is hoped that an understanding of the photoresponse mechanism will shed some light on the nature of superconductivity in the HTSCs.

One of the main criteria for distinguishing between a bolometric and a nonbolometric photoresponse has been to look for deviations from the predicted temperature dependence of a bolometric response described in Fig. 1.8 and Eq. (1.2). The bolometric response is therefore peaked at T_C where dR/dT is a maximum, and any photoresponse seen below T_C

where dR/dT is zero must then be due to some nonbolometric mechanism. This analysis is valid for photoresponse experiments using low light levels or chopped radiation where the temperature transients induced in the film are small. However, in pulsed laser experiments with large fluences, the temperature transients can be quite large and this approach becomes invalid. In this case, the nonlinearity of the resistive transition near T_C must be considered.[198,201,207,240,247-250] (Papers A to D)

Another criteria used to distinguish bolometric from nonbolometric has been the speed of response of the signals. Photoresponse wave forms contain fast and slow components, and it was usually assumed that the fast component was nonbolometric since thermal response times were considered to be too slow. However, it has been shown that fast resistive bolometric voltage transients with decay times of about a nanosecond are possible from very thin films.[200,205]

Accurate thermal modelling of the heat transfer between the HTSC film and the substrate is essential in order to properly distinguish between bolometric and nonbolometric photoresponse signals.[204-209] For films with thickness d much larger than the optical penetration depth δ of about 90 nm, diffusion of heat from the front face of the film where the energy is deposited to the back of the film limits the cooling rate. The thermal time constant τ will scale as d^2, and the decay in the voltage transient due to a resistive bolometric response will fall as $t^{-½}$, where t is the elapsed time. For thinner films with more uniform heating, it has been established that the thermal boundary resistance R_{BD} between the film and the substrate limits the rate of heat escape from the film.[200,205,206] In this case, $\tau \propto d$ and the voltage transient due to a resistive response bolometric will fall exponentially as $e^{-t/\tau}$. The thermal escape is then given by

$$\tau = d \quad C \quad R_{BD} \tag{3.1}$$

where C is the heat capacity in J/cm^3K. R_{BD} has been found to be temperature independent from 90 to 200 K,[205] and has a value of about 10^{-3} K cm^2/W for YBCO on nearly all types of substrates.[200,205,207-209,227,248] (Paper B) This is much larger than R_{BD} predicted by acoustic mismatch theory at 90 K, which scales as $1/T^3$, and which will become significant for YBCO films at temperatures below about 30 K.[205] At 78 K, C ≈ 1.0 J/cm^3K, and so Eq. (3.1) gives

τ = 3 ns for a 30 nm film and 20 ns for a 200 nm film. Examples of resistive bolometric signals seen from films with different thicknesses are shown in Fig. 3.1. Notice that the thinnest film has the fastest fall time and is about 1 ns wide. As discussed in Paper B, the fall time of the voltage transient due to a resistive bolometric response can be faster than the actual thermal escape time due to the nonlinear nature of the resistive transition.

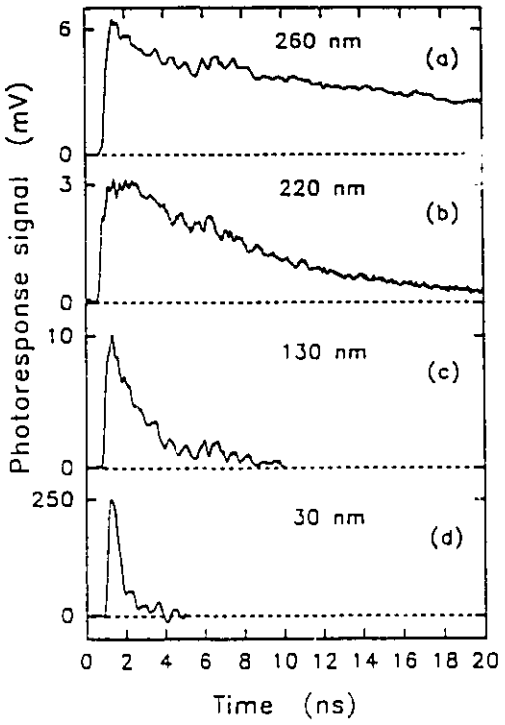

Fig. 3.1. Examples of resistive bolometric photoresponse signals observed from films with thicknesses of (a) 260 nm, (b) 220 nm, (c) 130 nm, and (d) 30 nm. The films are biased in their resistive transition regions (Paper B). The decay time is longest for the thickest film and gets progressively shorter as the films get thinner, as predicted by Eq. (3.1). The resistive bolometric response can be very fast, as shown for the 30 nm film in (d) where the decay time is about one nanosecond.

The change in temperature induced in a film by a laser pulse with duration $\tau_p << \tau$ will then be (Appendix B)

$$\Delta T = \frac{F}{C\,d}\,\frac{E_{ABS}}{E_0} \tag{3.2}$$

where F is the incident laser fluence in $\mu J/cm^2$ and E_{ABS}/E_0 is the fraction of incident pulse energy absorbed in the film given by

$$\frac{E_{ABS}}{E_0} = (1 - R)(1 - \exp(-d / \delta)) \qquad (3.3)$$

where R is the reflectance (R ≈ 0.1). Thinner films will absorb less energy because they are more transmissive than thicker films, but the temperature transient induced in them will be larger due to their smaller heat capacity. For example, for 30 and 200 nm films, Eq. (3.3) predicts E_{ABS}/E_0 ≈ 0.26 and 0.80, respectively. The corresponding temperature transients from Eq. (3.2) for an incident laser pulse fluence of F = 10 μJ/cm^2 will then be 0.87 K for the 30 nm film and 0.40 K for the 200 nm film. Knowing the size of the temperature transient, the change in resistance can be predicted from a plot of the resistance of the sample as a function of temperature and bias current in the resistive transition region. If ΔT calculated from Eq. (3.2) gives a change in resistance of the sample which is too small to account for the observed voltage transient, then the signal must be due to some mechanism other than the resistive bolometric response.

With thermal decay times in the nanosecond region, observations of picosecond voltage transients cannot be attributed to a resistive bolometric response and have usually been used as evidence for a nonbolometric response. However, the electrical bandwidth of the apparatus measuring the signals must be large enough to observe transients faster than those expected for thermal processes. The rise time τ_r in picoseconds for a system with a bandwidth Δf in GHz is given by

$$\tau_r\,(ps) = \frac{350}{\Delta f\,(GHz)} \quad . \qquad (3.4)$$

Since the fastest resistive bolometric response will be of the order of a nanosecond, then it is important to have a measuring bandwidth larger than 1 GHz if the time duration of transients is to be used as a means of distinguishing between bolometric and nonbolometric photoresponse signals. As discussed in Section 1.4, voltage transients can be measured directly on an oscilloscope with bandwidths up to 50 GHz, which would give a theoretical rise time of 7 ps. A large bandwidth is therefore important for distinguishing between resistive bolometric voltage transients with nanosecond decay times and faster nonbolometric

signals with sub-nanosecond transients, and for resolving the actual time evolution of any nonbolometric response so that its origin can be identified. As discussed in Chapter 5, the voltage transients we have seen are too fast to be explained by a resistive bolometric response. We attribute the fast response to the KIB model which will be discussed in Chapter 4. For comparison, an overview of some of the experiments that have been interpreted as providing evidence for nonbolometric mechanisms is given below.

3.2. Photoresponse of granular films and grain boundaries

Some of the first photoresponse experiments were performed with granular films.[174-187] Granular films consist of networks of small superconducting grains that are weakly coupled to each other at the grain boundaries, as shown in Fig. 3.2. One possible nonbolometric photoresponse mechanism for granular films originates from light-induced suppression of superconductivity in the weak links between the grains.[174] The critical current I_C of these films is determined by the critical currents of the junctions formed at the grain boundaries. For temperatures less than $T_C/2$, the critical current of a junction is proportional to the magnitude of the gap parameter Δ in the junction.[15,174] If the film is biased with a current I just less than I_C, then light incident on the film will suppress Δ in the grain boundaries, I_C will be reduced, and a voltage transient will appear if I exceeds the suppressed I_C.[174] Experiments with polycrystalline BaPbBiO films (T_C ~ 13 K) have demonstrated the viability of superconducting granular films for detection of wavelengths

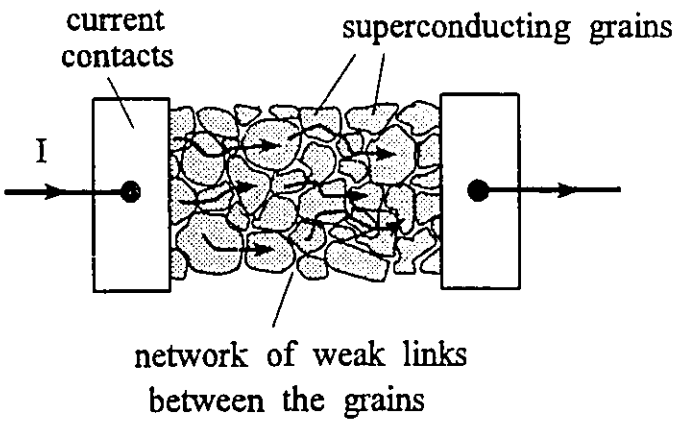

Fig. 3.2. Granular superconducting film showing how a bias current I makes its way through a network of grains connected by weak links. Light incident on the film will weaken the superconductivity in the weak links between the grains which may cause the critical current of the film to be exceeded and give rise to a voltage transient.

from 1 to 8 μm at modulation frequencies up to 1.3 GHz and responsivities of 10^4 V/W, which is well suited for optical communications systems.[174]

Experiments with granular NbN films[175,176] (T_c = 6 K) have revealed different nonbolometric mechanisms. In one case,[175] it was found that the peak in the photoresponse occurred at the Kosterlitz-Thouless transition temperature just below T_c, and was attributed to light-induced vortex-antivortex depairing. The same mechanism was used to explain the photoresponse in granular YBCO thin films.[179,180] Gousev *et al.*[176] have developed fast NbN detectors sensitive from the visible part of the spectrum to submillimetre wavelengths with 50 ps response times, but have interpreted the fast response in terms of nonequilibrium electron heating effects and gap suppression rather than vortex dynamics. Using the same nonequilibrium heating mechanism, Gershenzon et al.[178] have predicted response times of a few picoseconds in YBCO granular films. Recently, Gol'tsman *et al.*[233] have compared the photoresponse in granular and epitaxial films to 20 ps laser pulses. A fast nonbolometric transient was observed in the zero-resistance superconducting state only for the granular films, and the responsivity in the resistive state for the granular films was several orders of magnitude larger than in epitaxial thin films. Nanosecond response times have also been seen in TlBaCaCuO granular films at FIR wavelengths from 10 μm to 500 μm.[183-185] It is interesting that in these experiments a nonbolometric response was seen only at wavelengths longer than 100 μm. The responsivity in granular films seems to be enhanced at longer wavelengths,[175,180,185] which has been attributed to direct modulation of the Josephson junction currents by light with energy below the gap.[175,180] Granular YBCO films have also been studied for use as sensitive detectors of microwave radiation.[186,187] Recently, a portable microwave detector consisting of a granular YBCO thin film bridge cooled by a closed-cycle refrigerator showed a responsivity of 180 V/W at 53 K,[187] which demonstrated the possibility of practical YBCO microwave detectors.

To understand the photoresponse mechanism in granular films, the photoresponse from single junctions or grain boundaries has been studied.[188-191] Bhattacharya *et al.*[190,191] have studied the photoresponse of ultrathin epitaxial YBCO thin films (~ 3 nm) and thicker epitaxial thin films (~ 50 nm) with single grain boundaries made by depositing YBCO onto a bicrystal of $SrTiO_3$. For the ultrathin epitaxial films,[190] there was no peak in the photoresponse observed at the Kosterlitz-Thouless transition temperature for the film,

thereby ruling out light-induced vortex-antivortex unbinding as a possible nonbolometric mechanism. The epitaxial film with a single grain boundary showed an enhanced optical response at the grain boundary compared to the rest of the film.[190] It was suggested that photon-induced depinning of vortices in the grain boundary was responsible for the enhanced response. In later work, the optical response of single grain boundaries in epitaxial films was found to be consistent with a bolometric response where heating of the junction by the incident light modulated the temperature and therefore the critical current of the junction.[191]

3.3. Photoresponse of epitaxial films

Epitaxial films with large critical currents ($> 10^6$ A/cm^2) do not consist of grains separated by weak links as in granular films which have much lower critical currents ($\approx 10^4$ A/cm^2), and so the origin of the nonbolometric mechanism in epitaxial films is less clear. In fact, some of the first experiments with chopped radiation on epitaxial films revealed only a bolometric photoresponse[197,198] determined by Eq. (1.2). The photoresponse of YBCO epitaxial films to 10 ns laser pulses was found to be resistive bolometric.[198] Fast signals seen below T_C could be explained by the large laser fluence heating a 280 nm film from 75 K well into the normal state above T_C. Carr *et al.*[200] used 1 ns pulses from a synchrotron source on 40 nm and 156 nm YBCO epitaxial films and found no evidence for a nonbolometric response. Kadin *et al.*[199] looked at the optical switching of very thick ($\approx$ 0.7 μm) YBCO films and found that the observed switching rise times could not be accounted for by heat diffusion across the thickness of the film. Instead, they proposed that hot electron transport was responsible for heat transport from the front to the back of the film. However, the response was still resistive bolometric since it was the change in resistance of the film due to the change in temperature of the lattice caused by transport of heat by the hot electrons. The optical switching experiments were continued by Gupta *et al.*[203] who found a predominantly bolometric response with an initial fast component whose origin was uncertain. Recently, Liu *et al.*[202] did not find any evidence for a nonequilibrium distribution of quasiparticles in a YBCO film illuminated with a CW argon-ion laser and probed with a terahertz pulse.

Frenkel first performed extensive studies of the photoresponse of YBCO epitaxial films as a function of temperature, bias current, laser fluence, laser pulse duration, and film

thickness.[216-218] With chopped radiation from a HeNe laser, only a resistive bolometric response was observed as predicted by Eq. (1.2) where the peak in the temperature dependence of the photoresponse coincided with the peak in dR/dT. Using 150 ps laser pulses, the thinnest films (40 nm) gave photoresponse transients as fast as 1 ns wide and the peak in the photoresponse occurred at temperatures below the peak in dR/dT. The thickest films (300 nm) did not show a nonbolometric response with fast voltage transients. Frenkel concluded that this was evidence for a nonbolometric response in the thinnest films. It was believed that a nonbolometric response could not be seen in optically thick films since any voltage transient from such a response would be short-circuited by unilluminated superconducting layers beneath the exposed surface of the film. However, Carr *et al.*[201] have recently shown that Frenkel's results can be explained in terms of a purely resistive bolometric response. Also, as discussed above in Section 3.1, nanosecond transients due to a resistive bolometric response can easily occur in 40 nm films.

Kwok et al.[220] also emphasized the need for optically thin films in order to see a nonbolometric photoresponse below T_C. Optically thin films would reduce phonon trapping in the film, and would allow faster recovery of superconductivity after absorption of energy by the laser pulse. In other words, optically thin films would show a faster response time and would therefore be necessary in order to make high speed superconducting photodetectors. The YBCO films used by Kwok *et al.* were 80 nm thick with a T_C of about 40 K at low bias current and 28 K at bias currents used to acquire the wave forms. Using 6 ns laser pulses with a fluence of 200 $\mu J/cm^2$, slowly decaying transients were seen above T_C, fast and slow transients were seen near T_C, and only a fast transient with a width of 15 ns (limited by the system bandwidth) was seen below T_C at 5 K. The amplitude of the slow component was very different from the dR/dT behaviour predicted by a resistive bolometric response. Kwok *et al.* estimated the temperature transient in the film to be only about 1 K, and therefore concluded that the fast response must be nonbolometric in origin since the temperature transient was too small to account for a resistive change in the sample. Equation (3.2), however, gives a much larger estimate for the temperature transient of about 25 K. This would be more than enough to bring the film from 5 K into the normal state above T_C for the bias current that was used. Nevertheless, Kwok *et al.*, who were not very specific as to the nature of the nonbolometric response, suggested quasiparticle induced gap suppression as

a possible mechanism.

Kwok's group (Shi et al.[222,223]) later developed a novel double-bridge voltage correlation technique for measuring fast transients in YBCO thin films without having to use a high speed oscilloscope. The technique is similar to optical auto-correlation techniques used to measure the duration of ultrashort laser pulses. In these experiments, a 40 ps laser pulse illuminated a YBCO bridge connected in parallel with a second identical bridge on the same substrate. A second laser pulse delayed with respect to the first pulse illuminated the second bridge. By changing the delay time of the second pulse with respect to the first, an auto-correlation of the voltage transient from a single bridge could be obtained simply by measuring the amplitude of the voltage developed across the two bridges connected in parallel as a function of delay time between the two pulses. The photoresponse of the double-bridge structure was therefore peaked at zero time delay between the two laser pulses. The observed voltage-versus-delay trace revealed both fast and slow transients in the photoresponse. For 15 nm films, the fast transients had characteristic times of about 40 ps and were attributed to a nonbolometric response since thermal time constants were much longer than this. The slow transients were of the order of 2 ns, and were consistent with a bolometric response governed by thermal escape from the film. It was found that the decay of the fast transient increased as the film thickness was increased, which provided evidence for the claim that phonon trapping was the limiting factor in the quasiparticle relaxation process. No difference in the decay time of the fast transient (40 ps) was seen when either 40 ps or 500 fs laser pulses were used, suggesting that the electron-phonon relaxation time was shorter than 500 fs or longer than 40 ps. There was little description of the origin of the fast component other than it was due to quasiparticle generation and decay. However, evidence for a light-induced nonequilibrium intermediate resistive state predicted by Elesin *et al.* (Section 2.2) was recently found by Shi et al.[224] using 200 ns long trains of 40 ps laser pulses at 13 ns intervals on YBCO films with single bridges. Only a thermal response was seen for a 150 nm film, whereas both thermal and nonthermal components were seen for a 10 nm film. The rise time of the oscilloscope was limited to 2 ns, which is longer than the 1 ns thermal escape time from a 10 nm film. It would therefore be difficult to distinguish between resistive bolometric and nonbolometric photoresponse signals from the 10 nm film. The fact that large laser fluences were used might have made a resistive

bolometric response possible in this case.

Fast photoresponse signals have been observed directly on oscilloscopes from YBCO epitaxial thin films which cannot be explained by slow thermal transients.[225,227,229-238,240,243-250] In 1992, Semenov et al.[225] saw bandwidth-limited 0.7 ns wide voltage transients using 5 ps laser pulses on a YBCO film with a thickness of 70 nm and biased in the resistive transition region. Bluzer[236-240] and Johnson[243] have used 300 fs laser pulses to look at voltage transients in the 10 ps to 10 ns range using one of the fastest digital sampling scopes in the world with a bandwidth of 70 GHz. Both have seen fast and slow components in the photoresponse wave forms, with Johnson[243] seeing 20 ps wide transients followed by a slowly decaying component in 80 nm films. Ghis *et al.*[244-246] have seen fast transients about 29 ps wide followed by components with nanosecond decay times in 30 nm films using the same digital sampling scope used in our experiments. We have also seen fast transients about 20 ps wide from films with thicknesses ranging from 30 to 200 nm and using 5 ps laser pulses,[249,250] (Papers C and D) but one of the major differences with our data is that we have seen fast transients in the superconducting state that were not followed by a slowly decaying component. *No other group has reported photoresponse transients less than 100 ps wide from epitaxial YBCO thin films that were <u>not</u> followed by a slow component.* Our interpretation of the origin of the fast response is also different from other groups. Semenov, Gol'tsman, Gershenzon, *et al.*,[225-235] Bluzer,[237-240] and Ghis *et al.*[244-246] all describe their fast photoresponse signals in terms of nonbolometric mechanisms. A description of these mechanisms is given below.

3.4. A survey of nonbolometric photoresponse mechanisms for epitaxial films

A breakdown of possible bolometric and nonbolometric photoresponse mechanisms of epitaxial YBCO thin films is shown in Fig. 3.3. A bolometric response arising from equilibrium heating of the electrons and the lattice ($T_e = T_{ph}$) by the laser pulse can result in a resistive bolometric response or a kinetic inductive bolometric (KIB) response (Chapter 4). A nonbolometric response can result from nonequilibrium heating where $T_e > T_{ph}$. This can produce either a rapid change in resistance of a film due to gap suppression or changes in the kinetic inductance. Transient flux dynamics has also been used to explain the origin of nonbolometric photoresponse signals, such as photoactivated flux flow and photofluxonic

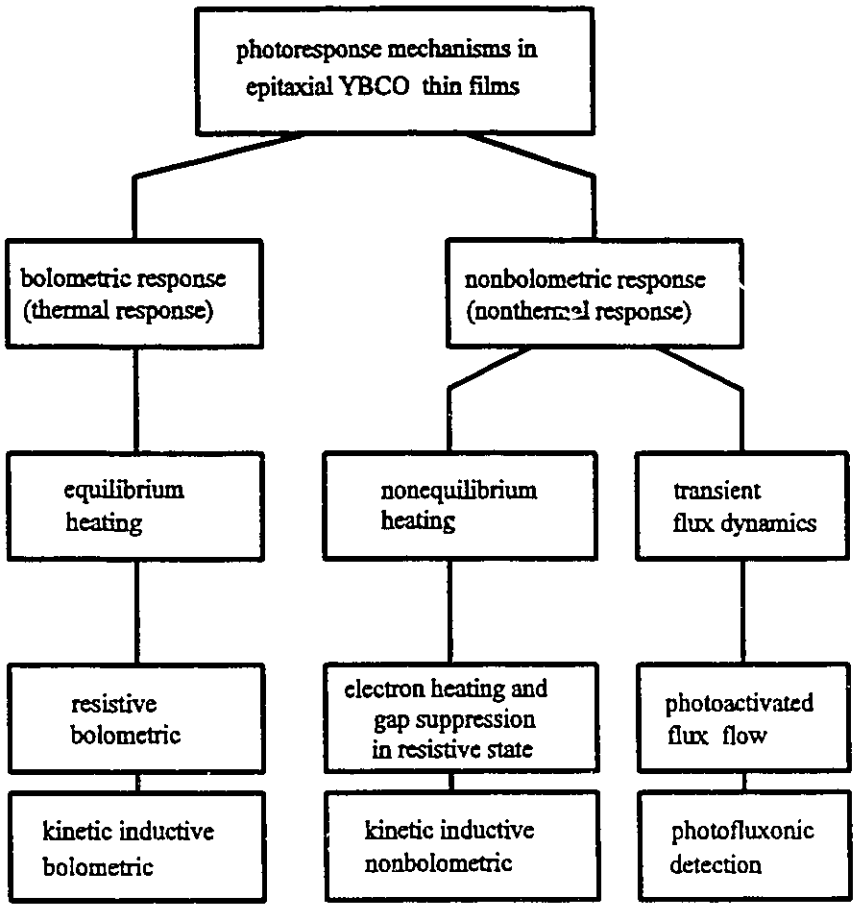

Fig. 3.3. Summary of bolometric and nonbolometric mechanisms that have been proposed to explain the origin of the photoresponse of epitaxial high-T_c thin films. A bolometric response arises from equilibrium heating of the film, whereas nonbolometric signals can be caused by nonequilibrium electron heating or transient flux dynamics.

detection. Some of the nonbolometric photoresponse mechanisms proposed by several groups such as (a) transient flux dynamics,[210-219] (b) nonequilibrium electron heating in the resistive state,[225-235] and (c) nonequilibrium changes in the kinetic inductance[233,236-242,244-246] are described below.

(a). Transient flux dynamics

As discussed in Section 1.2, vortices (fluxons, fluxoids) in superconductors each carry a quantum of magnetic flux ϕ_0. If a current is passed through the superconductor, each vortex will experience a Lorentz force perpendicular to this current given by [13,14]

$$\boldsymbol{F}_L = \boldsymbol{J} \times \boldsymbol{B} \qquad (f_L = J \times \phi_0) \tag{3.5}$$

where $\mathbf{F_L}$ is the Lorentz force per unit volume on a flux bundle, $\mathbf{f_L}$ is the Lorentz force per unit length of a single vortex ϕ_0, J is the current density, and **B** is the average magnetic field penetrating the superconductor. Without pinning, the vortices will be free to move under the influence of the Lorentz force, and will induce an electric field **E** along the direction of the current density

$$E = B \times v \tag{3.6}$$

where **v** is the velocity of the vortices. An electric field generated across a superconductor due to vortex motion means that power must be dissipated. This is possible because the vortices experience a frictional force due to a viscosity η in the material which is opposite to the Lorentz force. This limits the velocity of the vortices to

$$v = \frac{J \phi_0}{\eta} \tag{3.7}$$

Vortex motion without pinning is called flux flow, and the electric field generated by the motion of vortices for a sample of length l is the flux flow voltage given by

$$V = B l v \tag{3.8}$$

The resistivity of the sample due to flux flow is then

$$\rho_{FF} = \rho_0 \frac{B}{B_{C2}} \tag{3.9}$$

where ρ_0 is the normal state resistivity and B_{C2} is the upper critical magnetic field.

In a pure superconductor, flux flow will occur for even the smallest applied J, and the property of zero-resistance will be lost. In real superconductors, defect sites in the material provide pinning sites for individual vortices. Only when the Lorentz force exceeds the force associated with the pinning sites can flux flow occur. However, at finite temperatures it is possible for vortices to hop out of their pinning sites due to thermal

excitations. The resistivity arising from this thermally activated flux flow (TAFF) has been used to describe the broadening of the resistive transition in the HTSCs subject to high magnetic fields.[251-253] If the energy required for a vortex to hop out of a pinning site is U, then the thermally activated behaviour of the resistivity will follow an exponential behaviour given by

$$\rho_{TAFF} \propto \exp\ (- U / k_B T) \qquad (3.10)$$

The value of U in YBCO depends on the exact model used to interpret the resistivity data, and is believed to be strongly dependent on the current density and applied field. Typical reported values for U range from about 1 eV [251] to less than 100 meV[252-254] in both single crystals and thin films. The validity of the TAFF model applied to resistive transition broadening in the HTSCs is still controversial,[256] and several other dissipative mechanisms have been proposed such as vortex unbinding at the Kosterlitz-Thouless transition,[255,256] dissipation in networks of weak links, and superconducting fluctuations.[256]

Nevertheless, aspects of the TAFF model have been used to describe nonbolometric photoresponse mechanisms in YBCO thin films.[210,211,216-219] In 1989, Zeldov *et al.*[210,211] suggested photoenhanced flux creep as the origin for a nonbolometric signal seen in YBCO films with thicknesses of 250 to 600 nm using chopped radiation from a HeNe laser. Frenkel[217] attributed fast photoresponse signals about 1 ns wide to photoactivated flux flow. The basic process for photoactivated flux flow is shown in Fig. 3.4 where incident photons induce the motion of vortices subject to a Lorentz force in a current-biased film. When the vortices move, they generate a voltage pulse which constitutes the nonbolometric photoresponse. However, the exact mechanism by which the photons enhance the motion of vortices is still uncertain. Zeldov *et al.* have suggested that energetic nonequilibrium phonons created by the incident light may be responsible for enhancing the thermally activated hopping of the vortices. Frenkel also implies that the photons create additional flux creep in the sample, and that the photon energy must be larger than the pinning energy U in order for this to occur.

Kadin *et al.*[212] have suggested photofluxonic detection as a new mechanism for nonbolometric (quantum) detection of infrared light. In this process, as described in Fig. 3.5,

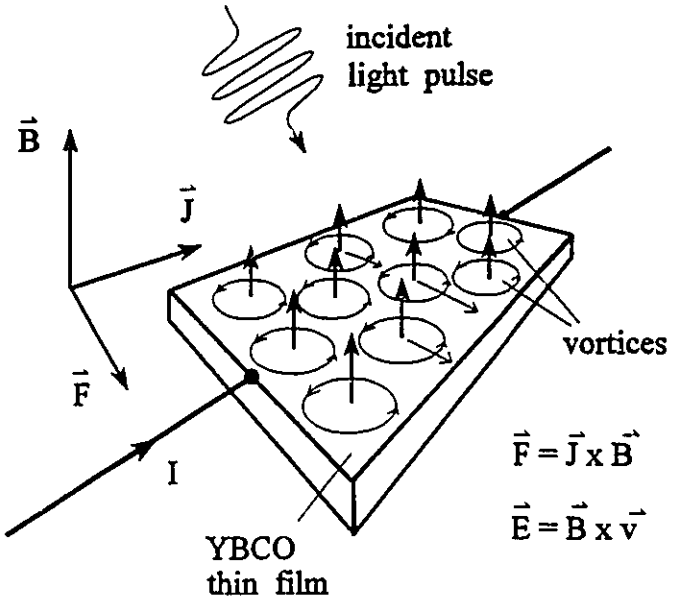

Fig. 3.4. Description of photoactivated flux flow. A bias current I through the film imposes a Lorentz force perpendicular to the direction of the current on vortices pinned in the film. Photons from an incident light pulse provide enough energy for the vortices to hop out of their pinning sites allowing them to move freely in the film. Once the vortices move, they dissipate energy and an electric field is created across the sample. The voltage produced by the motion of the vortices results in a photoresponse signal.

an incident photon is absorbed and creates a hot spot in the superconductor. The current passing through the superconductor will be diverted around this hot spot resulting in the formation of a vortex-antivortex pair. The Lorentz force from the current breaks the pair apart, and the vortices travel to the edges of the film where they are annihilated. The voltage generated due to their motion is $V = \phi_0 / t$, where t is the transit time across the film. The response time of such a detector will therefore depend on how fast the vortices move across the film, which may be as fast as 100 ps.[212] However, just like in semiconductor detectors with creation of electron-hole pairs, there is a minimum photon energy required for creation of vortex-antivortex pairs in a photofluxonic detector. For a very thin film with thickness $d < \xi$, the minimum energy is

$$E_{MIN} = \frac{\phi_0^{\,2}\, d}{2\,\pi\,\mu_0\,\lambda^2} \tag{3.11}$$

Equation (3.11) explains why the Kosterlitz-Thouless transition with vortex unbinding

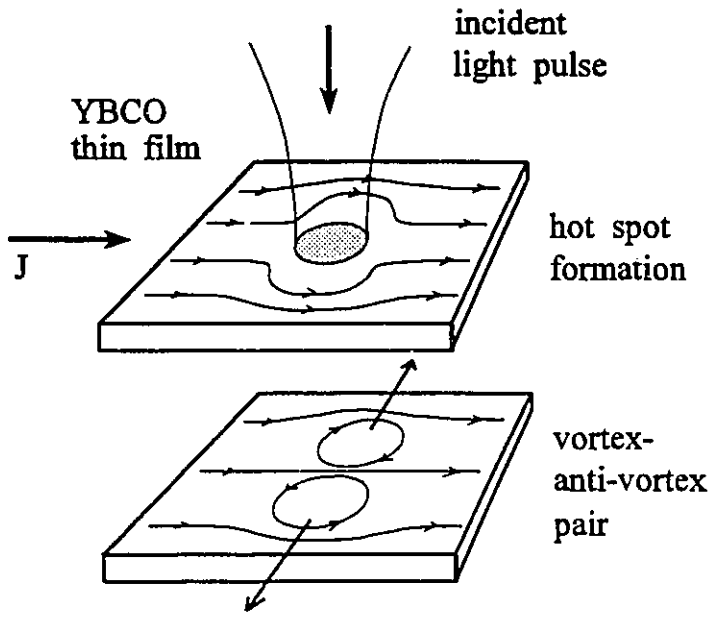

Fig. 3.5. Photofluxonic detection mechanism proposed by Kadin *et al.* (Ref. 212). An incident laser pulse creates a hot spot in a superconducting film forcing the current to divert around it. The resulting current distribution leads to the creation of a vortex-antivortex pair, with each vortex being swept away by the Lorentz force to opposite sides of the film. A voltage pulse is generated as the vortices move across the film..

energies of $E_{MIN} = k_B T_{KT}$ is usually seen in very thin films and only close to T_C where λ diverges. For the HTSCs, λ is already much larger than in the conventional superconductors, and such a transition has been seen in films with thicknesses of 120 nm[255] and may also explain the mechanism for resistive transition broadening.[256] If the film is thicker than the coherence length ($d > \xi$), then photons absorbed inside the superconductor will create vortex rings with circumference ξ and the Lorentz force from the current will cause the rings to expand. When the rings become as large as the film thickness, they become vortex-antivortex pairs and are swept to the edges of the film. The minimum energy required in this case ($d > \xi$) is

$$E_{MIN} \approx \frac{\phi_0^{\,2}\,\xi}{2\,\pi\,\mu_0\,\lambda^2} \tag{3.12}$$

For a 150 nm YBCO film with $\lambda \sim 150$ nm and $\xi \sim 1$ nm, Eq. (3.12) gives a minimum energy for creation of a vortex ring of about 0.1 eV, which is in the infrared region ($\lambda \approx 12$ μm).[212] Kadin *et al.*[212] have confirmed some of the results of photofluxonic

detection with NbN films, but no data supporting such a mechanism has been shown for YBCO films. It would be interesting to measure the wavelength dependence of the photoresponse to see if there is a minimum energy cutoff as predicted by photofluxonic detection. Photofluxonic detection should also be seen in all types of films, whether they are granular or epitaxial, or whether they are made from low or high-T_C materials. The tunability of E_{MIN} would also be useful for detector applications. Recently, a DC SQUID has been used to confirm the nonbolometric (quantum) nature of the photofluxonic detection process in In-InO_x granular thin films.

Finally, the Nernst effect[14] has also been used to explain the origin of voltage transients from Tl-Ba-Ca-Cu-O films.[214,215] In these experiments, 80 ns laser pulses heated the front surface of the film creating a temperature gradient across its thickness. A magnetic field was imposed parallel to the surface of the film and perpendicular to the current which ran through the bridge. The vortices were forced by the Nernst effect to travel from the hot front surface to the colder regions at the back of the film. The resulting voltage transients had rise times as fast as the laser pulse and microsecond fall times due to heat diffusion in the 1 μm thick films. By increasing the laser fluence and therefore the size of the temperature gradient, it was possible to distinguish between the different flux motion regimes such as TAFF, flux creep, and flux flow.

(b). Nonequilibrium electron heating and gap suppression in the resistive state

As discussed in Section 2.3 and shown in Fig. 2.10(d), short laser pulses can heat the electron system in a metal to a temperature T_e much greater than the temperature T_{ph} of the phonon system (or lattice). Nonequilibrium heating of electrons has been used by several groups to explain the fast component in photoresponse signals observed in YBCO films biased in the resistive transition region.[225-235] The equations governing the time evolution of T_e and T_{ph} are similar to Eqs. (2.7) and are given by [234,235]

$$C_e \frac{\partial T_e}{\partial t} = P(t) - C_e \frac{(T_e - T_{ph})}{\tau_{e\text{-}ph}} \qquad (3.13)$$

where τ_γ is the escape time for heat out of the film and T_0 is the temperature of the heat sink (substrate). It is *assumed* that T_e determines the resistance of the sample. Equivalently,

$$C_{ph}\frac{\partial T_{ph}}{\partial t} = C_e\frac{(T_e - T_{ph})}{\tau_{e\text{-}ph}} - C_{ph}\frac{(T_{ph} - T_0)}{\tau_\gamma}$$

since the gap is already suppressed in the resistive state, an increase in T_e will inject more quasiparticles into the system which will then suppress the gap further thereby increasing the resistance of the sample. If the resistance follows T_e, then one should expect a fast resistive transient on the picosecond time scale as T_e equilibrates to T_{ph} followed by a slowly decaying transient on the nanosecond time scale determined by the slow rate of heat escape out of the film. A typical photoresponse signal observed in the resistive transition region by Semenov *et al.*[229] using 20 ps laser pulses is shown in Fig. 3.6. The width of the fast component was limited by the system rise time of about 100 ps. The exponentially decaying slow component (dashed line in Fig. 3.6) had a decay time of 3.9 ns which agreed with the thermal escape time for a 45 nm film at a temperature of 76 K. The fast component was therefore attributed to a nonbolometric response since the 100 ps time scale was too fast to be explained by a thermal process. The wavelength dependence of the fast and slow

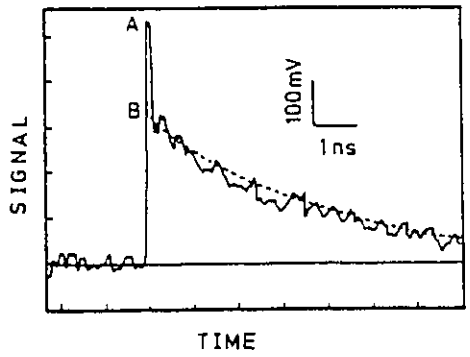

Fig. 3.6. Photoresponse signal observed by Semenov *et al.* (Ref. 229) from a 45 nm YBCO film using 20 ps laser pulses with a fluence of 8 μJ/cm². The sample was biased in the resistive transition region at a temperature of 76 K. The dashed line represents a thermal decay with a time constant of 3.9 ns. Notice how the wave form consists of both fast and slow components. The origin of the fast component was attributed to gap suppression by nonequilibrium electron heating in the resistive state. The width of the fast component was limited by the 100 ps rise time of the system.

components was also tested using $\lambda = 0.63$ and 1.54 μm laser pulses.[227,229] The amplitude of the slow resistive bolometric component was unaffected by the change in wavelengths, but the fast component increased slightly in magnitude at the longer wavelength. This ruled out the possibility that the fast component was due to some quantum response such as photofluxonic detection. No photoresponse was seen by these groups for epitaxial films in the superconducting state.[225-235] As mentioned earlier, however, Gol'tsman *et al.*[233] have recently compared the photoresponse between epitaxial and granular YBCO films and found not only a fast response in the superconducting state for the granular films but also a much larger responsivity in the resistive state for granular films. The fast response in the superconducting state for the granular films was interpreted in terms of a nonequilibrium kinetic inductive response, as discussed in Section 3.4(c).

Measurements studying the light modulation frequency response of YBCO photodetectors up to 10 GHz have proven useful in extracting information on $\tau_{e\text{-}ph}$ by eliminating the need for fast oscilloscopes.[230-232] Using fits to the modulation data, the transient photoresponse in the resistive state has been modelled using Eqs. (3.13) with $\tau_{e\text{-}ph} \approx 2$ ps and $C_{ph}/C_e \approx 40$. For Tl-Ba-Ca-Cu-O films, transients were modelled with $\tau_{e\text{-}ph} \approx 1$ ps and $C_{ph}/C_e \approx 130$. Recent simulations of photoresponse signals by Semenov *et al.*[235] have revealed electron-phonon relaxation times of 1.8 ps for Tl films, 1.5 to 3.5 ps for YBCO films, and 17 ps for NbN films. The effects of finite bandwidth for the experimental setup were also considered to give a more accurate prediction of the observed photoresponse.

(c). Kinetic inductive nonbolometric response

Bluzer[236-238] has developed a model for the nonbolometric response of YBCO films in the superconducting state based on nonequilibrium changes in the kinetic inductance of the sample. The transient photoimpedance measurements were performed with 300 fs, 665 nm, laser pulses on a sample connected directly to the end of a coaxial transmission line. The resulting "Corbino disk" geometry was used to minimize effects due to flux motion. The coaxial line, which was kept as short as possible (≈ 5 cm), connected the sample at temperatures as low as 7 K to a bias-tee and an ultra high speed digital sampling scope (70 GHz) at room temperature. The rise time of the system was limited to about 40 ps due

to time jitter in the trigger electronics. Photoresponse signals were taken in the normal state above T_C, in the resistive transition region, and in the superconducting state. In the normal state and within the resistive transition region, the change in impedance of the sample could be explained by a change in resistance. In the superconducting state, the impedance change was dominated by changes in the kinetic inductance resulting from breaking of Cooper pairs by the laser pulse.

The kinetic inductance of a superconductor arises from the inertia of the Cooper pairs. A superconductor will have zero resistance only if a DC current passes through the material. If an AC current is applied, the Cooper pairs have to be accelerated each time the current switches direction. Since the Cooper pairs are made up of electrons which have mass, then an electric field must exist when they are being accelerated in order to keep pace with the changing current. This means that a voltage can exist across a superconductor in the superconducting state if the current through the superconductor changes with time. This is similar to the voltage produced by an AC current with frequency ω across an inductive element L in a circuit, where $V = I\omega L$. The inductive reactance of the superfluid in a superconductor is characterized by the kinetic inductance L_{KIN}. For a superconducting bridge with length l, width w, and thickness $d < \lambda$ so that the current distribution is approximately uniform, the kinetic inductance is given by [15,258,259]

$$L_{KIN} = \frac{m}{n_{SC}\, e^2}\left(\frac{l}{w\ d}\right) = \mu_0 \lambda_L^{\,2}\left(\frac{l}{w\ d}\right) = \frac{1}{\epsilon_0 \omega_P^{\,2}}\left(\frac{1}{f_{SC}}\right)\left(\frac{l}{w\ d}\right) \qquad (3.14)$$

where m is the electron mass, e is the charge of an electron, n_{SC} is the superfluid density, f_{SC} is the superfluid fraction, and ω_P is the plasma frequency. The London penetration depth is $\lambda_L = (m/\mu_0 n_{SC} e^2)^{1/2} = c/\omega_P$. The plasma frequency, which can be determined experimentally from FIR measurements on YBCO films, is used in the last form shown in Eq. (3.14) to eliminate the need for determining the mass m and the carrier density n separately since $\omega_P^{\,2} = ne^2/\epsilon_0 m$. If the current I changes with time, then a voltage will develop across the bridge given by $V = L_{KIN}\, dI/dt$. If instead the current is kept constant, then a voltage can still appear across the superconductor if the kinetic inductance changes with time such as [236-238,248] (Paper B)

$$V_{KIN} = I \frac{d L_{KIN}}{d t} \tag{3.15}$$

According to Eq. (3.14), the *kinetic inductance is inversely proportional to the superfluid fraction.* If incident light breaks Cooper pairs, then the superfluid fraction will decrease and the kinetic inductance will increase. Any time the kinetic inductance changes with time, Eq. (3.15) predicts that a voltage should develop across the superconductor. The *rate of change of the kinetic inductance determines the magnitude of the voltage transient.*

The nonbolometric mechanism suggested by Bluzer for the photoresponse in the superconducting state is described in Fig. 3.7. From time t_0 to t_1, a fast laser pulse breaks Cooper pairs in the superconducting film and generates energetic quasiparticles. These energetic quasiparticles break more Cooper pairs in an avalanche process as they relax back down to the gap edge. For quasiparticle energies well above the gap energy, the electron-electron interaction resulting in an avalanche process dominates over the electron-phonon interaction and is extremely fast. Closer to the gap edge, the excited quasiparticles relax by emitting optical phonons which can break more Cooper pairs but at a slower rate from time t_1 to t_2. As an example, if the gap was 20 meV and incident photons had an energy of 2 eV, each photon would excite a quasiparticle which would cascade 4 times breaking 16 Cooper pairs and then would emit ~ 32 phonons with energies of about 50 meV.[237] At time t_2, enough phonons have escaped from the film to allow net recombination of quasiparticles back into Cooper pairs and the superfluid fraction slowly recovers back to its original value. At time t_3 the superfluid has completely recovered. The change in superfluid fraction is shown in Fig. 3.7(b). The corresponding change in the kinetic inductance, which varies as $1/f_{SC}$, is shown in Fig. 3.7(c). The rate of change of the kinetic inductance produces a voltage signal V_{KIN} from Eq. (3.15) as shown in Fig. 3.7(d). *The voltage is positive when there is a net generation of quasiparticles and negative when quasiparticles recombine.*

The photoresponse signals observed by Bluzer contained both fast and slow components. In a 50 nm film biased in the superconducting state, a laser induced transition to the normal state was observed in a photoresponse signal with a fast kinetic inductive spike followed by a slow resistive response.[237] The signal went negative about 6 ns after the

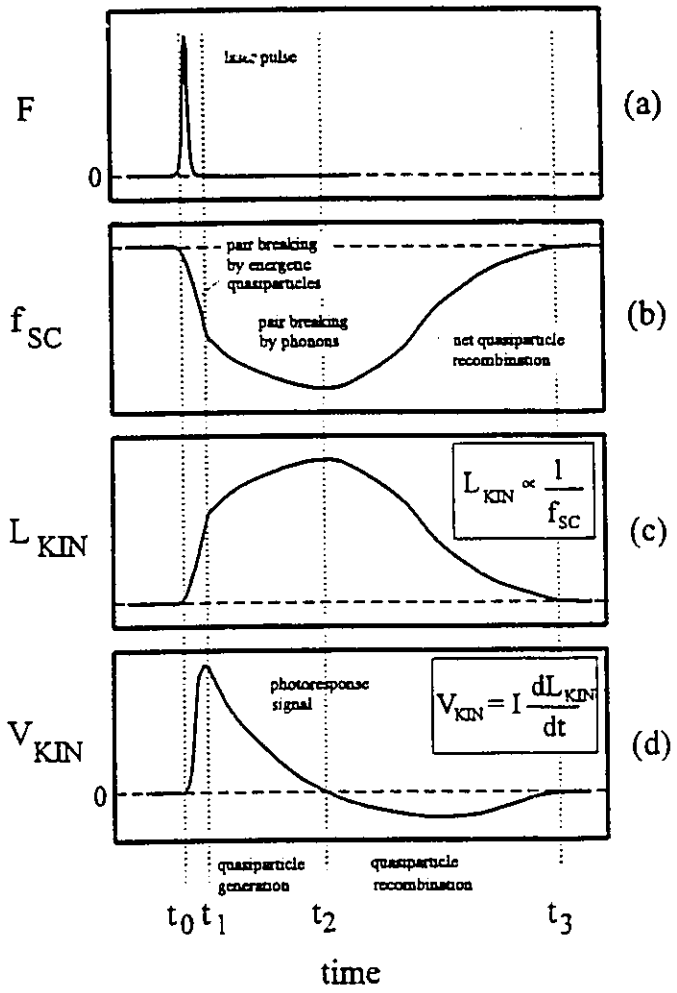

Fig. 3.7. Description of nonbolometric photoresponse mechanism proposed by Bluzer (Ref. 236-238) using nonequilibrium changes in the kinetic inductance of the superconducting film. The laser pulse (a) with fluence F excites quasiparticles to high energies which then lose their energy by breaking more Cooper pairs in an avalanche process. This rapidly reduces the superfluid fraction f_{SC} (b) between times t_0 and t_1. After several cascades, the quasiparticles lose the rest of their energy by emitting phonons which break more Cooper pairs but at a slower rate between times t_1 and t_2. This results in a change in kinetic inductance (c) which produces a rapid positive rise in voltage (d) followed by a slower decay over a few nanoseconds. After time t_2, there is a net recombination of quasiparticles resulting in a negative voltage transient which returns to zero at time t_3.

initial spike, which signified the sample re-entering the superconducting state and is consistent with a 5 ns thermal time constant. However, the photoresponse signal from a 30 nm film in the superconducting state at T = 6.8 K far below T_C (85 K) consisted of a fast rise time followed by a slow decay which did not cross zero until some time after 10 ns (the maximum time for the wave forms was limited to 10 ns).[238] Bluzer implied that this was indicative of net quasiparticle recombination occurring at times greater than 10 ns. In other words, net quasiparticle generation was still happening 10 ns after absorption of the laser

pulse. This time seems a bit long considering that the Pb films probed by Federici *et al.*[152] showed that the pair-breaking process induced by 100 fs laser pulses occurred in times less than 1 ps. Bluzer later interpreted the fast component in some photoresponse signals observed just below T_c as due to nonlinearities in the resistive transition.[240] Bluzer has also recently developed a novel superconducting quantum detector based on kinetic inductance effects.[241,242]

Ghis *et al.*[244-246] have also interpreted their results in terms of nonequilibrium changes in the kinetic inductance of their sample using an experimental setup similar to that of Bluzer's. Fast photoresponse transients 29 ps wide were seen followed by a slowly decaying nanosecond component, as shown in Fig. 3.8. A small dip in the signal seen in Fig. 3.8(a) was attributed to the negative component of the inductive response superimposed on a thermal component. The fast component was not seen by itself in the superconducting state. Ghis *et al.* have also studied the feasibility of YBCO films as fast detectors of FIR radiation generated by pulsed free electron lasers.[246]

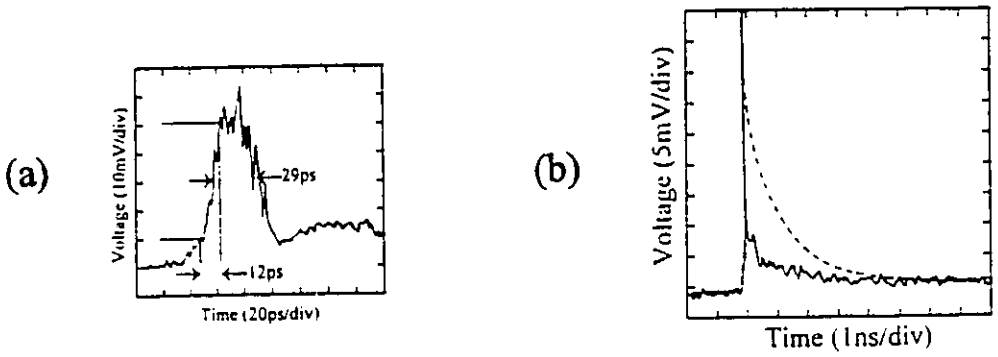

Fig. 3.8. Photoresponse signals observed by Ghis et al. (Ref. 245) from 30 nm YBCO films using 1.5 ps laser pulses (F = 1 μJ/cm^2) and a high-speed digital sampling oscilloscope with a bandwidth of 50 GHz. As shown in (a), transients as fast as 29 ps wide were seen followed by a slower component with a decay over several nanoseconds (b). The effect of a larger bias current and laser fluence (5 μJ/cm^2) is shown by the dashed line in (b). The fast response was attributed to nonequilibrium changes in the kinetic inductance induced by the laser pulse in the film. The slow component is due to a resistive response. A small dip in the signal just after the fast transient in (a) was believed to arise from recombination of nonequilibrium quasiparticles back into Cooper pairs.

3.5. A different interpretation

Figure 3.9(a) illustrates the typical photoresponse signal observed by several groups

from epitaxial thin films. It consists of a fast component with a width in the picosecond range followed by a slow component with a decay in the nanosecond range. The usual interpretation has been that the fast component is due to some kind of nonbolometric mechanism whereas the slow component can be explained very well in terms of a thermal, or more specifically, resistive bolometric response.

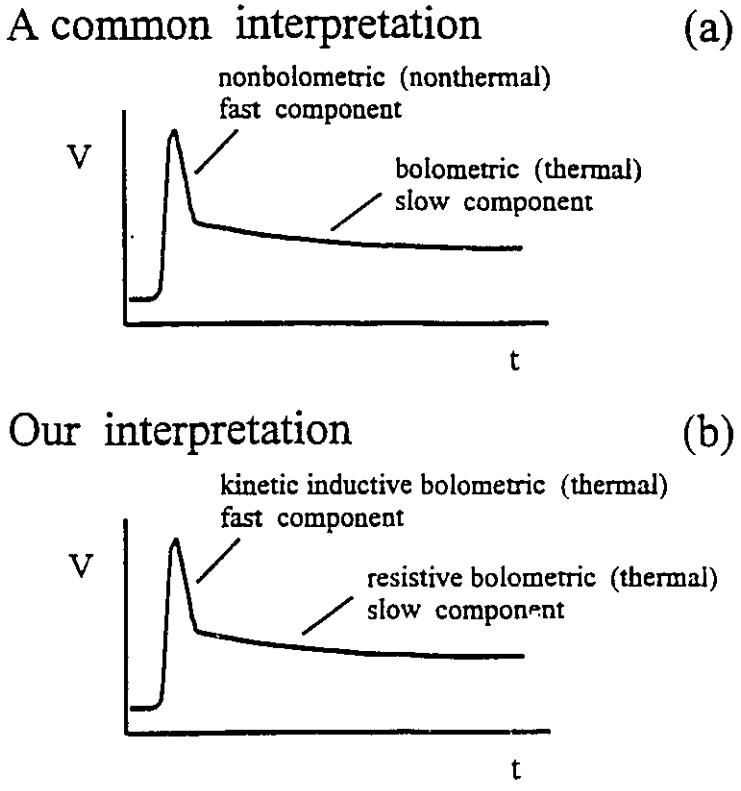

Fig. 3.9. Typical wave form observed in many photoresponse experiments and comparison between a common interpretation (a) and our interpretation (b) of the origin of fast and slow components. In both cases, the slow component with a nanosecond decay time has been attributed to a resistive bolometric response. However, the origin of the fast component in (a) has usually been explained in terms of a nonbolometric mechanism whereas in (b) it is due to a bolometric mechanism based on the KIB model (for 5 ps and 100 ps laser pulses).

We have also seen photoresponse signals with fast transients followed by slow components, but our interpretation is a little different from that described in Fig. 3.9(a). As shown in Fig. 3.9(b), we also believe that the slow component is due to a resistive bolometric response with a time constant determined by the thermal escape time from the film. However, for 100 ps and 5 ps laser pulses, we do not believe that the observed fast component must be due to a nonbolometric process. Instead, we believe the fast component

can be adequately and simply explained by a thermal mechanism called the kinetic inductive bolometric (KIB) response. The KIB response relies on changes in kinetic inductance in the film due to thermally induced changes in the superfluid fraction. Whereas Bluzer discusses kinetic inductance changes due to nonequilibrium processes, we assume only an equilibrium heating mechanism. The next few chapters discuss how the KIB model may provide a better alternative to some of the nonbolometric mechanisms described above when looking at photoresponse signals from 5 ps and 100 ps laser pulses.

4. THE KINETIC INDUCTIVE BOLOMETRIC (KIB) RESPONSE

4.1. Description of the KIB model

We have developed the KIB model to explain the origin of fast photoresponse signals seen in our experiments from epitaxial YBCO thin films.[248-250] (Papers B, C, and D) The model is based on changes in the kinetic inductance of a current-biased bridge arising from changes in the superfluid fraction determined by *equilibrium* heating of the lattice by an incident laser pulse. The following is a basic description of how the KIB model works.

Consider a sample cooled to an initial temperature $T_i < T_c$, as shown in Fig. 4.1. An incident laser pulse rapidly heats the film and induces a temperature transient ΔT (Eq. (3.2)) in the film such that the instantaneous temperature T does not exceed T_c. The variation of the superfluid fraction as a function of lattice temperature is also shown in Fig. 4.1 which may be of the form given in Eq. (2.2). Since the temperature of the lattice has increased by ΔT due to equilibrium heating by the laser pulse, the superfluid fraction will have to decrease. The decrease in superfluid fraction increases the kinetic inductance of the bridge

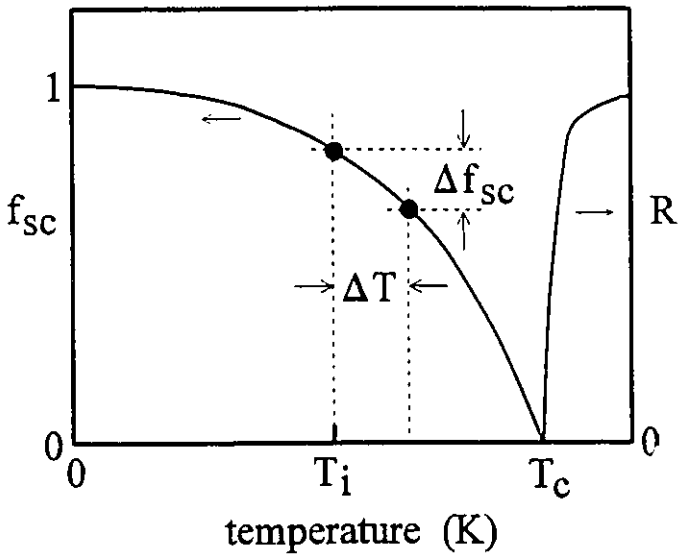

Fig. 4.1. Superfluid fraction f_{sc} and resistance R of a superconducting film as a function of temperature showing change in superfluid fraction when the film is heated by ΔT from an initial temperature of T_i below T_c. If ΔT is not large enough to bring the film into the resistive state, then it is possible to see a voltage transient if a bias current is applied due to the resulting change in kinetic inductance of the film.

according to Eq. (3.14). If a current bias I is applied to the bridge, then Eq. (3.15) will give a voltage proportional to the *rate of change* of this kinetic inductance. Figure 4.2 shows schematically the entire sequence of events involved in the KIB model. It is important to keep in mind the relative time scales involved in the process. Heating of the film occurs over the duration of the laser pulse which can be in the picosecond range. The temperature rapidly increases from T_i to $T_i + \Delta T$, as shown in Fig. 4.2(b), and then begins to cool over the nanosecond time scale depending on the characteristic thermal escape time of the film determined by Eq. (3.1). The superfluid fraction and the kinetic inductance will follow the

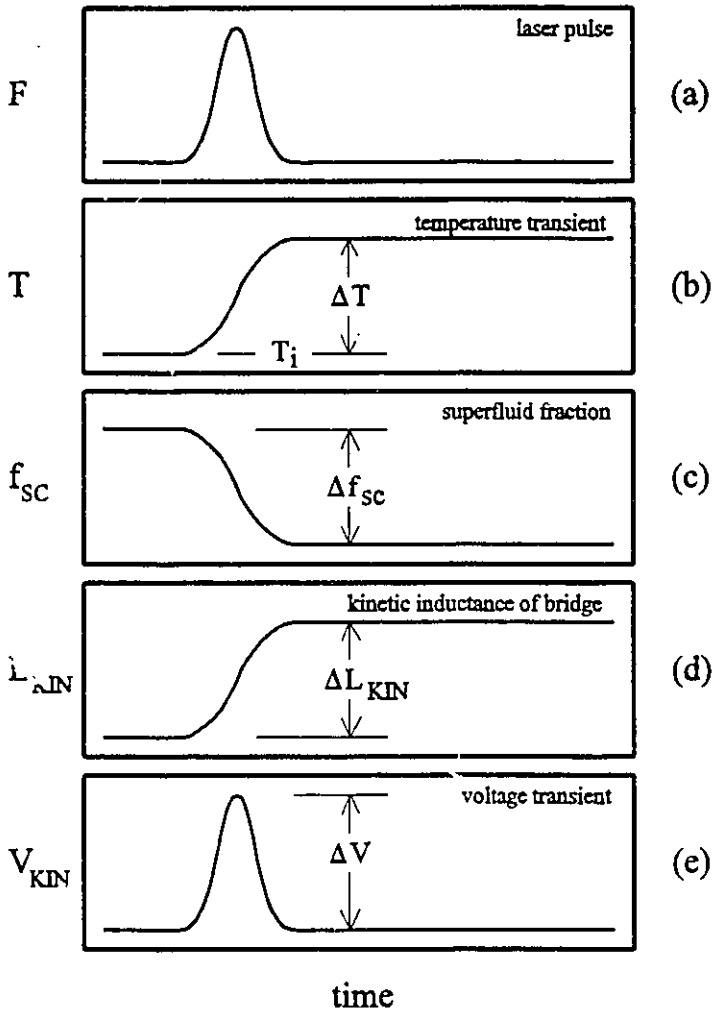

Fig. 4.2. Description of the KIB model. A laser pulse (a) heats a film by ΔT from an initial temperature T_i (b) which reduces the superfluid fraction (c). The thermal escape time from the film is much longer than the duration of the laser pulse in this case. The reduction in superfluid fraction causes the kinetic inductance (d) of the film to increase. The change in kinetic inductance produces a voltage transient across the bridge if a bias current is applied. The width of the voltage transient is roughly the same as that of the laser pulse, and the amplitude of the voltage transient is determined by the rate of change of the kinetic inductance.

same behaviour with a rapid initial change followed by a slow recovery back to their initial values. Since the voltage transient across the bridge depends on the rate of change of the kinetic inductance, a photoresponse signal will be seen only during the time the laser pulse is heating the film, as shown in Fig. 4.2(e). This means that the voltage transient can be quite fast even though the heat escape out of the film is very slow.

Figure 4.3 provides a circuit analogy of the KIB response. The kinetic inductance of a superconducting bridge is modelled by an inductor with a bias current passing through it. A resistor in parallel with the inductor representing the normal fluid fraction has been neglected but will be considered in Section 4.4. In Fig. 4.3(a), the sample is in the zero-resistance superconducting state with V = 0. In Fig. 4.3(b), the effect of the laser pulse is to suddenly increase the inductance of the inductor in the circuit, which results in a positive voltage transient across the inductor. The inductance remains at the higher value until the heat has escaped from the film. If the inductance recovers quickly, as in the case where heat escape is very fast, then a negative voltage transient might be seen. Since the initial increase in inductance due to heating by the laser pulse is usually so much faster than the recovery of the inductance back to its original value determined by the thermal escape time, then typically

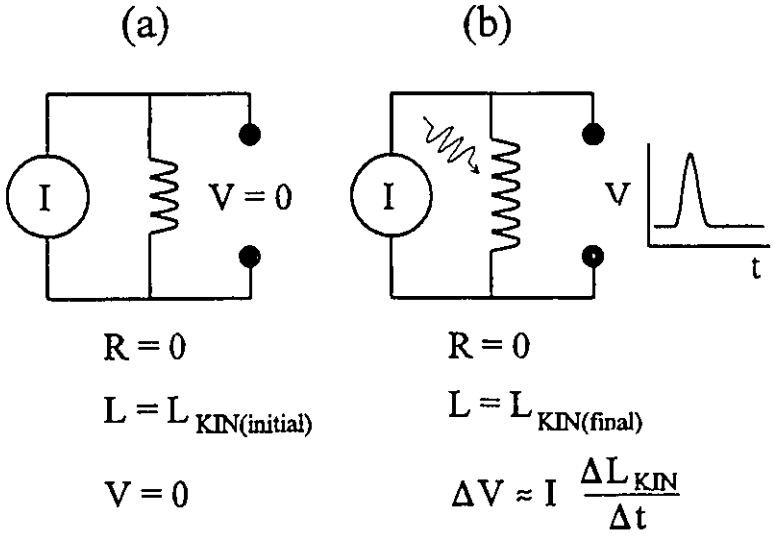

Fig. 4.3. Description of the KIB model by (a) representing the kinetic inductance of a superconducting bridge with an inductive element biased with a constant current I. In the superconducting state with R = 0, the voltage across the inductor is zero. If the kinetic inductance of the bridge is suddenly increased by heating from a laser pulse, then the inductance in the circuit will suddenly increase (b) and a voltage transient will appear across the inductor even though the resistance in the circuit is still zero.

only positive-going voltage transients are seen. Also, shorter laser pulses produce faster changes in inductance resulting in larger photoreponse signals.

It is easy to get an estimate of the amplitude of such voltage transients. Consider a typical YBCO thin film bridge 10 μm wide, 200 nm thick, and with a length illuminated by the laser pulse of 35 μm. If $\Delta T = 0.4$ K and the initial temperature is 77.4 K ($T_c = 89$ K), then using Eq. (2.2) the superfluid fraction will decrease from 0.244 to 0.236 and the kinetic inductance will increase by 0.10 pH from 2.91 to 3.01 pH. If this change in inductance occurs over the time scale of a 5 ps laser pulse, then the voltage transient will have an

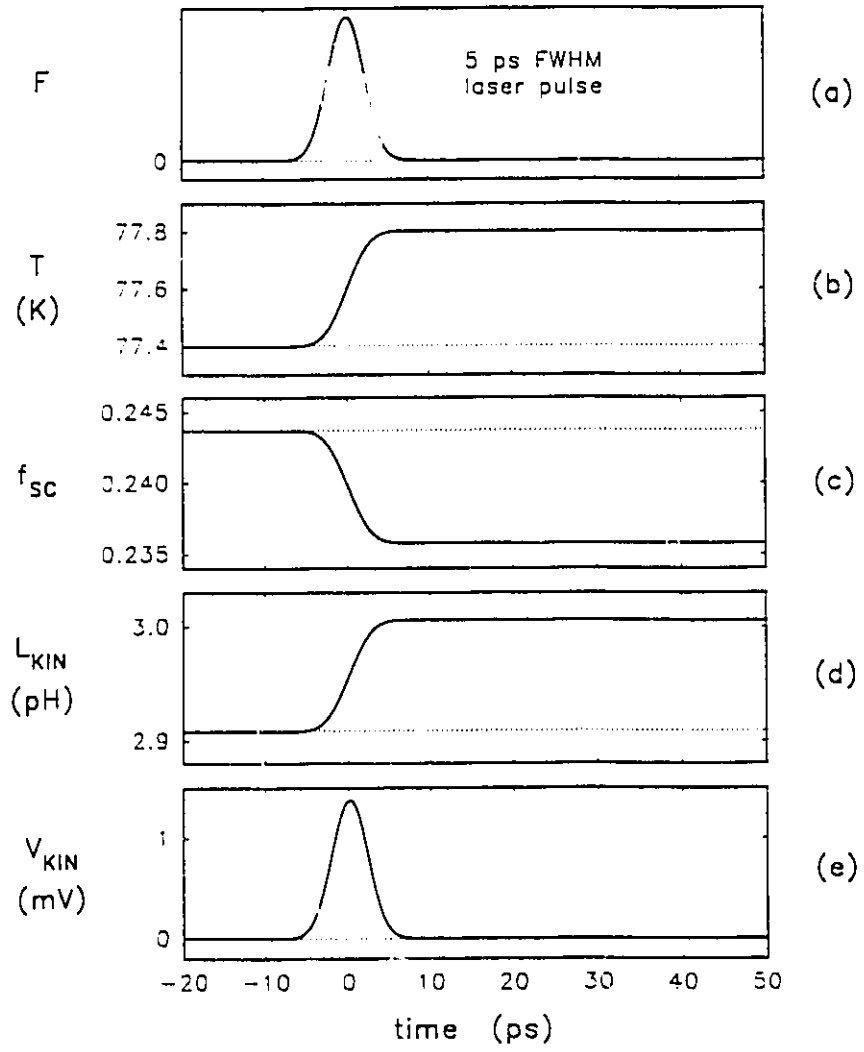

Fig. 4.4. Simulation of the KIB response from a 200 nm YBCO bridge cooled with liquid nitrogen (77.4 K) and illuminated by 5 ps FWHM laser pulses (a) at a fluence of 10 μJ/cm² (Papers C and D). A temperature transient (b) of 0.4 K is induced in the bridge which lowers the superfluid fraction (c) and increases the kinetic inductance (d). A voltage (e) appears across the bridge only when the kinetic inductance changes with time. The amplitude of the voltage transient in (e) is about 1.38 mV and has a width equal to that of the laser pulse of 5 ps.

amplitude of about 0.4 mV for a current bias of 20 mA (10^6 A/cm^2). A full simulation of the KIB response for the same conditions but at a current bias of 75 mA (3.75 x 10^6 A/cm^2) is shown in Fig. 4.4 giving a voltage amplitude of 1.38 mV. The fast photoresponse signals observed in our experiments for the same bridge had amplitudes on the order of 1 mV, which is consistent with the KIB model. This is a very small voltage transient, but it is still possible to observe sub-millivolt signals on a digital sampling scope (see Chapter 5). The observation of such low-level transients was one of the main challenges of the work described here, and the fact they are so small may be the reason why other groups have failed to see fast transients without any slow components from epitaxial films.

The KIB response is an extremely simple photoresponse mechanism which does not require knowledge of the superconducting energy gap or nonequilibrium processes. The KIB model:

1. assumes the current distribution in the bridge is uniform,
2. assumes uniform illumination by the laser pulse over a section of the bridge,
3. assumes uniform heating within the bridge by the laser pulse,
4. assumes equilibrium heating with the lattice,
5. neglects the effect of the normal fluid channel on the response which can reduce the amplitude of the predicted response, and
6. has only one adjustable parameter: the temperature dependence of the superfluid fraction.

Despite these simplifications, the KIB model has provided excellent qualitative as well as reasonable quantitative agreement with the observed photoresponse data, as discussed in Chapter 5. The sensitivity of the KIB model to variations in the experimental parameters such as initial temperature, laser fluence, and choice of plasma frequency of the film is presented in Appendix C. The purpose of introducing the KIB model was not to refute the existence of nonbolometric mechanisms, but merely to provide an alternative explanation for the origin of fast photoresponse transients. It is possible that deviations of photoresponse signals from the predicted KIB response could be used to identify nonbolometric components.

4.2. Predictions of the KIB model

The KIB model predicts the following:

1. From Eq. (3.14), $L_{KIN} \sim \lambda^2$ and so Eq. (3.15) predicts a temperature dependence of the amplitude of the photoresponse signal that is largest near T_c and smallest at low temperatures. This behaviour has been observed in our photoresponse data.
2. The amplitude of the KIB photoresponse is linear with bias current according to Eq. (3.15). We have observed this behaviour in all the films we have studied when only the fast response was present in the wave form.
3. Since the photoresponse relies on the rate of change of the kinetic inductance, the amplitude of the voltage transient increases as the laser pulse gets shorter for the same ΔT induced in the film. The width of the voltage transient should also be about the same width as the laser pulse. Such effects have been observed in our photoresponse data.
4. A fast response should be seen in optically thick films since the kinetic inductance of the bridge will change even if only the superfluid fraction in the top-most layers is decreased by the incident light. This is contrary to the belief that very thin films are needed in order to see a fast response. We have seen the fastest reported transients in 200 nm films (Papers C and D).

Chapter 5 presents the experimental evidence which supports the KIB model.

4.3. Some notes on kinetic inductance

The inductance of a metal or superconductor can be separated into a magnetic inductance L_M due to energy stored in the magnetic field surrounding the material as a result of a current passing through it and a kinetic inductance L_{KIN} due to the kinetic energy of the carriers. The magnetic inductance for a wire of length l is $L_M \approx \mu_0 l$,[93] which is normally much larger than L_{KIN} since $\lambda^2 << wd$. For example, if $L_{KIN} \approx 1$ pH, then $L_M \approx 0.1$ to 1 nH ($d \approx \lambda$, $w \approx 100$ d) and the magnetic inductance dominates. For a microstrip transmission line where a thin strip of superconductor with width w is placed at a distance h from a

ground or shield plane such that w >> h, the magnetic inductance of the microstrip can be greatly reduced and is given be $L_M \approx \mu_0 h/w$.[260] In this case, it is possible to make $L_{KIN} > L_M$ so that the kinetic inductance dominates. The phase velocity for propagation of microwaves on such a microstrip transmission line, given by $v_{phase} = c/(LC)^{1/2}$, will vary greatly with temperature since $L = L_M + L_{KIN}$. The fact that $L_{KIN} \sim \lambda^2$ allows accurate measurements of the temperature dependence of λ using microwave resonant transmission line circuits, as discussed earlier in Section 2.1.[89-92,260] The temperature dependence of the kinetic inductance has also been used in the design of ultrasensitive thermometers[261,262] and infrared detectors[263,264]. Variable microwave delay lines have been made by optically modulating the kinetic inductance of a YBCO microstrip with a 10 mW HeNe laser.[265] The effect was attributed to a bolometric change in the kinetic inductance of the line due to heating of the film by the laser. Optically modulated microwave interferometers[266] and filters[267] have been developed which also rely on thermally-induced changes in the kinetic inductance of superconductor films.

Equation (3.14) for the kinetic inductance is valid only if the current distribution in the superconducting film is uniform.[15,93,259,268-270] The current distribution is uniform for a microstrip transmission line if w >> h,[259,260] but becomes peaked at the edges of the strip if w > h or if $wd > \lambda^2$.[259,268-270] The latter condition is met in our experiments where $w \approx 10$ μm, $d \approx 100$ nm, and $h = 500$ μm, and so a nonuniform current distribution is expected. However, Lemberger[268] has shown for a 10 μm wide bridge with a thickness of 100 nm and using $\lambda = 220$ nm that the peak current density at the edges is only about twice the average value. The minimum current density at the centre is only about 0.75 the average value. The assumption of uniform current density is therefore not an unreasonable approximation, especially when considering that a larger source of error probably is in determining the average laser fluence illuminating the film.

4.4. Effect of the normal-fluid channel

The equivalent circuit representation of a superconductor in the two-fluid model is shown in Fig. 4.5. The superfluid channel is represented by an inductance L_{SC} given by

$$L_{SC} = \frac{m}{n_{SC}\, e^2} \frac{l}{w\, d} \tag{4.1}$$

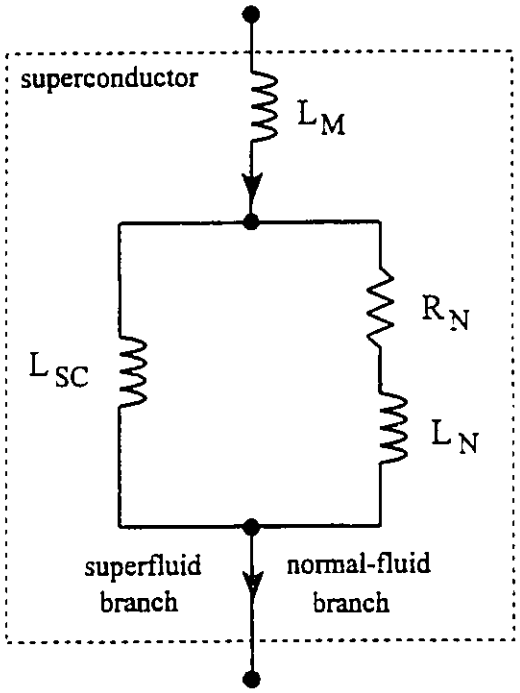

Fig. 4.5. Equivalent circuit of a superconductor in the two-fluid model. The circuit consists of a purely inductive (L_{SC}) superfluid branch and a resistive (R_N) and inductive (L_N) normal-fluid branch connected in parallel. L_M is the magnetic inductance associated with the superconducting element. In the steady state, current will always pass through the non-resistive superfluid branch. If the current or L_{SC} changes, then a voltage will appear across the two branches which will force current through the resistive normal-fluid channel resulting in dissipation.

which is simply the kinetic inductance from Eq. (3.14). The resistive normal-fluid channel is represented by a resistor R_N in series with a kinetic inductance L_N for carriers in the normal state. R_N is given by

$$R_N = \frac{m}{n_N\, e^2} \frac{l}{w\, d} \frac{1}{\tau_S} \tag{4.2}$$

where n_N is the normal fluid density and τ_S is the electron-phonon scattering rate. The normal channel kinetic inductance is then

$$L_N = \frac{m}{n_N e^2} \frac{l}{w\ d} \tag{4.3}$$

which can usually be neglected since the inductive impedance ωL_N will be much less than R_N for $\omega << 1/\tau_S$.

In the superconducting state with a DC bias current, all the current will pass through the inductor L_{SC}. If the current through the inductor changes with time a voltage will develop across L_{SC} which will also appear across R_N. This will result in a current flowing through R_N which leads to dissipation as long as $T > 0$. If L_{SC} increases abruptly due to absorption by a laser pulse, the impedance of the superfluid branch will suddenly increase and the normal-fluid channel resistance will shunt current away from L_{SC}. The time constant for shunting of current through the resistive channel as a result of a sudden change in the impedance of the inductance in the superfluid channel is

$$\tau_J = \frac{L_{SC}}{R_N} = \tau_S \frac{f_N}{f_{SC}} \tag{4.4}$$

This is the same as the supercurrent response time to a sudden change in current density.[271] At 77 K, $\tau_S \approx 0.2$ ps (Fig. 2.4), $f_{SC} = 0.268$ and $f_N = 1 - f_{SC} = 0.732$ ($T_C = 90$ K) so that Eq. (4.4) gives a relaxation time for shunting of current through the resistive channel of $\tau_J \approx 0.5$ ps. As shown in Fig. 2.4 for YBCO, there is a sudden drop in $1/\tau_S$ below T_C and so one might expect τ_J to increase as the temperature is lowered. At 20 K, τ_S may be as large as 10 ps in good quality single crystals, but if one assumes that $f_N = (T/T_C)^2$, then Eq. (4.4) gives $\tau_J \approx 0.52$ ps which is about the same value as that calculated earlier at 77 K. The temperature dependence of τ_J is shown in Fig. 4.6. A supercurrent response time of less than 1 ps means that the attenuation of voltage transients due to shunting of current through the resistive channel will not be significant for the 5 ps laser pulses used in some of the experiments described here. However, if shorter laser pulses were used, a reduction in the photoresponse amplitude will occur. Figure 4.7 shows the effect of the normal-fluid channel on fast voltage transients induced by changes in kinetic inductance of the superfluid at a temperature of 77.4 K. For 5 ps laser pulses as shown in Fig. 4.7(a), the normal fluid

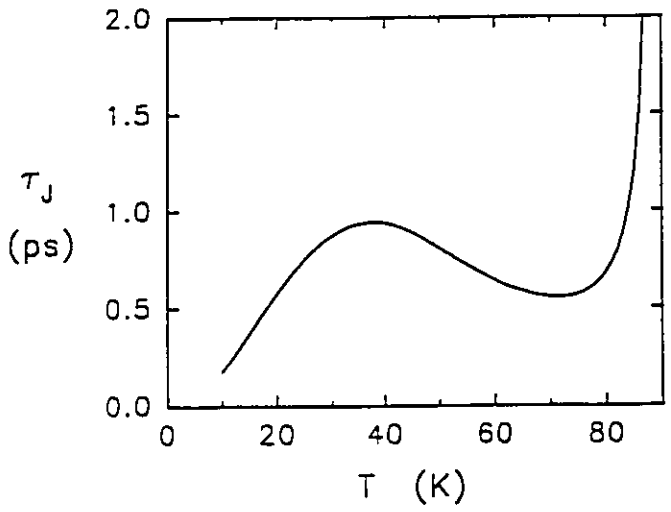

Fig. 4.6. Plot of the supercurrent response time τ_J calculated from Eq. (4.4) as a function of temperature for a YBCO film. Voltage transients with widths comparable to τ_J will be greatly attenuated by dissipation in the normal fluid channel.

channel has little effect on the amplitude predicted by the basic KIB model. If the laser pulse width is reduced to 147 fs, the KIB model predicts a voltage transient with approximately the same width as the laser pulse. However, the signal will be strongly attenuated by the normal-fluid channel and will have a decay time equal to τ_J of about 0.5 ps. The supercurrent response time τ_J imposes a limit on the response time of a superconducting photodetector based on changes in kinetic inductance.

4.5. Effect of nonuniform heating

Another assumption of the KIB model is that heating by the laser pulse is uniform across the thickness of the high-T_C film. The optical penetration depth δ in YBCO films is about 90 nm, and so uniform heating may apply only to very thin films. For films thicker than 100 nm, the incident light pulse will heat the front surface to a higher temperature than the back surface of the film. The change in kinetic inductance will then be larger near the illuminated surface. It is possible to simulate the effect of nonuniform heating by dividing the film thickness into several layers. The heat deposited at each layer by the laser pulse determines the kinetic inductance of that layer. The total kinetic inductance of the bridge can

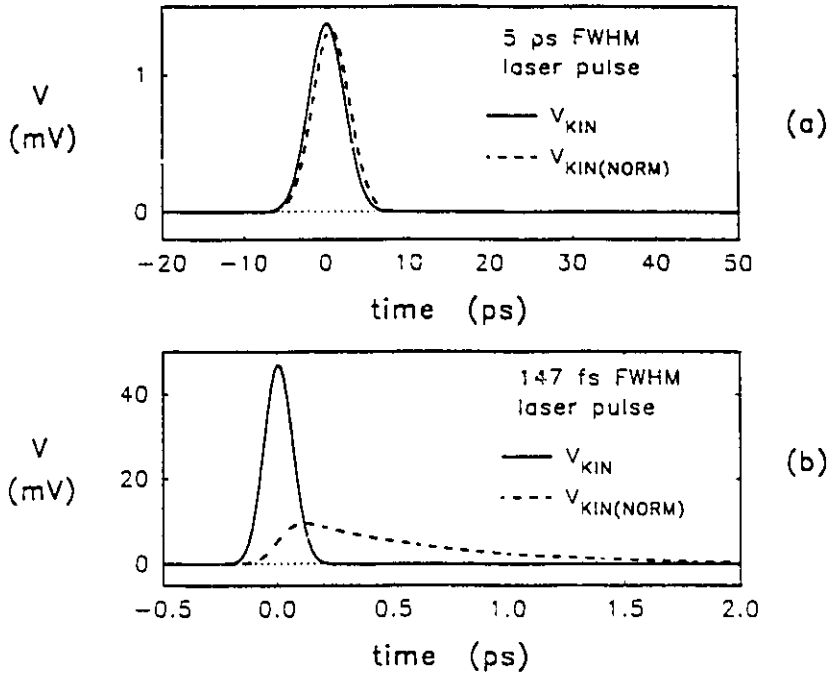

Fig. 4.7. Simulation of the effect of the normal-fluid channel on voltage transients generated by 5 ps (a) and 147 fs (b) laser pulses. The voltage response V_{KIN} predicted by the KIB model is represented by a solid line. The simulation parameters are identical to the ones used in Fig. 4.4. Notice how the shorter laser pulse generates a larger voltage transient, as predicted by the KIB model. The dashed line shows the same response attenuated by the normal-fluid channel. The effect of the normal-fluid channel is much stronger for transients generated by the 147 fs pulse in (b).

then be taken as the parallel combination of the inductances from each layer. As shown in Fig. 4.4, the KIB simulation predicts a voltage transient of 1.38 mV for a 200 nm film exposed to 5ps laser pulses. The temperature change is about 0.40 K assuming uniform heating. Nonuniform heating due to δ = 90 nm results in a voltage transient with a maximum amplitude of about 1.30 mV. This is not very different from the KIB simulation result, even though the nonuniform heat distribution in the film just after the laser pulse is 0.88 K at the front surface and 0.11 K at the back.

The ability of the KIB model to provide reasonable quantitative agreement with the

observed photoresponse data seems surprising in light of all the approximations and assumptions discussed above. The next chapter gives an overview of trends seen in the photoresponse data and how this data supports the KIB photoresponse mechanism in epitaxial YBCO thin films.

5. PICOSECOND PHOTORESPONSE MEASUREMENTS

5.1. Trend observed in the photoresponse data

A general trend has been observed in the temperature and bias-current dependence of the photoresponse data, as described in Papers B and C. Figure 5.1 plots the behaviour of the DC voltage across a bridge at two different bias currents. This is equivalent to the resistance of the sample at a given bias current, but voltage is shown instead so that temperature transients ΔT induced by the laser pulse can be directly translated into voltage transients ΔV in a resistive bolometric response. The evolution of the photoresponse as the temperature is lowered is also shown in Fig. 5.1. It was necessary to perform experiments at high current densities (~ 10^6 A/cm^2) in order to see fast photoresponse signals above the noise level of the oscilloscope. However, large current densities tend to broaden the resistive transition.[257] For a small bias current I_1, the resistive transition is very sharp and falls to zero at $T_{C0} \approx 90$ K (for YBCO films). At a larger bias current I_2, the transition is much broader and the zero-resistance temperature T_{C0} is significantly lowered.* Operating at bias current I_2, the photoresponse signals taken at temperatures well within the resistive transition region will have large amplitudes and nanosecond decay times, consistent with a resistive bolometric response. The amplitude of the resistive bolometric (slow) component at a given bias current is given by

$$\Delta V_{slow} = V_{DC}(T_i + \Delta T) - V_{DC}(T_i) = I\,[R(T_i + \Delta T) - R(T_i)] \qquad (5.1)$$

where T_i is the initial temperature of the sample. Eq. (5.1) must be used rather than Eq. (1.2) for predicting the amplitude of the resistive bolometric response when large temperature transients are involved (i.e. $\Delta T > 0.1$ K). As the temperature is lowered, the amplitude of

* The criteria used for the onset of resistance in superconductors depends on the resolution of the voltmeter used to take measurements. Most sensitive voltmeters can easily measure 10^{-7} V, and so the convention for onset of resistance is usually taken as 1 μV/cm, or 10^{-7} V across a 1 mm-long sample. In our experiments, the onset of resistance across 200 μm or 100 μm-long bridges is taken at the temperature where the voltage across the bridge is also 10^{-7} V, or about 5 μV/cm or 10 μV/cm, respectively, for the bridges.

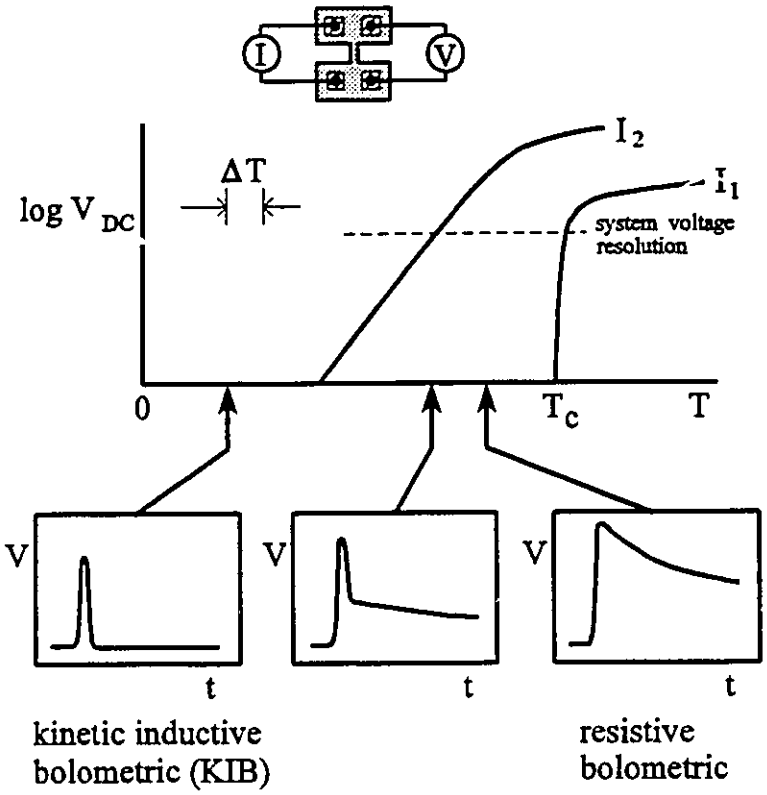

Fig. 5.1. General trend observed in the photoresponse data as the temperature is lowered below T_c. At a low bias current I_1, the resistive transition is sharp and falls to zero at $T_c \approx 89$ K for YBCO films. At a higher bias current I_2, the resistive transition is broadened and T_c is reduced. Plotting the DC voltage V_{DC} across the bridge as a function of temperature and bias current can be used to identify resistive bolometric photoresponse signals. If the bridge is biased with current I_2 and is at a temperature well within the resistive transition, the photoresponse signal is due to a resistive bolometric response and is very large with a long decay time on the nanosecond time scale. As the temperature is lowered, the slow component is reduced in amplitude and a fast component appears at the start of the slow component. The amplitude of the slow component will completely disappear (as seen on an oscilloscope) if the temperature transient ΔT cannot change the voltage across the bridge by an amount greater than the system voltage resolution. Reducing the temperature further so that the temperature transient ΔT induced by the laser pulse cannot bring the film into the resistive region, only the fast component is observed. The fast component is attributed to a KIB response.

the slow component decreases and a fast component appears superimposed on top of the slow component. At temperatures well below the resistive transition region such that the temperature transient ΔT induced by the laser pulse is insufficient to raise the temperature of the sample into the resistive region, the slow component has completely disappeared and only the fast component remains due to the KIB response. The noise level for DC voltage measurements using a sensitive voltmeter (~ 0.1 μV) is much lower than the noise level on a fast oscilloscope for measuring fast voltage transients (~ 0.1 mV). The slow component can only be seen if its amplitude given by Eq. (5.1) is larger than the noise level of the

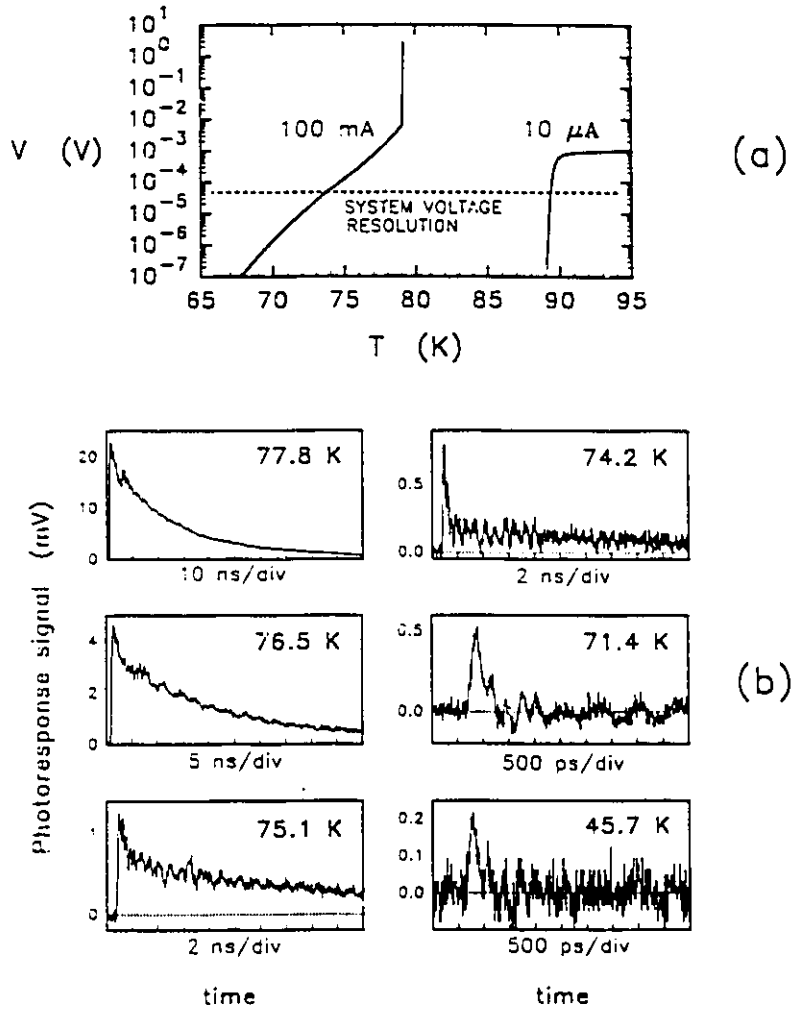

Fig. 5.2. Photoresponse signals seen from a 260 nm YBCO film exposed to 100 ps laser pulses at a fluence of 100 μJ/cm^2 (Paper B). In (a), it is seen that the resistive transition at a bias of 100 mA through the bridge is much broader than the transition at 10 μA. The system voltage resolution is about 0.05 mV as determined by the noise level on the fast oscilloscope. The photoresponse signals taken at a bias of 100 mA are shown in (b). The general trend described in Fig. 5.1 is seen here. Well within the resistive region above 76 K, only a slow component with a large amplitude is observed. As the temperature is lowered slightly, a fast component begins to appear. At 71 K, the slow component has completely disappeared and only the fast component remains even though the sample is still in the resistive region. This is because the temperature transient of about 3 K is insufficient to raise the temperature of the bridge to a value which would make the voltage across it exceed the system voltage resolution. At 45.7 K, which is well below the resistive region, the fast component is still observed. The width of the fast component in this case was limited to 400 ps by the 1 GHz bandwidth of the system.

oscilloscope, which is shown in Fig. 5.1 by a dashed line labelled as the system voltage resolution. It is therefore possible to see only the fast component from the KIB response while in the resistive transition region as long as ΔT does not increase the temperature of the sample to the point where V_{DC} is larger than the system noise resolution.

Figure 5.2(a) shows the resistive transition broadening observed for a YBCO thin

film bridge at bias currents of 10 μA and 100 mA (Paper B). At 10 μA, the transition is very sharp and T_{c0} is about 89 K. Increasing the bias current to 100 mA broadens the transition region and reduces T_{c0} to 68 K. The temperature at which V_{DC} exceeds the system voltage resolution is about 74 K. In these experiments, which are described in Paper B, 100 ps, 532 nm laser pulses with a fluence of 100 μJ/cm^2 induced temperature transients $\Delta T \approx 3$ K in a YBCO film with a thickness of 260 nm. The bandwidth of the apparatus was limited by a voltage amplifier (gain of 10) to about 1 GHz ($\tau_r \approx 350$ ps). The photoresponse wave forms are shown as a function of temperature in Fig. 5.2(b), and the trend closely follows that described in Fig. 5.1. Above 76 K, only the resistive bolometric component is observed with a large amplitude and slow decay time. At 75 and 74 K, the amplitude of the slow component has been greatly reduced and a fast component appears at the start of the signal. At 71 K, which is still within the resistive transition region, only a fast component is seen because ΔT is insufficient to bring the temperature of the sample to a level where V_{DC} exceeds the system voltage resolution. At temperatures well below the resistive transition region (i.e. 46 K), the fast component can still be seen with a width of less than 400 ps. The amplitude of the fast component is smaller than the real amplitude due to bandwidth limitations. The fast component is attributed to the KIB response.

Plots of the temperature dependence of the amplitude of the photoresponse signal can be found in Paper B (Figs. 17 and 19). Excellent qualitative agreement with the KIB model was obtained. Quantitatively, the observed amplitudes were lower by a factor of 3.5 from those predicted by the KIB model using 100 ps laser pulses and a temperature dependence for the superfluid fraction given by Eq. (2.2). However, the agreement improves if one realizes that the amplitude of 100 ps wide voltage transients predicted by the KIB model will be reduced by a factor of 4 if bandwidth limitations increase the width of the transients to 400 ps. This quantitative agreement with a model whose only adjustable parameter is the temperature dependence of the superfluid fraction provides further support for the KIB model. As shown in Fig. 2.3, the superfluid fraction has several postulated forms as a function of temperature. In Paper B, these forms were inserted into the KIB model and compared to the observed temperature dependence of the photoresponse data. It was found that using $f_{SC} = 1 - t^4$ in the KIB model did *not* agree with the observed temperature dependence of the photoresponse data. A detailed comparison could not be

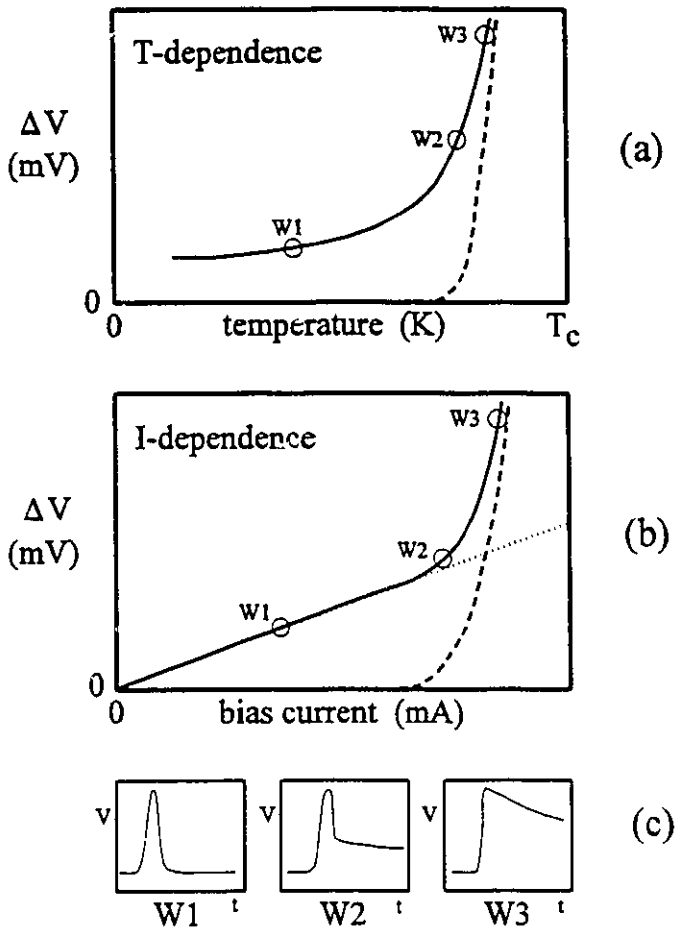

Fig. 5.3. General trends observed in the temperature (a) and bias current (b) dependence of the amplitude of the voltage transients observed in the photoresponse data. The dashed line represents the amplitude of the slow component only. When the slow component has disappeared, the amplitude of the fast component is always observed to be linear with the applied current. Typical wave forms at various points in the curves are shown in (c).

made, however, between the other forms due to the cold head being limited to temperatures above 40 K.

A schematic of the temperature dependence of the photoresponse signal amplitude is shown in Fig. 5.3(a). The dashed line represents the amplitude of the slow component. Below a certain temperature, the slow component disappears and only the fast component remains. Examples of wave forms are shown in Fig. 5.3(c), and can be compared with those seen in Fig. 5.2(b). As shown in Fig. 5.3(b), the amplitude of the fast photoresponse when no slow component is present is directly proportional to the bias current. This is exactly what the KIB model predicts, as discussed in Chapter 4. This trend has been observed in all the films we have studied with thicknesses ranging from 30 nm to 260 nm, which provides

further support for our claim that the fast photoresponse we are seeing is due to the KIB mechanism. As the bias current is increased, the bridge is biased far enough into the resistive transition region so that the resistive bolometric signal can be seen on the oscilloscope. When this happens, the amplitude of the photoresponse signal increases nonlinearly with the applied bias current until the slow component dominates. The shape of the photoresponse wave form can therefore be changed quite easily from signals with only the fast component to signals with only the slow component simply by increasing the temperature of the sample or by increasing the bias current through the bridge. Examples of the bias-current dependence of the photoresponse signal amplitude can be found in Paper B (Figs. 7 and 9), Paper C (Fig. 8), and Paper D (Figs. 3 and 4).

5.2. Measuring fast photoresponse signals

The KIB model has been shown to provide an accurate description of the fast photoresponse of YBCO films exposed to 100 ps laser pulses. This might not be too surprising over this time scale since equilibrium heating with $T_e \cong T_{ph}$ is probably a good approximation. The next step in experimentation was to see if a nonequilibrium response could be seen using shorter laser pulses about 5 ps wide. The results from these experiments are discussed in Papers C and D. The challenge was to get the maximum possible bandwidth

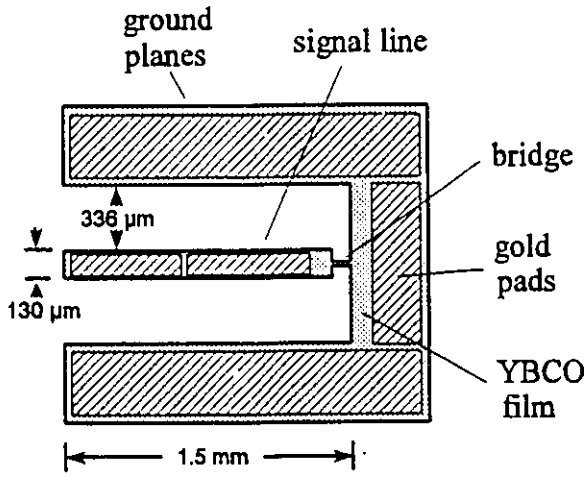

Fig. 5.4. Coplanar transmission line structure used for measuring fast photoresponse transients. The laser pulse is focused onto the bridge, and the voltage transient propagates down the central signal line.

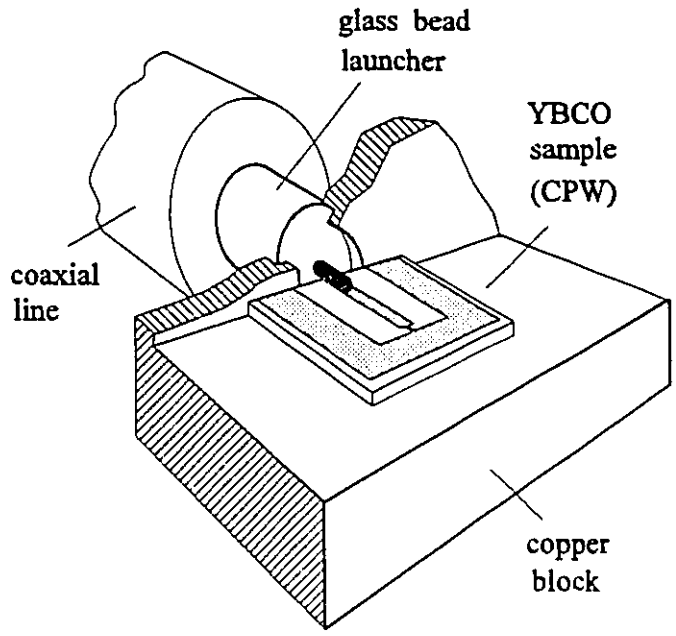

Fig. 5.5. Cutaway view of the sample mount showing how the voltage transient from the YBCO coplanar waveguide (CPW) is launched into a coaxial cable.

from the apparatus so that the temporal evolution of the fast component could be resolved. Besides the obvious requirement of a fast digital sampling scope with a bandwidth of 50 GHz ($\tau_r \approx 7$ ps), it was important to properly launch the fast voltage transient from the YBCO bridge into a coaxial line.

This was done by patterning the YBCO thin film into a coplanar transmission line structure, as shown in Fig. 5.4. The narrow bridge which was to be illuminated by the laser pulse terminated one end of the transmission line. Gold contact pads allowed 4-point probe measurements of the I-V characteristics of the bridge structure, which helped in analyzing the resistive bolometric response. The sample was mounted on a copper block cooled to 77 K with liquid nitrogen, as shown in Figs. 5.5 and 5.6. The other end of the coplanar transmission line was connected to a pin mounted in a hermetic glass bead structure, which allowed launching of the voltage transient into a 50 Ω coaxial line with a bandwidth of 65 GHz. The hermetic seal also allowed the coaxial cable to be cooled directly with liquid nitrogen with the sample mounted in vacuum, as shown in Fig. 5.6. The laser pulse illuminated the bridge through a quartz window about 30 mm from the sample. Since the coaxial cable had to be kept as short as possible to minimize losses, direct cooling of the cable with liquid nitrogen was necessary in order to reduce heating of the sample by thermal

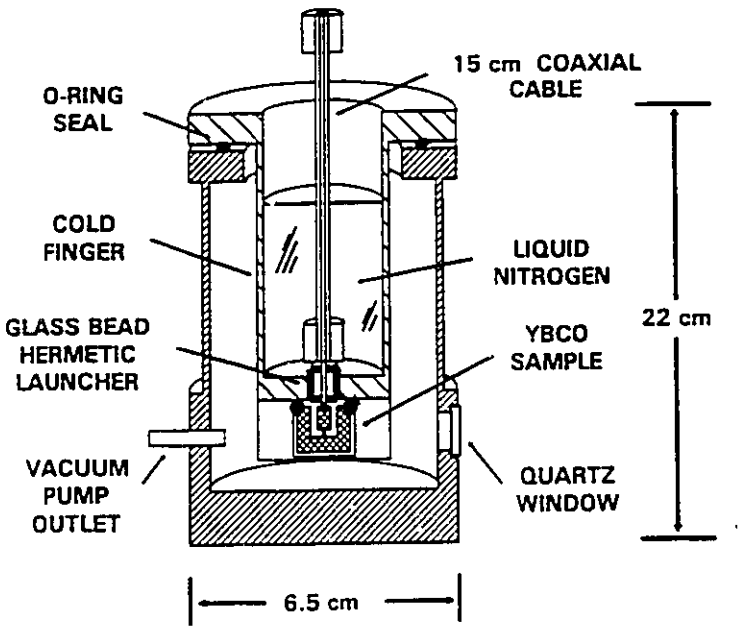

Fig. 5.6. Sample chamber used to cool samples with liquid nitrogen.

conduction through the coaxial line. The sample chamber was made as compact as possible for easy portability and cooled with liquid nitrogen only to demonstrate the viability of practical high speed YBCO photodetectors. As shown in Fig. 5.7, a bias-tee (0.1 to 60 GHz) allowed a bias current from a current source to be applied to the bridge. The bias-tee was also connected to a fast digital sampling scope (50 GHz) for direct observation of the fast voltage transients.

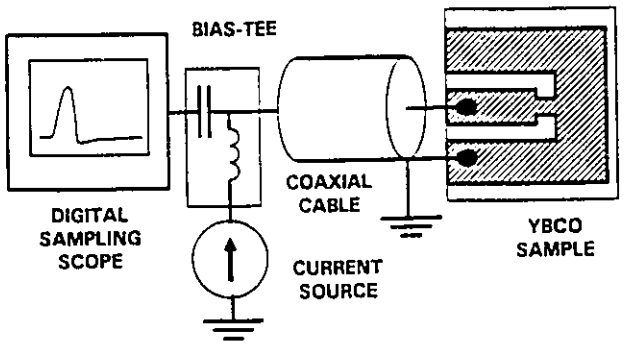

Fig. 5.7. High speed photoresponse measurement circuit.

In a typical experiment, wave forms were taken after 512 averages on the sampling scope, giving a voltage resolution of about 0.05 mV. Wave forms at positive and negative

bias currents were also taken and then subtracted to eliminate base-line effects on the scope. Since liquid nitrogen was used, all the measurements using this chamber were performed at a temperature of 77.4 K. The 5 ps, 820 nm laser pulses were focused onto the bridge at one end of the coplanar transmission line with a fluence of about 10 $\mu J/cm^2$. Examples of photoresponse signals can be seen in Papers C and D. With the sample biased in the resistive transition region, both fast and slow components were seen, as shown in Fig. 5.8 for a 135 nm film. As discussed in Sections 3.3 and 3.4, several other groups have seen photoresponse signals consisting of fast transients followed by slowly decaying components. Fig. 5.8 can be compared to the photoresponse signals seen by Semenov *et al.* in Fig. 3.6 or by Ghis *et al.* in Fig. 3.8(b). The slow component is consistent with a resistive bolometric response. For a 135 nm film, the thermal escape time should be about 13 ns at 77 K. The faster decay of about 3 ns observed for the slow component in Fig. 5.8 is due to the lower cutoff of the bias-tee of 0.1 GHz ($\tau_{fall} \approx 3.5$ ns).

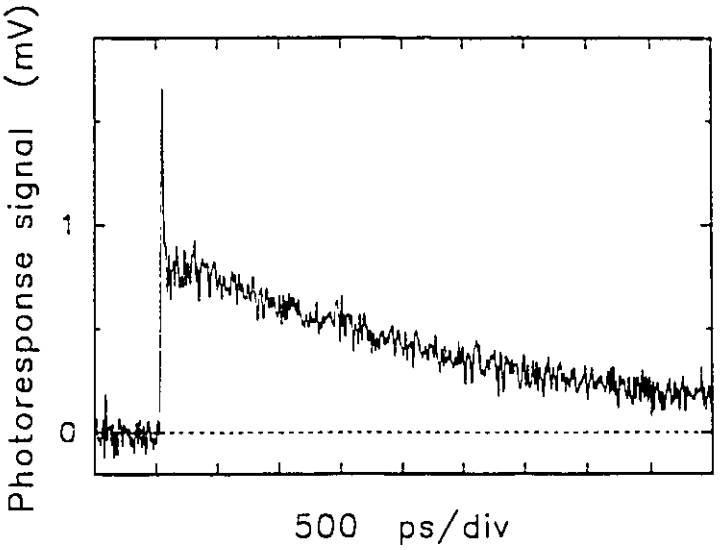

Fig. 5.8. Photoresponse signal from a 135 nm YBCO film with 5 ps laser pulses (Papers C and D). The bridge was biased in the resistive transition region, and so the slow component is due to a resistive bolometric response. The fast component is due to the KIB response. This wave form is very similar to those observed by other groups, as shown in Figs. 3.6 and 3.8.

Figure 5.9 compares the 16 ps wide transient seen from a 200 nm film (shown earlier in Fig. 1.3) to the response predicted by a simulation based on the KIB model (Fig. 4.4, Paper D). The KIB model gives a voltage transient with an amplitude of 1.38 mV and a width of 5 ps equal to that of the laser pulse. Limiting the simulation transient to a 50 GHz

bandwidth gives a voltage transient 11 ps wide with an amplitude of 0.69 mV. This is close to the observed photoresponse of about 1 mV. The discrepancy in the amplitudes may be due to errors in some estimates used for the parameters in the KIB model, such as the laser fluence (see Appendix C for a more detailed error analysis). Considering the simplicity of the KIB model, the predicted response is a surprisingly good estimate of the observed amplitude. This suggests that the observed photoresponse is predominantly due to an equilibrium response where $T_e = T_{ph}$. In other words, the electron-phonon energy relaxation time in YBCO films must be much shorter than 5 ps. This is discussed further in the next chapter.

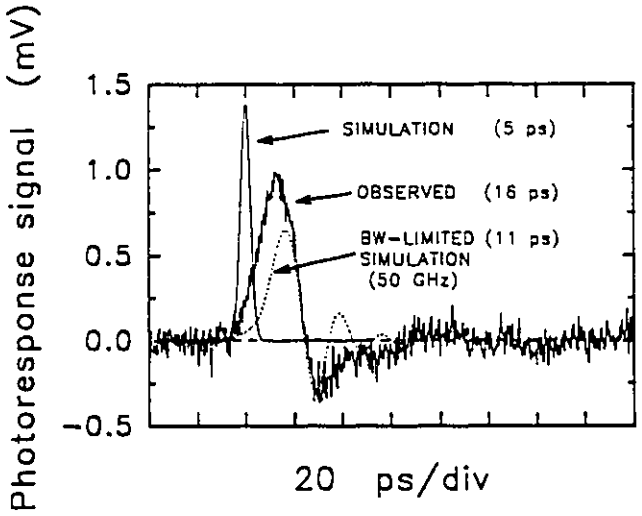

Fig. 5.9. Comparison of the observed photoresponse signal from a 200 nm film to a simulation based on the KIB model (solid line). (Papers C and D) The KIB model response has an amplitude of 1.38 mV and the same width as the laser pulse. The dashed line represents the KIB model response limited by the 50 GHz bandwidth of the oscilloscope resulting in a width of 11 ps and an amplitude of about 0.7 mV. This is very close to the amplitude of the observed response of about 1 mV.

Of course, as mentioned earlier deviations in the observed photoresponse from the KIB response could possibly be used to identify nonbolometric mechanisms. The amplitude of the observed signal in Fig. 5.9 is a little larger than the predicted response, but this may be due to the sensitivity of the KIB model to variations in the experimental parameters rather than any nonbolometric mechanism. What is curious in Fig. 5.9, however, is the negative going transient in the observed response with a decay of about 30 ps. As mentioned in section 3.4(c), a negative response due to changes in kinetic inductance signifies quasiparticle

recombination back into Cooper pairs. The negative signal in Fig. 5.9 may therefore be indicative of nonequilibrium quasiparticle recombination. The effect of dispersion from the limited bandwidth of the scope input alone is seen in the oscillations at the tail end of the bandwidth-limited simulation pulse in Fig. 5.9. Even though these oscillations have negative-going transients, there is no negative-going signal that has a decay over 30 ps. The effect of dispersion from the YBCO coplanar transmission line and time jitter in the trigger timing circuit for the scope, which were not included in the broadening of the simulation pulse, must also be considered in order to make any conclusions regarding nonbolometric or nonequilibrium mechanisms.

What is clear from this analysis is that a large part of the observed photoresponse with 5 ps laser pulses can be attributed to the KIB mechanism which is based on equilibrium heating of the YBCO film. The fact that the amplitude of the 20 ps wide photoresponse transients varied linearly with the bias current supports the KIB model (Papers C and D). This was seen in YBCO films with thicknesses ranging from 47 to 200 nm. We believe that nonequilibrium processes should appear with much shorter laser pulses, but it will be difficult to observe them directly on an oscilloscope. Suggestions for future experiments are given in the next chapter. At this point, our experimental results suggest that, despite claims made by other groups, there is no evidence for nonequilibrium processes over a 5 ps time scale in superconducting YBCO thin films.

6. DISCUSSION

6.1. Successes and limitations of the KIB model

The KIB model has been quite successful in explaining the origin of the fast photoresponse signals observed in our experiments. The temperature and bias-current dependence of the fast photoresponse are consistent with a KIB mechanism. As discussed in Sections 4.3 to 4.5, simplifying approximations made in the model do not adversely affect the validity of the model. Assuming uniform current and heat distributions within the film still provided reasonable estimates of the photoresponse amplitude. It was also found that the damping effect of the normal-fluid channel was not large and could be neglected when using 5 ps laser pulses. In the KIB model, there is no need to consider complicated nonequilibrium processes which rely on accurate knowledge of the nature of the superconducting order parameter in the material. Phonon trapping effects do not even play a role in observing a fast response since it is the rate of change of heating in the film by the laser pulse that determines the width of the photoresponse voltage transient. The fact that 16 ps wide signals were seen in 200 nm films emphasizes that ultrathin films ($d < 30$ nm) are not necessary to see a fast photoresponse signal.

The trend observed in the photoresponse experiments (Section 5.1) revealed that once the slow resistive bolometric signal had disappeared, the amplitude of the fast component that remained was linear with bias current. This is an extremely important observation since it eliminates the possibility of the fast photoresponse arising from some other nonbolometric mechanisms. For instance, the voltage generated by a photoactivated flux flow mechanism (section 3.4(a), Eq. (3.8)) is directly proportional to the magnetic field B and the velocity v of the vortices. Since both B and v (Eq. (3.7)) are proportional to the current density J, then the voltage response generated by photoactivated flux flow would have to vary as J^2. The observed voltage amplitude is linear with J, and so photoactivated flux flow cannot be used to explain the origin of the fast response. Furthermore, vortex pinning energies also decrease with current density,[211,253] and so one would expect voltage transients to increase even faster than J^2 for photoactivated flux flow.

In the case of photofluxonic detection (Section 3.4(a)), the width of the voltage

transient depends on the time for a vortex to cross the width of a bridge. At large bias currents, vortex velocities of the order of 5 x 10^5 m/s have been observed in flux flow devices at 77 K.[47,272] For a 10 μm wide bridge, the transit time would then be about 20 ps, which is the width of the voltage transient observed using 5 ps laser pulses in our experiments. Since Eq. (3.7) states that $v \propto J$, and Eq. (3.8) gives $V \propto v$, then the amplitude of the voltage transient should also be linear with current. However, the energy required to unbind vortex-antivortex pairs given in Eqs. (3.11) and (3.12) will be reduced as the bias current is increased[212,255] due to the Lorentz force (Eq. (3.5)). A reduced unbinding energy should increase the quantum response of the photofluxonic detection mechanism, which would lead to signals that increase faster than linear as the bias current is increased. The steady-state V-I characteristics of the Kosterlitz-Thouless transition are already very nonlinear,[255] and in general $V \propto I^{\alpha}$ where α is some constant greater than 1. The fact that the observed photoresponse signal in our experiments varied linearly with current eliminates the possibility of a photofluxonic detection mechanism as the origin of the fast photoresponse signal.

The linear dependence of the amplitude of the fast photoresponse signal with bias current also eliminates the possibility that the fast response is due to the film entering the resistive or the normal state, as suggested by Bluzer.[240] The resistive transition is very nonlinear with bias current, as seen in Papers B, C, and D. The slow component, which is due to a resistive response, increases faster than linear with bias current, as shown schematically by the dashed line in Fig. 5.3(b).

The most significant assumption made by the KIB model is equilibrium heating of the film by the laser pulse. The fact that the KIB model provides reasonably good estimates of the observed photoresponse amplitude using 5 ps laser pulses suggests that the electron-lattice interaction is fast enough in YBCO to allow a good approximation to equilibrium heating over this time scale. The negative-going component of the observed signal shown in Fig. 5.9 which is not present in the KIB simulation shown in Figs. 4.4 and 5.9 may be an indication of nonequilibrium recombination of quasiparticles back into Cooper pairs, but more work is needed to understand the characteristics of the coplanar transmission line structure in case dispersion effects are causing the negative response.

As discussed in section 3.4(b), Semenov *et al.*,[227,235] Gol'tsman *et al.*,[233] and Lindgren

et al.[230] have studied the photoresponse from YBCO films biased in the resistive state and using 20 ps laser pulses. They have concluded that nonequilibrium heating was taking place over the time scale of the laser pulse. Typical values for $\tau_{e\text{-}ph}$ in YBCO were around 1.5 ps, and the ratio of lattice to electronic heat capacities was $C_{ph}/C_e \approx 40$. Fig. 6.1 shows a simulation of the predicted response for the same conditions described in Figs. 4.4 and 5.9 but with nonequilibrium heating of the electron gas. In Fig. 6.1(b), the electron temperature changes by as much as 4.2 K before reaching equilibrium with the lattice just after the laser pulse with a total change in lattice temperature of 0.4 K. If the superfluid fraction depends on T_e as described in Fig. 6.1(c), then the rapid rise in kinetic inductance (Fig. 6.1(d)) as the electrons are heated produces a positive voltage transient with an amplitude of 33 mV, as shown in Fig. 6.1(e). As the electrons cool to the lattice, the kinetic inductance rapidly decreases resulting in a voltage signal with an amplitude of -29 mV. These transients are much larger than the 1.38 mV predicted by the KIB model in Fig. 4.4 as well as the observed response of about 1 mV shown in Fig. 5.9. The effect of the normal fluid component on this response is shown by the dashed line in Fig. 6.1(e), but has little effect on the amplitude. Limiting the response, with the effect of the normal fluid channel included, to a 50 GHz bandwidth results in a positive transient of 6.8 mV and negative transient of -9.0 mV. This cannot account for the observed response of about 1 mV, especially since the observed response did not exhibit such a pronounced negative transient. Thus a nonequilibrium model using $\tau_{e\text{-}ph} = 1.5$ ps and $C_{ph}/C_e = 40$ suggested by Semenov and coworkers does not seem to agree with our data, assuming that it is the electron temperature T_e which determines f_{SC}. However, even if the KIB model can provide reasonable estimates of the amplitude of the photoresponse signal with 5 ps laser pulses, it does not necessarily mean that nonequilibrium heating must be ruled out.

Large nonequilibrium electron temperatures will be obtained if C_{ph}/C_e is large. The electronic heat capacity is given by $C_e = \gamma T_e$, where γ is the Sommerfeld constant.[18,19] In copper, $\gamma \approx 0.097$ mJ/cm^{3}K^2 so that $C_{ph}/C_e \approx 120$ at room temperature and about 230 at 100 K.[19,143,144] Gold has similarly large heat capacity ratios.[19,147] Niobium, on the other hand, has a much larger value for γ of about 0.72 mJ/cm^{3}K^2 giving $C_{ph}/C_e \approx 10$ at room temperature.[19,141] Indeed, the heavy fermion compounds[273] exhibit some of the largest values for γ due to the extremely large electron effective masses. The value for γ in YBCO has

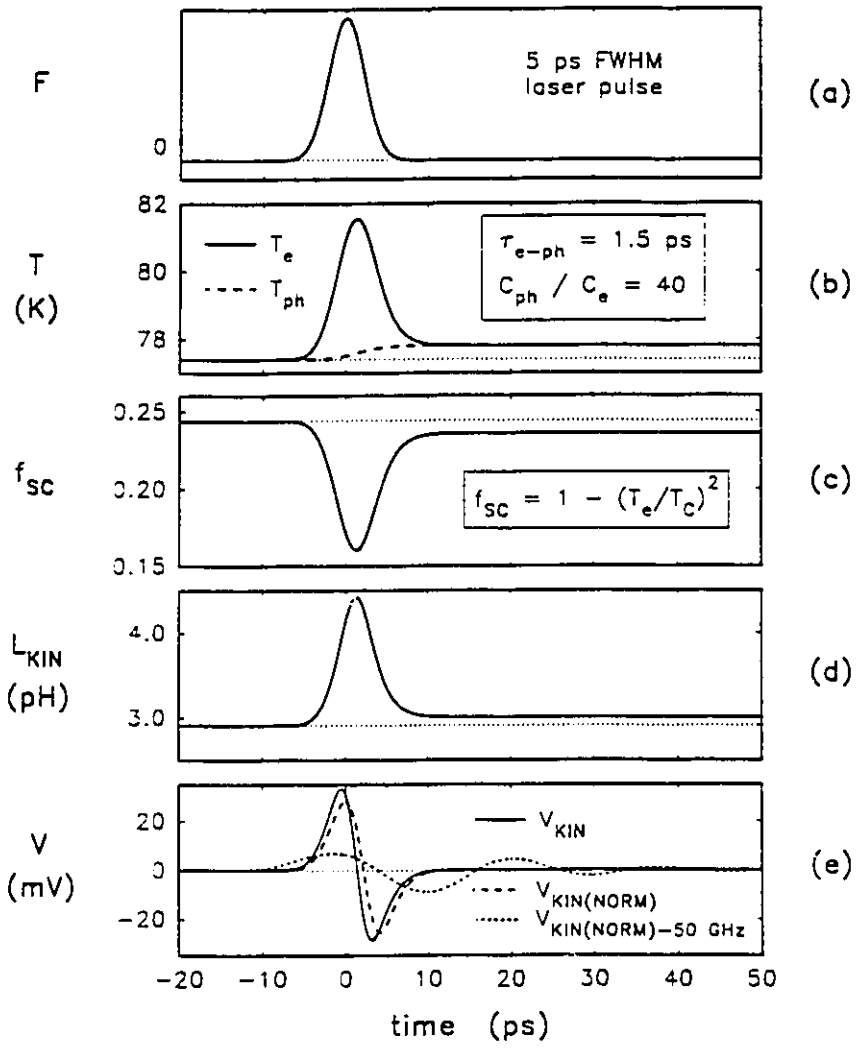

Fig. 6.1. Simulation of the voltage response for the same conditions as Figs. 4.4 and 5.9 but allowing for nonequilibrium heating with τ_{e-ph} = 1.5 ps and C_{ph}/C_e = 40. The nonequilibrium electron temperature T_e is shown in (b). Assuming that the electron temperature determines the superfluid fraction (c), then the kinetic inductance change (d) will produce (e) a large voltage signal (solid line) with positive and negative components which will be slightly attenuated by the normal-fluid channel (long dashes). The short-dashed line shows the response limited by the 50 GHz bandwidth of the oscilloscope. The nonequilibrium response is too large to account for the observed photoresponse in Fig. 5.9.

been studied by several groups,[17,274,275] and has an approximate value of 0.3 mJ/cm^{3}K^2 (~ 30 mJ/mole K^2). This gives C_{ph}/C_e = 30 at room temperature and about 40 from 70 K to 100 K. Below 70 K, C_{ph}/C_e decreases and C_e becomes dominant below 10 K. The extraction of γ from heat capacity data for YBCO can be obtained by looking at the jump in heat capacity ΔC at T_c or by subtracting the calculated phonon contribution. In a BCS superconductor, $\Delta C/\gamma T_c$ = 1.43, and γ has been obtained for YBCO using this relation.[17] The difficulty with this is the assumption of BCS superconductivity for the HTSCs, which

Table 6.1. Comparison of simulation results assuming nonequilibrium heating as in Fig. 6.1. The maximum change in T_{ph} was 0.4 K in all cases. The maximum change in the electron temperature T_e is shown to give an idea of the degree of the induced nonequilibrium. Results from the KIB model and observed response are shown for comparison..

			$V_{KIN(NORM)}$		**BW limited (50 GHz)**	
$\tau_{e\text{-}ph}$	C_{ph}/C_e	ΔT_e	V_{max}	V_{min}	V_{max}	V_{min}
(ps)		(K)	(mV)	(mV)	**(mV)**	(mV)
1.5	**40**	4.16	27.92	-25.69	**6.78**	-9.02
0.2	**40**	0.83	3.97	-2.33	**1.15**	-0.88
0.2	**30**	0.68	3.17	-1.53	**0.99**	-0.65
0.2	**20**	0.54	2.41	-0.79	**0.85**	-0.44
0.2	**10**	0.43	1.72	-0.16	**0.74**	-0.29
0.5	**10**	0.61	2.73	-1.10	**0.91**	-0.54
1.0	**10**	0.93	4.36	-2.66	**1.29**	-1.09
1.5	**10**	1.21	5.78	-3.86	**1.68**	-1.66
0.5	**20**	0.96	4.68	-3.03	**1.31**	-1.12
20	**0.8**	0.60	2.18	-0.32	**1.00**	-0.59
0.2	**0.5**	0.40	1.34	-0.0003	**0.69**	-0.24
KIB		0.40	1.34	-0.0003	**0.69**	-0.24
OBSERVED		--	--	--	1	-0.3

is still the subject of controversy (Section 2.1). The use of $C_{ph}/C_e = 40$ at temperatures between 70 K and 100 K by Semenov and coworkers is not unreasonable, but the accurate determination of γ in the HTSCs is still controversial.

Table 6.1 summarizes simulation results based on nonequilibrium heating as described in Fig. 6.1. The effect of the normal fluid fraction is included, and the amplitude of the signal limited to a bandwidth of 50 GHz is also given. Photoresponse signals close to the observed amplitude of about 1 mV are possible for $C_{ph}/C_e = 40$ if $\tau_{e\text{-}ph}$ is reduced to 0.2 ps. Reducing the heat capacity ratio allows larger relaxation times to be used to get the same result, such as $\tau_{e\text{-}ph} = 1.0$ ps and $C_{ph}/C_e = 10$, but this also results in the bandwidth-

limited wave form having a negative component which approaches the amplitude of the initial positive voltage transient. Such large negative transients were not seen in our experiments.

A fast electron-phonon relaxation time in YBCO would be consistent with the success of the KIB model for 5 ps laser pulses. Even though there is always some finite amount of nonequilibrium heating when laser pulses are absorbed in metals, the assumption of equilibrium heating will be a reasonable approximation if the following two conditions are met. First, it is necessary that $\tau_{e\text{-}ph} << \tau_p$, where τ_p is the width of the laser pulse. Second, the heat capacity ratio C_{ph}/C_e cannot be too large. From Table 6.1, it is seen that for $\tau_{e\text{-}ph}$ = 0.2 ps and C_{ph}/C_e = 40 there is still significant nonequilibrium heating with $\Delta T_{e(max)} \approx 2\Delta T_{ph(max)}$. On the other hand, reducing C_{ph}/C_e to 10 results in very little nonequilibrium heating with $\Delta T_e \approx \Delta T_{ph}$. Increasing the width of the laser pulse may not necessarily result in equilibrium heating either. Significant nonequilibrium heating will occur even for 70 ps laser pulses with $\tau_{e\text{-}ph}$ = 1.5 ps and C_{ph}/C_e = 40. However, experiments performed using 70 ps laser pulses produced photoresponse signals which were consistent with the approximation of equilibrium heating.

A short relaxation time in YBCO implies that energy relaxation due to the electron-phonon interaction must be very strong. This is certainly the case for Nb where $\tau_{e\text{-}ph} \approx 0.36$ ps, as discussed in Section 2.3. The pump-probe experiments by Brorson *et al.*[151] gave relaxation times in NbN limited by the duration of the 60 fs laser pulses used in the experiment. Photoemission experiments[149] using 30 ps laser pulses on tungsten and 2 ps laser pulses on zirconium showed no evidence for nonequilibrium electron heating in these materials. Only when 75 fs pulses were used did nonequilibrium heating become apparent in tungsten.[149] Pump-probe experiments on YBCO show fast relaxation times less than 0.5 ps in the normal state, as shown in Fig. 2.12(b). Many of the pump-probe results on YBCO reveal relaxation times less than 0.2 ps in the normal state. However, the observed relaxation times seem to increase to about 2 ps when cooled below T_C. The scattering time τ_S determined by microwave measurements (Fig. 2.4) also shows a sudden rise just below T_C, with a value of about 0.2 ps at 77 K.[95] Furthermore, this sudden drop in $1/\tau_S$ has been used as evidence to support the idea that the main scattering mechanism for electrons in YBCO is electronic in origin rather than due to the electron-phonon interaction.[95,276] The linear resistivity of most HTSC samples which extrapolates to zero at T = 0 is inconsistent

with an electron-phonon scattering mechanism and requires some other mechanism to account for it.[277] On the other hand, some groups believe that the electron-phonon interaction in the HTSCs is very strong and can even explain the high values for T_c [109,110] with strong coupling to 65 meV optical phonons.[278] Anomalous broadening of phonon lines investigated by Raman spectroscopy seem to indicate significant coupling of phonons to the electronic system.[279] The carriers which produce the broad absorption band observed in FIR spectroscopy and referred to as the mid-infrared band interact strongly with 52 meV phonons in YBCO producing a notch-like feature in the mid-infrared band.[276] The strength of the electron-phonon interaction in YBCO and the HTSCs is still a major source of controversy. What is needed for equilibrium heating in the KIB model to be a good approximation is efficient coupling of electrons excited by the laser pulse to the lattice so that the condition $T_e \approx T_{ph}$ can be maintained.

Finally, it is interesting that the value for T_c of the film used in the KIB simulations is the one obtained at low bias currents (i.e. $T_c = 89$ K) even though the measurements were taken at high bias currents with a broadened resistive transition and reduced T_c. In other words, despite the appearance of resistance in the bridge due to a large bias current below T_c, the superfluid fraction f_{sc} seems to be determined by the value of T_c for very low bias currents. This suggests that the bias-current-induced resistive broadening in YBCO bridges has no effect on the superfluid fraction in the bridge, which may provide insight into the dissipation mechanism responsible for such broadening.

6.2. Characteristics of a high speed photodetector based on the KIB model

A YBCO thin film photodetector based solely on the KIB model would produce voltage transients the same width as the incident laser pulse and with amplitudes which increased as the laser pulse width decreased. Unlike semiconductor detectors, a KIB photodetector would be sensitive to a broad range of wavelengths from the UV to the FIR region. The KIB detector is also extremely simple to make, since it has only a single YBCO layer and a single gold contact layer which can both be processed very easily. The sensitive area at the YBCO bridge can also be made larger than that of fast semiconductor detectors, which makes optical alignment easier. Light hitting the edges of the bridge will not affect the performance of the device, unlike some fast semiconductor detectors where carriers

generated in low-field regions take longer to be swept out of the device. The response time of the KIB detector will normally be limited by the bandwidth of the measuring electronics, transmission lines, and connectors, as is the case for semiconductor photodetectors. Since ultrathin films are not needed, good quality films with thicknesses around 100 nm can be used. For operation at 77 K, the bias current can be increased to make the bridge enter the resistive region. This will make the photoresponse signals quite large (and with long decays) so that the alignment procedure can be made easier. Once the device has been aligned, the bias current is reduced to the point where the slow resistive component disappears leaving behind only the fast component. The disadvantages of a KIB photodetector compared to semiconductor detectors is the requirement for cooling to 77 K, which makes the detector housing physically larger than most semiconductor devices. The KIB detector is also much less sensitive (about 10^4 times) than a semiconductor detector. Also, since the voltage response from a KIB detector relies on changes in kinetic inductance in the bridge, the KIB detector can only respond to pulsed light. The fact that the responsivity is so low requires that only laser pulses with enough intensity be used (i.e. 0.1 nJ for ~ 1 ps pulses, and 1 nJ for longer pulses). The KIB detector would not be practical for laser pulses longer than 100 ps, unless low-noise, high-gain , and broadband amplifiers are added. Since most laser systems have high repetition rates (i.e. 76 to 100 MHz), the average laser power for 0.1 to 1 nJ per pulse is large enough to significantly increase the average temperature of the sample. This, however, will not affect the response time of the KIB detector even though the thermal escape time is of the order of the time between laser pulses. Recently, fast 20 ps transients without any slow components were observed from a 100 nm film using 5 ps laser pulses at a repetition rate of 76 MHz and an average power of about 10 mW.

The fundamental limit in the response time of a KIB detector is determined by dissipation in the normal-fluid channel of the bridge. As shown in Fig. 4.6, attenuation by the normal-fluid channel imposes a limit in the response time of about 0.5 to 1 ps. The response time can be decreased further if the scattering rate $1/\tau_s$ is increased, as is the case for thin films compared to single crystals (see Fig. 2.4). The responsivity of the detector is also reduced by the attenuating effect of the normal channel. However, the effect of the normal fluid channel will be significant only for pulses shorter than a few picoseconds for operation at 77 K. For shorter pulses, nonequilibrium effects will become significant and the

KIB model will no longer be valid.

6.3. Suggestions for future experiments

The controversy surrounding the origin of the fast photoresponse observed in YBCO epitaxial thin films is by no means over. The KIB model has provided some new insight, but many questions still remain. The experimental data with 100 ps pulses presented in Paper B was limited to a 1 GHz bandwidth. It would be useful to improve on those measurements by looking at the temperature dependence again but with a 20 GHz system. This would allow a more accurate determination of the photoresponse amplitude as a function of temperature for a more precise comparison with the KIB model. Extending the range to lower temperatures would help in distinguishing between the various postulated temperature-dependencies of the superfluid fraction as shown in Fig. 2.3. Such data could be used to extract the temperature dependence of the penetration depth in the YBCO film. A temperature dependence of the photoresponse from 5 ps laser pulses would also be very useful in order to examine more closely the origin of the negative component in the observed response. This could be accompanied by more accurate modelling of the characteristics of the coplanar transmission line. Studying the photoresponse signal as a function of laser pulse width might reveal the onset of nonequilibrium processes. Finally, subpicosecond pulses could be used to investigate nonequilibrium effects. The fast voltage transients could be probed by electro-optic techniques (Section 1.4). Pump-probe measurements could be done simultaneously with electrical transient measurements to better understand nonequilibrium phenomena in YBCO films.

7. CONCLUSIONS

The photoresponse of epitaxial YBCO thin films has been investigated using 100 ps and 5 ps laser pulses. Both fast and slow components are observed in the photoresponse signals. We have seen a trend in the shape of the photoresponse wave form as a function of temperature and bias current. At temperatures or bias currents well within the resistive region of the bridge, only a slow component is observed. As the temperature or bias current is lowered, the amplitude of the slow component decreases and a fast component appears on top of the rising edge of the slow component. At temperatures below the resistive region, only the fast component is observed. The slow component, which has a decay time over several nanoseconds, is attributed to a resistive bolometric response. The fast component has a width in the subnanosecond range. Transients as fast as 16 ps wide have been seen from a 200 nm YBCO film, which is the fastest photoresponse transient observed directly with an oscilloscope from epitaxial YBCO films. We are also the first group to have observed fast photoresponse signals less than 100 ps wide which were not followed by a slow component in the wave form. This has enabled us to clearly identify the resistive bolometric response.

We attribute the origin of the fast component to a kinetic inductive bolometric (KIB) mechanism. The KIB model has provided excellent qualitative and reasonable quantitative agreement with the temperature and bias-current dependence of the observed photoresponse. The KIB model assumes equilibrium heating by the laser pulse such that the electron and lattice temperatures are approximately equal. The decrease in superfluid fraction from the change in temperature induced by the laser pulse increases the kinetic inductance of the bridge. A voltage transient is generated while the kinetic inductance is changing, which produces photoresponse signals the same width as the laser pulse. The amplitude of the photoresponse signal will also increase if the duration of the laser pulse is made shorter. However, the attenuating effect of the normal fluid channel will limit the ultimate response time to just under 1 ps.

The response to 5 ps laser pulses can be adequately modelled by the KIB mechanism. This implies that there is little nonequilibrium heating over the time scale of the 5 ps laser

pulse, which suggests that the coupling between excited electrons and the lattice must be strong. A predominantly equilibrium response over a 5 ps time scale is not consistent with claims made by other groups that nonequilibrium heating was seen using 20 ps laser pulses.

The KIB model is also the first bolometric (equilibrium) model used to explain the origin of subnanosecond photoresponse transients from YBCO films. We do not claim that nonbolometric mechanisms will not occur with shorter laser pulses. However, we do claim that the fast voltage transients observed in our experiments with 5 ps laser pulses are not consistent with transient flux dynamics mechanisms or large nonequilibrium electron heating. Nonequilibrium heating will always occur to some degree, but the approximation of equilibrium heating made by the KIB model seems to be reasonable for 5 ps laser pulses. The photoresponse signals observed for 5 ps laser pulses show possible signs of nonequilibrium effects in the negative part of the response, but more work is needed in characterizing dispersion effects in the coplanar transmission line to see if the negative response is real.

The only way to probe nonequilibrium mechanisms directly on a faster time scale will be to use electro-optic sampling techniques which will allow picosecond voltage transients to be measured. With the sample cooled well below T_C, it is possible for 100 fs laser pulses to induce nonequilibrium electron temperatures which can easily exceed T_C. If the superfluid fraction is determined by the electron temperature, then such transients in the electron temperature will cause the sample to enter the normal state. This has already been explored by other groups, but no one has looked at the voltage transients by electro-optic sampling. Plans are currently under way to perform such measurements.

APPENDIX A

YBCO film growth and processing

Film growth by laser ablation:

The YBCO films were grown epitaxially by laser ablation on $LaAlO_3$ substrates with the c-axis perpendicular to the substrate.[24] The laser source consisted of a KrF excimer laser (Lumonics EX-700; $\lambda = 249$ nm) which provided energy densities of about 2 $\mu J/cm^2$ at a YBCO target inside the chamber. The repetition rate of the laser was 2 Hz, and the laser pulse duration was about 30 ns. The substrates were typically 6 mm x 6 mm x 0.5 mm (0.020"), and were cleaned with acetone and methanol before being mounted with gold paste on the surface a furnace inside the laser ablation chamber. After reaching a vacuum of about 2×10^{-6} Torr, the heater in the furnace was turned on and 300 mTorr of oxygen was admitted into the chamber. The YBCO target had a diameter of 1" and was rotated so that new material could be exposed to each new laser pulse. With a shutter in the closed position in front of the heated substrate, a cleaning run of the target was made by ablating material from the target for one full rotation. Once the furnace had stabilized at 790 ^{0}C, the shutter was opened and material from the YBCO target was deposited onto the substrate. At a pulse repetition rate of 2 Hz, the deposition time was typically 13 minutes for a 200 nm film, or about 15 nm/min. After deposition, the furnace was turned off and the sample allowed to cool in 0.5 atm of oxygen.

Since the $LaAlO_3$ substrates were highly twinned, the epitaxial YBCO films were also twinned. Nevertheless, the YBCO films had excellent values for T_c of around 90 K and high critical current densities at 77 K of more than 10^6 A/cm^2. In appearance, the YBCO films are black and almost opaque for thicknesses around 200 nm.

Film processing:

Processing of the YBCO films consisted of patterning the films using standard photolithographic techniques and a wet chemical etch, followed by deposition of gold for

contact pads with subsequent annealing. The processing procedure has been modified over the past few years as new techniques and experience were acquired. Some of the processing steps and techniques mentioned below were developed by other members of our group, namely Darcy Poulin and Steve Moffat. The processing is also dependent on the specific photoresist and developer available in the clean room. We currently use Shipley's microposit 1400-33 positive photoresist. The developer, which must be diluted with 5 parts de-ionized (DI) water, is Shipley's microposit MF-351. The following is a description of the currently recommended procedure developed by our group for processing YBCO thin films.

Patterning of YBCO layer:

- clean sample with acetone and methanol in ultrasound
- mount sample on 1" diam. glass cover slip using crystal bond (120 ^{0}C on hot plate)
- spin on photoresist at 5000 rpm for 30 s. ($\approx$ 1μm thick)
- soft bake at 120 ^{0}C for 2 minutes (recent alternative: 90 ^{0}C for 90 s)
- position sample in mask aligner (Karl Suss MJB3) under mask for YBCO layer
- expose for 10 s
- develop for 30 s
- rinse with DI water and blow dry with N_2
- hard bake at 140 ^{0}C for 6 minutes (recent alternative: 110 ^{0}C for 2 minutes)
- etch YBCO layer in acid solution. There are two possible wet etches:
    1) 0.1mL HCl and 0.1mL HNO_3 in 200 mL DI water which can etch a 200 nm in about 20 s, or
    2) a 0.001 M citric acid solution with an etch time of about 6 minutes
- rinse in DI water for 15 to 30 s, blow dry with N_2
- remove photoresist with spray of acetone and then methanol.
- place sample in oxygen plasma barrel etcher for 3 min at 100 W to remove remaining photoresist and other organics from surface
- inspect sample under microscope

Opening of contact pads on top of YBCO layer

- spin on photoresist at 5000 rpm for 30 s
- let air dry for at least 10 minutes
- soft bake at 80 ^{0}C for 1 minute
- position sample in mask aligner under mask for gold contact pads
- expose 30 s to 1 minute (depending on size of contact pads)
- now proceed 1 sample at a time with the following steps:
    - soak 6 minutes in toluene to harden the top surface of the photoresist
    - blow dry with N_2
    - develop for about 90 s to make sure that photoresist is undercut
    - rinse in DI water and blow dry with N_2
- leave photoresist on for deposition of gold

Gold deposition, lift-off, and annealing

- mount samples in gold evaporator unit
- deposit about 200 nm of gold
- remove samples from evaporator and soak in petri dish filled with acetone
- photoresist will dissolve and gold will be lifted off from areas outside of the contact pads. Slight agitation of the films with a cotton swab will speed up the lift off process
- remove samples from glass cover slips (crystal bond will dissolve in acetone)
- spray clean samples in acetone and methanol (do not use ultrasound or else gold pads might come off the YBCO film)
- place samples in barrel etcher for final cleaning (3 minutes at 100 W)
- anneal samples for 30 minutes at 400 ^{0}C in flowing oxygen (1 atm.)
- test room-T resistance of YBCO bridges to see if resistivity is about 400 $\mu\Omega$ cm

The sample processing had little effect on the original T_C and J_C measured with the unpatterned films. T_{C0} for bridges 200 μm long and 10 μm wide was typically around 89 K, and J_C was greater than 10^6 A/cm^2. Films with thicknesses less than 100 nm seemed to suffer more degradation of superconducting properties after processing.

The processing steps are continuously being modified. The HCl / HNO_3 etch is very fast and results in poor side wall definition in the bridges. The citric acid etch, recently introduced by Darcy Poulin, produces smoother edges. Forcing nitrogen bubbles through the citric acid solution while the samples are being etched removes CO_2 dissolved in the DI water which can otherwise degrade the superconducting properties of the films. More work is needed to identify processing steps which enhance or degrade the film properties.

APPENDIX B

Heat transfer analysis for YBCO thin films

A simplified thermal model :

As discussed in Sections 1.4 and 3.1, correct thermal modelling is essential in order to distinguish between thermal and nonthermal photoresponse signals from YBCO thin films. In its simplest form, heat absorbed in a YBCO strip at a temperature T_{YBCO} is transferred to the underlying substrate through a thermal boundary resistance R_{BD} at the interface. It is assumed that the substrate is at a constant temperature T_{SUB} equal to that of the heat sink T_0, and so diffusion effects in the substrate are neglected. The equivalent thermal model is shown in Fig. B1. Two cases are considered: 1) continuous heating of the YBCO strip by a constant power P, and 2) transient heating of the YBCO strip by energy absorbed from a laser pulse. Specific considerations for photoresponse experiments will be discussed, and a comparison between thermal and electrical parameters is given to help in understanding thermal analysis.

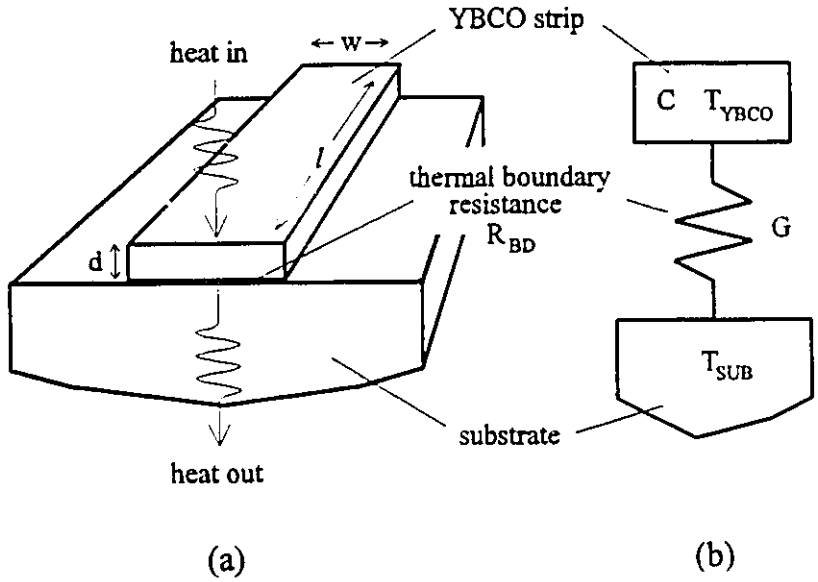

Fig. B1. (a) YBCO strip on substrate and (b) simplified equivalent thermal model.

1) Continuous heating of the YBCO strip

We wish to find the time evolution of the temperature T_{YBCO} of the YBCO strip when a continuous power P is applied to the strip after time t = 0. At time t = 0, $T_{YBCO} = T_{SUB}$ such that $\Delta T = T_{YBCO} - T_{SUB} = 0$. It is assumed that $T_{SUB} = T_0$ and is constant for all times. The total power dissipated in the strip is

$$P_{TOTAL} = P_{IN} - P_{OUT}$$

and so

$$C \frac{\Delta T}{\Delta t} = P - G \Delta T$$

$$\frac{d T_{YBCO}}{dt} = \frac{P}{C} - \frac{G}{C} \Delta T$$

which has a solution for ΔT given by

$$\Delta T = \frac{P}{G} (1 - e^{-t/\tau}) \qquad \text{(B1)}$$

The thermal time constant for heating the strip is

$$\tau = \frac{C}{G} = R C \qquad \text{(B2)}$$

where C is the heat capacity, G is the thermal conductance, and R is the thermal resistance (R = 1/G). Units for these parameters can be found in the last section of this appendix. After several time constants ($t >> \tau$), the maximum temperature reached by the film for a constant power dissipation P is

$$\Delta T_{MAX} = \frac{P}{G} = R P \qquad \text{(B3)}$$

If the input power P is switched off, the temperature in the YBCO film will equilibrate with

that of the substrate with the same time constant given in Eq. (B2).

The thermal boundary resistance R_{BD} at the film-substrate interface is related to the thermal resistance R by

$$R = \frac{R_{BD}}{A} \tag{B4}$$

where $A = w\,l$ is the area of the interface between the strip and the substrate. Combining Eq. (B4) with Eq. (B3) gives

$$\boxed{\Delta T_{MAX} = \frac{R_{BD}\,P}{A}} \tag{B5}$$

For example, if P = 100 mW is dissipated in a bridge with a width of 20 μm and a length of 200 μm, then Eq. (B5) gives $\Delta T = 2.5$ K using $R_{BD} = 10^{-3}$ Kcm^2/W (Section 3.1). However, the temperature of the sample is usually measured with a transducer near the sample but in thermal contact with the heat sink at temperature T_0. The thermal resistance for heat transport across the substrate material to the heat sink can add an extra thermal gradient between the temperature reading at the transducer and the temperature of the YBCO strip. We have measured ΔT between the YBCO strip and the temperature transducer as a function of the power P dissipated in the YBCO strip. This provided an effective thermal boundary resistance of $R_{BD(effective)} \approx 9 \times 10^{-3}$ Kcm^2/W which can be used in place of R_{BD} in Eq. (B5) to give a temperature difference of

$$T_{YBCO} - T_0 = \frac{R_{BD\ (effective)}\,P}{A} \tag{B6}$$

For 100 mW dissipated in a 20 μm x 200 μm bridge, Eq. (B6) predicts a temperature increase of the YBCO strip above T_0 of 22.5 K. If the heat sink is at $T_0 = 77.4$ K, then the final temperature of the YBCO strip would be about 100 K, which is well above T_C.

2) Transient heating of the YBCO strip

A laser pulse with energy E_0 incident on a YBCO film will be partially reflected and transmitted. Assuming that there is no reflection from the film-substrate interface and no multiple reflections within the film, the energy E_{ABS} absorbed in the strip is given by

$$E_{ABS} = E_0 - R E_0 - (1 - R) E_0 e^{(-d/\delta)}$$

where R is the reflectance and δ is the optical penetration depth. This simplifies to

$$\frac{E_{ABS}}{E_0} = (1 - R)(1 - e^{-d/\delta})$$

which is about 0.8 for a 200 nm film (R = 0.1, δ = 90 nm). The temperature transient induced by the laser pulse in the YBCO strip is then ($\tau_P \ll \tau$)

$$\Delta T = \frac{\Delta E_{ABS}}{C} = \left(\frac{E_{ABS}}{E_0}\right) \frac{E_0}{C_V\, l\, w\, d}$$

$$\boxed{\Delta T = \left(\frac{E_{ABS}}{E_0}\right) \frac{F}{C_V\, d}} \qquad \text{(B7)}$$

where $F = E_0 / l\, w$ is the incident laser fluence in $\mu J/cm^2$ and $C_V = C/V$ is the specific heat capacity of the YBCO strip in J/cm^3K. A plot of C_V as a function of temperature can be found in Paper B. For a 200 nm film with a laser fluence of 10 $\mu J/cm^2$, Eq. (B7) gives $\Delta T = 0.4$ K. From Eqs. (B2) and (B4), the thermal escape time from the film will then be

$$\boxed{\tau = R_{BD}\, C_V\, d} \qquad \text{(B8)}$$

which is about 20 ns for a 200 nm film.

Considerations for photoresponse experiments

One of the major concerns in transient photoresponse experiments is that the average power P from the laser source will raise the average temperature of the strip above that of the temperature transducer at T_0. The average laser power is given by $P = E_0 f$, where f is the repetition rate of the laser. For 100 ps laser pulses (Paper B), a fluence of about 100 $\mu J/cm^2$ is needed to see a fast photoresponse signal, or about 4 nJ in a spot size of 20 μm x 200 μm. At a repetition rate of 76 MHz with 4 nJ per pulse, the average laser power is about 300 mW, or 7500 W/cm^2 in the laser spot. For a 200 nm film, the absorbed power is about 6000 W/cm^2 ($E_{ABS}/E_0 = 0.8$) so that Eq. (B6) gives a temperature increase in the YBCO film of 54 K using $R_{BD(effective)} = 9 \times 10^{-3}$ Kcm^2/W. This is, of course, unacceptable for photoresponse experiments with YBCO operating at 77 K. Maintaining the same laser fluence, the average laser power can be reduced by decreasing the repetition rate of the laser source. In our experiments, a pulse picker was used to reduce the repetition rate from 76 MHz to 12 kHz for 100 ps pulses or 38 kHz for 5 ps laser pulses. This decreases the average laser power by more than 2000 times from its value at 76 MHz, which allows accurate measurements of the sample temperature from the transducer reading alone.

It is also important to keep the contact resistance R_C as low as possible to avoid heat dissipation at the contact pads when a bias current is applied to the bridge. The total R_C is typically less than 0.5 Ω at 77 K. If I = 100 mA and $R_C = 0.5$ Ω, then $P = I^2R_C = 5$ mW, which will not significantly increase the temperature of the film since the area of the contact pads is much larger than that of the bridge.

As a final note, we have recently observed 20 ps wide transients from a 100 nm film using 5 ps laser pulses at a repetition rate of 76 MHz and an average laser power of 5 to 10 mW. This has confirmed that even though the time between laser pulses is of the order of the thermal escape time, the speed of the response remains unchanged. This is because the average laser power only increases the average temperature of the film above that of the heat sink. To predict the response according to the KIB model, the temperature of the film is calculated using Eq. (B6) rather than using the reading from the transducer at T_0.

Comparison between thermal and electrical parameters:

Table B1 below provides a list of thermal parameters and units with the corresponding electrical parameters. The analogy helps in understanding some of the formulas used in thermal analysis.

Table B1. Comparison of thermal and electrical parameters.

Thermal parameter			Corresponding electrical parameter		
symbol	units	description	symbol	units	description
T	[K]	temperature	V	[V]	voltage
E, Q	[J]	heat energy	Q	[C]	charge
P	[W]	power	I	[A]	current
P	[W/cm^2]	power density	J	[A/cm^2]	current density
∇T	[K/m]	temp. gradient	E	[V/m]	electric field
C	[J/K]	heat capacity	C	[F=C/V]	capacitance
κ	[W/cmK]	conductivity	σ	[$\Omega^{-1}m^{-1}$]	conductivity
G	[W/K]	conductance	S	[Ω^{-1}]	conductance
R	[K/W]	resistance	R	[Ω]	resistance
R_{BD}	[Kcm^2/W]	boundary res.	R_C	[Ωcm^2]	contact resistance
$\Delta T = P / G = R P$			$\Delta V = I R$		
$P = \kappa \nabla T$			$J = \sigma E$		
$\tau = C / G = R C$			$\tau = R C$		

APPENDIX C

Sensitivity of KIB model to variations in parameters

Variations in experimental parameters:

The simulation of the KIB model shown in Fig. 4.4 for a 200 nm film exposed to 5 ps laser pulses results in a photoresponse amplitude of about 1.38 mV. Most of the parameters put into the KIB simulation are experimental values such as the laser fluence, bridge thickness, etc. Table C1 below shows how variations in these parameters affect the amplitude of the voltage transient predicted by the KIB model. It seen that :

- the most sensitive experimental parameters are T_{C0} , T_i , d , and ω_P,
- the least sensitive experimental parameters are δ and R, and
- parameters for which $\delta x/x = |\delta V/V|$ are F, I, τ_p, l, and w.

Table C1. Change in voltage amplitude V_{KIN} predicted by the KIB model simulation of Fig. 4.4 for large variations (δx) in experimental parameters (x). The KIB model predicts $V_{KIN}(x) = 1.38$ mV .

x		δx		$V_{KIN}(x+\delta x)$	$V_{KIN}(x-\delta x)$	$-\delta V_{KIN}$
T_{C0}	89 K	± 2 K	± 2.2 %	1.98 mV	1.02 mV	± 35 %
T_i	77.4 K	± 2 K	± 2.6 %	1.95	1.04	± 33 %
F	10 μJ/cm^2	± 3 μJ/cm^2	± 30 %	1.81	0.96	± 30 %
δ	90 nm	± 20 nm	± 22 %	1.29	1.46	∓ 6 %
R	0.1	± 0.05	± 50 %	1.30	1.46	∓ 6 %
I	75 mA	± 5 mA	± 6.7 %	1.47	1.29	± 7 %
τ_p	5 ps	± 1 ps	± 20 %	1.15	1.72	∓ 21 %
l	35 μm	± 5 μm	± 14 %	1.57	1.18	± 14 %
w	10 μm	± 2 μm	± 20 %	1.15	1.72	∓ 21 %
d	200 nm	± 20 nm	± 10 %	1.16	1.65	∓ 18 %
ω_P	1.67x10^{15} s^{-1} (1.10 eV)	± 0.17x10^{15} s^{-1} (± 0.11 eV)	± 10 %	1.14	1.71	∓ 20 %

Despite the sensitivity of the KIB model to T_{C0}, T_i, d, and ω_P, the KIB model provides reasonable quantitative agreement with the observed photoresponse. The most sensitive parameters are T_{C0} and T_i ($T_i \approx 77$ K). T_{C0} can be determined to within 0.2 K. For $T_{C0} = 89.0 \pm 0.2$ K ($\pm$ 0.22 %), the KIB model gives $V_{KIN} = 1.38 \pm 0.05$ mV ($\pm$ 3.6 %) which is the noise level of photoresponse wave forms observed in our experiments.

Variations in adjustable parameters :

The KIB model simulation shown in Fig. 4.4 assumes that the superfluid fraction varies as $f_{SC} = 1-t^2$, where $t = T/T_C$ is the reduced temperature. Table C2 shows how the KIB simulation amplitude is affected by the form chosen for the temperature dependence f_{SC}. Some common forms for f_{SC} are seen in Fig. 2.3. The corresponding amplitudes of the voltage transients calculated with the KIB model are also provided. For the results shown in Table C2, the temperature of the film is at 77 K and so the BCS result gives the same value as that for a $1 - t^2$ dependence. This can be understood by the similarity between the BCS and the $1 - t^2$ curve near 77 K in Fig. 2.3. The temperature dependence of the photoresponse amplitude over a much broader range of temperatures would allow identification of the correct form for f_{SC}.

Table C2. Dependence of the KIB simulation amplitude on the variation of the superfluid fraction.

superfluid fraction variation	V_{KIN} (mV)
$f_{SC} = 1 - t$	2.77
$f_{SC} = 1 - t^2$	1.38
$f_{SC} = 1 - t^4$	0.68
f_{SC} : BCS	1.38
f_{SC} : Hardy *et al.*[88]	0.78

REFERENCES

History of superconductivity

1. **H. Kamerlingh Onnes**, Comm. Physical Lab., Univ. of Leiden, Suppl. 34b to 133-144 (1911).
2. **J. R. Gavaler**, Appl. Phys. Lett. 23, 480 (1973).
3. **J. G. Bednorz and K. A. Muller**, "Possible high T_C superconductivity in the Ba-La-Cu-O system", Z. Phys. B 64, 189 (1986).
4. **M. K. Wu**, J. R. Ashburn, C. J. Torng, P. H. Hor, R. L. Meng, L. Gao, Z. J. Huang, Y. Q. Wang, and C. W. Chu, "Superconductivity at 93 K in a new mixed phase Y-Ba-Cu-O compound system at ambient pressure", Phys. Rev. Lett. 58, 908 (1987).
5. **H. Maeda**, Y. Tanaka, M. Fukutomi, and T. Asano, "A new high-T_C oxide superconductor without a rare earth element", Jap. J. Appl. Phys. Lett. 27, L209 (1988).
6. **Z. Z. Sheng**, W. Kiehl, J. Bennett, A. El Ali, D. Marsh, G. D. Mooney, F. Arammash, J. Smith, D. Viar, and A. M. Hermann, "New 120 K Tl-Ca-Ba-Cu-O superconductor", Appl. Phys. Lett. 52, 1738 (1988).
7. **A. Schilling**, M. Cantoni, J. D. Guo, and H. R. Ott, Nature 363, 56 (1993).

   L. Gao, Z. J. Huang, R. L. Meng, J. G. Lin, F. Chen, L. Beauvais, Y. Y. Xue, and C. W. Chu, Physica C 213, 261 (1993).

   L. Gao, Y. Y. Xue, F. Chen, Q. Xiong, R. L. Meng, D. Ramirez, C. W. Chu, J. H. Eggert, and H. K. Mao, "Superconductivity up to 164 K in $HgBa_2Ca_{m-1}Cu_mO_{2m+2+\delta}$ (m = 1, 2, and 3) under quasihydrostaticpressures", Phys. Rev. B 50, 4260 (1994).
8. **J. Bardeen, L. N. Cooper, and J. R. Schrieffer,** "Theory of Superconductivity", Phys. Rev. 108, 1175 (1957).
9. **P. L. Richards and M. Tinkham**, "Far-infrared energy gap measurements in bulk superconducting In, Sn, Hg, Ta, V, Pb, and Nb", Phys. Rev. 119, 575 (1960).

FIR properties of HTSCs and energy gap

10. **T. Timusk and D. B. Tanner**, "Infrared properties of high-T_C superconductors", in *Physical Properties of High Temperature Superconductors I*, ed. D. M. Ginsberg (World Scientific, Singapore, 1989), p. 339. See also

K. Kamarás, S. L. Herr, C. D. Porter, N. Tache, D. B. Tanner, S. Etemad, T. Venkatesan, E. Chase, A. Inam, X. D. Wu, M. S. Hegde, and B. Dutta, "In a clean high-T_C superconductor you do not see the gap", Phys. Rev. Lett. 64, 84 (1990).

J. Orenstein, G. A. Thomas, A. J. Millis, S. L. Cooper, D. H. Rapkine, T. Timusk, L. F. Schneemeyer, and J. V. Waszczak, "Frequency and temperature dependent conductivity in $YBa_2Cu_3O_{6+x}$ crystals", Phys. Rev. B 42, 6342 (1990).

F. Gao, G. L. Carr, C. D. Porter, D. B. Tanner, S. Etemad, T. Venkatesan, A. Inam, B. Dutta, X. D. Xu, G. P. Williams, and C. J. Hirschmugl, "Far-infrared transmittance and reflectance studies of oriented $YBa_2Cu_3O_{7-\delta}$ thi films", Phys. Rev. B 43, 10383 (1991).

D. Miller, P. L. Richards, S. Etemad, A. Inam, T. Venkatesan, B. Dutta, X. D. Wu, C. B. Eom, T. H. Geballe, N. Newman, and B. F. Cole, "Correspondence between microwave and submillimeter absorptivity in epitaxial thin films of ", Phys. Rev. B 47, 8076 (1993).

- - - - -

11. **C. J. Gorter and H. G. B. Casimir**, Physica 1, 306 (1934).
12. **J. P. Carbotte**, "Properties of boson exchange superconductors", Rev. Mod. Phys. 62, 1027 (1990).

General books on superconductivity

13. **M. Tinkham**, *Introduction to Superconductivity*, (Robert E. Krieger, Malabar, FL., 1980).
14. **A. C. Rose-Innes and E. H. Rhoderick**, *Introduction to Superconductivity*, (Pergamon, Oxford, 1978).

15. **T. Van Duzer** and C. W. Turner, *Principles of superconductive devices and circuits*, (Elsevier, New York, 1981).

16. **J. D. Doss**, *Engineer's guide to high-temperature superconductivity*, (Wiley, New York, 1989).

17. **G. Burns**, *High-temperature superconductivity: an introduction*, (Academic Press, Boston, 1992).

- - - - -

18. **C. Kittel**, *Introduction to solid state physics*, 5th ed. (Wiley, New York, 1976).

19. **N. W. Ashcroft and N. D. Mermin**, "Solid state physics", (Saunders College, Philadelphia, 1976).

20. **T. A. Friedmann**, M. W. Rabin, J. Giapintzakis, J. P. Rice, D. M. Ginsberg, "Direct measurement of the anisotropy of the resistivity in the ab-plane of twin-free, single-crystal, superconducting $YBa_2Cu_3O_{7-\delta}$", Phys. Rev. B 42, 6217 (1990).

Processing of HTSCs

21. **S. Martin**, A. T. Fiory, R. M. Fleming, L. F. Schneemeyer, J. V. Waszczak, "Normal-state transport properties of $Bi_{2+x}Sr_{2-y}CuO_{6\pm\delta}$ crystals", Phys. Rev. B 41, 846 (1990).

22. **A. Davidson**, J. Talvacchio, M. G. Forrester, and J. R. Gavaler, "High-T_C materials expand superconductive circuit applications", Microwaves & RF, April 1994, p. 140.

23. **R. Simon**, "High-T_C thin films and microwave devices", Physics Today, June 1991, p. 64.

24. **R. Hughes**, "The optical properties of high-T_C superconductors grown by laser deposition", Ph.D. Thesis, McMaster University, 1992.

25. **X.X. Xi, T. Venkatesan**, Q. Li, X. D. Wu, A. Inam, C. C. Chang, R. Ramesh, D. M. Hwang, T. S. Ravi, A. Findikoglu, D. Hemmick, S. Etemad, J. A. Martinez, B. Wilkens, "Preparation of thin film high temperature superconductors", IEEE Trans. Magn. MAG-27, 982 (1991).

26. **R. G. Humphreys**, J. S. Satchell, N. G. Chew, J. A. Edwards, S. W. Goodyear, S.

E. Blenkinsop, O. D. Dosser, and A. G. Cullis, "Physical vapour deposition techniques for the growth of $YBa_2Cu_3O_{7-\delta}$ thin films", Supercond. Sci. Technol. 3, 38 (1990).

27. **B. F. Cole**, G.-C. Liang, N. Newman, K. Char, and G. Zaharchuk, "Large-area $YBa_2Cu_3O_{7-\delta}$ thin films on sapphire for microwave applications", Appl. Phys. Lett. 61, 1727 (1992).

28. **B. J. Hinds**, D. L. Schultz, D. A. Neumayer, B. Han, T. J. Marks, Y. Y. Wang, V. P. Dravid, J. L. Schindler, T. P. Hogan, and C. R. Kannewurf, "Metal-organic vapor deposition/open flow thallium annealing route to epitaxial $Tl_2Ba_2Ca_2Cu_3O_{10}$ thin films", Appl. Phys. Lett. 65, 231 (1994).

29. **X. D. Wu**, S. R. Foltyn, R. E. Meunchausen, D. W. Cooke, A. Pique, D. Kalokitis, V. Pendrick, and E. Belohoubek, "Buffer layers for high-T_C thin films on sapphire", J. Supercon. 5, 353 (1992).

30. **Q. Y. Ma**, C. Shu, E. S. Yang, C.-A. Chang, and C. E. Farrell, "Patterning of high-T_C superconducting thin films on Si substrates", SPIE Proc. 1292, 38 (1990).
Q. Y. Ma, P. Dosanjh, A. Wong, J. F. Carolan, and W. N. Hardy, "Inhibition patterning of oxide superconducting films with Si ion implantation", Supercon. Sci. Technol. 7, 294 (1994).

31. **C. H. Ashby**, J. Martens, T. A. Plut, D. S. Ginley, and J. M. Phillips, "Improved aqueous etch for high T_C superconductor materials", Appl. Phys. Lett. 60, 2147 (1992).

32. **L. Alff**, G. M. Fischer, R. Gross, F. Kober, A. Beck, K. D. Husemann, T. Nissel, F. Schmidl, and C. Burckhardt, "Dry-etching processes for high-tempertaure superconductors", Physica C 200, 277 (1992).

33. **J. Schneider**, H. Kohlstedt, and R. Wördenweber, "Nanobridges of optimized $YBa_2Cu_3O_{7-\delta}$ thin films for superconducting flux-flow type devices", Appl. Phys. Lett. 63, 2426 (1993).

34. **R. Barth**, B. Spangenberg, C. Jaekel, H. G. Roskos, H. Kurz, and B. Holzapfel, "Optimization of $YBa_2Cu_3O_{7-\delta}$ submicrometer structure fabrication", Appl. Phys. Lett. 63, 1149 (1993).

35. **R. Sobolewski**, W. Xiong, W. Kula, and J. R. Gavaler, "Laser patterning of Y-Ba-Cu-O thin-film devices and circuits", Appl. Phys. Lett. 64, 643 (1994).

36. **S. Proyer**, E. Stangl, P. Schwab, D. Bäuerle, P. Simon, and C. Jordan, "Patterning of YBCO films by excimer-laser ablation", Appl. Phys. A 58, 471 (1994).

HTSC SQUID devices

37. **G. Friedl**, M. Vildic, B. Roas, D. Uhl, F. Bömmel, M. Römheld, B. Hillenbrand, B. Stritzker, and G. Daalmans, "Low 1/f noise single-layer $YBa_2Cu_3O_{7-\delta}$ dc SQUID at 77 K", Appl. Phys. Lett. 60, 3048 (1992).

38. **N. Missert**, T. E. Harvey, R. H. Ono, and C. D. Reintsema, "High-T_C multilayer step-edge Josephson junctions and SQUIDs", Appl. Phys. Lett. 63, 1690 (1993).

39. **M. Schilling**, D. Reimer, and U. Merkt, "$YBa_2Cu_3O_{7-\delta}$ direct current-superconducting quantum interference devices with artificial $PrBa_2Cu_3O_{7-\delta}$ barriers above 77 K", Appl. Phys. Lett. 64, 2584 (1994).

40. **J. W. M. Hilgenkamp**, G. C. S. Brons, J. G. Soldevilla, R. P. J. Ijsselsteijn, J. Flokstra, and H. Rogalla, "Four layer monolithic integrated high T_C dc SQUID magnetometer", Appl. Phys. Lett. 64, 3497 (1994).

41. **M. J. Ferrari**, F. C. Wellstood, J.J. Kingston, and J. Clarke, "Suppression of magnetic-flux noise in $YBa_2Cu_3O_{7-\delta}$ by a supercurrent", Phys. Rev. Lett. 67, 1346 (1991).

42. **A. H. Miklich**, J. Clarke, M. S. Colclough, and K. Char, "Flicker (1/f) noise in biepitaxial grain boundary junctions of $YBa_2Cu_3O_{7-\delta}$ ", Appl. Phys. Lett. 60, 1899 (1992).

43. **C. E. Cunningham**, G. S. Park, B. Cabrera, and M. E. Huber, "Noise reduction in low-frequency SQUID measurements with laser-driven switching", Appl. Phys. Lett. 63, 1152 (1993).

44. **S. Tanaka**, H. Itozaki, H. Toyoda, N. Harada, A. Adachi, K. Okajima, H. Kado, and T. Nagaishi, "Four-channel $YBa_2Cu_3O_{7-\delta}$ dc SQUID magnetometer for biomagnetic measurements", Appl. Phys. Lett. 64, 514 (1994).

45. **R. C. Black**, A. Mathai, F. C. Wellstood, E. Dantsker, A. H. Miklich, D. T. Nemeth, J. J. Kingston, and J. Clarke, "Magnetic microscopy using liquid nitrogen cooled $YBa_2Cu_3O_{7-\delta}$ superconducting quantum interference device", Appl. Phys. Lett. 62, 2128 (1993).

- - - - -

46. **H. Hübner** and A.A. Valenzuela, "Radio frequency performance of superconducting thin films in high magnetic fields", Appl. Phys. Lett. 64, 3491 (1994).

SFFTs and integration of HTSCs with semiconductor electronics

47. **J. S. Martens**, D. S. Ginley, J. B. Beyer, J. E. Nordman, and G. K. G. Hohenwarter, "A model equivalent circuit for a superconducting flux flow transisitor", IEEE Trans. Appl. Supercon. 1, 95 (1991).

48. **J. S. Martens**, V. M. Hietala, T. E. Zipperian, S. R. Kurtz, D. S. Ginley, C. P. Tigges, J. M. Phillips, and N. Newman, "High temperature superconducting transresistance amplifiers for far infrared detectors", IEEE Trans. Appl. Supercon. 2, 111 (1992).

49. **M. J. Burns**, P. R. de la Houssaye, S. D. Russell, G. A. Garcia, S. R. Clayton, W. S. Ruby, and L. P. Lee, "Demonstration of $YBa_2Cu_3O_{7-\delta}$ and complementary metal-oxide-semiconductor device fabrication on the same sapphire substrate", Appl. Phys. Lett. 63, 1282 (1993).

50. **C. Hilbert**, U. Ghoshal, H. Kroger, J. S. Martens, V. M. Hietala, and T. A. Plut, "Superconducting readout of semiconductor memory at liquid nitrogen temperature", Appl. Phys. Lett. 64, 2442 (1994).

HTSC microwave devices and high-speed interconnects

51. **N. Newman**, W. G. Lyons, "High-temperature superconducting microwave devices: fundamental issues in materials, physics, and engineering", J. Supercon. 6, 119 (1993).

52. **R. W. Ralston**, "Microwave applications of superconductor electronics", Supercon.

Sci. Technol. 4, 386 (1991).

53. **M. C. Nuss**, K. W. Woods, P. M. Mankiewich, R. E. Howard, B. L. Straughn, G. W. Berkstresser, and C. D. Brandle, "$YBa_2Cu_3O_{7-\delta}$ superconductors for high-speed interconnects", IEEE Electron Device Lett. 11, 200 (1990).

Optical properties of HTSC films

54. **W. Markowitsch**, W. Mayr, P. Schwab, X. Z. Wang, "Optical constants of YBaCuO from polarized reflectance measurements", Physica C 223, 117 (1994).
A. El. Azrak, R. Nahoum, N. Bontemps, M. Guilloux-Viry, C. Thivet, A. Perrin, S. Labdi, Z. Z. Li, and H. Raffy, "Infrared properties of $YBa_2Cu_3O_{7-\delta}$ and $Bi_2Sr_2Ca_{n-1}Cu_nO_{2n+1}$ thin films", Phys. Rev. B 49, 9846 (1994).

55. **T. Strach**, "Transport and optical properties of ion irradiated $YBa_2Cu_3O_{7-\delta}$", M.Sc. Thesis, McMaster University, 1992.

56. **H. Yasuoka**, H. Mazaki, T. Terashima, and Y. Bando, "Optical absorption spectra of single crystal $YBa_2Cu_3O_{7-\delta}$ films", Physica C 175, 192 (1991).

HTSC bolometers

57. **P. L. Richards**, "Bolometers for infrared and millimter waves", J. Appl. Phys. 76, 1 (1994).

58. **J. Clarke**, G. I. Hoffer, P. L. Richards, and N.-H. Yeh, "Superconductive bolometers for submillimetre wavelengths", J. Appl. Phys. 48, 4865 (1977).

59. **C. L. Bertin and K. Rose**, "Comparison of superconducting and semiconducting bolometers", J. Appl. Phys. 42, 163 (1971).

60. **P. L. Richards**, J. Clarke, R. Leoni, Ph. Lerch, S. Verghese, M. R. Beasley, T. H. Geballe, R. H. Hammond, P. Rosenthal, and S. R. Spielman, "Feasibility of the high-T_C superconducting bolometer", Appl. Phys. Lett. 54, 283 (1989).

61. **S. Verghese**, P. L. Richards, S. A. Sachtjen, and K. Char, "Sensitive bolometers using high-T_C superconducting thermometers for wavelengths 20-300 μm", J. Appl.

Phys. 74, 4251 (1993).

62. **Q. Li, D. B. Fenner**, W. D. Hamblen, and D. G. Hamblen, "Epitaxial bolometers on micromachined windows in silicon wafers", Appl. Phys. Lett. 62, 2428 (1993).
63. **I. S. McLean**, "Astronomers see distant stars more clearly in a new light", Laser Focus World (July 1994), p. 81.
64. Superconductivity group, AFR Inc., 87 Church Street, East Hartford, Conneticut

High-speed semiconductor photodetectors and sampling techniques

65. DC to 60 GHz visible photodetector, 400 to 900 nm, 6 ps rise time, 5 V/W, model 1002, New Focus, Inc., 1275 Reamwood Ave., Sunnyvale, California (1993).
66. DC to 60 GHz ultrafast photodetector with 7 ps FWHM response, 400 to 900 nm, manufactured by Picometrix for Newport Corporation, model PX-D7 (1994).
67. **G. A. Mourou**, "Electro-optic sampling: device embodiments and possibilities", Proc. SPIE 795, 300 (1987).
68. **M. Y. Frankel**, J. F. Whitaker, and G. A. Mourou, "Optoelectronic characterization of ultrafast devices", IEEE J. Quantum Electron. 28, 2313 (1992).
69. **S. A. Alexandrou**, C.-C. Wang, T. Y. Hsiang, M. Y. Liu, and S. Y. Chou", Appl. Phys. Lett. 62, 2507 (1993).
70. **S. Gupta**, S. L. Williamson, J. F. Whitaker, Y. Chen, and F. W. Smith, "Epitaxial methods produce robust ultrafast detectors", Laser Focus World (June 1992). p. 97.
71. **C.-C. Wang**, S. Alexandrou, D. Jacobs-Perkins, and T. Y. Hsiang, "Comparison of the picosecond characteristics os silicon and silicon-on-sapphire metal-semiconductor-metal photodiodes", Appl. Phys. Lett. 64, 3578 (1994).
72. **B. J. Van Zeghbroeck**, W. Patrick, J.-M. Halbout, and P. Vettiger, "105-GHz bandwidth metal-semiconductor-metal photodiode", IEEE Electron Device Lett. 9, 527 (1988).
73. **Y. Chen**, S. Williamson, and T. Brock, "1.9 picosecond high-sensitivity sampling optical temporal analyzer", Appl. Phys. Lett. 64, 551 (1994).
74. **E. Hecht and A. Zajac**, *Optics*, (Addison-Wesley, Reading, 1974).

Propagation of broadband pulses on YBCO transmission lines

75. **J. F. Whitaker**, R. Sobolewski, D. R. Dykaar, T. Y. Hsiang, and G. A. Mourou, "Propagation model for ultrafast signals on superconducting dispersive striplines", IEEE Trans. Microwave Theory Tech. MTT-36, 277 (1988).

76. **D. R. Dykaar, R. Sobolewski**, J. M. Chwalek, J. F. Whitaker,T. Y. Hsiang, G. A. Mourou, D. K. Lathrop, S. E. Russek, and R. A. Buhrman, "High-frequency characterization of thin-film Y-Ba-Cu oxide superconducting transmission lines", Appl. Phys. Lett. 52, 1444 (1988).

77. **M. C. Nuss**, P. M. Mankiewich, R. E. Howard, B. L. Straughn, T. E. Harvey, C. D. Brandle, G. W. Berkstresser, K. W. Goossen, and P. R. Smith. "Propagation of terahertz bandwidth electrical pulses on $YBa_2Cu_3O_{7-\delta}$ transmission lines on lanthanum aluminate", Appl. Phys. Lett. 54, 2265 (1989).

- - - - -

78. **S. D. Gunapala**, K. M. S. V. Bandara, B. F. Levine, G. Sarusi, J. S. Park, T. L. Lin, W. T. Pike, and J. K. Liu, "High performance InGaAs/GaAs quantum well infrared photodetectors", Appl. Phys. Lett. 64, 3431 (1994).

Equilibrium properties of HTSCs

79. **H. Fukuyama**, "Conference summary: mechanisms and theories", Physica C 185-189, xxv (1991).

80. **J. Rossat-Mignod**, L. P. Regnault, C. Vettier, P. Burlet, J. Y. Henry and G. Lapertot, "Investigation of the spin dynamics in $YBa_2Cu_3O_{6+x}$ by inelastic neutron scattering", Physica B 169, 58 (1991).

81. **D. Pines**, "Understanding high-temperature superconductivity: a progress report", Physica B 199 & 200, 300 (1994).

82. **P. Monthoux and D. Pines**, "$YBa_2Cu_3O_7$: a nearly antiferromagnetic Fermi liquid", Phys. Rev. B 47, 6069 (1993).

83. **P. Monthoux and D. J. Scalapino**, "Properties of the $d_{x^2-y^2}$ gap in the two-dimensional Hubbard model", Physica B 199 & 200, 294 (1994).

84. **P. Monthoux and D. J. Scalapino,** "Self-consistent $d_{x^2-y^2}$ pairing in a two-dimensional Hubbard model", Phys. Rev. Lett. 72, 1874 (1994).

85. **K. Maki and H. Won,** "D-wave superconductivity in high-T_C copper oxides", Physica B 199 & 200, 298 (1994).

H. Won and K. Maki, "d-wave superconductor as a model of high-T_C superconductors", Phys. Rev. B 49, 1397 (1994).

86. **D. A. Wollman, D. J. Van Harlingen,** W. C. Lee, D. M. Ginsberg, and A. J. Leggett, "Experimental determination of the superconducting pairing state in YBCO from the phase coherence of YBCO-Pb dc SQUIDS", Phys. Rev. Lett. 71, 2134 (1993).

87. **C. C. Tsuei,** J. R. Kirtley, C. C. Chi, L. S. Yu-Jahnes, A. Gupta, T. Shaw, J. Z. Sun, and M. B. Ketchen, "Pairing symmetry and flux quantization in a tricrystal superconducting ring of $YBa_2Cu_3O_{7-\delta}$", Phys. Rev. Lett. 73, 593 (1994).

88. **W. N. Hardy, D. A. Bonn,** D. C. Morgan, R. Liang, and K. Zhang, "Precision measurements of the temperature dependence of λ in $YBa_2Cu_3O_{6.95}$: strong evidence for nodes in the gap function", Phys. Rev. Lett. 70, 3999 (1993).

89. **J. Annett,** N. Goldenfield, and S. R. Renn, "Interpretation of the temperature dependence of the electromagnetic penetration depth in $YBa_2Cu_3O_{7-\delta}$", Phys. Rev. B 43, 2778 (1991).

90. **S. Anlage** and D.-H. Wu, "Magentic penetration depth measurements in cuprate superconductors", J. Supercond. 5, 395 (1992).

91. **A. Porch,** M. J. Lancaster, R. G. Humphreys and N. G. Chew, "Surface impedance measurements of $YBa_2Cu_3O_{7-\delta}$ thin films using coplanar resonators", IEEE Trans. Appl. Supercond. 3, 1719 (1993).

92. **W. Rauch,** E. Gornik, G. Sölkner, A. A. Valenzuela, F. Fox, and H. Behner, "Microwave properties of $YBa_2Cu_3O_{7-\delta}$ thin films studied with coplanar transmission line resonators", J. Appl. Phys. 73, 1866 (1993).

93. **J. Y. Lee and T. Lemberger,** "Penetration depth $\lambda(T)$ of $YBa_2Cu_3O_{7-\delta}$ films determined from kinetic inductance", Appl. Phys. Lett. 62, 2419 (1993).

94. **F. Gao,** J. W. Kruse, C. E. Platt, M. Feng, and M. V. Klein, "Microwave surface

impedance at 10 GHz and quasiparticle scattering in $YBa_2Cu_3O_{7-\delta}$ films", Appl. Phys. Lett. 63, 2274 (1993).

95. **D. A. Bonn**, R. Liang, T. M. Riseman, D. J. Baar, D. C. Morgan, K. Zhang, P. Dosanjh, T. L. Duty, A. MacFarlane, G. D. Morris, J. H. Brewer, W. N. Hardy, C. Kallin and A. J. Berlinsky, "Microwave determination of the quasiparticle scattering time in $YBa_2Cu_3O_{7-\delta}$ ", Phys. Rev. B 47, 11314 (1993). See also comment by O. Klein, Phys. Rev. Lett. 72, 1390 (1994) and reply by D. Bonn et al., ibid, p. 1391.

96. **Z. Ma**, R. C. Taber, L. W. Lombardo, A. Kapitulnik, M. R. Beasley, P. Merchant, C. B. Eom, S. Y. Hou, and J. M. Phillips, "Microwave penetration depth measurements on $Bi_2Sr_2CaCu_2O_8$ single crystals and $YBa_2Cu_3O_{7-\delta}$ thin films", Phys. Rev. Lett. 71, 781 (1993).

97. **S. D. Brorson**, R. Buhleier, J. O. White, I. E. Trofimov, H.-U. Habermeier, and J. Kuhl, "Kinetic inductance and penetration depth of thin superconducting films measured by THz-pulse spectroscopy", Phys. Rev. B 49, 6185 (1994).

98. **P. Arberg**, M. Mansor, and J. P. Carbotte, "Penetration depth for a 2D d-wave superconductor", Solid State Commun. 86, 671 (1993).

99. **W. N. Hardy**, S. Kamal, **D. A. Bonn**, K. Zhang, R. Liang, E. Klein, D. C. Morgan, and D. J. Baar, "Microwave surface impedance of the cuprate superconductor $YBa_2Cu_3O_{7-\delta}$ ", Physica B 197, 609 (1994). For a different view, see
D. A. Bonn, S. Kamal, K. Zhang, R. Liang, D. J. Baar, E. Klein, and **W. N. Hardy**, "Comparison of the influence of Ni and Zn impurities on the electromagnetic properties of $YBa_2Cu_3O_{6.95}$", Phys. Rev. B 50, 4051 (1994).

100. **D. B. Romero**, C. D. Porter, D. B. Tanner, L. Forro, D. Mandrus, L. Mihaly, G. L. Carr, and G. P. Williams,"Quasiparticle damping in $Bi_2Sr_2CaCu_2O_8$ and $Bi_2Sr_2CuO_6$", Phys. Rev. Lett. 68, 1590 (1992).

101. **S. M. Quinlan, D. J. Scalapino, and N. Bulut**, "Superconducting quasiparticle lifetimes due to spin-fluctuation scattering", Phys. Rev. B 49, 1470 (1994).

102. **N. Bulut and D. J. Scalapino**, "Analysis of NMR data in the superconducting state of $YBa_2Cu_3O_{7-\delta}$ ", Phys. Rev. Lett. 68, 706 (1992).

103. **J. Rossat-Mignod**, L. P. Regnault, P. Bourges, P. Burlet, C. Vettier, and J. Y.

Henry, "Neutron scattering study of the high-T_C superconducting system $YBa_2Cu_3O_{6+x}$", in *Selected Topics in Superconductivity*, eds. L. C. Gupta and M. S. Multani (World Scientific, Singapore, 1993). p.265.

104. **B. J. Sternlieb**, G. Shirane, J. M. Tranquada, M. Sato and S. Shamato, "Temperature dependence of the dynamic susceptibility $\chi''(\omega)$ in superconducting $YBa_2Cu_3O_{6.6}$ (T_C = 53 K)", Phys. Rev. B 47, 5320 (1993).

105. **T. E. Mason**, G. Aeppli, S. M. Hayden, A. P. Ramirez, and H. A. Mook, "Low energy excitations in superconducting $La_{1.86}Sr_{0.14}CuO_4$", Phys. Rev. Lett. 71, 919 (1993).

106. **K. Levin**, Y. Zha, R. J. Radtke, Q. Si, M. R. Norman, and H.-B. Schüttler, "Spin dynamics and implications for superconducivity: some problems with the d-wave scenario", J. Supercond. 7, 563 (1994).

107. **T. Ekino** and J. Akimitsu, "Tunneling spectroscopy of copper oxide superconductors", in *Selected Topics in Superconductivity*, eds. L. C. Gupta and M. S. Multani (World Scientific, Singapore, 1993). p.477.

108. **W. Weber** and L. F. Mattheiss, "Electron-phonon interaction in $Ba_2YCu_3O_7$", Phys. Rev. B 37, 599 (1988).

109. **R. E. Cohen**, W. E. Pickett, and H. Krakauer, "Theoretical determination of strong electron-phonon coupling in $YBa_2Cu_3O_{7-\delta}$ ", Phys. Rev. Lett. 64, 2575 (1990).

110. **V. Z. Kresin** and S. Wolf, "Symmetry, mechanism of pairing, and the isotope effect in the cuprates", J. Supercond. 7, 531 (1994).

W. W. Fuller-Mora, S. A. Wolf, and V. Z. Kresin, "Electron-phonon coupling as a mechanism for high-temperature superconductivity", *ibid.*, p.543.

111. **J. C. Phillips**, "A prosaic explanation for linearly temperature-dependent penetration depths in $YBa_2Cu_3O_{6.95}$", Physica C 228, 171 (1994).

112. **W. Y. Chang**, Y. Xu, G.-L. Zhao, K. W. Wong, and F. Zandiehnadem, "Electronic structure and excitonic-enhanced superconducting mechanism in $YBa_2Cu_3O_{7-\delta}$", Phys. Rev. Lett. 59, 1333 (1987).

R. E. Cohen, "Elelctrons, phonons, and electron-phonon interactions in high-temperature superconductors", Computers in Phys. 8, 34 (1994).

Photoinduced superconductivity in the HTSCs

113. **G. Nieva**, E. Osquiguil, J. Guimpel, M. Maenhoudt, B. Wuyts, Y. Bruynseraede, M. B. Maple, and I. K. Schuller, "Photoinduced enhancement of superconductivity", Appl. Phys. Lett. 60, 2159 (1992).

114. **D. Lederman**, E. Osquiguil, G. Nieva, J. Guimpel, J. Hasen, Y. Bruynseraede, and I. K. Schuller, "Photoinduced enhancement of superconductivity", J. Supercond. 7, 127 (1994).

115. **K. Tanabe**, S. Kubo, F. H. Teherani, H. Assano, and M. Suzuki, "Effects of photoinduced hole doping on normal-state and superconducting transport in oxygen deficient $YBa_2Cu_3O_{7-\delta}$ ", Phys. Rev. Lett. 72, 1537 (1994).

Nonequilibrium properties of superconductors

116. **D. N. Langenberg and A. I. Larkin** (eds.), *Nonequilibrium Superconductivity*, (North Holland, Amsterdam, 1986).

117. *NATO Advanced Study Institute on Nonequilibrium Superconductivity, Phonons, and Kapitza Boundaries*, (Plenum, New York, 1981).

118. **R. Tidecks**, "Nonequilibrium superconductivity", in *Selected Topics in Superconductivity*, eds. L. C. Gupta and M. S. Multani (World Scientific, Singapore, 1993). p. 211.

119. **A. Rothwarf and B. N. Taylor**, "Measurement of recombination lifetimes in superconductors", Phys. Rev. Lett. 19, 27 (1967).

120. **K. E. Gray**, "Steady state measurements of the quasiparticle lifetime in superconducting aluminum", J. Phys. F: Metal Phys. 1, 290 (1971).

121. **S. B. Kaplan, C. C. Chi, D. N. Langenberg, J. J. Chang, S. Jafarey, and D. J. Scalapino**, "Quasiparticle and phonon lifetimes in superconductors", Phys. Rev. B 14, 4854 (1976).

122. **J.-J. Chang and D. J. Scalapino**, "Nonequilibrium superconductivity", J. Low Temp. Phys. 31, 1 (1978).

J.-J. Chang and D. J. Scalapino, " ' Hot superconductors ' : the physics and applications of nonequilibrium superconductivity", in Superconductor Applications: SQUIDS and Machines, eds. B. B. Schwartz and S. Foner (Plenum, New York, 1977), p. 447.

123. **P. Hu, R. C. Dynes, V. Narayanamurti**, H. Smith, and W. F. Brinkman, "Quasiparticle propagation and recombination in bulk, superconducting Pb", Phys. Rev. Lett. 38, 361 (1977).

V. Narayanamurti, R. C. Dynes, P. Hu, H. Smith, and W. F. Brinkman, "Quasiparticle and phonon propagation in bulk, superconducting lead", Phys. Rev. B 18, 6041 (1978).

124. **C. C. Chi**, M. M. T. Loy, and D. C. Cronmeyer, "Transient responses of superconducting lead films measured with picosecond laser pulses", Phys. Rev. B 23, 124 (1981).

125. **M. Johnson**, "Direct real time measurement of quasiparticle lifetimes in a superconductor", Phys. Rev. Lett. 67, 374 (1991).

126. **I. Schuller and K. E. Gray**, "Experimental observation of the relaxation time of the order parameter in superconductors", Phys. Rev. Lett. 36, 429 (1976).

127. **J. A. Pals and J. Wolter**, "Measurement of the order-parameter relaxation in superconducting Al-strips", Phys. Lett. 70A, 150 (1979).

D. J. Frank, M. Tinkham, A. Davidson, and S. M. Faris, "Transient response of superconducting indium microbridges to supercritical current pulses", Phys. Rev. Lett. 50, 1611 (1983).

J.-P. Maneval, J.-C. Villegier, and F. S. Jelila, "Current-induced switching of epitaxial YBaCuO films into a dissipative state", Proc. SPIE, presented at OE/LASE '94, Los Angeles, January 23-28, 1994.

128. **L. R. Testardi**, "Destruction of superconductivity by laser light", Phys. Rev. B 4, 2189 (1971).

129. **C. S. Owen and D. J. Scalapino**, "Superconducting state under the influence of external dynamic pair breaking", Phys. Rev. Lett. 28, 1559 (1972).

130. **W. H. Parker and W. D. Williams**, "Photoexcitation of quasiparticles in

nonequilibrium superconductors", Phys. Rev. Lett. 29, 924 (1972).

131. **G. A. Sai-Halasz**, C. C. Chi, A. Denenstein, and D. N. Langenberg, "Effects of dynamic pair breaking in superconducting thin films", Phys. Rev. Lett. 33, 215 (1974).

132. **W. H. Parker**, "Modified theory of nonequilibrium superconductors", Phys. Rev. B 12, 3667 (1975).

133. **J. Fuchs**, P. W. Epperlein, M. Welte, and W. Eisenmenger, "Energy gap reduction in superconducting tin films by quasiparticle injection", Phys. Rev. Lett. 38, 919 (1977).

134. **V. F. Elesin**, Sov. Phys. JETP 39, 862 (1974).

135. **A. I. Golovashkin, V. F. Elesin**, O. M. Ivanenko, K. V. Mitsen, and G. P. Motulevich, "Conditions for the appearance of spatially inhomogeneous states in superconductors under laser pumping conditions", Sov. Phys. Solid State 22, 60 (1980).

136. **R. Sobolewski**, D. P. Butler, T. Y. Hsiang, C. V. Stancampiano, and G. A. Mourou, "Dynamics of the intermediate state in nonequilibrium superconductors", Phys. Rev. B 33, 4604 (1986).

137. **X.-H. Hu, T. Juhasz**, and W. E. Bron, "Transient electric field generated by nonequilibrium states in superconducting Pb films", Appl. Phys. Lett. 59, 3333 (1991).

138. **I. Iguchi** and H. Konno, "New instability model for the inhomogeneous gap states of a nonequilibrium superconductor", Phys. Rev. B 28, 4040 (1983).

I. Iguchi and Y. Suzuki, "Spatial structure of a tunnel-injected nonequilibrium superconductor", *ibid.*, p. 4043.

Y. Nisida, T. Nishimura, A. Nishiura, and I. Iguchi, "Optical probing of the inhomogeneous gap distribution in nonequilibrium superconductors", Solid State Commun. 50, 553 (1984).

139. **T. Kobayashi**, S. Sawada, and K. Fujisawa, "Nonequilibrium superconductivity based on quasithermal phonon and quasiparticle distributions", Phys. Rev. B 31, 6150 (1985).

140. **I. Iguchi**, K. Nukui, and K. Lee, "Dynamic Cooper-pair breaking by tunnel injection of quasiparticles into a high-T_C $YBa_2Cu_3O_{7-\delta}$ superconductor", Phys. Rev. B 50, 457 (1994).

Pump-pobe experiments of normal metals

141. **K. M. Yoo**, X. M. Zhao, M. Siddique, R. R. Alfano, D. P. Osterman, M. Radparvar, and J. Cunniff, "Femtosecond thermal modulation measurements of electron-phonon relaxation in niobium", Appl. Phys. Lett. 56, 1908 (1990).
M. Mihailidi, Q. Xing, K. M. Yoo, and R. R. Alfano, "Electron-phonon relaxation dynamics of niobium metal as a function of temperature", Phys. Rev. B 49, 3207 (1994).

142. **S. L. Anisimov**, B. L. Kapeliovich, and T. L. Perel'man, Sov. Phys. JETP 39, 375 (1975).

143. **G. L. Eesley**, "Generation of nonequilibrium electron and lattice temperatures in copper by picosecond laser pulses", Phys. Rev. B 33, 2144 (1986).

144. **H. E. Elsayed-Ali**, T. B. Norris, M. A. Pessot, and G. A. Mourou, "Time-resolved observation of electron-phonon relaxation in copper", Phys. Rev. Lett. 58, 1212 (1987).

145. **R. W. Schoenlein**, W. Z. Lin, J. G. Fujimoto, and G. L. Eesley, "Femtosecond studies of nonequilibrium electronic processes in metals", Phys. Rev. Lett. 58, 1680 (1987).

146. **H. E. Elsayed-Ali** and T. Juhasz, "Femtosecond time-resolved thermomodulation of thin gold films with different crystal structures", Phys. Rev. B 47, 13599 (1993).

147. **C.-K. Sun**, F. Vallée, L. Acioli, E. P. Ippen, and J. G. Fujimoto, "Femtosecond investigation of electron thermalization in gold", Phys. Rev. B 48, 12365 (1993).

148. **W.-Z. Lin**, R. W. Schoenlein, J. G. Fujimoto, and E. P. Ippen, "Femtosecond absorption saturation studies of hot carriers in GaAs and AlGaAs", IEEE J. Quantum Electron. 24, 267 (1988).

149. **J. G. Fujimoto**, J. M. Liu, E. P. Ippen, and N. Bloembergen, "Femtosecond laser

interaction with metallic tungsten and nonequilibrium electron and lattice temperatures", Phys. Rev. Lett. 53, 1837 (1984).

150. **J. R. Goldman** and J. A. Prybyla, "Ultrafast dynamics of laser-excited electron distributions in silicon", Phys. Rev. Lett. 72, 1364 (1994).

Pump-probe experiments of conventional superconductors

151. **S. D. Brorson**, A. Kazeroonian, J. S. Moodera, D. W. Face, T. K. Cheng, E. P. Ippen, M. S. Dresselhaus, and G. Dresselhaus, "Femtosecond room-temperature measurement of the electron-phonon coupling constant λ in metallic superconductors", Phys. Rev. Lett. 64, 2172 (1990).

152. **J. F. Federici**, B. I. Greene, P. N. Saeta, D. R. Dykaar, F. Sharifi, and R. C. Dynes, "Direct picosecond measurement of photoinduced Cooper-pair breaking in lead", Phys. Rev. B 46, 11153 (1992).

J. F. Federici, B. I. Greene, P. N. Saeta, D. R. Dykaar, F. Sharifi, and R. C. Dynes, "Cooper pair breaking in lead measured by pulsed terahertz spectroscopy", IEEE Trans. Appl. Supercond. 3, 1461 (1993).

Pump-probe experiments of HTSCs

153. **S. D. Brorson, A. Kazeroonian, D. W. Face**, T. K. Cheng, G. L. Doll, M. S. Dresselhaus, G. Dresselhaus, E. P. Ippen, T. Venkatesan, X. D. Wu, and A. Inam, "Femtosecond thermomodulation study of high-T_C superconductors", Solid State Commun. 74, 1305 (1990).

154. **D. W. Face, S. D. Brorson, A. Kazeroonian**, J. S. Moodera, T. K. Cheng, G. L. Doll, M. S. Dresselhaus, G. Dresselhaus, E. P. Ippen, T. Venkatesan, X. D. Wu, and A. Inam, "Femtosecond thermomodulation studies of low and high-T_C superconductors", IEEE Trans. Magn. 27, 1556 (1991).

155. **A. S. Kazeroonian**, T. K. Cheng, **S. D. Brorson**, Q. Li, E. P. Ippen, X. D. Wu, T. Venkatesan, S. Etemad, M. S. Dresselhaus, G. Dresselhaus, "Probing the fermi level of $Y_{1-x}Pr_xBa_2Cu_3O_{7-\delta}$ by femtosecond spectroscopy", Solid State Commun. 78, 95

(1991).

156. **S. G. Han**, Z. V. Vardeny, K. S. Wong, O. G. Symko, and G. Koren, "Femtosecond optical detection of quasiparticle dynamics in high-T_C $YBa_2Cu_3O_{7-\delta}$ superconducting thin films", Phys. Rev. Lett. 65, 2708 (1990).

157. **S. G. Han**, Z. V. Vardeny, O. G. Symko, and G. Koren, "Femtosecond dynamics of quasiparticles in $YBa_2Cu_3O_{7-\delta}$ superconductor films", IEEE Trans. Magn. 27, 1548 (1991).

158. **G. L. Eesley**, J. Heremans, M. S. Meyer, G. L. Doll, and S. H. Liou, "Relaxation time of the order parameter in a high-temperature superconductor", Phys. Rev. Lett. 65, 3445 (1990).

159. Comment by **Han** *et al.*, Phys. Rev. Lett. 67, 1053 (1991). Reply by **Eesley** *et al.*, *ibid.*, p. 1054.

160. **J. M. Chwalek, C. Uher, J. F. Whitaker**, G. A. Mourou, J. Agostinelli, and M. Lelental, "Femtosecond optical absorption studies of nonequilibrium electronic processes in high T_C superconductors", Appl. Phys. Lett. 57, 1696 (1990).

161. **J. M. Chwalek, C. Uher, J. F. Whitaker**, G. A. Mourou, and J. A. Agostinelli, "Subpicosecond time-resolved studies of coherent phonon oscillations in thin film $YBa_2Cu_3O_{7-\delta}$ ($x < 0.4$)", Appl. Phys. Lett. 58, 980 (1991).

162. **Y. Liu, J. F. Whitaker, C. Uher**, J.-L. Peng, Z. Y. Li, and R. L. Greene, "Ultrafast nonequilibrium carrier relaxation in single-crystal $Nd_{1.85}Ce_{0.15}CuO_{4-y}$", Appl. Phys. Lett. 63, 979 (1993).

163. **S. V. Chekalin**, V. M. Farztdinov, V. V. Golovlyov, V. S. Letokhov, Y. E. Lozovik, Y. A. Matveets, and A. G. Stepanov, "Femtosecond spectroscopy of $YBa_2Cu_3O_{7-\delta}$: electron-phonon measurement and energy-gap observation", Phys. Rev. Lett. 67, 3860 (1991).

164. **D. H. Reitze**, A. M. Weiner, A. Inam, and S. Etemad, "Fermi-level dependence of femtosecond response in nonequilibrium high-T_C superconductors", Phys. Rev. B 46, 14309 (1992).

165. **W. Albrecht**, Th. Kruse, and H. Kurz, "Time-resolved observation of coherent phonons in superconducting $YBa_2Cu_3O_{7-\delta}$ thin films", Phys. Rev. Lett. 69, 1451

(1992).

166. **W. Albrecht**, Th. Kruse, K. Leo, and H. Kurz, "Oxygen dependence of the Fermi-level and electron-phonon coupling costant in $YBa_2Cu_3O_{7-\delta}$ films", Appl. Phys. A. 56, 463 (1993).

167. **T. Gong**, L. X. Zheng, W. Xiong, W. Kula, Y. Kostoulas, R. Sobolewski, and P. M. Fauchet, "Femtosecond optical response of Y-Ba-Cu-O thin films: The dependence on optical frequency, excitation intensity, and electric current", Phys. Rev. B 47, 14495 (1993).

168. **L. Shi, T. Gong**, W. Xiong, X. Weng, Y. Kostoulas, R. Sobolewski, and P. M. Fauchet, "Femtosecond reflectivity of 60 K Y-Ba-Cu-O thin films", Appl. Phys. Lett. 64, 1150 (1994).

169. **A. N. Zherikhin**, V. A. Lobastov, V. M. Petnikova, and V. V. Shuvalov, "Nonlinear spectroscopy of Y-Ba-Cu-O nonequilibrium states excited by picosecond optical pumping", Physica C 221, 311 (1994).

HTSC band structure

170. **S. L. Cooper**, D. Reznik, A. Kotz, M. A. Karlow, R. Liu, M. V. Klein, W. C. Lee, J. Giapintzakis, D. M. Ginsberg, B. W. Veal, and A. P. Paulikas, "Optical studies of the a-, b-, and c-axis charge dynamics in $YBa_2Cu_3O_{8-x}$ ", Phys. Rev. B 47, 8233 (1993).

171. **S. Uchida**, T. Ido, H. Takagi, T. Arima, Y. Tokura, and S. Tajima, "Optical spectra of $La_{2-x}Sr_xCuO_4$: effect of carrier doping on the elecetronic structure of the CuO_2 plane", Phys. Rev. B 43, 7942 (1991).

172. **W. Kress**, U. Schröder, J. Prade, A. D. Kulkarni, and F. W. de Witte, "Lattice dynamics of the high-T_C superconductor $YBa_2Cu_3O_{7-\delta}$", Phys. Rev. B 38, 2906 (1988).

Photoresponse mechanisms

173. For a recent conference proceedings, see *High-Temperature Superconducting*

Detectors: Bolometric and Nonbolometric, M. Mahum and J.-C. Villegier eds., Proc. SPIE 2159, (1994).

Granular films: BaPbBiO and NbN

174. **Y. Enomoto and T. Murakami**, "Optical detector using superconducting $BaPb_{0.7}Bi_{0.3}O_3$ thin films", J. Appl. Phys. 59, 3807 (1986).

175. **U. Strom, J. C. Culbertson**, S. A. Wolf, S. Perkowitz, and G. L. Carr, "Far-infrared photoresponse of quasi-two-dimensional granular NbN/BN films", Phys. Rev. B 42, 4059 (1990).

176. **Y. P. Gousev, G. N. Gol'tsman, A. D. Semenov, E. M. Gershenzon, R. S. Nebosis**, M. A. Heusinger, and **K. F. Renk**, "Broadband ultrafast superconducting NbN detector for electromagnetic radiation", J. Appl. Phys. 75, 3695 (1994).

Granular films: HTSC, and response to microwave radiation

177. **M. Leung**, P. R. Broussard, J. H. Claassen, M. Osofsky, S. A. Wolf, and **U. Strom**, "Optical detection in thin granular films of Y-Ba-Cu-O at temperatures between 4.2 K and 100 K", Appl. Phys. Lett. 51, 2046 (1987).

178. **E. M. Gershenzon, G. N. Gol'tsman, A. D. Semenov**, and **A. V. Sergeev**, "Mechanism of picosecond response of granular YBaCuO films to electromagnetic radiation", IEEE Trans. Magn. 27, 1321 (1991).

179. **J. C. Culbertson, U. Strom**, S. A. Wolf, and W. W. Fuller, "Response of granular superconducting $YBa_{2.1}Cu_{3.4}O_{7-\delta}$ to light", Phys. Rev. B 44, 9609 (1991).

180. **U. Strom, J. C. Culbertson**, S. A. Wolf, F. Gao, D. B. Tanner, and G. L. Carr, "Far-infrared photoresponse of granular $YBa_{2.1}Cu_{3.4}O_{7-\delta}$ ", Phys. Rev. B 46, 8472 (1992).

181. **J.-P. Maneval**, F. Chibane, and R. W. Bland, "Electron-phonon decoupling in the photoresponse of YBaCuO granular films at low temperature", Appl. Phys. Lett. 61, 339 (1992).

182. **Y. Cai**, P. L. Leath, and Z. Yu, "Simulation of below-gap photoresponse of thin film superconductors by Josephson-junction arrays", Phys. Rev. B 49, 4015 (1994).

183. **Gi. Schneider, H. Lengfellner**, J. Betz, **K. F. Renk**, and **W. Prettl**, "Infrared detection by Tl-Ba-Ca-Cu-O superconducting films", Int. J. Infrared and Millimeter Waves 12, 1 (1991).

184. **P. G. Huggard, Gi. Schneider**, T. O'brien, P. Lemoine, W. Blau, and **W. Prettl**, "Fast nonlinear photoresponse of current biased thin-film $Bi_2Sr_2CaCu_2O_8$ to pulsed far-infrared radiation", Appl. Phys. Lett. 58, 2549 (1991).

185. **P. G. Huggard, Gi. Schneider**, C. Richter, R. Rickler, and **W. Prettl**, "Wavelength-dependent power-law Josephson photoresponse of a $Tl_2Ba_2CaCu_2O_8$ thin film", Phys. Rev. B 49, 9949 (1994).

186. **J. Konopka, R. Sobolewski**, G. Jung, W. Kula, P. Gierlowski, A. Konopka, and S. J. Lewandowski, "Microwave detectors based on granular high-T_C thin films", IEEE Trans. Microwave Th. Techn. 38, 160 (1990).

187. **M. Takai**, K. Niki, T. Ikemachi, S. Yoshikawa, Y. Yoshisato, and S. Nakano, "A practical microwave detection system using a high-impedance microbridge and a miniature refrigerator", IEEE Trans. Appl. Supercond. 3, 2156 (1993).

Photoresponse of YBCO Josephson junctions and grain boundaries

188. **S. B. Kaplan, C. C. Chi**, P. Chaudhari, D. Dimos, R. Gross, A. Gupta, and G. Koren, "Response of $YBa_2Cu_3O_{7-\delta}$ grain-boundary junctions to short light pulses", Phys. Rev. B 43, 8627 (1991).

189. **E. J. Cukauskas**, L. H. Allen, R. T. Holm, G. K. Sherrill, P. K. Van Damme, "Photoresponse os shallow step, weak-link bridges using inverted cylindrical magnetron-sputtered $YBa_2Cu_3O_{7-\delta}$ thin films", J. Appl. Phys. 71, 1878 (1992).

190. **S. Bhattacharya**, X. X. Xi, M. Rajeswari, C. Kwon, S. N. Mao, Q. Li, and T. Venkatesan, "Optical response of an ultrathin film and a large-angle grain-boundary in superconducting $YBa_2Cu_3O_{7-\delta}$ ", Appl. Phys. Lett. 62, 3510 (1993).

191. **S. Bhattacharya**, M. Rajeswari, I. Takeuchi, X. X. Xi, S. N. Mao, C. Kwon, Q. Li,

and T. Venkatesan, "Low temperature optical response of a single grain boundary in superconducting $YBa_2Cu_3O_{7-\delta}$ thin films", Appl. Phys. Lett. 63, 2279 (1993).

Laser-induced voltages in normal state without current bias

192. **C. L. Chang, A. Kleinhammes**, W. G. Moulton, and **L. R. Testardi**, "Symmetry-forbidden laser-induced voltages in $YBa_2Cu_3O_{7-\delta}$ ", Phys. Rev. B 41, 11564 (1990).

193. **A. Kleinhammes, C. L. Chang**, W. G. Moulton, and **L. R. Testardi**, "Nonbolometric laser-induced voltage signals in $YBa_2Cu_3O_{7-\delta}$ thin films at room temperature", Phys. Rev. B 44, 2313 (1991).

194. **L. R. Testardi**, "Anomalous laser-induced voltages in $YBa_2Cu_3O_{7-\delta}$ and "off-diagonal" thermoelectricity", Appl. Phys. Lett. 64, 2347 (1994).

195. **H. S. Kwok, J. P. Zheng**, and S. Y. Dong, "Origin of the anomalous photovoltaic signal in Y-Ba-Cu-O", Phys. Rev. B 43, 6270 (1991).

196. **H. Lengfellner**, G. Kremb, A. Schnellbögl, J. Betz, **K. F. Renk**, and **W. Prettl**, "Giant voltages upon surface heating in normal $YBa_2Cu_3O_{7-\delta}$ films suggesting an atomic layer thermopile", Appl. Phys. Lett. 60, 501 (1992).

Epitaxial films: bolometric response only

197. **M. G. Forrester**, M. Gottlieb, J. R. Gavaler, and A. I. Braginski, "Optical response of epitaxial films of $YBa_2Cu_3O_{7-\delta}$ ", Appl. Phys. Lett. 53, 1332 (1988).

198. **W. S. Brocklesby**, D. Monroe, A. F. J. Levi, M. Hong, S. H. Liou, J. Kwo, C. E. Rice, P. M. Mankiewich, and R. E. Howard, "Electrical response of superconducting $YBa_2Cu_3O_{7-\delta}$ to light", Appl. Phys. Lett. 54, 1175 (1989).

199. **A. M. Kadin, P. H. Ballentine,** and **W. R. Donaldson**, "Relaxation processes in optically excited high-T_c films", Physica B 165 & 166, 1507 (1990).

200. **G. L. Carr**, M. Quijada, D. B. Tanner, C. J. Hirschmugl, G. P. Williams, S. Etemad, B. Dutta, F. DeRosa, A. Inam, and T. Venkatesan, "Fast bolometric response by high-T_c detectors measured with subnanosecond synchrotron radiation", Appl. Phys. Lett. 57, 2725 (1990).

201. **G. L. Carr**, D. B. Tanner, S. Etemad, and A. Inam, "Thin YBCO films as fast infrared detectors: model calculations and experimental results", Proc. SPIE 2159 (1994).

202. **Y. Liu, F. Gao, J. F. Whitaker, C. Uher**, C. E. Platt, "Study of optical response of high-T_C YBaCuO and BaKBiO thin films by terahertz spectroscopy", Proc. SPIE 2159 (1994).

Optical switching of YBCO films

203. **D. Gupta, W. R. Donaldson**, K. Kortkamp, and **A. M. Kadin**, "Optically triggered switching of optically thick YBCO films", IEEE Trans. Appl. Supercond. 3, 2895 (1993).

Thermal models and thermal boundary resistance

204. **M. I. Flik**, P. E. Phelan, and C. L. Tien, "Thermal model for bolometric response of high-T_C superconducting films to optical pulses, Cryogenics 30, 1118 (1990).

205. **M. Nahum, S. Verghese, P. L. Richards**, and K. Char, "Thermal boundary resistance for $YBa_2Cu_3O_{7-\delta}$ films", Appl. Phys. Lett. 59, 2034 (1991).

206. **C. G. Levey**, S. Etemad, and I. Inam, "Optically detected transient thermal response of high-T_C epitaxial films", Appl. Phys. Lett. 60, 126 (1992).

207. **S. Zeuner, H. Lengfellner**, J. Betz, **K. F. Renk**, and **W. Prettl**, "Heat propagation in high-T_C films investigated by optical response measurements", Appl. Phys. Lett. 61, 973 (1992).

208. **C. D. Marshall**, A. Tokmakoff, I. M. Fishman, C. B. Eom, J. M. Phillips, and D. C. Fayer, "Thermal boundary resistance and diffusivity measurements on thin $YBa_2Cu_3O_{7-\delta}$ films with MgO and $SrTiO_3$ substrates using the transient grating method", J. Appl. Phys. 73, 850 (1993).

209. **A. V. Sergeev, A. D. Semenov**, P. Kouminov, V. Trifonov, **I. G. Goghidze, B. S. Karasik, G. N. Gol'tsman,** and **E. M. Gershenzon**, "Transparency of $YBa_2Cu_3O_{7-\delta}$

film/substrate interface for thermal phonons measured by means of voltage response to radiation", Phys. Rev. B 49, 9091 (1994).

Transient flux dynamics

210. **E. Zeldov**, N. M. Amer, G. Koren, and A. Gupta, "Nonbolometric optical response of $YBa_2Cu_3O_{7-\delta}$ epitaxial films", Phys. Rev. B 39, 9712 (1989).

211. **E. Zeldov**, N. M. Amer, G. Koren, A. Gupta, R. J. Gambino, and M. W. McElfresh, "Optical and electrical enhancement of flux creep in $YBa_2Cu_3O_{7-\delta}$ epitaxial films", Phys. Rev. Lett. 62, 3093 (1989).

212. **A. M. Kadin, M. Leung**, A. D. Smith, and J. M. Murdock, "Photofluxonic detection: A new mechanism for infrared detection in superconducting thin films", Appl. Phys. Lett. 57, 2847 (1990).

A. M. Kadin, M. Leung, A. D. Smith, and J. M. Murduck, "Infrared photodetector based on the photofluxonic effect in superconducting thin films", Proc. SPIE 1477, 156 (1991).

213. **J. P. Walko**, S. V. Rao, and **D. J. Van Harlingen**, "Photon-induced vortex-antivortex pair creation in superconducting films", Supercond. Sci. Technol. 7, 246 (1994).

214. **T. Puig, P. G. Huggard**, M. Pont, **Gi. Schneider**, J. S. Muñoz, and **W. Prettl**, "Fast flux motion in $YBa_2Cu_3O_{7-\delta}$ films in an ac magnetic field activated by laser heating", Phys. Rev. B 49, 7004 (1994).

215. **S. Zeuner, W. Prettl, K. F. Renk,** and **H. Lengfellner**, "Nernst effect in Tl-Ba-Ca-Cu-O high-T_c superconducting thin films", Phys. Rev. B 49, 9080 (1994).

Frenkel *et al.*: photoactivated flux flow and gap suppression

216. **A. Frenkel**, M. A. Saifi, T. Venkatesan, C. Lin, X. D. Wu, and A. Inam, "Observation of fast nonbolometric optical response of nongranular high-T_c $YBa_2Cu_3O_{7-\delta}$ superconducting thin films", Appl. Phys. Lett. 54, 1594 (1989).

217. **A. Frenkel**, M. A. Saifi, T. Venkatesan, P. England, X. D. Wu, and A. Inam,

"Optical response of nongranular high-T_C $YBa_2Cu_3O_{7-\delta}$ superconducting thin films", J. Appl. Phys. 67, 3054 (1990).

218. **A. Frenkel**, "High temperature superconducting thin films as broadband optical detectors", Physica C 180, 251 (1991).

219. **A. Frenkel**, "Mechanism of nonequilibrium optical response of high-temperature superconductors", Phys. Rev. B 48, 9717 (1993).

Kwok, Zheng, Shi, Huang, *et al.*: gap suppression and phonon trapping effects

220. **H. S. Kwok**, **J. P. Zheng**, Q. Y. Ying, and R. Rao, "Nonthermal optical response of Y-Ba-Cu-O thin films", Appl. Phys. Lett. 54, 2473 (1989).

221. **J. P. Zheng**, Q. Y. Ying, and **H. S. Kwok**, "Y-Ba-Cu-O thin film infrared detectors", Physica C 168, 322 (1990).

222. **L. Shi, G. L. Huang**, C. Lehane, **J. P. Zheng**, and **H. S. Kwok**, "Generation and measurement of picosecond voltage pulses in $YBa_2Cu_3O_{7-\delta}$ thin films", Appl. Phys. Lett. 61, 489 (1992).

223. **L. Shi, G. L. Huang**, C. Lehane, D. Kim, **H. S. Kwok**, J. Swiatkiewicz, G. C. Xu, and P. N. Prasad, "Picosecond photoresponse in Y-Ba-Cu-O ultrathin films", Phys. Rev. B 48, 6550 (1993).

224. **L. Shi, G. L. Huang**, C. Lehane, D. H. Kim, and **H. S. Kwok**, "Study of photoresponse of high-T_C Y-Ba-Cu-O superconducting ultrathin films using a picosecond laser pulse train", Appl. Phys. Lett. 63, 2830 (1993).

Semenov, Gol'tsman, Gershenzon, Lindgren, Karasik, Goghidze, Sergeev, Nebosis, Renk, *et al.*: gap suppression, nonequilibrium electron heating and kinetic inductance

225. **A. D. Semenov, G. N. Gol'tsman, I. G. Goghidze, A. V. Sergeev, E. M. Gershenzon**, P. T. Lang, and **K. F. Renk**, "Subnanosecond photoresponse of YBaCuO thin film to infrared and visible radiation by quasiparticle induced suppression of superconductivity", Appl. Phys. Lett. 60, 903 (1992).

226. **R. S. Nebosis**, R. Steinke, P. T. Lang, W. Schatz, M. A. Heusinger, **K. F. Renk, G. N. Gol'tsman, B. S. Karasik, A. D. Semenov**, and **E. M. Gershenzon**, "Picosecond $YBa_2Cu_3O_{7-\delta}$ detector for far-infrared radiation", J. Appl. Phys. 72, 5496 (1992).

227. **A. D. Semenov, I. G. Goghidze, G. N. Gol'tsman, A. V. Sergeev**, E. E. Aksaev, and **E. M. Gershenzon**, "Non-equilibrium quasiparticle response to radiation and bolometric effect in YBaCuO films", IEEE Trans. Appl. Supercond. 3, 2132 (1993).

228. **R. S. Nebosis**, M. A. Heusinger, W. Schatz, **K. F. Renk, G. N. Gol'tsman, B. S. Karasik, A. D. Semenov**, and **G. M. Gershenzon**, "Ultrafast photoresponse of a structured $YBa_2Cu_3O_{7-\delta}$ thin film to ultrashort FIR laser pulses", IEEE Trans. Appl. Supercond. 3, 2160 (1993).

229. **A. D. Semenov, I. G. Goghidze, G. N. Gol'tsman, A. V. Sergeev**, and **E. M. Gershenzon**, "Evidence for the spectral dependence of nonequilibrium picosecond photoresponse of YBaCuO thin films", Appl. Phys. Lett. 63, 681 (1993).

230. **M. Lindgren**, V. Tifonov, M. Zorin, **M. Danerud**, D. Winkler, **B. S. Karasik, G. N. Gol'tsman**, and **E. M. Gershenzon**, "Transient resistive photoresponse of $YBa_2Cu_3O_{7-\delta}$ films using low power 0.8 and 10.6 μm laser radiation", Appl. Phys. Lett. 64, 3036 (1994).

231. **M. Danerud**, D. Winkler, **M. Lindgren**, M. Zorin, V. Trifonov, **B. S. Karasik, G. N. Gol'tsman**, and **E. M. Gershenzon**, "Nonequilibrium and bolometric photoresponse in patterned $YBa_2Cu_3O_{7-\delta}$ thin films", J. Appl. Phys. 76, 1902 (1994).

232. **B. Karasik, M. Lindgren**, M. Zorin, **M. Danerud**, D. Winkler, V. Trifonov, **G. Gol'tsman**, and **E. M. Gershenzon**, "Picosecond detection and broadband mixing of near-infrared radiation by YBaCuO films", Proc. SPIE 2159, (1994).

233. **G. N. Gol'tsman**, **I. G. Goghidze**, P. B. Kouminov, **B. S. Karasik**, **A. D. Semenov**, and **E. M. Gershenzon**, "Influence of grain boundary weak links on the nonequilibrium of YBaCuO thin films to short laser pulses", J. Supercond. 7, 751 (1994).

G. N. Gol'tsman, P. B. Kouminov, **I. G. Goghidze**, **B. S. Karasik**, and **E. M. Gershenzon**, "Nonbolometric and fast bolometric responses of YbaCuO thin films

in superconducting, resistive, and normal states", Proc. SPIE 2159, (1994).

G. Gol'tsman, P. Kouminov, **I. Goghidze**, and **E. Gershenzon**, "Nonequilibrium kinetic inductive reponse of YbaCuO thin films to low-power laser pulses", preprint received Sept. 13, 1994.

234. **R. S. Nebosis**, M. A. Heusinger, W. Schatz, A. Piehler, R. Löw, N. Reschauer, **K. F. Renk, A. D. Semenov**, P. Kouminov, **I. G. Goghidze**, and **E. M. Gershenzon**, "A TlBa2Ca2Cu3O9 film for detection of visible and far-infrared radiation", Proc. SPIE 2159, (1994).

235. **A. D. Semenov, R. S. Nebosis**, Y. P. Gousev, M. A. Heusinger, and **K. F. Renk**, "Analysis of the nonequilibrium photoresponse of superconducting films to pulses radiation by use of a two-temperature model", preprint received from A. D. Semenov, Aug. 4, 1994.

Bluzer *et al.*: kinetic inductive nonbolometric

236. **N. Bluzer**, D. K. Fork, T. H. Geballe, M. R. Beasley, M. Y. Reizer, S. R. Greenfield, J. J. Stankus, and M. Fayer, "Superconducting, transition, and normal state photoresponse in YBCO observed at different temperatures", IEEE Trans. Magn. 27, 1519 (1991).

237. **N. Bluzer**, "Temporal relaxation of nonequilibrium in Yba-Cu-O measured from transient photoimpedance response", Phys. Rev. B 44, 10222 (1991).

238. **N. Bluzer**, "Temporal relaxation measurements of photoinduced nonequilibrium in superconductors", J. Appl. Phys. 71, 1336 (1992).

239. **N. Bluzer**, "Temporal relaxation of photoinduced nonequilibrium in niobium", Phys. Rev. B 46, 1033 (1992).

240. **N. Bluzer**, "Biexponential decay and delay artifact in the photoresponse of superconductors", IEEE Trans. Appl. Supercond. 3, 2869 (1993).

241. **N. Bluzer** and **M. G. Forrester**, "Superconducting quantum detectors", Opt. Engin. 33, 697 (1994).

242. **N. Bluzer** and **M. G. Forrester**, "Superconducting quantum detectors in YBCO",

J. Supercond. 7, 395 (1994).

Johnson: nonbolometric photoresponse in YBCO

243. **M. Johnson**, "Nonbolometric photoresponse of $YBa_2Cu_3O_{7-\delta}$ films", Appl. Phys. Lett. 59, 1371 (1991). See also Ref. 125.

Ghis, Villegier, et al.: kinetic inductive nonbolometric

244. **A. Ghis**, S. Pfister, **J.-C. Villegier**, M. Nail, and **J. P. Maneval**, "Ultrafast nonbolometric photoresponse of $YBa_2Cu_3O_{7-\delta}$ thin films", IEEE Trans. Appl. Supercond. 3, 2136 (1993).

245. **A. Ghis, J.-C. Villegier**, S. Pfister, M. Nail, and Ph. Gibert, "Electrical picosecond measurements of the photoresponse in $YBa_2Cu_3O_{7-\delta}$ ", Appl. Phys. Lett. 63, 551 (1993).

246. **A. Ghis, J.-C. Villegier**, M. Nail, and S. Striby, "Ultrafast combined bolometric and nonbolometric infrared detector", Proc. SPIE 2159, (1994).

Hegmann *et al.*: kinetic inductive bolometric

247. **F. A. Hegmann** and **J. S. Preston**, "Identification of nonbolometric photoresponse in $YBa_2Cu_3O_{7-\delta}$ thin films based on magnetic field dependence", Appl. Phys. Lett. 62, 1158 (1993). (Paper A)

248. **F. A. Hegmann** and **J. S. Preston**, "Origin of the fast photoresponse of epitaxial $YBa_2Cu_3O_{7-\delta}$ thin films", Phys. Rev. B 48, 16023 (1993). (Paper B)

249. **F. A. Hegmann, R. A. Hughes**, and **J. S. Preston**, "High speed kinetic inductive bolometric photoresponse of epitaxial $YBa_2Cu_3O_{7-\delta}$ thin films", Proc. SPIE 2159, (1994). (Paper C)

250. **F. A. Hegmann, R. A. Hughes**, and **J. S. Preston**, "Picosecond photoresponse of epitaxial $YBa_2Cu_3O_{7-\delta}$ thin films", Appl. Phys. Lett. 64, 3172 (1994). (Paper D)

Dissipative mechanisms, TAFF, and resistive transition broadening

251. **T. T. M. Palstra**, B. Batlogg, R. B. van Dover, L. F. Schneemeyer, and J. V. Waszczak, "Dissipative flux motion in high-temperature superconductors", Phys. Rev. B 41, 6621 (1990).

252. **P. P. Nguyen**, Z. H. Wang, A. M. Rao, M. S. Dresselhaus, J. S. Moodera, G. Dresselhaus, H. B. Radousky, R. S. Glass, and J. Z. Liu, "Transport and magnetic properties of $YBa_2Cu_3O_{7-\delta}Br_y$ single crystals", Phys. Rev. B 48, 1148 (1993).

253. **M. Leghissa**, A. Königer, M. Lippert, W. Dorsch, M. Kraus, and G. Saemann-Ischenko, "Dissipative flux motion in $YBa_2Cu_3O_{7-\delta}$ films - Investigation by means of transport I-V curves", Z. Phys. B 92, 163 (1993).

254. **R. Kumar**, S. K. Malik, S. P. Pai, P. R. Apte, R. Pinto, R. Vijayaraghavan, and D. Kumar, "Self-field-induced flux creep in $YBa_2Cu_3O_{7-\delta}$ thin films", Phys. Rev. B 46, 5766 (1992).

255. **Q. Y. Ying** and **H. S. Kwok**, "Kosterlitz-Thouless transition and conductivity fluctuations in Y-Ba-Cu-O thin films", Phys. Rev. B 42, 2242 (1990).

256. **K. Kadowaki**, Y. Songliu, and K. Kitazawa, "Lorentz-force-independent dissipation in high-temperature superconductors", Supercond. Sci. Technol. 7, 519 (1994).

257. **C. Y. Chang**, C.-S. Lue, and Y. C. Chou, "Analysis of the I-V characteristics of $YBa_2Cu_3O_{7-\delta}$ superconductive films in the transition region", Phys. Rev. B 49, 1488 (1994).

Kinetic inductance: theory and devices

258. **R. Meservey** and **P. M. Tedrow**, "Measurements of the kinetic inductance of superconducting linear structures", J. Appl. Phys. 40, 2028 (1969).

259. **J. W. Baker**, J. D. Lejeune, and D. G. Naugle, "Effects of a nonuniform current distribution on the kinetic inductance of a thin superconducting film", J. Appl. Phys. 45, 5043 (1974).

260. **J. M. Pond**, J. H. Claassen, and W. L. Carter, "Kinetic inductance microstrip delay

lines", IEEE Trans. Magn. 23, 903 (1987).

261. **D. G. McDonald**, "Novel superconducting thermometer for bolometric applications", Appl. Phys. Lett. 50, 775 (1987).

262. **J. E. Sauvageau** and **D. G. McDonald**, "Superconducting kinetic inductance bolometer", IEEE Trans. Magn. 25, 1331 (1989).

263. **J. E. Sauvageau, D. G. McDonald**, and **E. N. Grossman**, "Superconducting kinetic inductance radiometer", IEEE Trans. Magn. 27, 2757 (1991).

264. **E. N. Grossman, D. G. McDonald**, and **J. E. Sauvageau**, "Far-infrared kinetic inductance detectors", IEEE Trans. Magn. 27, 2677 (1991).

265. **E. K. Track**, R. E. Drake, and C. K. G. Hohenwarter, "Optically modulated superconducting delay lines", IEEE Trans. Appl. Supercond. 3, 2899 (1993).

266. **J. C. Culbertson**, H. S. Newman, **U. Strom, J. M. Pond**, D. B. Chrisey, J. S. Horwitz, and S. A. Wolf, "Detection of light using high temperature superconducting microstrip lines", IEEE Trans. Magn. 27, 1536 (1991).

267. **D. Zhang**, D. V. Plant, H. R. Fetterman, K. Chou, S. Prakash, C. V. Deshpandey, and R. F. Bunshah, "Optical control of millimeter wave high T_C superconducting quasi-optical bandpass filters", Appl. Phys. Lett. 58, 1560 (1991).

Current distribution in superconducting bridges

268. **T. R. Lemberger**, in *Physical Properties of High Temperature Superconductors III*, ed. D. M. Ginsberg (World Scientific, Singapore, 1992), p. 490.

269. **L. H. Lee**, T. P. Orlando, and W. G. Lyons, "Current distribution in superconducting thin-film strips", IEEE Trans. Appl. Supercond. 4, 41 (1994).

270. **D. M. Sheen**, S. M. Ali, D. E. Oates, R. S. Withers, and J. A. Kong, "Current distribution, resistance, and inductance for superconducting strip transmission lines", IEEE Trans. Appl. Supercond. 1, 108 (1991).

- - - - -

271. **A. M. Kadin** and A. M. Goldman, "Dynamical effects in nonequilibrium superconductors: some experimental perspectives", *ibid* Ref. 116, p.270.

272. **P. Bernstein**, J. F. Hamet, B. Blanc-Guihon, S. Flamet, C. Dubuc, J. Bok, X. Q. Zhang, J. P. Contour, and F. R. Ladan, "A mean field description of the transition to the mixed state of superconducting microbridges with low vortex pinning forces", J. Appl. Phys. 76, 2929 (1994).

273. **F. Steglich**, U. Ahlheim, C. D. Bredl, C. Geibel, M. Lang, A. Loidl, and G. Sparn, "Superconductivity and magnetism in heavy-fermion compounds", in *Selected Topics in Superconductivity*, eds. L. C. Gupta and M. S. Multani (World Scientific, Singapore, 1993). p. 527.

Electronic heat capacity in YBCO

274. **M. E. Reeves**, D. A. Ditmars, S. A. Wolf, T. A. Vanderah, and V. Z. Kresin, "Evidence for strong electron-phonon coupling from the specific heat of $YBa_2Cu_3O_{7-\delta}$", Phys. Rev. B 47, 6065 (1993).

M. E. Reeves, V. Z. Kresin, and S. A. Wolf, "Thermodynamic determination of the electron-phonon coupling strength in $YBa_2Cu_3O_{7-\delta}$", J. Supercond. 7, 257 (1994).

275. **A. Junod**, E. Bonjour, R. Calemczuk, J. Y. Henry, J. Muller, G. Triscone, and J. C. Vallier, "Specific heat of an single crystal in fields up to 20 T", Physica C 211, 304 (1993).

A. Junod, "Specific heat of high temperature superconductors: a review", in *Physical Properties of High Temperature Superconductors II*, ed. D. M. Ginsberg (World Scientific, Singapore, 1990).

Electron-phonon interaction in YBCO

276. **T. Timusk**, C. D. Porter, and D. B. Tanner, "Strong electron-phonon interaction in the high-T_C superconductors: evidence from the infrared", Phys. Rev. Lett. 66, 663 (1991).

277. **M. Gurvitch** and **T. Fiory**, "Resistivity of $La_{1.825}Sr_{0.175}CuO_4$ and $YBa_2Cu_3O_{7-\delta}$ to 1100 K: absence of saturation and its implications", Phys. Rev. Lett. 59, 1337 (1987).

278. **G. L. Zhao** and J. Callaway, "Strong electron-phonon interaction in $YBa_2Cu_3O_{7-\delta}$", Phys. Rev. B 49, 6424 (1994).

279. **B. Friedl**, C. Thomsen, and M. Cardona, "Determination of the superconducting gap in $YBa_2Cu_3O_{7-\delta}$", Phys. Rev. Lett. 65, 915 (1990).

- - - - -

Paper A

"Identification of nonbolometric photoresponse in $YBa_2Cu_3O_{7-\delta}$ thin films based on magnetic field dependence"

F. A. Hegmann and J. S. Preston, Appl. Phys. Lett. 62, 1158-1160 (1993).

Summary:

Paper A contains some of the earliest work performed by our group on the photoresponse of epitaxial YBCO thin films using 100 ps laser pulses. Photoresponse signals with fast and slow components were observed. To distinguish between bolometric and nonbolometric behaviour, a novel technique was developed which used a small magnetic field to modulate the resistance of the bridge in the resistive transition region. The amplitude of the slow component was affected by the field and was therefore attributed to a resistive bolometric response. On the other hand, the fast component was not affected by the field and therefore could not be explained by a resistive bolometric response. Since at that time the KIB model had not yet been developed, we concluded that the fast response was evidence for a nonbolometric response. The paper was unique in that it offered an alternative technique to identify a resistive response rather than relying solely on thermal models. The paper also emphasized the importance of "mapping" the resistive transition as a function of temperature and bias current so that proper identification of a resistive response could be made.

Identification of nonbolometric photoresponse in $YBa_2Cu_3O_{7-\delta}$ thin films based on magnetic field dependence

F. A. Hegmann
Department of Physics and Astronomy, McMaster University, Hamilton, Ontario L8S 4M1, Canada

J. S. Preston
Department of Engineering Physics, McMaster University, Hamilton, Ontario L8S 4M1, Canada

(Received 22 September 1992; accepted for publication 23 December 1992)

Optically induced transient voltages across a current-biased bridge structure fabricated from an epitaxial $YBa_2Cu_3O_{7-\delta}$ thin film are reported. A novel technique consisting of applying a small magnetic field perpendicular to the sample was used to identify any bolometric contribution to the photoresponse. Comparison to resistance versus temperature curves with and without the field establishes a slow component in the photoresponse as bolometric and unambiguously identifies a fast component as a nonthermal transient.

Nonbolometric transient voltage signals have been studied in granular films of high-T_c superconductors by a number of authors.[1] In many cases, these systems have been successfully modeled as a network of Josephson weak links. For epitaxial thin films with high critical currents the issue is more contentious. Numerous authors have reported nonbolometric signals[2-5] while a comparable number have interpreted the observed voltage transients as being solely thermal in origin.[6,7] In the cases where the transient voltage signal has been assigned a nonbolometric origin, most authors have relied on the short duration of the transient and its weak dependence on the ambient temperature in identifying the nonbolometric contribution.[2] Mechanisms for nonbolometric response have been attributed to light-induced nonequilibrium superconductivity,[3-5] photoenhanced flux creep,[3,8] photofluxonic detection,[9] and kinetic inductance effects.[10] It has been shown,[11,12] however, that thermal transients can have short recovery times approaching 1 ns[11] and, due to their high speed, may have been misinterpreted as being nonthermal in origin. The uncertainty in the thermal properties and the complexity of the thermal processes make the unambiguous identification of a nonthermal photoresponse difficult.[11]

In this letter, application of a small magnetic field assists in distinguishing between the thermal and nonthermal components of a photoresponse signal. The field broadens the resistance versus temperature characteristic of a $YBa_2Cu_3O_{7-\delta}$ (YBCO) thin-film bridge without affecting the optical or thermal properties of the sample. The field will therefore modify any bolometric response in accordance with the measured broadening.

The sample used in these experiments was a 1200 Å, c-axis oriented $YBa_2Cu_3O_{7-\delta}$ epitaxial thin film grown by laser ablation on $LaAlO_3$. The film was patterned into a bridge 50 μm wide and 200 μm long using standard photolithographic techniques resulting in a T_c of 89 K and a transition width of 1 K, as shown in Fig. 1.

The laser source provided 100 ps, 532 nm pulses at a repetition rate of 12.7 kHz. A cylindrical lens was used to focus the beam down to a 20×200 μm^2 elliptical spot with the major axis perpendicular to the length of the bridge, resulting in an energy of 1 nJ per pulse (~ 100 $\mu J/cm^2$) incident on the bridge.

The sample was mounted in vacuum on the cold finger of a closed cycle He gas refrigerator, and was biased with currents up to 100 mA through two of four contacts on the sample. The other two contacts were connected to a 35 cm SMA coaxial cable which brought the high-speed signal to a bias-T just outside the chamber. A nanovoltmeter connected to the inductor side of the bias-T monitored the dc voltage across the sample with a resolution of about 50 nV, allowing accurate measurements of the dc resistance of the sample during photoresponse measurements. A 20 dB amplifier with a frequency range of 0.1 MHz to 1 GHz was inserted between the capacitor side of the bias T and a 20 GHz sampling oscilloscope. The total system response time with the sample in place was estimated to be 400 ps. A magnetic field of 100 Gauss oriented perpendicular to the sample could be applied by placing two large ring-shaped permanent magnets outside the chamber.

Broadening of the resistive transition due to the applied magnetic field at various bias currents is shown in Fig. 1. Since the field is weak the broadening is significant only at high current densities, and is shown on an expanded scale in Fig. 2 at a bias of 100 mA (1.7×10^6 A/cm^2). Both curves in Fig. 2 are roughly exponential as

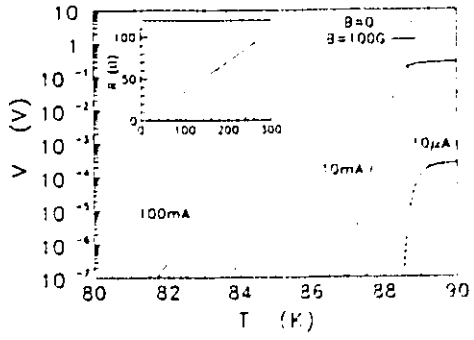

FIG. 1. The dc voltage measured across the 200 μm long YBCO thin film bridge structure as a function of temperature, bias current, and magnetic field. The broadening due to the 100 Gauss field increased with bias current. The inset shows the resistance of the bridge as a function of temperature with $T_c=89$ K and $\Delta T_c=1$ K at a bias current of 10 μA.

 0003-6951/93/101158-03$06.00

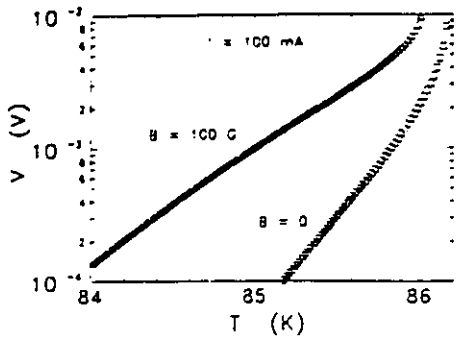

FIG. 2. Expanded view of the dc voltage across the bridge as a function of temperature showing the resistive broadening due to the field at a bias current of 100 mA. This figure is used to directly estimate transient temperatures from the amplitudes of the observed photosignals.

a function of temperature except for sharp upturns above 86 K due to self-heating. Figure 2 will be used to convert the bolometric photoresponse to an effective transient temperature of the illuminated portion of the bridge. Two factors need to be accounted for before this conversion can be made. First, only the 20 μm irradiated portion of the 200 μm bridge is responsible for the transient photosignal. Second, an amplifier with a $\times 10$ voltage gain was inserted for the photoresponse measurements. These two factors cancel, so that Fig. 2 can be used directly to estimate the maximum temperature reached by the exposed region of the film.

A simple estimate of the transient temperature ΔT in the film assumes that the energy from the incident laser pulse is absorbed instantaneously and uniformly in the film. The heat capacity of YBCO single crystals[13] increases with temperature from nominally 1.0 J/cm^3 K at 80 K to 1.16 J/cm^3 K at 90 K, where a density of 6.39 g/cm^3 has been used. In a volume of 20 μm$\times$50 μm$\times$1200 Å, the temperature change per nJ *absorbed* in the film is about 8.3 K at 80 K and 7.2 K at 90 K. An optical penetration depth of 900 Å at 532 nm results in 25% transmission through the film.[14] With a reflectance[15] of approximately 10%, the transient temperature induced in the film per *incident* nJ is $\Delta T \approx 5$ K.

In Fig. 3, the photoresponse for an incident fluence of 1 nJ and a bias current of 100 mA is shown for three different temperatures in zero field. From initial tempera-

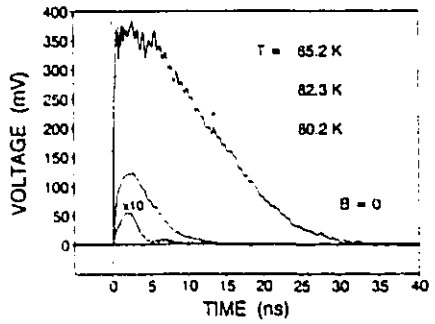

FIG. 3. Photoresponse signals seen at three temperatures with a bias of 100 mA, an incident fluence of 1 nJ, and zero magnetic field. The signal at 80.2 K is multiplied by a factor of 10.

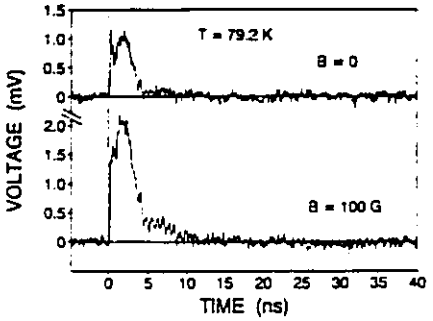

FIG. 4. Effect of the applied magnetic field on the photoresponse at 79.2 K with a bias of 100 mA and a fluence of 1 nJ. With the field applied, the slow component was larger than the fast component.

tures of 85.2 and 82.3 K, a ΔT of 5 K is consistent with final temperatures well above the sharp upturn at 86 K in Fig. 2 resulting in large photosignals which were relatively insensitive to the applied magnetic field. At 80.2 K, a 5.5 mV signal was observed corresponding to a transient of 6 K, which is very close to the estimated ΔT of 5 K. There was a weak magnetic field dependence observed in this case.

As the temperature was lowered further to 79.2 K, a double-peak structure emerged with distinct fast and slow components, as shown in Fig. 4. The effect of the applied field was to increase the amplitude of the slow component by a factor of 2 without significantly changing the fast component. (The fast component can be visualized as being superimposed on top of the rising edge of the slower component.) This implies that the fast component is nonbolometric since it was unaffected by the resistive broadening introduced by the applied magnetic field. Using Fig. 2, the amplitudes of the slow components in Fig. 4 correspond to peak transient temperatures of 6.2 and 6.6 K. The agreement between these two values and the estimated ΔT of 5 K support a bolometric origin for the slow component.

In Fig. 5, the incident fluence was lowered to 0.65 nJ at 80.2 K. Without the magnetic field, only a fast component less than 500 ps wide was observed. The resolution of this fast component was limited by the time response of the system. With the magnetic field applied, this fast component was unchanged but was superimposed on a 0.2 mV

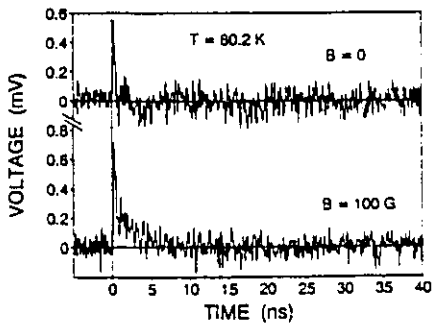

FIG. 5. Effect of the applied magnetic field on the photoresponse at 80.2 K with a fluence of 0.65 nJ. Only a very fast spike was seen in zero field. With the field aplied, both a fast spike and a slow tail were observed. The width of the fast spike was less than 500 ps.

slow component corresponding to a temperature transient of 4 K. Note that if we take ΔT as 6.6 K for 1 nJ, then an energy of 0.65 nJ should give $\Delta T = 4.3$ K in agreement with the observed transient. Without the field, no bolometric component was observed since a 4 K thermal transient from 80.2 K corresponds to a voltage well below the noise level of the system.

With nonuniform absorption, diffusion of heat through a film of thickness d will have a characteristic time constant $\tau_{diff} = d^2/D$, where D is the thermal diffusivity given by $D = \kappa/C$, where κ is the thermal conductivity and C is the heat capacity. The thermal conductivity of YBCO single crystals[16] increases below T_c and peaks around 40–50 K. Nominal values for κ are 0.11 W/cm K at 80 K and 0.09 W/cm K at 90 K, giving $D \approx 0.11$ cm^2/s and 0.08 cm^2/s and $\tau_{diff} \approx 1.3$ and 1.8 ns, respectively, for a 1200 Å film. The separation between the peaks of the fast and slow components seen in Fig. 4 at 79.2 K is about 1.7 ns, suggesting the slow rise of the slow component may be due to heat diffusing to the back of the film. However, studies of the anisotropy of the thermal conductivity[17] have found κ_c approximately 4–5 times smaller than κ_{ab}. Since the film was c-axis oriented, this would result in longer thermal diffusion times of 5–9 ns making the interpretation of the delay uncertain.

Heat conduction out of the film and into the substrate material[11,12] will occur in a time $\tau_{diss} = C/G = C R_{bd}/A$, where G is the thermal boundary conductance at the film-substrate interface, R_{bd} is the thermal boundary resistance, and A is the area of the interface. Using $R_{bd} \approx 1.0 \times 10^{-3}$ K cm^2/W[7,11] for YBCO on $LaAlO_3$, $C \approx 0.13$ nJ/K, and $A = 20 \times 50\ \mu m^2$ gives $\tau_{diss} \approx 13$ ns for heat to dissipate out of the film and into the substrate. This is consistent with pulse widths of 16 ns observed at 85.2 K in Fig. 3, but cannot explain the faster recovery times seen at lower temperatures. Nevertheless, none of the characteristic thermal time constants estimated above can predict a transient less than 500 ps wide.

Many authors reporting nonbolometric photosignals[2,4,5] have observed fast transient peaks followed by monotonically decaying slow components. A *double-peak* structure similar to the response shown in Fig. 4 has also been observed elsewhere[10] and has been attributed to changes in the kinetic inductance of the sample. However, the negative voltage transients[10] that result from kinetic inductance modulation were not observed in our experiments.

In summary, we have developed a simple technique using the resistive broadening induced by a small magnetic field to help identify thermal and nonthermal components in the photoresponse of high T_c superconducting thin films. A fast transient less than 500 ps wide was observed which was not modified by the applied field. We believe this fast transient is evidence for a nonbolometric photoresponse in epitaxial YBCO thin films.

The authors gratefully acknowledge Thomas Strach for his assistance with the film growth. This work was supported by the Ontario Centre for Materials Research and the Natural Sciences and Engineering Research Council of Canada.

[1] Y. Enomoto, T. Murakami, and M. Suzuki, Physica C **153–155**, 1592 (1988); M. Leung, P. R. Broussard, J. H. Claassen, M. Osofsky, S. A. Wolf, and U. Strom, Appl. Phys. Lett. **51**, 2046 (1987); G. Schneider, H. Lengfellner, J. Betz, K. F. Renk, and W. Prettl, Int. J. IR MM Waves **12**, 1 (1991); J. C. Culbertson, U. Strom, S. A. Wolf, and W. W. Fuller, Phys. Rev. B **44**, 9609 (1991); U. Strom, E. S. Snow, R. L. Henry, P. R. Broussard, J. H. Claassen, and S. A. Wolf, IEEE Trans. Magn. **MAG-25**, 1315 (1989).
[2] H. S. Kwok, J. P. Zheng, Q. Y. Ying, and R. Rao, Appl. Phys. Lett. **54**, 2473 (1989).
[3] A. Frenkel, M. A. Saifi, T. Venkatesan, P. England, X. D. Wu, and A. Inam, J. Appl. Phys. **67**, 3054 (1990).
[4] M. Johnson, Appl. Phys. Lett. **59**, 1371 (1991).
[5] A. D. Semenov, G. N. Gol'tsman, I. G. Gogidze, A. V. Sergeev, E. M. Gershenzon, P. T. Lang, and K. F. Renk, Appl. Phys. Lett. **60**, 903 (1992).
[6] W. S. Brocklesby, D. Monroe, A. F. J. Levi, M. Hong, S. H. Liou, J. Kwo, C. E. Rice, P. M. Mankiewich, and R. E. Howard, Appl. Phys. Lett. **54**, 1175 (1989); W. R. Donaldson, A. M. Kadin, P. H. Ballentine, and R. Sobolewski, *ibid*, 2470 (1989); A. M. Kadin, P. H. Ballentine, and W. R. Donaldson, Physica B **165 & 166**, 1507 (1990).
[7] G. L. Carr, M. Quijada, D. B. Tanner, C. J. Hirschmugl, G. P. Williams, S. Etemad, B. Dutta, F. DeRosa, A. Inam, T. Venkatesan, and X. Xi, Appl. Phys. Lett. **57**, 2725 (1990).
[8] E. Zeldov, N. M. Amer, G. Koren, A. Gupta, R. J. Gambino, and M. W. McElfresh, Phys. Rev. Lett. **62**, 3093 (1989); E. Zeldov, N. M. Amer, G. Koren, and A. Gupta, Phys. Rev. B **39**, 9712 (1989).
[9] A. M. Kadin, M. Leung, A. D. Smith, and J. M. Murduck, Appl. Phys. Lett. **57**, 2847 (1990).
[10] N. Bluzer, Phys. Rev. B **44**, 10222 (1991); N. Bluzer, J. Appl. Phys. **71**, 1336 (1992).
[11] M. Nahum, S. Verghese, and P. L. Richards, Appl. Phys. Lett. **59**, 2034 (1991).
[12] S. Zeuner, H. Lengfellner, J. Betz, K. F. Renk, and W. Prettl, Appl. Phys. Lett. **61**, 973 (1992).
[13] E. Bonjour, R. Calemczuk, J. Y. Henry, and A. F. Khoder, Physica B **165 & 166**, 1343 (1990); A. Schilling, H. R. Ott, J. D. Guo, S. Rusiecki, J. Karpinski, and E. Kaldis, Physica C **185–189**, 1755 (1991).
[14] H. Yasuoka, H. Mazaki, T. Terashima, and Y. Bando, Physica C **175**, 192 (1991).
[15] T.-W. Nee, J. Appl. Phys. **71**, 6002 (1992).
[16] S. D. Peacor, R. A Richardson, F. Nori, C. Uher, Phys. Rev. B **44**, 9508 (1991); J. L. Cohn, S. A. Wolf, T. A. Vanderah, V. Selvamanickam, and K. Salama, Physica C **192**, 435 (1992).
[17] S. J. Hagen, Z. Z. Wang, and N. P. Ong, Phys. Rev. B **40**, 9389 (1989); M. Sera, S. Shamoto, M. Sato, I. Watanabe, S. Nakashima, and K. Kumagai, Solid State Commun. **74**, 951 (1990).

Paper B

"Origin of the fast photoresponse of epitaxial $YBa_2Cu_3O_{7-\delta}$ thin films"

F. A. Hegmann and J. S. Preston, Phys. Rev. B 48, 16023-16039 (1993).

Summary:

Paper B first introduced the KIB model through an extensive study of the temperature, bias current, and film-thickness dependence of the photoresponse of epitaxial YBCO thin films exposed to 100 ps laser pulses. The theory behind the KIB model is presented, and fits of the KIB model to the observed data are made. It is concluded that the observed photoresponse signals from 100 ps laser pulses can be adequately described by the KIB model. Although nonequilibrium changes in the kinetic inductance had already been used by other groups to explain the origin of fast photoresponse signals, Paper B marked the first time that fast photoresponse signals were attributed to changes in kinetic inductance due to *equilibrium* (bolometric) heating of the film by the laser pulse.

Origin of the fast photoresponse of epitaxial $YBa_2Cu_3O_{7-\delta}$ thin films

F. A. Hegmann
Department of Physics and Astronomy, McMaster University, Hamilton, Ontario, Canada L8S 4M1

J. S. Preston
Department of Engineering Physics, McMaster University, Hamilton, Ontario, Canada L8S 4M1
(Received 9 July 1993)

We have measured the photoresponse of current-biased bridge structures of epitaxial $YBa_2Cu_3O_{7-\delta}$ thin films on $LaAlO_3$ using 100 ps, 532 nm laser pulses. Voltage transients with fast and slow components were observed below T_c. The amplitude of the slow component agrees with a resistive bolometric response where the laser pulse heats the bridge into the resistive transition region. The decay time of the slow component is consistent with a thermal time constant for heat loss out of the film governed by the thermal boundary resistance at the interface between the film and the substrate. We show that the fast component can be explained by changes in the kinetic inductance of the bridge due to *temperature-induced* changes in the superfluid density from heating of the bridge by the laser pulse. Our interpretation of the origin of the fast component, therefore, is bolometric in nature over the time scale of the laser pulse contrary to some of the nonequilibrium or nonbolometric mechanisms that have been proposed. A simulation of this kinetic inductive bolometric effect provides reasonable agreement with the temperature dependence of the observed photoresponse, and a comparison is made between the various postulated temperature dependencies of the superfluid fraction in $YBa_2Cu_3O_{7-\delta}$. The simulation further shows that the speed of the kinetic inductive bolometric photoresponse is not limited by the thermal escape time out of the film, but is determined by the *rate* at which the incident laser pulse initially heats the film and is therefore the same duration in time as the laser pulse. Evidence for negative voltage transients observed in the photoresponse data consistent with the simulation results is also presented.

I. INTRODUCTION

The photoresponse of high-T_c superconductors has been actively studied over the past few years. The motivation behind most of the research has been the development of photodetectors sensitive to a very broad range of wavelengths. The ability to cool high-T_c superconducting films with liquid nitrogen has made them quite attractive for use as sensitive transition-edge bolometers.[1-4] Such detectors rely on heating from incident radiation inducing a large resistive change in the film biased in the sharp transition region. The response time of transition-edge bolometers is limited by the rate of heat loss out of the film, but thermal response times as short as 1 ns are possible.[5] Relatively well established with conventional superconductors, application of this technology with high-T_c superconductors has progressed to the point where one company[6] has marketed a superconducting bolometer for infrared detection using a patterned $YBa_2Cu_3O_{7-\delta}$ (YBCO) line on a micromachined silicon wafer.

Granular and epitaxial high-T_c thin films offer the possibility of developing very fast photodetectors which rely on nonequilibrium or nonbolometric (nonthermal) mechanisms for detection. Studying the nonbolometric photoresponse may also offer insight into the nature of superconductivity in the high-T_c oxides. The photoresponse in granular films[7-11] has been attributed to light-induced phase-slip processes in the Josephson junction weak links between the grains. Nanosecond response times have been observed in polycrystalline Tl-Ba-Ca-Cu-O thin films[10] at wavelengths larger than 100 μm, and response times of a few picoseconds have been predicted[11] in granular YBCO thin films.

It is not so clear that intergrain phase-slip processes can explain the fast photoresponse in epitaxial thin films characterized by high critical currents. Indeed there has been some controversy over whether or not high-T_c epitaxial thin films exhibit a nonbolometric photoresponse at all. In some experiments, only a bolometric photoresponse in epitaxial thin films was observed[12-14] where the voltage transients could be explained by the laser pulses heating the film within or into the resistive region. In other experiments, both bolometric and nonbolometric signals were observed,[15-25] where bolometric usually implied a resistive mechanism and nonbolometric was a term used by many authors to refer to signals that were too fast or had too little temperature dependence below T_c to be due to the resistive bolometric mechanism.[15] While in some cases, nanosecond thermal transients may have been misinterpreted as nonbolometric transients,[5] the 30 ps wide voltage transients recently observed[25] in epitaxial YBCO thin films cannot be explained by characteristic thermal response times.

Nonbolometric signals have also been identified by deviations of the observed transient voltage ΔV from a simple resistive bolometric response governed by $\Delta V = I\, dR/dT\, \Delta T$, where I is the bias current, dR/dT is the temperature derivative of the resistance, and ΔT is

the transient temperature generated in the film by the incident light. It should be noted that this approach is invalid for the large ΔT produced by intense laser pulses since the resistance curve of a superconductor is highly nonlinear near T_c. Using the actual $R(T)$ is preferred; however, precise values of ΔT are required to make a clear and unambiguous identification of a nonthermal photoresponse which relies on accurate thermal modeling.[5,26,27] A magnetic field has been used in a technique to help distinguish between bolometric and nonbolometric components in the photoresponse of epitaxial YBCO thin films.[28]

Among the groups that have reported a nonbolometric photoresponse, there has been little consensus regarding the origin of the nonbolometric mechanism in epitaxial thin films. The nonbolometric photoresponse has been discussed in terms of optically generated quasiparticles suppressing the superconducting order parameter[16–18,20,22–24,33] or changing the sample's kinetic inductance,[16,18–20,23,25] or attributed to optically induced flux motion phenomena such as photoenhanced flux creep,[29] photoactivated flux flow,[17] and photofluxonic detection.[30] Fast current switching of optically thick YBCO films by intense laser pulses[31] was explained by nonequilibrium hot electrons inducing a bolometric response after having traveled to the back of the film. A related set of experiments involves pump-probe measurements of YBCO thin films which have examined quasiparticle thermalization times,[32–35] electron-phonon coupling parameters,[36] and quasiparticle recombination times[32] over subpicosecond and picosecond time scales. However, interpretation of the results from these experiments remains controversial.[37]

In this paper, we argue that the fast photoresponse observed below T_c in epitaxial YBCO thin-film bridge structures due to 100 ps laser pulses, which we previously attributed to a nonbolometric mechanism,[28] can be explained by temperature-induced changes of the kinetic inductance in the bridge and is, therefore, essentially bolometric in origin. Kinetic inductance arises from the inertia of the superconducting electrons and, as discussed later, is inversely proportional to the superfluid density (or proportional to λ_L^2, where λ_L is the London penetration depth). The superfluid density depends on temperature, so the temperature transient induced by the laser pulse will change the kinetic inductance of the bridge. At constant current bias, a change in kinetic inductance will produce a voltage transient across the bridge which constitutes the photoresponse. The voltage transient is potentially the same width as the laser pulse, or 100 ps in this case. However, bandwidth limitations in the measuring circuit (see Sec. II) have limited the observed widths to just under 500 ps. The fast component can therefore be described as a kinetic inductive bolometric response. Slower components in the photoresponse with nanosecond decay times observed near the transition region are due to a resistive bolometric response.

The study of kinetic inductance in superconductors is not a new subject. The kinetic inductance of microwave superconducting microstrip transmission lines has been studied extensively.[38] The temperature variation of the kinetic inductance has been used in YBCO microstrip resonators to measure the temperature dependence of the London penetration depth[39] (providing information on the superfluid fraction) and in variable delay YBCO microstrip delay lines.[40] Recently, an optically modulated superconducting delay line has been constructed which relies on the bolometric modulation of the kinetic inductance in a YBCO microstrip.[41] Kinetic inductance bolometers have also been developed[42] which operate below T_c and require a superconducting quantum interference device (SQUID) to sense changes in the inductance of the circuit. The kinetic inductive bolometric mechanism we are proposing for the fast photoresponse is similar to the detection principle of a kinetic inductance bolometer. To our knowledge, this is the first time such a mechanism has been used to explain the origin of the fast photoresponse in high-T_c epitaxial thin films.

The remainder of the paper is organized as follows. The YBCO film characteristics and photoresponse measurement techniques are discussed in the Sec. II. Section III discusses the broadening of the resistive transition due to the bias current, shows some typical transient voltage wave forms, describes the temperature and current dependence of the photoresponse, and analyzes the resistive bolometric response due to heating from the laser pulse in the transition region. The origin of the fast photoresponse is discussed in terms of kinetic inductance, and a simulation of the photoresponse based on the kinetic inductive bolometric response mechanism is compared with our observations. Finally, a summary is given in Sec. IV.

II. EXPERIMENT

Epitaxial thin films of YBCO were deposited on $LaAlO_3$, substrates by laser ablation. The c-axis films were grown at 760 °C in 300 mTorr oxygen, then allowed to cool in 0.5 atm oxygen. Film thickness ranged from 30 to 260 nm, and substrate sizes were nominally $6\times6\times0.5$ mm^3. The films were patterned into bridge structures using standard photolithographic techniques and a wet chemical etch of 0.1% HCl and HNO_3 in deionized water. Etch times were typically 10–20 s, thus minimizing the exposure time of the films in water. Standard lift-off techniques were used to pattern 200-nm-thick gold pads on the YBCO film. Contact resistance was less than 0.1 Ω after annealing at 500 °C for 30 min in 1 atm flowing oxygen. The annealing process also improved the adhesion of the gold pads to the YBCO film.

Table I gives the characteristics after processing for the four films described here. The zero resistance critical temperature T_{c0} ranged from 86 to 90 K, and transition widths ΔT_c varied from 3 K for the thinnest film to about 1 K for the thickest films. Degradation of T_{c0} due to processing was about 2 K for the thinnest films and less than 0.5 K for the thickest films. In particular, the 30 nm film degraded further in time as a result of oxygen loss from the bridge. The critical current density J_c for the bridges at 77 K was nominally 1×10^6 A/cm^2 after processing, using a voltage criteria of 10^{-7} V across the 200 μm bridges or 5 μV/cm. Bridge resistivities were typically

TABLE I. Specifications for the four films described in the paper. The patterned bridges have a thickness d, width w, and length l. $T_{c0(R=0)}$ is the zero resistance transition temperature after patterning using a 10^{-7} V criteria (5 μV/cm), and ΔT_c is the width of the superconducting transition. The critical current I_c at 77 K (5 μV/cm criteria) for each bridge is shown from which the critical current density J_c at 77 K is calculated. The resistance R of the bridge at 100 K is used to estimate the corresponding resistivity ρ. When referring to a specific film in the text, the film thickness d will be used.

d (nm)	w (μm)	l (μm)	$T_{c0(R=0)}$ (K)	ΔT_c (K)	I_c at 77 K (mA)	J_c at 77 K (A/cm^2)	R at 100 K (Ω)	ρ at 100 K ($\mu\Omega$ cm)
30	20	200	86	3	5	8.3×10^5	600	180
130	20	200	87	2	25	9.6×10^5	120	160
220	20	200	90	<1	100	2.3×10^6	50	110
260	10	200	89	1	45	1.7×10^6	110	140

150 $\mu\Omega$ cm at 100 K.

A frequency doubled Nd:YAG laser provided 100 ps, 532 nm (2.33 eV) mode-locked pulses at a repetition rate of 76 MHz. The 1.5 W average laser power from this source resulted in excessive sample heating and made photoresponse measurements difficult. In order to maintain a high energy per pulse but lower the average power in the beam, a pulse extraction system was used to select individual pulses at a repetition rate of 12.7 kHz. This lowered the average beam power at the sample to less than 0.4 mW while providing 4 nJ per selected pulse. The contrast ratio of the pulse selection system was typically 300:1. Variations in the contrast ratio had little effect on the amplitude of the selected pulse, but had a large effect on the average beam power. It was estimated that the average beam power of 0.4 mW increased the temperature of the sample by less than 0.1 K. Power dissipation at the current contacts was at most about 1 mW and therefore did not contribute significantly to heating of the sample. A cylindrical lens was used to focus the laser pulse to a 20 μm$\times$200 μm elliptical spot on the bridge, producing a fluence of about 100 μJ/cm^2. The long axis of the spot was oriented perpendicular to the bridge to minimize beam misalignment due to thermal drift of the sample holder in the chamber.

The samples were mounted in vacuum on the end of a cold finger of a closed cycle He gas refrigerator. The measuring circuit is shown in Fig. 1. A constant current source provided bias currents up to 100 mA through two of the four gold contacts on the YBCO film. The other two contacts were connected to a 50 Ω SMA coaxial cable 40 cm long which brought the transient voltage signal from the bridge structure to a bias T and amplifier. The bias T had a rise time of 20 ps and a lower cutoff of 0.5 MHz. The amplifier, which had a gain of 20 dB ($\times$10 voltage gain) from 0.1 MHz to 1 GHz, enabled low level transients to be observed on a 20 GHz sampling oscilloscope, resulting in a system rise time of 400 ps. We did observe photoresponse transients with full widths at half maximum (FWHM) less than 500 ps, but we assume these were attenuated due to the finite frequency response of our circuit. A nanovoltmeter attached to the bias-T allowed *in situ* four-point probe voltage measurements across the bridge with a resolution of 50 nV. Each wave form acquired on the sampling oscilloscope was averaged 128–512 times. Wave forms were taken at positive and negative current bias and then subtracted to remove dc offsets and noise pickup, resulting in a noise limit on the wave forms acquired from the oscilloscope of about 0.05 mV.

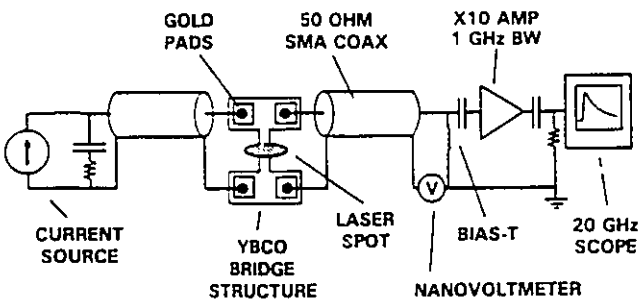

FIG. 1. Schematic of the experimental setup used for the photoresponse measurements.

III. RESULTS

A. Broadening of the resistive transition due to bias current

Before photoresponse measurements on a sample were taken, the steady state (dc) voltage across the bridge was plotted as a function of temperature and various bias currents, as shown in Fig. 2(a) for the 260 nm film. This provided a detailed "map" of the resistive transition region which enabled identification of the resistive bolometric photoresponse. As the current bias increased, the value for T_{c0} decreased (10^{-7} V criteria) and the width of the transition increased. The critical current I_c is a linear function of temperature from 65 to 85 K, which is consistent with the temperature dependence of the critical current density J_c observed in YBCO thin films.[43] With the bias current held constant, increasing the temperature beyond a certain point resulted in a very sharp and sudden upturn in the measured voltage which may have been due to runaway thermal effects from the generation of hot spots in the bridge.[44] Figure 2(b) plots the resistance of the bridge as a function of temperature and bias current on a linear scale to emphasize the broadening. Several photoresponse studies[12,17,28,29] have

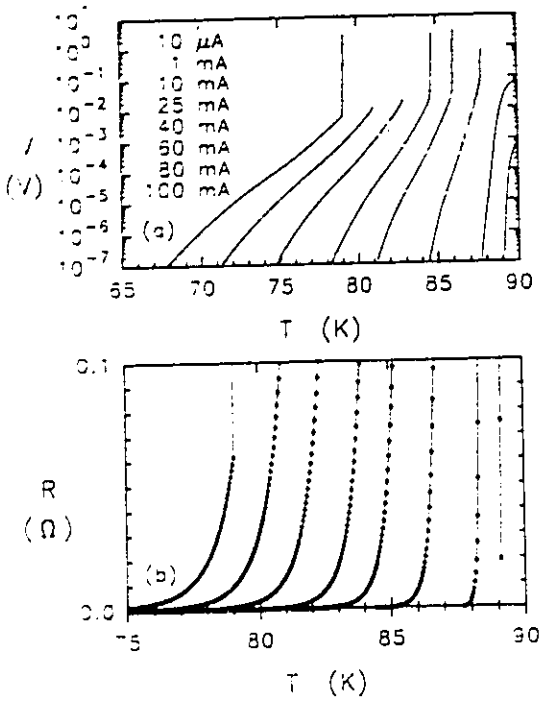

FIG. 2. Resistive transition broadening as a function of bias current observed for the 260 nm film under steady-state (dc) conditions and zero external field. In (a), the dc voltage V measured across the 200 μm long bridge is plotted on a logarithmic scale as a function of temperature T. The rightmost curve is for a bias current of 10 μA, and the leftmost curve with the broadest transition was taken at 100 mA. The corresponding bridge resistance R is plotted on a linear scale in (b) as a function of temperature to emphasize the broadening of the transition and lowering of T_{c0} due to the bias current. The lines drawn in (b) are only guides to the eye. Similar plots were made for the other films providing maps of the resistive transitions for each film.

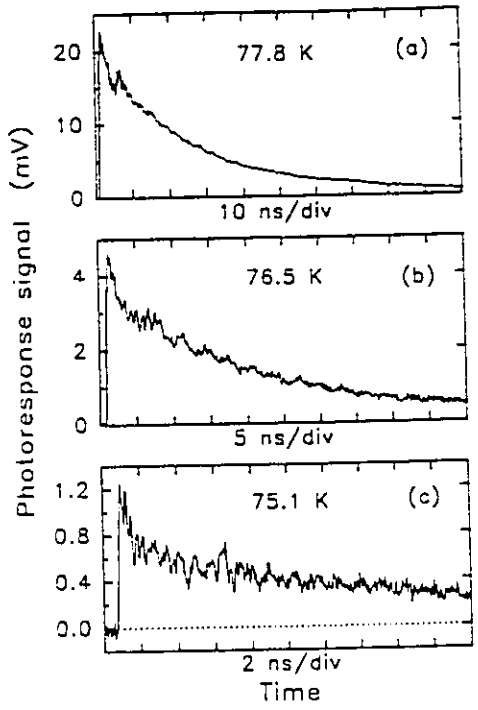

FIG. 3. Photoresponse signals observed in the resistive transition region of the 260 nm film at a bias of 100 mA and laser fluence of 100 μJ/cm^2. Notice the change in the time scale for each of the wave forms. In (a), at a temperature of 77.8 K, the signal is quite large and has a long decay. As the temperature is lowered to 76.5 K in (b), the slowly decaying component has decreased dramatically in amplitude, but a fast component begins to appear at the start of the wave form. In (c) at 75.1 K, the fast component is becoming more prominent and the slow component has decreased further in amplitude.

examined the effect of current bias on the resistive transition.

Considering that only 20 μm of the 200-μm-long bridge was illuminated by the laser spot and the amplifier had a gain of 10, it was possible to use the resistive transition map for each sample to directly convert observed voltage transients to transient temperatures if the photoresponse was resistive bolometric in origin. Examples of this method are discussed in the next section and more thoroughly in Sec. III E.

B. Typical photoresponse wave forms

The observed transient voltages for the 260 nm film with 100 mA bias are shown in Figs. 3 and 4 for various temperatures. Figure 5 shows an expanded view of the 100 mA resistive transition curve from Fig. 2(a). Figure 3(a) shows the transient response of the bridge at a temperature of 77.8 K which is close to the sudden upturn seen in Fig. 5(a) at 79 K. The amplitude of the signal is large and the decay time is close to 30 ns. As the temperature is lowered to 76.5 and 75.1 K, a fast transient peak appears at the start of the slowly decaying component as shown in Figs. 3(b) and 3(c). In Fig. 4(a), the fast component dominates over slow component at 74.2 K, and in Fig. 4(b) the slow component has completely vanished below our noise limit at 71.4 K and all that remains is the fast component with a pulse width less than 500 ps. The fast component persists with decreasing amplitude even to lower temperatures. This is shown in Fig. 4(c) where the temperature has been reduced to 45.7 K.

We will show that the temperature transient induced by the laser pulse in the current-biased bridge produces two types of photoresponse: (1) a slow component due to a resistive bolometric photoresponse which dominates when the maximum temperature attained by the temperature transient in the bridge is within the resistive transition region, and (2) a fast component due to a kinetic inductive bolometric photoresponse which can be seen at temperatures below the resistive transition. Photoresponse signals consisting of a fast component followed by a slow component have been reported by other groups studying the photoresponse of epitaxial YBCO thin films.[15,18,20–23,25,45]

The resistive transition curve shown in Fig. 5 can be used to determine the resistive bolometric nature of the slow component and demonstrate the nonresistive nature of the fast component.[28] In Fig. 3(b), the amplitude of

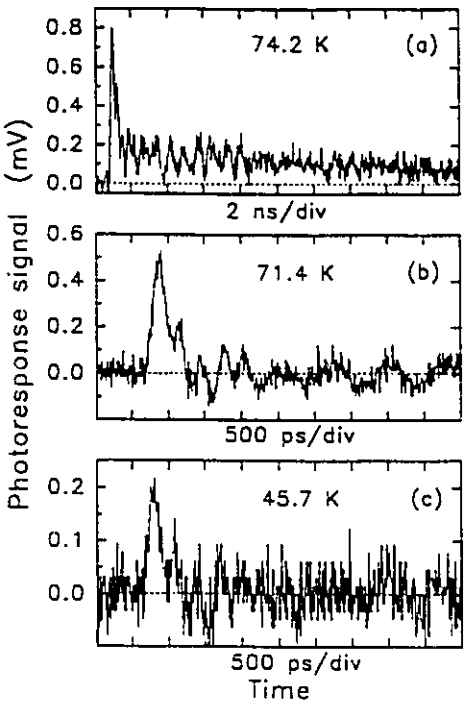

FIG. 4. Photoresponse signals observed in the resistive transition region and at lower temperatures for the 260 nm film at a bias of 100 mA and laser fluence of 100 $\mu J/cm^2$. The sequence of wave forms presented here is continued from Fig. 3. Notice the change in time scale for the wave forms. In (a), at a temperature of 74.2. K, the fast component at the start of the wave form dominates over the slow component. At 71.4 K in (b), the slow component has completely disappeared below the noise level of the oscilloscope and only the fast component remains. The fast component persists to lower temperatures with a decreased amplitude as shown in (c) at a temperature of 45.7 K well below the resistive transition region. The fast photoresponse in (c) is less than 500 ps wide.

the slow component is roughly 3.5 mV. At an initial temperature $T_{INITIAL}$ of 76.5 K, Fig. 5(b) indicates that the initial dc voltage across the bridge is about 0.4 mV. Since the sample is ac coupled to the scope, a voltage transient ΔV of 3.5 mV due to a change in resistance of the bridge produces a maximum voltage across the bridge of 3.9 mV, which corresponds to a maximum temperature T_{MAX} of 78.7 K in Fig. 5(b) or a temperature transient ΔT of 2.2 K. From the analysis given in Sec. III E below, a simple thermal model provides an estimate of 3.4 K for the temperature transient, which is close to the observed value in this case of 2.2 K. Interpreting the 0.2 mV fast response seen at 45.7 K in Fig. 4(c) to a change in resistance of the bridge would require a transient temperature of almost 30 K according to Fig. 5. This is quite different from a 7.8 K transient predicted by the simple thermal model, implying that the fast response cannot be due to a resistive bolometric effect. The fact that the fast response can be explained by kinetic inductance effects will be demonstrated by a simulation of the photoresponse data given in Sec. III F.

C. Temperature dependence of the photoresponse

The amplitude of the photoresponse as a function of temperature and at a constant bias current for the 260 nm film is shown in Fig. 6. Examples of wave forms observed in this temperature range are shown in Figs. 3 and 4. The rapid decrease of the signal as the temperature is lowered below the resistive transition region is evident. However, the photoresponse is seen to persist to lower temperatures. The inset of Fig. 6 shows more clearly the amplitude of the fast and slow components as a function of temperature below the resistive transition. Notice how the slow component, which is attributed to resistive bolometric effects, disappears quite sharply below the resistive transition region. Below 72 K, the slow component has completely vanished and only the fast component remains which decreases more slowly in amplitude as the temperature is lowered further.

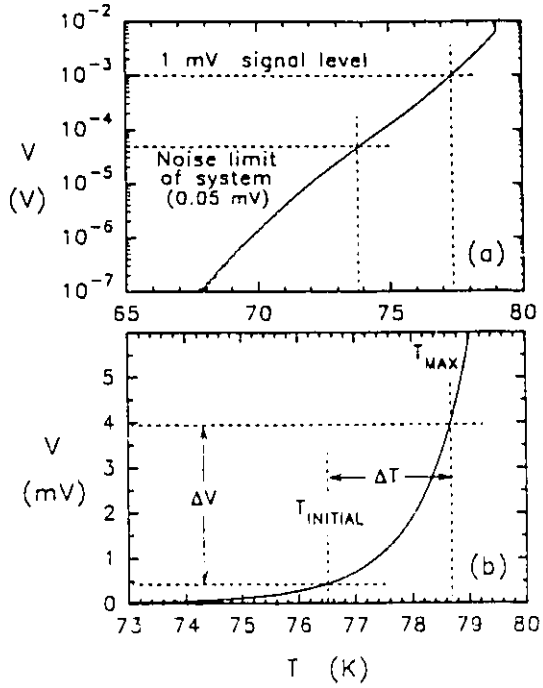

FIG. 5. Expanded view of the dc voltage V measured across the 200-μm-long bridge as a function of temperature for the 260 nm film at a bias of 100 mA taken from Fig. 2(a). The curve can be used to determine if the observed photoresponse was due to temperature transients induced by the laser pulse bringing the temperature of the bridge into the resistive region. In (a), the noise limit of 0.05 mV determines the minimum temperature ($\approx$73.8 K) needed to be reached at the peak of the temperature transient in the film in order for a resistive photoresponse to be observed. In other words, resistive bolometric voltage transients would not be seen on the oscilloscope if this minimum temperature requirement were not satisfied. If the peak temperature reached by the film were around 77.3 K and the initial temperature was less than 70 K, then the resistive photoresponse signal would be about 1 mV. The transition curve is plotted on a linear scale in (b). The parameters shown in (b) are described in the text.

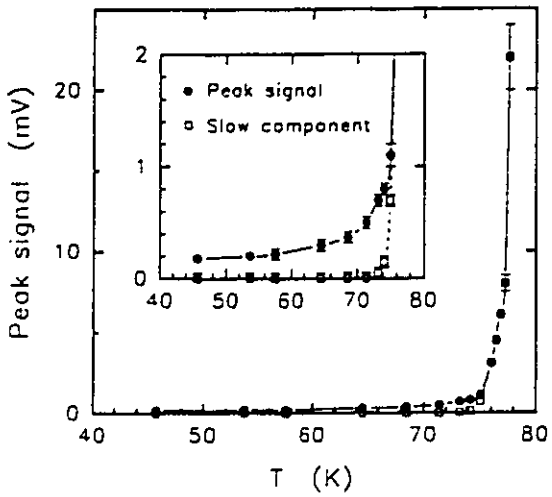

FIG. 6. Temperature dependence of the peak photoresponse signal for the 260 nm film at a bias of 100 mA and laser fluence of 100 $\mu J/cm^2$. Examples of some of the wave forms for these points are shown in Figs. 3 and 4. The inset shows the low-temperature region more clearly and plots the peak amplitude of the photoresponse signal (filled circles) and the amplitude of the slow component only (open squares) which follows the fast transient. The slow component rapidly disappears as the temperature is lowered, and only the fast component remains at temperatures less than 72 K. The lines are a guide to the eye.

D. Current dependence of the photoresponse

Figure 7 shows the amplitude of the photoresponse signal as a function of current bias for the 260 nm film at a constant temperature of 78 K. Figure 8 shows typical wave forms associated with the data points in Fig. 7. The

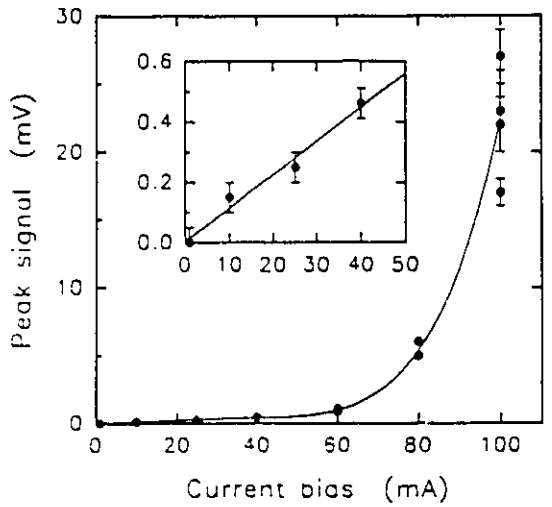

FIG. 7. Bias current dependence of the peak photoresponse signal for the 260 nm film at a temperature of 78 K and laser fluence of 100 $\mu J/cm^2$. The inset shows the linear dependence of the photoresponse with bias current at low current values. In the linear regime, only the fast photoresponse is observed. The sudden increase in signal amplitude seen above 60 mA is due to the film entering the resistive region at these higher current levels. The line in the main plot is only a guide to the eye. The line in the inset is a linear regression fit to the low current data. Examples of some of the wave forms for these points are shown in Fig. 8.

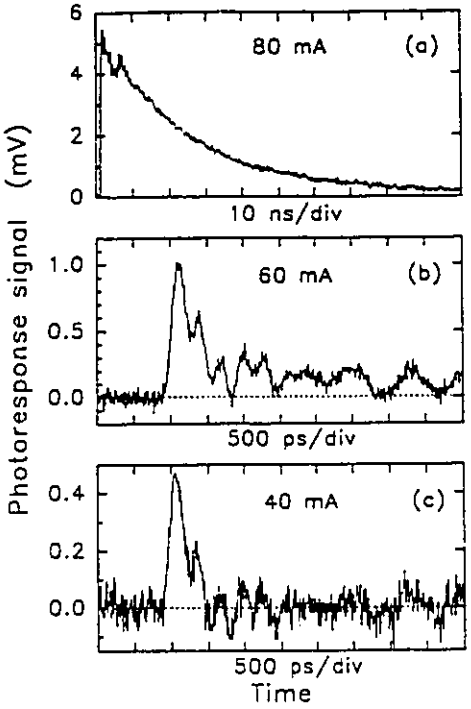

FIG. 8. Bias current dependence of the observed photoresponse wave forms for the 260 nm film at a temperature of 78 K and a laser fluence of 100 $\mu J/cm^2$. Notice the change in time scale for the wave forms. The amplitudes of these transients are plotted in Fig. 7. At high bias currents, the signal is resistive bolometric and has a long decay time as shown in (a). As the current is lowered to 60 mA in (b), the slow component is almost gone. Only the fast component remains in (c) since a bias of 40 mA is insufficient to bring the film into the resistive region. Below 40 mA, the amplitude of the fast response is linear with current, as shown in the inset of Fig. 7.

sudden rise in amplitude of the photoresponse above 60 mA corresponds to the induced temperature transient entering the broadened resistive region at higher bias currents, as can be seen by examining Fig. 2(a). The scatter in the peak signal readings at 100 mA in Fig. 7 is due to small changes in laser fluence near the highly nonlinear upturn of the resistive transition shown in Fig. 5. A slow component in the photoresponse was observed for currents above 60 mA, as shown in Fig. 8(a) at 80 mA and Fig. 8(b) at 60 mA. Below 60 mA, which was out of the resistive transition region, only a fast photoresponse was observed, as seen in Fig. 8(c) for a 40 mA bias. What is important to note here is that the fast photoresponse observed below 60 mA varied *linearly* with current, as shown more clearly in the inset of Fig. 7. A linear dependence of the fast photoresponse with bias current has also been observed elsewhere.[17–19,23,24]

Similar behavior in the photoresponse was also seen in the 30 nm film, as shown in Fig. 9, and the 130 and 220 nm films. Figure 10 shows wave forms for some of the data points in Fig. 9. The voltage transient seen in Fig. 10(a) for the 30 nm film at a bias of 60 mA is a resistive bolometric response with a width of about 650 ps

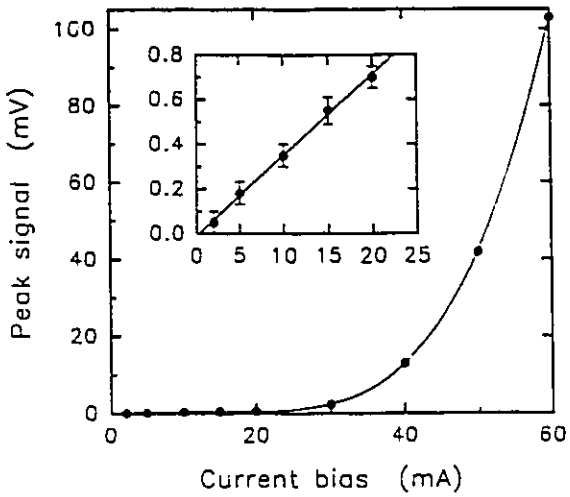

FIG. 9. Bias current dependence of the peak photoresponse signal for the 30 nm film at a temperature of 54 K and laser fluence of 100 $\mu J/cm^2$. The inset shows the linear dependence of the photoresponse with bias current at low current values. As in Fig. 7 for the 260 nm film, only the fast photoresponse was observed in this linear regime. The line in the main plot is only a guide to the eye. The line in the inset is a linear regression fit to the low current data. Examples of some of the wave forms for these points are shown in Fig. 10.

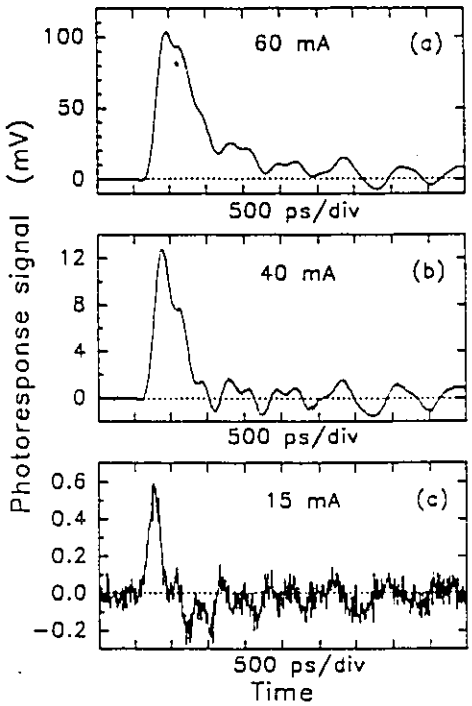

FIG. 10. Bias current dependence of the observed photoresponse wave forms for the 30 nm film at a temperature of 54 K and a laser fluence of 100 $\mu J/cm^2$. The amplitudes of these transients are plotted in Fig. 9. The fast, 650 ps FWHM transient with 60 mA bias seen in (a) is a resistive bolometric response. In (b) at 40 mA, the film is still in the resistive region and the response is still resistive bolometric despite its 450 ps FWHM pulse width. The film leaves the resistive region for currents below 30 mA and only the fast response is seen, as shown in (c) at a bias of 15 mA. In this current region, the fast photoresponse is linear with bias current, as shown in the inset of Fig. 9.

FWHM. Reducing the current to 40 mA in Fig. 10(b) produces a transient still in the resistive region with a width of about 450 ps FWHM. In Fig. 10(c), the current level is low enough to bring the film out of the resistive transition region, and the amplitude of the fast response is linear with current, as shown in the inset of Fig. 9. The width of the transient in Fig. 10(c) is about 220 ps FWHM. As mentioned earlier, the amplitude of these short transients will be attenuated due to the finite bandwidth of the measuring circuit.

E. Analysis of the resistive bolometric (slow) photoresponse

Examples of resistive bolometric wave forms from the four films at temperatures and bias currents in the resistive transition region are shown in Fig. 11. The decay time of the voltage transients decreases as the film thickness is reduced. This is consistent with faster thermal decay times for thinner films, but the magnitude of the thermal escape time cannot be read directly from the voltage transient wave forms due to the nonlinearity of the resistive transition. The temperature transient as a function of time induced in the film by the laser pulse can be determined by finding the temperature in the dc resistance transition curve at which the dc voltage equals the voltage in the photoresponse transient at a given time.

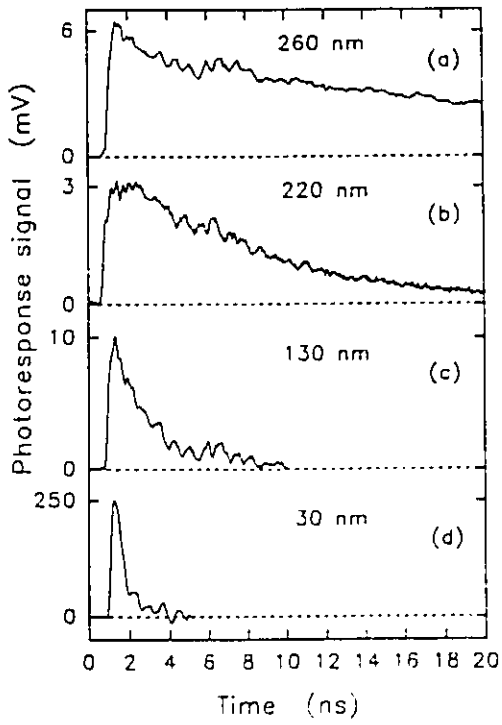

FIG. 11. Examples of resistive bolometric photoresponse signals seen in the four films biased in their resistive transition regions. The decay time for the 260 nm film in (a) is greater than 20 ns, but gets progressively shorter as the film thickness is decreased becoming as short as 1 ns for the 30 nm film in (d). The temperature at which each of the wave forms was taken is given in Table II. The laser fluence was 100 $\mu J/cm^2$, and the current bias was 100 mA in (a), 80 mA in (b), 75 mA in (c), and 20 mA in (d).

An example of this technique, which gives more accurate estimates of thermal escape times, is described below.

A voltage transient from the 130 nm film at 70 K is shown in Fig. 12. A current of 75 mA was enough to bias the bridge into the resistive transition region, as seen in Fig. 13. The temperature transient shown in Fig. 12 was obtained by converting the voltage transient values in Fig. 12 to equivalent temperatures using Fig. 13. Due to the nonlinear nature of the resistive transition, the decay of the transient voltage signal is much faster than the decay of the temperature transient. The same technique was used on the resistive bolometric signals from the other films shown in Fig. 11, and the normalized temperature transients are shown in Fig. 14. The main feature of Fig. 14 is the faster thermal decay observed for thinner films. The amplitudes and thermal decay times (exponential fit) of the observed temperature transients for the four films are given in Tables II and III, respectively.

A simple thermal model using the thermal boundary resistance between the film and the substrate[5] can be used to estimate the amplitude of the transient temperature

$$\Delta T_{\text{ESTIMATE}} = \frac{F}{Cd}\frac{E_{\text{ABS}}}{E_0} \tag{1}$$

and the thermal decay time for heat loss out of the film

$$\tau_{\text{ESTIMATE}} = CR_{\text{BD}}d\ , \tag{2}$$

where F is the incident laser fluence in J/cm^2, C is the heat capacity of the film in J/cm^3 K, d is the thickness of the film in cm, and R_{BD} is the thermal boundary resistance in K cm^2/W. The factor E_{ABS}/E_0 is the fraction of the total incident energy absorbed in the film and takes into account transmission of the laser pulse through the film and reflection from the front surface given by

$$E_{\text{ABS}}/E_0 = (1-R)[1-\exp(-d/\delta)]\ , \tag{3}$$

where R is the reflectivity and δ is the optical penetration depth. Equation (3) neglects reflection from the back surface of the film and multiple reflections in thin films.

The heat capacity[46,47] of YBCO decreases almost

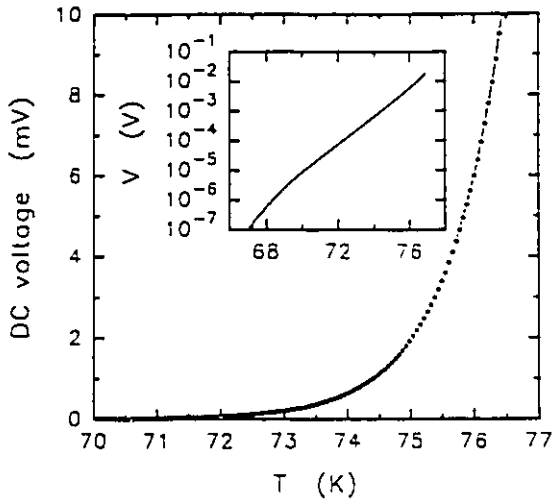

FIG. 13. dc voltage measured across the 200-μm-long bridge as a function of temperature for the 130 nm film at a bias of 75 mA. This curve was used to determine the temperature transient induced in the film shown in Fig. 12. The line is a guide to the eye. The inset plots the voltage on a logarithmic scale showing an exponential voltage dependence over most of the temperature range for this sample.

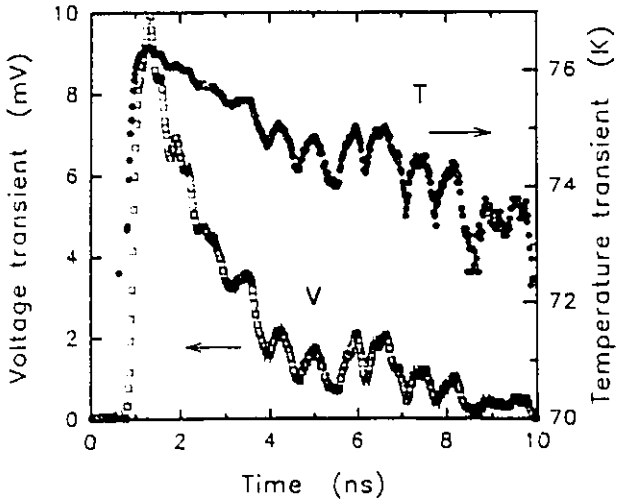

FIG. 12. Voltage transient (V, open squares) observed from the 130 nm film biased in the resistive transition region ($T=70$ K, $I=75$ mA, $F=100$ μJ/cm^2) and corresponding temperature transient (T, closed circles) interpolated from the measured dc resistive transition curve shown in Fig. 13. Due to the nonlinear nature of the resistive transition, the voltage transient has a faster fall time than the temperature transient. The voltage transient is the same as that shown in Fig. 11(c).

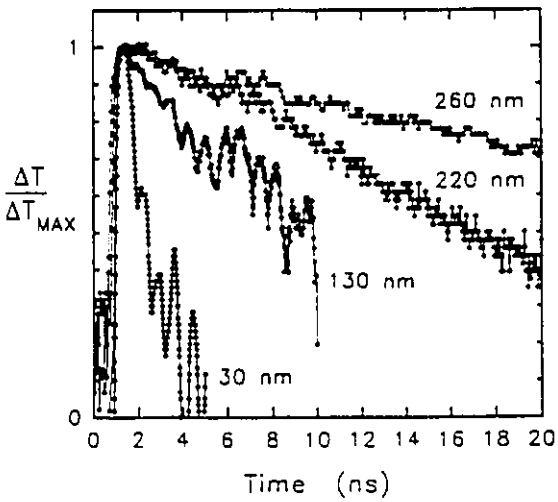

FIG. 14. Normalized temperature transients interpolated from photoresponse signals (shown in Fig. 11) taken in the resistive transition regions of the four films. As discussed in the text, the faster thermal decay time observed for the thinner films is consistent with Eq. (2). Exponential fits to this data provided values for the maximum temperature transients ΔT_{MAX} and thermal decay times τ_{OBSERVED} for each of the films, as shown in Tables II and III.

linearly from a value of 1.0 J/cm^3 at 78 K to 0.4 J/cm^3 at 45 K (see Fig. 16 in Sec. III F). The thermal boundary resistance[5] between YBCO thin films and $LaAlO_3$ substrates is nominally 1.0×10^{-3} K cm^2/W and independent of temperature from 90 to 200 K. At lower temperatures,

$$R_{BD}=B/T^3 , \tag{4}$$

where $B\approx17$ K^4 cm^2/W for YBCO on sapphire.[5] Therefore, the T^{-3} behavior of R_{BD} will become significant for temperatures below 30 K, and will have the effect of increasing the thermal escape time from the film. At 532 nm (2.33 eV), the reflectivity[48] of bulk single-crystal YBCO is about 10% ($R=0.1$), and the absorption coefficient α of YBCO thin films[49] is approximately 1.1×10^5 cm^{-1} which gives an optical penetration depth of $\delta=1/\alpha\approx90$ nm. Using Eq. (3), E_{ABS}/E_0 will be 0.85 for the 260 nm film and 0.26 for the more transmissive 30 nm film. If a shorter optical penetration depth[50] of 60 nm at 532 nm is used, the values for E_{ABS}/E_0 change to 0.89 and 0.35, respectively, which will not seriously affect the results. However, even though the thinner film absorbs less energy from the laser pulse, the temperature transient induced in the thinner film will be larger. As an example, if the laser fluence is 100 μJ/cm^2 and the heat capacity is 1.0 J/cm^3 K ($T=78$ K), then from Eq. (1) we find that ΔT induced by the laser pulse is 3.3 K for the 260 nm film and as high as 8.7 K for the 30 nm film. From Eq. (2), the thermal escape times will then be 26 ns for the 260 nm film and only 3 ns for the 30 nm film at 78 K.

Table II compares the transient temperatures extracted from the analysis above to estimates of ΔT using Eq. (1). The agreement is within a factor of 2, which is reasonable considering the uncertainty in some of the parameters. The agreement is also quite reasonable in Table III when comparing estimates of the thermal escape time using Eq. (2) to exponential fits of the decay times for the observed temperature transients shown in Fig. 14. If it is not assumed that $R_{BD}=1.0\times10^{-3}$ K cm^2/W (Ref. 5), then R_{BD} can be estimated using the observed thermal decay times. The average value of the estimates for R_{BD} given in Table III is $(1.1\pm0.6)\times10^{-3}$ K cm^2/W, which is in good agreement with other reported values.[5,14,23,51] This analysis supports the claim that the slow component is a resistive bolometric photoresponse with a decay time determined by the thermal boundary resistance between the YBCO film and the $LaAlO_3$ substrate.

TABLE II. Comparison of observed transient temperature amplitudes $\Delta T_{OBSERVED}$ for the four films of thickness d to estimates of the transient temperature $\Delta T_{ESTIMATE}$ using Eq. (1). The estimates use the heat capacity C of the YBCO film at an initial temperature T_i. E_{ABS}/E_0 is the fraction of incident laser pulse energy absorbed in the film, as described by Eq. (3). ($F=100$ μJ/cm^2, $R=0.1$, $\delta=90$ nm.)

d (nm)	T_i (K)	C (J/cm^3 K)	E_{ABS}/E_0	$\Delta T_{OBSERVED}$ (K)	$\Delta T_{ESTIMATE}$ (K)
30	73	0.91	0.26	~5	9.5
130	70	0.85	0.69	6.3	6.2
220	84	1.11	0.82	1.7	3.4
260	77	0.98	0.85	2.3	3.3

We now consider characteristic thermal diffusion times given by

$$\tau_{DIFF}=\frac{d^2}{D}=\frac{d^2C}{\kappa} , \tag{5}$$

where D is the thermal diffusivity in cm^2/s and κ is the thermal conductivity W/cm K. Using τ_{DIFF} as an estimate for the rate of heat loss out of the film and into the substrate would assume that there is no thermal mismatch at the boundary between the YBCO film and the $LaAlO_3$ substrate. Values for κ in YBCO single crystals[52] depend on sample quality and direction of heat flow[53] but are nominally 0.12 W/cm K in the ab plane near 80 K and roughly 4 to 5 times smaller[53] along the c axis. This would give $D_{ab}\approx0.12$ cm^2/s and $D_c\approx0.026$ cm^2/s near 80 K. Since the epitaxial films used here have the c axis perpendicular to the substrate, we consider the thermal diffusivity along the c axis for heat flow out of the film and into the substrate. Upper estimates for τ_{DIFF} along the c axis are shown in Table III using Eq. (5) with $\kappa_c\approx0.026$ W/cm K and $C\approx1$ J/cm^3 K. For the thinnest films, a thermal boundary resistance model is in better agreement with the data. Thermal diffusion time constants will become significant in thicker films since the incident light is absorbed mainly in the first 100 nm of the film thickness.

F. Discussion of the origin of the fast photoresponse

1. Kinetic inductance interpretation

Under dc bias, a superconductor will ideally exhibit zero resistance. If an alternating bias is supplied, a finite voltage will appear across the superconductor due to the inertia of the superconducting carriers. The kinetic inductance, which gives rise to this impedance in the superconductor, for a superconducting strip of length l, width w, and thickness d can be expressed[38] in several ways as

$$L_{KIN}=\frac{m}{n_{SC}e^2}\left|\frac{l}{wd}\right|=\mu_0\lambda_L^2\left|\frac{l}{wd}\right| =\frac{1}{\varepsilon_0\omega_{P_{SC}}^2}\left|\frac{l}{wd}\right|=\frac{1}{\varepsilon_0\omega_P^2}\left|\frac{1}{f_{SC}}\right|\left|\frac{l}{wd}\right| \tag{6}$$

where m is the effective mass of the superconducting carriers, n_{SC} is the density of superconducting carriers in a two fluid model, μ_0 is the permeability of free space, ε_0 is the permittivity of free space, λ_L is the temperature-dependent London penetration depth, ω_P is the plasma frequency, and f_{SC} is the superfluid fraction equal to n_{SC}/n, where n is the total density of carriers. The kinetic inductance of a superconducting bridge is therefore proportional to the square of the London penetration depth or inversely proportional to the superfluid fraction. The forms with λ_L and ω_P in Eq. (6) are useful in that λ_L and ω_P can be determined more accurately than n_{SC} or

TABLE III. Comparison of observed thermal decay times $\tau_{OBSERVED}$ for the four films of thickness d to estimates $\tau_{ESTIMATE}$ of the thermal decay time using Eq. (2) with the heat capacity C at an initial temperature T_i and a thermal boundary resistance of $R_{BD}=1.0\times10^{-3}$ K cm^2/W (Ref. 5). An exponential fit to the observed temperature transients shown in Fig. 14 for the four films is used to determine the thermal decay times $\tau_{OBSERVED}$. $R_{BD\ ESTIMATE}$ is obtained using the observed decay times in Eq. (2), giving an average value for R_{BD} of about $(1.1\pm0.6)\times10^{-3}$ K cm^2/W. τ_{DIFF} is an estimate of the thermal diffusion time along the c axis as discussed in the text using Eq. (5).

d (nm)	T_i (K)	C (J/cm^3 K)	$\tau_{OBSERVED}$ (ns)	$\tau_{ESTIMATE}$ (ns)	$R_{BD\ ESTIMATE}$ (K cm^2/W)	τ_{DIFF} (ns)
30	73	0.91	1.5	2.7	5.5×10^{-4}	0.31
130	70	0.85	12	11	1.1×10^{-3}	5.5
220	84	1.11	18	24	7.4×10^{-4}	21
260	77	0.98	52	25	2.0×10^{-3}	25

m. A laser pulse absorbed in the superconductor will break Cooper pairs and reduce the superfluid fraction from its initial value, thereby increasing the kinetic inductance.

The superfluid current density is given by

$$J_{SC}=n_{SC}ev_{SC}\ , \tag{7}$$

where v_{SC} is the velocity of the superfluid carriers. If a constant current bias is applied to the bridge, then the velocity of the superfluid carriers will have to increase in order to maintain a constant current density due to the decrease of superfluid carriers in the illuminated region. The resulting acceleration of the superfluid carriers will produce a voltage across the bridge. This can be understood using a simple model where the effect of this voltage on the normal carriers is not considered. Differentiating Eq. (7) with respect to time gives

$$\frac{\partial J_{SC}}{\partial t}=n_{SC}e\frac{\partial v_{SC}}{\partial t}+ev_{SC}\frac{\partial n_{SC}}{\partial t}\ . \tag{8}$$

From the condition of constant bias current I, Eq. (8) becomes

$$0=\frac{n_{SC}e^2}{m}E+J_{SC}\frac{1}{n_{SC}}\frac{\partial n_{SC}}{\partial t}\ , \tag{9}$$

where E is the electric field generated across the bridge by the acceleration of the carriers. The voltage V across the bridge can be found by substituting $E=V/l$ and $J_{SC}=I/wd$ into Eq. (9) giving

$$\begin{aligned}V&=-I\frac{ml}{e^2wd}\frac{1}{n_{SC}^2}\frac{\partial n_{SC}}{\partial t}\\&=I\frac{d}{dt}\left|\frac{ml}{n_{SC}e^2wd}\right|\\&=I\frac{d}{dt}L_{KIN}\ ,\end{aligned} \tag{10}$$

where the first form of Eq. (6) has been used for the kinetic inductance. The voltage can be estimated from

$$V_{KIN}=I\frac{d}{dt}L_{KIN}\cong I\frac{\Delta L_{KIN}}{\Delta t}\ , \tag{11}$$

where ΔL_{KIN} is the change in kinetic inductance over some time increment Δt. If $f_{SC\ initial}$ and $f_{SC\ final}$ are the initial and final superfluid fractions at time t and $t+\Delta t$, respectively, then

$$\Delta L_{KIN}=\frac{1}{\varepsilon_0\omega_P^2}\left[\frac{l}{wd}\right]\left[\frac{1}{f_{SC\ final}}-\frac{1}{f_{SC\ initial}}\right]\ . \tag{12}$$

Equation (11) predicts a positive voltage while the superfluid fraction is decreasing followed by a negative voltage as the superfluid density recovers to its initial value. At temperatures close to T_c, Eq. (12) will diverge as $f_{SC\ final}$ approaches zero. The resulting divergence of Eq. (11) will not occur if the effect of the normal fluid component is considered in a more complete analysis. Equation (11) also predicts a linear dependence of the photoresponse with bias current. This is exactly what was observed for the fast photoresponse as discussed in Sec. III D and shown in Figs. 7 and 9.

To estimate the magnitude of the voltage generated by changes in kinetic inductance, we use the 260 nm bridge biased at 100 mA as an example. The plasma frequency for YBCO thin films[54] is about 1.67×10^{15} s^{-1} (≈1.1 eV), which gives $\lambda_L(T=0)\approx180$ nm using $\lambda_L(T=0)=c/\omega_P$, where c is the velocity of light. If initially at low temperature so that $f_{SC\ initial}\approx1$, then a 10% decrease in superfluid fraction to $f_{SC\ final}=0.9$ over the 100 ps time scale of the laser pulse ($l=20$ μm, amplifier voltage gain=10) will produce a change in kinetic inductance according to Eq. (12) of about 35 fH and voltage transient using Eq. (11) of about 0.35 mV. If the 30 nm film biased at 15 mA is used as an example, the change in kinetic inductance would be about 150 fH producing a transient voltage of 0.22 mV.

A significant change in the superfluid fraction is possible from heating of the bridge by the laser pulse. For instance, using Eq. (1) for the 260 nm film at 50 K with $C\approx0.49$ J/cm^3 K and $F=100$ μJ/cm^2 gives a temperature transient of about 6.7 K. If f_{SC} varies as $1-(T/T_c)^2$, as measured[55,56] for YBCO thin films, then the superfluid fraction will change from 0.68 to 0.59 ($T_c=89$ K). This is a 13% change in f_{SC}, which is large enough to produce observable transient kinetic inductance signals with a 100 ps laser pulse. A simulation of this process provides estimates for voltage transients well within an order of magnitude of the observed photoresponse, as discussed below.

2. Simulation results

The parameters used in the simulation are given in Table IV. The simulation involved calculating the temperature as a function of time in the 260 nm film as the 100 ps FWHM laser pulse heated the bridge. The change in temperature ΔT as a function of time t was obtained by solving

$$\frac{d\Delta T(t)}{dt}=\frac{G(t)}{C(t,T)}-\frac{\Delta T(t)}{\tau(t,T)}\ , \tag{13}$$

where G is the heat generation term in W/cm^3 and τ is the thermal escape time given by Eq. (2). The generation term was given by

$$G(t)=G_0 e^{-(t/\tau_P)^2}\ , \tag{14}$$

where τ_P is the pulse width term and

$$G_0=\frac{F}{\sqrt{\pi}\,d\,\tau_P}\left[\frac{E_{\rm ABS}}{E_0}\right]\ , \tag{15}$$

so that integrating Eq. (14) over all time gives the total energy absorbed in the bridge per pulse. Figure 15(a) shows the generation term due to the laser pulse and the temperature $T(t)$ in the bridge as a function of time for an initial temperature of 75 K. Figure 15(b) shows the resulting variation in the superfluid fraction as a function of time using a two-fluid model $1-(T/T_c)^2$ dependence of the superfluid fraction. The kinetic inductance of the bridge, calculated from Eq. (6), is also shown in Fig. 15(b). The change in kinetic inductance for each time increment was calculated using Eq. (12), and the voltage generated from this change in kinetic inductance is shown as the dashed line in Fig. 15(c) using Eq. (11) multiplied by the voltage gain AV of the amplifier. The simulation also incorporated an exponential fit to the resistive transition at 100 mA for the 260 nm film shown in Fig. 5. The simulation shows from the dotted line in Fig. 15(c) that the induced temperature transient is large enough to bring the temperature of the bridge far enough into the resistive transition region to give a resistive bolometric response. The total photoresponse is the sum of the kinetic inductance component and the resistive component, which resembles the wave form seen in Fig. 3(c) where a fast voltage transient is followed by a slower response. The simulation shows that the fast component is the kinetic inductive bolometric photoresponse and the slow component is the resistive bolometric photoresponse. The kinetic inductive component is roughly the same width as the incident laser pulse, and does not depend on the slow thermal escape time from the film.

A fit to the heat capacity[46,47] as a function of temperature for YBCO is shown in Fig. 16. Using this fit, the simulation was able to provide values for the maximum amplitude of the temperature change $\Delta T_{\rm MAX\ (Simul.)}$ as a function of temperature in the 260 nm film. Approximate values $\Delta T_{\rm MAX\ (Approx.)}$ obtained from Eq. (1) assuming C is the value for the heat capacity at the initial temperature T provide reasonable estimates of the simulated transient temperatures only above 40 K. Due to the small heat capacity at low temperatures, the transient temperatures below 30 K can be quite high.

Using a $1-(T/T_c)^2$ dependence in the superfluid fraction, the peak voltage response as a function of temperature from the simulation is shown in Fig. 17. Multiplying the observed data points by a factor of 3.5 provides good agreement with the simulation results. Above 70 K, the resistive bolometric component becomes significant and eventually dominates over the kinetic inductive response as the temperature is increased further. Below 70 K, only the fast kinetic inductive component is observed. The simulation provides better than order of magnitude estimates for the temperature variation of the peak photoresponse signal and the onset of the slow resistive component. The factor of 3.5 needed to provide good agreement may be due to uncertainties in the laser fluence and the absorbed energy, in addition to attenuation of the broadband signals in the experimental setup. Simulation results have shown an almost linear dependence of the peak voltage signal as a function of laser fluence from 0

TABLE IV. List of parameter values used in the simulation described in the text. Values for ω_P, δ, R, and $R_{\rm BD}$ were taken from Refs. 54, 49, 48, and 5, respectively.

Parameter	Symbol	Value	Units
Bridge thickness	d	260	nm
Bridge width	w	10	μm
Length of bridge exposed to laser	l	20	μm
Critical temperature	T_c	89	K
Bias current	I	100	mA
Current density	J	3.8×10^6	A/cm^2
Plasma frequency	ω_P	1.67×10^{15}	s^{-1}
Pulse width term for 100 ps FWHM	τ_P	60	ps
Laser fluence	F	100	μJ/cm^2
Optical penetration depth at 532 nm	δ	90	nm
Reflectivity at 532 nm	R	0.1	
Ratio of absorbed to incident energy	$E_{\rm ABS}/E_0$	0.85	
Thermal boundary resistance	$R_{\rm BD}$	1.0×10^{-3}	K cm^2/W
Generation term constant	G_0	3.074×10^{10}	W/cm^3
Amplifier voltage gain	AV	10	

to 150 $\mu J/cm^2$ and in a temperature range from 40 to 70 K. Preliminary observations on a different sample have revealed a linear dependence of the fast photoresponse on laser fluence below 100 $\mu J/cm^2$. The simulation also predicts a fast photoresponse with approximately the same duration as the laser pulse, which means attenuation of the broadband pulses will be independent of temperature. Multiplying the observed results by a temperature independent factor to account for uncertainties in laser fluence and signal attenuation in order to obtain a better fit with the simulation is reasonable. Given the simplicity of the simulation model with no adjustable parameters other than the temperature dependence of the superfluid fraction as discussed below, better than order of magnitude agreement between the observed data and the simulation results is very encouraging.

Recently, Hardy *et al.*[57] showed from microwave

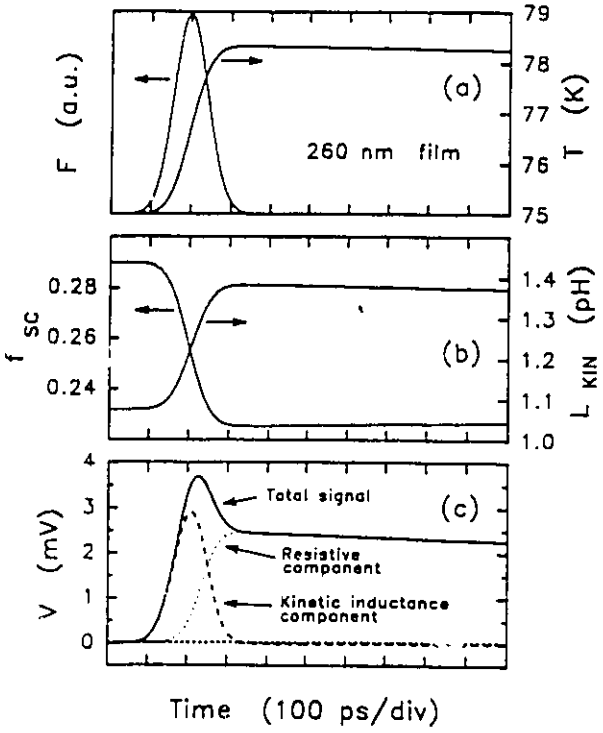

FIG. 15. Simulation results plotted as a function of time for the 260 nm film at a temperature of 75 K, 100 mA bias current, and laser fluence of 100 $\mu J/cm^2$. The parameters used in the simulation are listed in Table IV. The laser pulse intensity F is plotted in (a), which induces a temperature transient T in the bridge. This temperature transient reduces the superfluid fraction f_{SC} which varies as $1-(T/T_c)^2$ in this case, and increases the kinetic inductance L_{KIN} of the bridge, as shown in (b). The increase in kinetic inductance produces a fast voltage transient indicated in (c) as the kinetic inductance component (dashed line). This is also referred to in the text as the kinetic inductive bolometric photoresponse. Since the temperature is within the resistive transition region, a resistive bolometric component (dotted line) is also produced. The total photoresponse signal (solid line), therefore, shows a fast component at the start of a slow component with a decay time determined by the thermal escape time from the film. Similar photoresponse signals were observed at 75 K, as seen in Fig. 3(c).

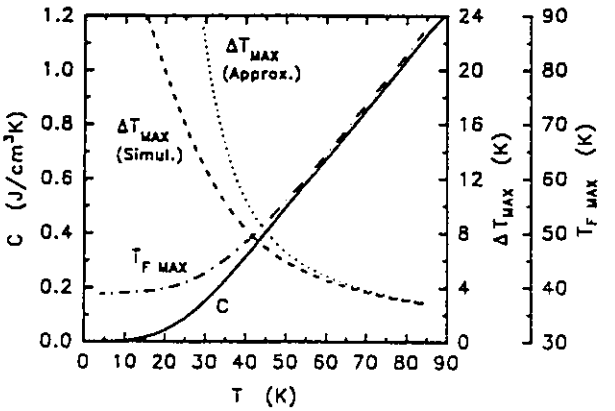

FIG. 16. Heat capacity C as a function of temperature T for YBCO. The plot for C is a fit to heat capacity data taken from Refs. 46 and 47. This heat capacity curve was used in the simulation to determine the temperature transients induced in the film by the laser pulse. For the 260 nm film with a fluence of 100 $\mu J/cm^2$, the maximum temperature transient $\Delta T_{MAX\ (Simul.)}$ from the simulation results can be compared to approximate estimates of the temperature transient $\Delta T_{MAX\ (Approx.)}$ calculated from Eq. (1). The maximum temperature T_{FMAX} reached in the film according to the simulation is also plotted as a function of the initial temperature T of the film, where $T_{FMAX} = T + \Delta T_{MAX\ (Simul.)}$.

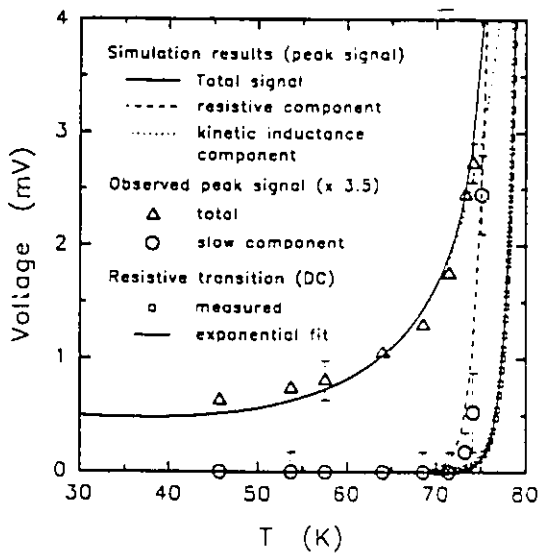

FIG. 17. Comparison of the voltage transient amplitudes obtained from the simulation to the observed peak signals (open triangles) as a function of temperature for the 260 nm film. The parameters used in the simulation are shown in Table IV. In this case, the simulation used a $1-(T/T_c)^2$ dependence of the superfluid fraction with temperature. The observed data values have been multiplied by a factor of 3.5 to obtain a reasonable fit to the simulation results. The rapid increase in the amplitude of the observed slow component (open circles) above 70 K coincides with the simulation results for the amplitude of the resistive component (dashed line). The amplitude of the kinetic inductance component (dotted line) is seen to fall below the peak signal amplitude (solid line) for temperatures above 70 K where the resistive component begins to take over. The measured resistive transition across the bridge (open squares) is shown with the exponential fit (solid line through the squares) used to determine the resistive photoresponse in the simulation.

penetration depth measurements that the superfluid fraction varied linearly at low temperatures for high-quality single crystals of YBCO. This is plotted in Fig. 18 along with $1-t^2$, $1-t^4$, and BCS[58] temperature dependencies of the superfluid fraction where $t=T/T_c$ is the reduced temperature. Figure 19 compares the observed data to the simulation results using each of the superfluid fraction curves from Fig. 18. Only a factor of 2 is needed to get the observed data in good agreement with the simulation results using the superfluid fraction determined by Hardy *et al.*[57] Both the $1-t^2$ and BCS dependencies give similar results above 50 K, but at lower temperatures the BCS curve falls below the $1-t^2$ fit. At this stage, the $1-t^4$ curve is incompatible with the data, however, extending the photoresponse measurements to lower temperatures would help to differentiate between the various dependencies.

The model used in the simulation for the origin of the fast photoresponse provides good agreement with the observed data, but several approximations and assumptions were made. The expression for kinetic inductance in Eq. (6) assumes the current distribution in the superconducting bridge is uniform. At microwave frequencies this is not the case, and many studies have been done[38,56,59] which look at the effect of current distribution on the kinetic inductance of microstrip transmission lines. Attenuation of the kinetic inductive voltage transient by the normal fluid component in the superconductor was considered in a separate simulation, but was found to be insignificant with normal carrier relaxation times shorter than 1 ps. A decrease in the peak amplitude was seen for relaxation times longer than 10 ps. Relaxation times longer than 10 ps will occur[55] at temperatures below about 40 K, but the decrease in normal fluid fraction will reduce the attenuation by the normal component.

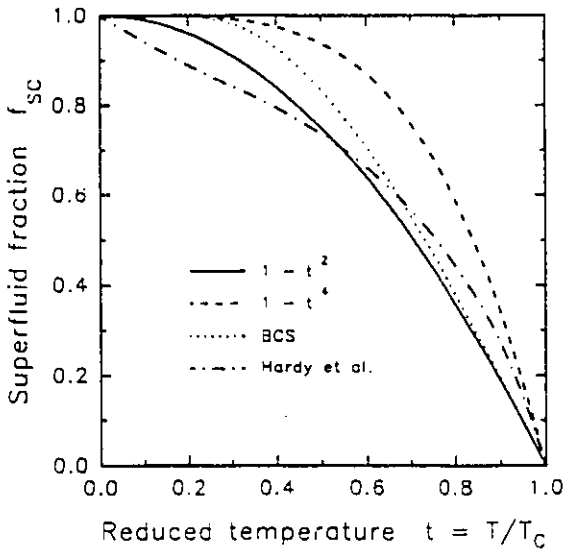

FIG. 18. Theoretical superfluid fraction f_{SC} as a function of reduced temperature $t=T/T_c$ for the following temperature dependencies: $1-t^2$ (solid line), $1-t^4$ (dashed line), BCS variation from Ref. 58 (dotted line), and as observed in YBCO single crystals by Hardy *et al.* from Ref. 57 (dash-dot line). Each of these superfluid fraction curves were used by the simulation to see which gave the best fit to the temperature dependence of the observed photoresponse data, as shown in Fig. 19.

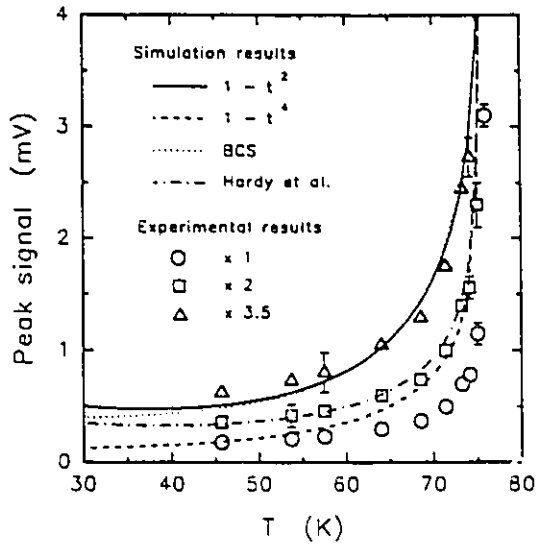

FIG. 19. Comparison of the peak signals obtained from the simulation results to those observed experimentally as a function of temperature for the 260 nm film. The simulation results for the peak signal amplitudes consist of four curves which use superfluid fractions (Fig. 18) varying as $1-t^2$ (solid line), $1-t^4$ (dashed line), BCS behavior from Ref. 58 (dotted line), and as observed by Hardy *et al.* in Ref. 57 for YBCO signal crystals (dot-dash line). The observed data (open circles) is multiplied by factors of 2 (open squares) and 3.5 (open triangles) to see which superfluid fraction variation used in the simulation gives the best fit.

The model also assumes uniform heating over the entire thickness of the bridge. This is clearly not the case for optically thick films, while for thinner films uniform heating is a reasonable approximation. It was also assumed that the optical penetration depth was relatively insensitive to temperature, which has been observed elsewhere[60] for transmittance measurements through 180 nm YBCO films between 10 and 300 K. The simulation only considered thermal escape times governed by thermal boundary resistance as described by Eq. (2) and did not take into account the effects of thermal diffusion times given by Eq. (5). The thermal boundary resistance was also assumed to be constant over the entire temperature range. This is true from 90 to 200 K,[5] but as discussed in Sec. III E in Eq. (4), R_{BD} will probably increase at temperatures below 30 K. This will increase the thermal escape time from the film which will tend to increase the signal amplitudes obtained from the simulation but will not affect the speed of the kinetic inductive response.

Uncertainties in laser spot size on the bridge and the energy in each pulse will affect the value for the laser fluence used in the simulation. The simulation approximated the Gaussian profile of the laser spot with a uniform fluence over an effective spot size. Finally, the value for the plasma frequency[54] of 1.67×10^{15} s^{-1} (1.1 eV) was obtained from far infrared measurements on similar YBCO films. Variations in sample quality may change

ω_P, thereby affecting the signal amplitude.

A further test of the validity of the kinetic inductive bolometric photoresponse model used to interpret the fast component in the observed wave forms is the prediction by Eq. (11) of negative voltage transients. Simulation results for the 30 nm film at 54 K with 20 mA bias are shown in Fig. 20. Figure 21 shows the simulation results for the 130 nm film at 61 K and 100 mA bias. Once the laser pulse has stopped heating the film, the films relax to their original starting temperatures at a rate determined by the thermal escape time. This can be seen by the faster decay time of the temperature transient in Fig. 20(a) for the 30 nm film compared to the slower decay in Fig. 21(a) for the 130 nm film. The resulting faster rate of increase in the superfluid fraction for the 30 nm film seen in Fig. 20(b) gives rise to a negative voltage transient in Fig. 20(c) a little less than 0.2 mV (≈ -0.14 mV). The negative voltage transient for the 130 nm film in Fig. 21(c) is hardly visible (≈ -0.024 mV) because the rate at which Cooper pairs reform as the heat escapes from the film is too slow.

Figure 22 shows fast photoresponse wave forms taken from the 30 and 130 nm films under operating conditions identical to those used in the simulation results of Figs. 20 and 21. Wave forms with approximately the same amplitude were chosen to make sure any negative transients were not due to spurious circuit effects. The photoresponse observed for the 30 nm film in Fig. 22(a)

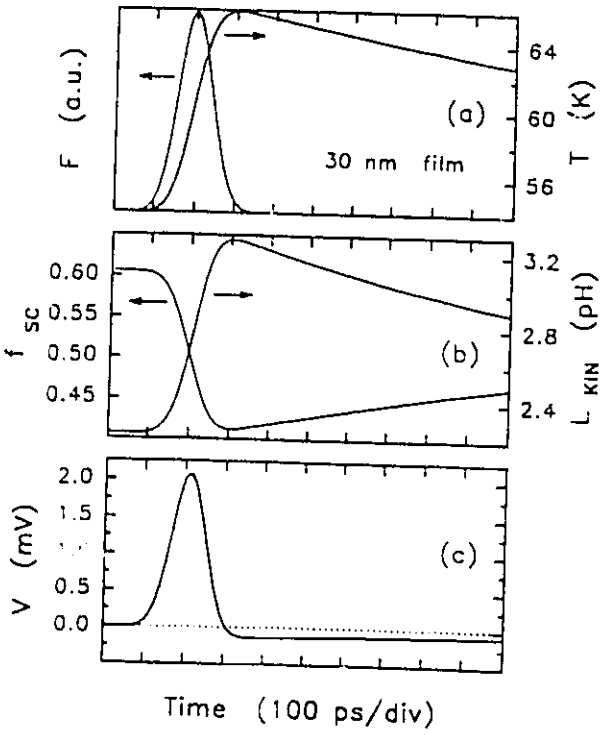

FIG. 20. Simulation results for the 30 nm film at a temperature of 54 K and a bias current of 20 mA. The film is biased below its resistive transition region, so only the kinetic inductive bolometric response appears in the simulation. Notice the negative voltage transient in (c) produced once the superfluid fraction in (b) starts to increase again and the kinetic inductance begins to drop.

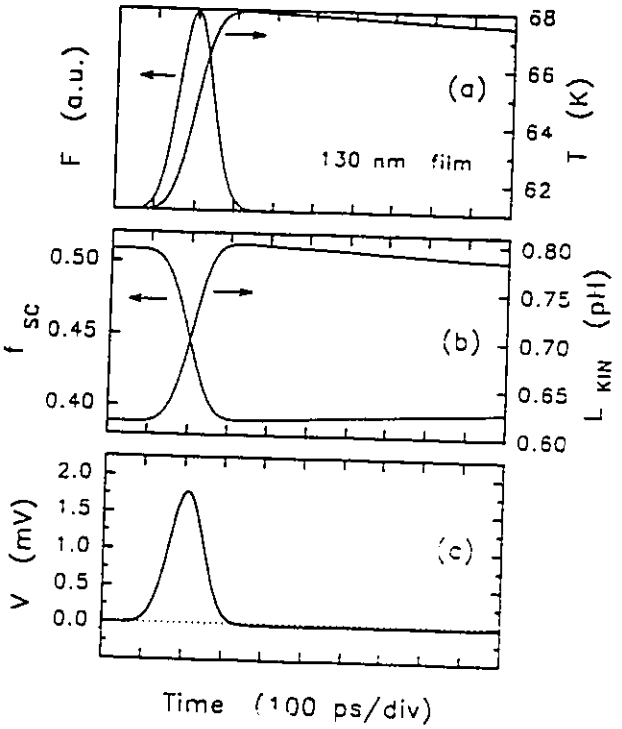

FIG. 21. Simulation results for the 130 nm film at a temperature of 61 K and a bias current of 100 mA. The film is biased below its resistive transition region, so only the kinetic inductive bolometric response appears in the simulation. Notice that the negative voltage transient in (c) produced once the superfluid fraction in (b) starts to increase again is much less than the negative transient expected from the 30 nm film shown in Fig. 20(c). This is because the thermal decay time in (a) is much slower than that for the 30 nm film seen in Fig. 20(a). The superfluid fraction takes longer to recover to its initial value than for the 30 nm film, which results in a slower change in L_{KIN} and a smaller negative voltage.

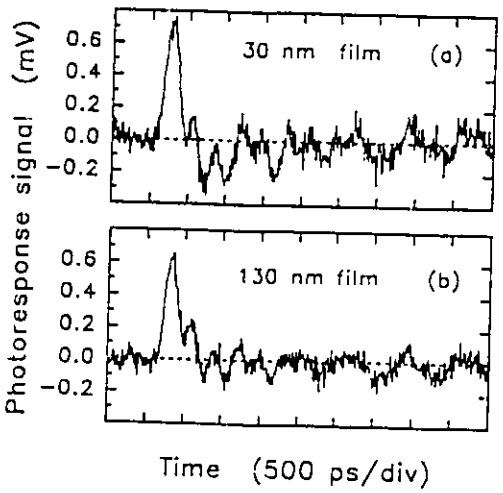

FIG. 22. Fast photoresponse signals observed from the (a) 30 nm and (b) 130 nm films. The 30 nm film was at a temperature of 54 K and biased at 20 mA. The signal from the 130 nm film was taken at 61 K and 100 mA. Both films were biased below their resistive transition regions. A small, negative transient is observed for the 30 nm film in (a) but not for the 130 nm film in (b). This is consistent with the simulation results shown in Figs. 20 and 21. Note the difference in time scale with Figs. 20 and 21.

shows a slight negative voltage transient less than 0.2 mV in amplitude, whereas no negative voltage transient is discernable in Fig. 22(b) for the 130 nm film. Notice that the oscilloscope noise is relatively flat before the transients are seen in Fig. 22. The increased noise seen after the fast transient is due to ringing and reflections of the fast voltage transient at the sample. The negative transient in Fig. 22(a) is seen as a negative-going trend in the average value of these oscillations, lasting about 1 ns after the fast positive-going pulse. A 60 nm film also exhibited a small negative voltage transient. As seen in Fig. 4(b), no negative voltage transient was observed for the 260 nm film. Figure 10(c) for the 30 nm film at a slightly smaller bias than that used in Fig. 22(b) also shows a small negative transient. The observation of negative voltage transients only in very thin films with faster thermal escape times supports the kinetic inductive bolometric photoresponse mechanism we are proposing for the origin of the fast photoresponse in YBCO thin films.

3. *Possibility of nonequilibrium effects*

In our simulation, we assumed that the distribution of quasiparticles was in equilibrium with the local temperature of the lattice. Of course, if a sufficiently short laser pulse is used to excite the superconductor, then this condition would not be initially satisfied. The nonbolometric kinetic inductive photoresponse that would then arise[16,18–20,23,25] might be identified by deviations from the simulated kinetic inductive bolometric response. This would provide insight into the complex quasiparticle dynamics and relaxation processes. Several authors have suggested that a single photon could be responsible for breaking many Cooper pairs due to impact ionization and emission of optical phonons which subsequently break more Cooper pairs.[18,32] Estimates based on conservation of energy have suggested[32] that as many as 100 Cooper pairs can be broken by a single optical photon. We note that these estimates are based on a minimum quasiparticle energy comparable to the BCS "*s*-wave" gap, and that any gap structure with nodes could lead to multiplication factors much higher than 100.

Pump-probe results suggest that during a 100 ps pulse the quasiparticles will be in equilibrium with the lattice temperature. The duration of the quasiparticle thermalization process has been measured in YBCO thin films[32] to be about 350 fs, and recombination back into Cooper pairs was believed to be complete after 5 ps.[32]

Suppression of the superconducting order parameter by the excess quasiparticle distribution has also been proposed as a nonbolometric mechanism and origin of the fast photoresponse in YBCO thin films.[16–18,20,22–24,33] If the gap is sufficiently suppressed, the critical current will be exceeded and the superconductor will enter a resistive state.[18,20] Signatures of this mechanism would be a nonlinear current dependence at threshold and a resistive rather than inductive signal. Whether this occurs with subpicosecond laser pulses is still unclear. The fact that the photoresponse was linear with bias current provides evidence that nonequilibrium gap suppression was probably not involved in our experiments.

4. *Possibility of photoactivated flux flow*

Laser-induced depinning of vortices has been proposed[17,29] as a mechanism for the fast photoresponse. Once the vortices have been freed, they move with a velocity governed by the Lorentz force generated by the current density J and the viscosity η for flux flow in the film. It is the motion of these photoactivated vortices perpendicular to the current which produces a voltage drop across the superconducting bridge. We now try to estimate the size of this effect for the 260 nm film.

Since no external fields have been applied, the only source of vortices is from the self-field of the current-carrying bridge. The current density and resulting magnetic field are peaked near the edges of the bridge.[61] The peak amplitude of the self-field at the edge of a 10 μm wide superconducting bridge has been calculated[61] to be about 190 G using a penetration depth of 220 nm and a current density of 10^7 A/cm^2. In a simple model, if one assumes that the laser pulse is able to activate the movement of a uniform magnetic field B of 100 G at a current density J of 5×10^6 A/cm^2 over a length l of 20 μm, then the flux flow voltage will be given by $V=Blv$, where v is the flux flow velocity. Using $v=J\phi_0/\eta$, where ϕ_0 is the flux quantum and $\eta\approx2\times10^{-7}$ N s/m^2 at 50 K for YBCO thin films,[62] the flux flow voltage would be about 1 mV after amplification with the $\times10$ amplifier. This is certainly within the correct order of magnitude of the observed fast photoresponse, but such a mechanism cannot account for the origin of the fast photoresponse. In the flux flow model, $v\sim J$ and $B\sim J$ making $V\sim J^2$. Furthermore, if the activation energy for depinning of vortices decreases with increasing current[29] then the photoresponse should increase even faster than J^2. This disagrees with the observed linear dependence of the fast photoresponse with the bias current. An external magnetic field of 100 G was applied perpendicular to the bridge of a different sample in experiments[28] similar to the ones described here, but no change in the amplitude of the fast photoresponse was observed implying the absence of photoactivated flux flow.

IV. SUMMARY

We have measured the photoresponse from current biased YBCO bridge structures exposed to 100 ps laser pulses in films ranging in thickness from 30 to 260 nm. Near the resistive transition, the photoresponse consisted of a fast component less than 500 ps wide followed by a slower component with a decay of several nanoseconds. Well below the resistive transition, only the fast component was observed which persisted to low temperatures. We have shown that the slow component is due to a resistive bolometric response where the laser pulse heats the film into the resistive transition region. The decay of the slow component is therefore determined by the thermal escape time from the film, which is faster for thinner films in agreement with predicted results. The

fast component is consistent with a kinetic inductive bolometric response. Heating from the laser pulse decreases the superfluid fraction in the superconductor which in turn increases the kinetic inductance of the bridge. This gives rise to a positive transient voltage which has the same width as the incident laser pulse. Fast transients were observed in both thin (30 nm) films and thick (260 nm) films. Negative voltage transients were only seen in the thinnest films where the thermal escape times were the fastest. This offers the possibility of using the amplitudes and decay times of the negative transients to estimate thermal escape times and thus the thermal boundary resistance as a function of temperature below T_c in thin films. The origin of the fast photoresponse of YBCO epitaxial thin films is therefore bolometric in nature over the duration of the 100 ps laser pulse, and arises from thermally induced changes in the kinetic inductance of the current-biased bridge. The observed linear dependence of the fast photoresponse with bias current is consistent with this mechanism.

A simulation based on the kinetic inductive bolometric response model provided reasonable agreement with the temperature dependence of the observed photoresponse data. Nonequilibrium or nonbolometric mechanisms were not required to explain the origin of the fast component. The only adjustable parameter in the simulation was the temperature dependence of the superfluid fraction. The simulation also provided a comparison between the various postulated temperature dependencies of the superfluid fraction in YBCO, but data at lower temperatures is required to determine the best fit.

Improvements in the electrical bandwidth of the photoresponse setup will be necessary in order to resolve the fast voltage transients. This will provide more accurate measurements of the amplitudes of the photoresponse signals for comparison with the simulation results. Since the amplitude of the positive portion of the kinetic inductive bolometric signal relies on the rate at which the laser pulse heats the film, shorter laser pulses should produce larger and faster voltage transients which could have interesting implications in the development of high speed optical detectors made from high-T_c superconductors.

ACKNOWLEDGMENTS

We would like to thank R. Hughes, A. McConnel, and T. Strach for their assistance with the film growth and for providing some of the laser ablated films. We are grateful for many useful discussions with T. Timusk regarding the plasma frequency and other optical properties of YBCO thin films. This work was supported by the Ontario Centre for Materials Research and the Natural Sciences and Engineering Research Council of Canada.

[1]P. L. Richards, J. Clarke, R. Leoni, Ph. Lerch, S. Verghese, M. R. Beasley, T. H. Geballe, R. H. Hammond, P. Rosenthal, and S. R. Spielman, Appl. Phys. Lett. 54, 283 (1989).
[2]Q. Hu and P. L. Richards, Appl. Phys. Lett. 55, 2444 (1989).
[3]S. Verghese, P. L. Richards, K. Char, D. K. Fork, and T. H. Geballe, J. Appl. Phys. 71, 2491 (1992).
[4]S. Verghese, P. L. Richards, D. K. Fork, K. Char, and T. H. Geballe, IEEE Trans. Appl. Superconductivity 3, 2115 (1993).
[5]M. Nahum, S. Verghese, P. L. Richards, and K. Char, Appl. Phys. Lett. 59, 2034 (1991).
[6]Advanced Fuel Research, 87 Church Street, East Hartford, CT 06108 (unpublished). Specifications: Response from near IR to the far IR, 10 kHz thermal response speed, 10 000 V/W responsivity, NEP $< 10^{-11}$ W/Hz$^{1/2}$, and $D^* > 10^{10}$ cm Hz$^{1/2}$/W. See also Q. Li, D. B. Fenner, W. D. Hamblen, and D. G. Hamblen, Appl. Phys. Lett. 62, 2428 (1993).
[7]J. C. Culbertson, U. Strom, S. A. Wolf, and W. W. Fuller, Phys. Rev. B 44, 9609 (1991).
[8]M. G. Forrester, M. Gottlieb, J. R. Gavaler, and A. I. Braginski, IEEE Trans. Magn. MAG-25, 1327 (1989).
[9]Y. Enomoto, T. Murakami, and M. Suzuki, Physica C 153-155, 1592 (1988).
[10]G. Schneider, H. Lengfellner, J. Betz, K. F. Renk, and W. Prettl, Int. J. IR MM Waves 12, 1 (1991).
[11]E. M. Gershenzon, G. N. Gol'tsman, A. D. Semenov, and A. V. Sergeev, IEEE Trans. Magn. MAG-27, 1321 (1991).
[12]M. G. Forrester, M. Gottlieb, J. R. Gavaler, and A. I. Braginski, Appl. Phys. Lett. 53, 1332 (1988).
[13]W. S. Brocklesby, D. Monroe, A. F. J. Levi, M. Hong, S. H. Liou, J. Kwo, C. E. Rice, P. M. Mankiewich, and R. E. Howard, Appl. Phys. Lett. 54, 1175 (1989).
[14]G. L. Carr, M. Quijada, D. B. Tanner, C. J. Hirschmugl, G. P. Williams, S. Etemad, B. Dutta, F. DeRosa, A. Inam, T. Venkatesan, and X. Xi, Appl. Phys. Lett. 57, 2725 (1990).
[15]H. S. Kwok, J. P. Zheng, Q. Y. Ying, and R. Rao, Appl. Phys. Lett. 54, 2473 (1989).
[16]L. Shi, G. L. Huang, C. Lehane, J. P. Zheng, and H. S. Kwok, Appl. Phys. Lett. 61, 489 (1992).
[17]A. Frenkel, M. A. Saifi, T. Venkatesan, P. England, X. D. Wu, and A. Inam, J. Appl. Phys. 67, 3054 (1990).
[18]N. Bluzer, Phys. Rev. B 44, 10 222 (1991).
[19]N. Bluzer, J. Appl. Phys. 71, 1336 (1992).
[20]N. Bluzer, IEEE Trans. Appl. Superconductivity 3, 2869 (1993).
[21]M. Johnson, Appl. Phys. Lett. 59, 1371 (1991).
[22]A. D. Semenov, G. N. Gol'tsman, I. G. Gogidze, A. V. Sergeev, E. M. Gershenzon, P. T. Lang, and K. F. Renk, Appl. Phys. Lett. 60, 903 (1992).
[23]A. D. Semenov, I. G. Goghidze, G. N. Gol'tsman, A. V. Sergeev, E. E. Aksaev, and E. M. Gershenzon, IEEE Trans. Appl. Superconductivity 3, 2132 (1993).
[24]R. S. Nebosis, M. A. Heusinger, W. Schatz, K. F. Renk, G. N. Gol'tsman, B. S. Karasik, A. D. Semenov, and G. M. Gershenzon, IEEE Trans. Appl. Superconductivity 3, 2160 (1993).
[25]A. Ghis, S. Pfister, J. C. Villegier, M. Nail, and J. P. Maneval, IEEE Trans. Appl. Superconductivity 3, 2136 (1993).
[26]M. I. Flik, P. E. Phelan, and C. L. Tien, Cryogenics 30, 1118 (1990).
[27]S. Zeuner, H. Lengfellner, J. Betz, K. F. Renk, and W. Prettl, Appl. Phys. Lett. 61, 973 (1992).
[28]F. A. Hegmann and J. S. Preston, Appl. Phys. Lett. 62, 1158 (1993).
[29]E. Zeldov, N. M. Amer, G. Koren, A. Gupta, R. J. Gambino,

and M. W. McElfresh, Phys. Rev. Lett. 62, 3093 (1989); E. Zeldov, N. M. Amer, G. Koren, and A. Gupta, Phys. Rev. B 39, 9712 (1989).

[30]A. M. Kadin, M. Leung, A. D. Smith, and J. M. Murduck, Appl. Phys. Lett. 57, 2847 (1990).

[31]W. R. Donaldson, A. M. Kadin, P. H. Ballentine, and R. Sobolewski, Appl. Phys. Lett. 54, 2470 (1989). A. M. Kadin, P. H. Ballentine, and W. R. Donaldson, Physica B 165&166, 1507 (1990).

[32]S. G. Han, Z. V. Vardeny, K. S. Wong, O. G. Symko, and G. Koren, Phys. Rev. Lett. 65, 2708 (1990).

[33]G. L. Eesley, J. Heremans, M. S. Meyer, G. L. Doll, and S. H. Liou, Phys. Rev. Lett. 65, 3445 (1990).

[34]J. M. Chwalek, C. Uher, J. F. Whitaker, G. A. Mourou, J. Agostinelli, and M. Lelental, Appl. Phys Lett. 57, 1696 (1990).

[35]T. Gong, L. X. Zheng, W. Xiong, W. Kula, Y. Kostoulas, R. Sobolewski, and P. M. Fauchet, Phys. Rev. B 47, 14495 (1993).

[36]S. D. Brorson, A. Kazeroonian, D. W. Face, T. K. Cheng, G. L. Doll, M. S. Dresselhaus, G. Dresselhaus, E. P. Ippen, T. Venkatesan, X. D. Wu, and A. Inam, Solid State Commun. 74, 1305 (1990); S. D. Brorson, A. Kazeroonian, J. S. Moodera, D. W. Face, T. K. Cheng, E. P. Ippen, M. S. Dresselhaus, and G. Dresselhaus, Phys. Rev. Lett. 18, 2172 (1990).

[37]S. G. Han, Z. V. Vardeny, O. G. Symko, and G. Koren, Phys. Rev. Lett. 67, 1053 (1991); G. L. Esley, J. Heremans, M. S. Meyer, and G. L. Doll, *ibid.* 67, 1054 (1991).

[38]J. M. Pond, J. H. Claassen, and W. L. Carter, IEEE Trans. Microwave Theory and Techniques MTT-35, 1256 (1987); W. H. Chang, Appl. Phys. Lett. 50, 8129 (1979); R. Meservey and P. M. Tedrow, J. Appl. Phys. 40, 2028 (1969).

[39]B. W. Langley, S. M. Anlage, R. F. W. Pease, and M. R. Beasley, Rev. Sci. Instrum. 62, 1801 (1991); J. M. Pond, K. R. Carroll, J. S. Horwitz, and D. B. Chrisey, IEEE Trans. Appl. Superconductivity 3, 1438 (1993).

[40]J. M. Pond, J. H. Claassen, and W. L. Carter, IEEE Trans. Magn. MAG-23, 903 (1987); G. K. G. Hohenwarter, J. S. Martens, J. B. Beyer, J. E. Nordman, and D. P. McGinnis, *ibid.* MAG-25, 1100 (1989).

[41]E. K. Track, R. E. Drake, and G. K. G. Hohenwarter, IEEE Trans. Appl. Superconductivity 3, 2899 (1993).

[42]J. E. Sauvageau, D. G. McDonald, and E. N. Grossman, IEEE Trans. Magn. MAG-27, 2757 (1991); E. N. Grossman, D. G. McDonald, and J. E. Sauvageau, *ibid.* MAG-27, 2677 (1991); J. E. Sauvageau and D. G. McDonald, *ibid.* MAG-25, 1331 (1989); D. G. McDonald, Appl. Phys. Lett. 50, 775 (1987).

[43]R. Kumar, S. K. Malik, S. P. Pai, P. R. Apte, R. Pinto, and R. Vijayaraghavan, Phys. Rev. B 46, 5766 (1992); S. Tahara, S. M. Anlage, J. Halbritter, C. B. Eom, D. K. Fork, T. H. Geballe, and M. R. Beasley, *ibid.* 41, 11 203 (1990).

[44]A. Frenkel, E. Clausen, C. C. Chang, T. Venkatesan, P. S. D. Lin, X. D. Wu, A. Inam, and B. Lalevic, Appl. Phys. Lett. 55, 911 (1989).

[45]D. Gupta, W. R. Donaldson, K. Kortkamp, and A. M. Kadin, IEEE Trans. Appl. Superconductivity 3, 2895 (1993).

[46]T. Atake, A. Honda, and H. Kawaji, Physica C 190, 70 (1991).

[47]D. Sanchez, A. Junod, J.-Y. Genoud, T. Graf, and J. Muller, Physica C 200, 1 (1992).

[48]A. Zibold, K. Widder, H. P. Geserich, T. Scherer, P. Marienhoff, M. Neuhaus, W. Jutzi, A. Erb, and G. Muller-Vogt, Appl. Phys. Lett. 61, 345 (1992); S. L. Cooper, D. Reznik, A. Kotz, M. A. Karlow, R. Liu, M. V. Klein, W. C. Lee, J. Giapintzakis, D. M. Ginsberg, B. W. Veal, and A. P. Paulikas, Phys. Rev. B 47, 8233 (1993).

[49]H. Yasuoka, H. Mazaki, T. Terashima, and Y. Bando, Physica C 175, 192 (1991).

[50]I. Bozovic, Phys. Rev. B 42, 1969 (1990).

[51]C. D. Marshall, A. Tokmakoff, I. M. Fishman, C. B. Eom, J. M. Phillips, and M. D. Fayer, J. Appl. Phys. 73, 850 (1993).

[52]S. D. Peacor, R. A. Richardson, F. Nori, and C. Uher, Phys. Rev. B 44, 9508 (1991); J. L. Cohn, S. A. Wolf, T. A. Vanderah, V. Selvamanickam, and K. Salama, Physica C 192, 435 (1992).

[53]S. J. Hagen, Z. Z. Wang, and N. P. Ong, Phys. Rev. B 40, 9389 (1989); Sera, S. Shamoto, M. Sato, I. Watanabe, S. Nakashima, and K. Kumagai, Solid State Commun. 74, 951 (1990).

[54]T. Timusk (private communication).

[55]D. A. Bonn, R. Liang, T. M. Riseman, D. J. Baar, D. C. Morgan, K. Zhang, P. Dosanjh, T. L. Duty, A. MacFarlane, G. D. Morris, J. H. Brewer, W. N. Hardy, C. Kallin, and A. J. Berlinsky, Phys. Rev. B 47, 11 314 (1993).

[56]J.-Y. Lee and T. R. Lemberger, Appl. Phys. Lett. 62, 2419 (1993).

[57]W. N. Hardy, D. A. Bonn, D. C. Morgan, R. Liang, and K. Zhang, Phys. Rev. Lett. 70, 3999 (1993).

[58]B. Muhlschlegal, Z. Phys. 155, 313 (1959).

[59]J. W. Baker, J. D. Lejeune, and D. G. Naugle, J. Appl. Phys. 45, 5043 (1974).

[60]I. Bozovic, D. Kirillov, A. Kapitulnik, K. Char, M. R. Hahn, M. R. Beasley, T. H. Geballe, Y. H. Kim, and A. J. Heeger, Phys. Rev. Lett. 59, 2219 (1987).

[61]T. R. Lemberger, in *Physical Properties of High Temperature Superconductors III*, edited by D. M. Ginsberg (World Scientific, Singapore, 1992), p. 490.

[62]M. S. Pambianchi, D. H. Wu, L. Ganapathi, and S. M. Anlage, IEEE Trans. Appl. Superconductivity 3, 2774 (1993).

Paper C

"High speed kinetic inductive bolometric photoresponse of epitaxial $YBa_2Cu_3O_{7-\delta}$ thin films"

F. A. Hegmann, R. A. Hughes, and J. S. Preston, in *High-Temperature Superconducting Detectors: Bolometric and Nonbolometric*, eds. M. Nahum and J.-C. Villegier, Proc. SPIE 2159, 88-97 (1994). (Paper presented at the OE/LASE '94 conference, Los Angeles, California, January 22-28, 1994.)

Summary:

Paper C provides an overview of the photoresponse results for 100 ps and 5 ps laser pulses. General trends observed in the photoresponse data consistent with the KIB model are discussed.

High speed kinetic inductive bolometric photoresponse of epitaxial $YBa_2Cu_3O_{7-\delta}$ thin films

Frank A. Hegmann, Robert A. Hughes

Department of Physics and Astronomy, McMaster University, Hamilton, Ontario, Canada L8S 4M1

John S. Preston

Department of Engineering Physics, McMaster University, Hamilton, Ontario, Canada L8S 4L7

ABSTRACT

A general trend is observed in the photoresponse of current biased epitaxial $YBa_2Cu_3O_{7-\delta}$ thin film bridge structures exposed to picosecond laser pulses. Both fast and slow components are seen in the photoresponse near the transition region. The slow component, which has a decay over several nanoseconds, is a resistive bolometric response due to heating of the film by the laser pulse in the resistive transition region. At lower temperatures, only the fast component is observed with an amplitude which is linear with bias current. The fast component has been observed in films ranging in thickness from 30 nm to 260 nm. Using 100 ps, 532 nm laser pulses, the origin of the fast component can be explained by a kinetic inductive bolometric response where the superfluid fraction is rapidly decreased by the laser pulse heating the bridge. Recent results using 5 ps, 820 nm laser pulses on samples maintained at liquid nitrogen temperature (77.4 K) in a high speed measurement setup have revealed fast components in the photoresponse as short as 16 ps full width at half maximum. To our knowledge, this is the fastest photoresponse signal observed to date from $YBa_2Cu_3O_{7-\delta}$ thin films. A large portion of this fast response can be attributed to a kinetic inductive bolometric response. The possibility of a nonbolometric component over this short time scale is discussed.

1. INTRODUCTION

1.1. Photoresponse experiments

In a typical photoresponse experiment, which is shown schematically in Fig. 1, a picosecond laser pulse is focused onto a narrow bridge patterned into a $YBa_2Cu_3O_{7-\delta}$ (YBCO) epitaxial thin film. When a current bias is applied, voltage transients can be seen on a fast oscilloscope. If the sample is biased in the resistive transition region, the photoresponse is due to a resistive bolometric response where the amplitude of the signal can be explained in terms of heating by the laser pulse changing the resistance of the bridge. The bolometric (thermal) nature of this response is apparent in the slow rate of decay of the signal over several nanoseconds which is determined by the thermal escape time from the film. However, it is possible to observe subnanosecond voltage transients when the sample is biased well below the transition region in the superconducting state.

Several groups[1-9] have studied this fast photoresponse from YBCO thin films which cannot be explained by a simple resistive bolometric response. Transients as fast as 30 ps wide have been reported.[3] The controversy that exists today is over the origin of this fast photoresponse in YBCO epitaxial thin films. Various nonbolometric (nonthermal) mechanisms have been proposed arising from laser induced nonequilibrium superconductivity such as kinetic inductance effects[3,4] and gap suppression by excess quasiparticles.[4-7] Since the

0-8194-1454-9/94/$6.00

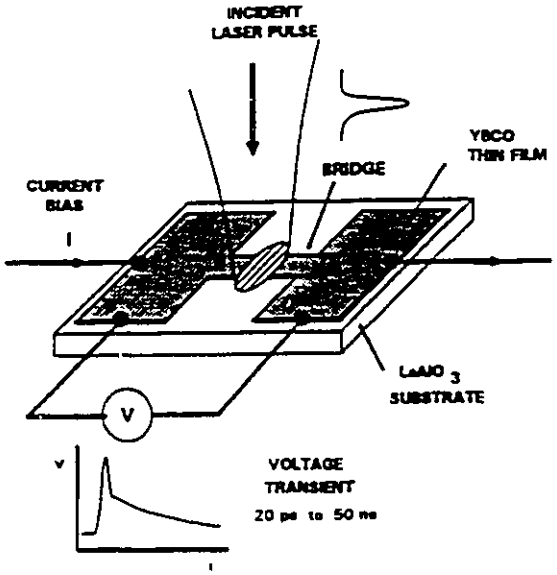

FIG. 1. Schematic of a typical photoresponse experiment.

motion of vortices in superconductors can generate voltages, mechanisms such as photoactivated flux flow[7] and photofluxonic detection[9] have also been proposed. We have already shown[1] that for 100 ps, 532 nm laser pulses the fast photoresponse can be explained using a kinetic inductive bolometric model, which is explained further in section 1.4. We have recently studied the photoresponse from YBCO films using 5 ps, 820 nm laser pulses and have observed 16 ps wide transients from a 200 nm thick film. One of the motivations behind these high speed photoresponse experiments is to find evidence for nonbolometric processes in the photoresponse, which would help improve our understanding of high-T_c superconductors. Another motivation was to assess the feasibility of a high speed YBCO photodetector cooled with liquid nitrogen.

1.2. General trend observed in the photoresponse data

We have observed a trend in all of our photoresponse measurements, as shown in Fig. 2 and discussed in more detail in Refs. 1 and 2. One of the first steps, however, was to measure the steady-state voltage (V_{DC}) across the bridge as a function of temperature and bias current in order to obtain a "map" of the resistive transition. This made it possible to identify a resistive bolometric response (slow component) in the photoresponse signals. The temperature transient ΔT induced by the laser pulse in the bridge determined the amplitude of the resistive bolometric response, and the decay time was determined by the characteristic thermal escape time from the film (see section 1.3). As shown in Fig. 2, the resistive transition gets broader as the bias current through the bridge is increased. If the bias current is kept constant at I_3, then a photoresponse measurement taken at a temperature T_1 will be almost completely a resistive response. At a temperature of T_2, however, ΔT will just be large enough to produce a voltage transient due to a change in resistance along the bridge which is greater than the resolution of the photoresponse measurement system. (For example, the system resolution for the wave forms described here was 0.05 mV, whereas the noise associated with the steady-state measurements V_{DC} across the bridge was less than 10^{-7} V.) A fast component is also seen on top of the slow component at this temperature. As the temperature is lowered further to T_3, only the fast component remains. The slow component, which is due to the resistive bolometric response, has completely disappeared since ΔT is insufficient to bring the transient temperature of the film to a resistive region above the noise level of the system.

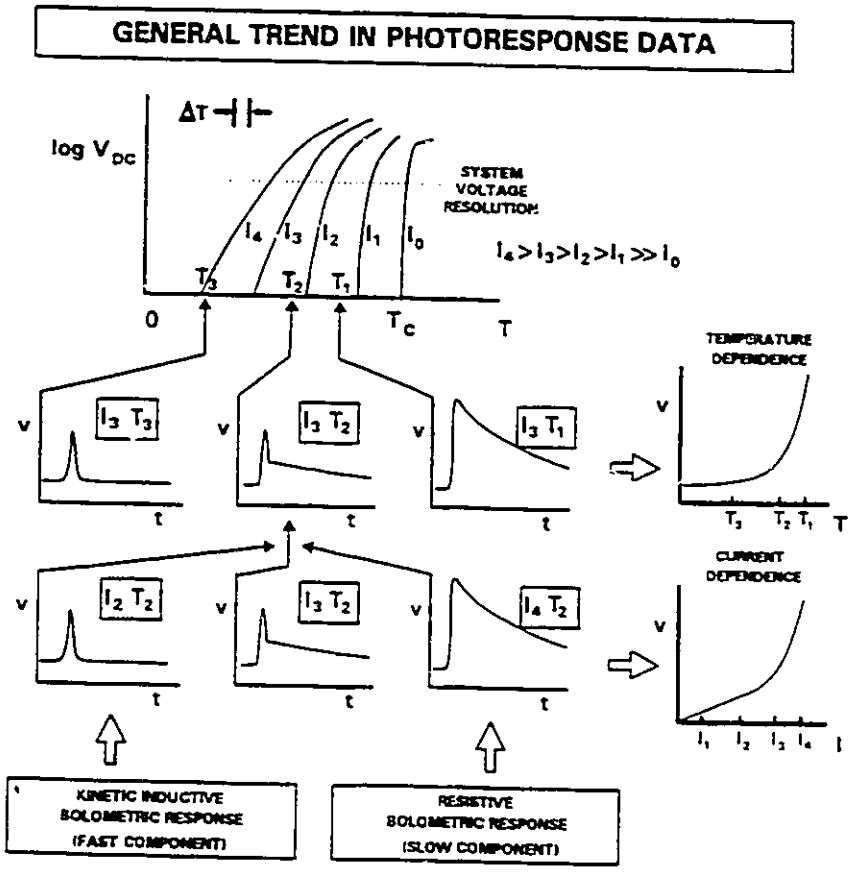

FIG. 2. General trend observed in the photoresponse data.

The fast response is due to a kinetic inductive bolometric response, as discussed in section 1.4. The amplitude of the fast response decreases more slowly as the temperature is lowered further.

If the temperature is kept at T_2, then biasing the sample with a current of I_4 will bring the sample into the resistive region and the response will be predominantly resistive bolometric. Decreasing the bias current to I_2 brings the film further away from the resistive transition region until the current is low enough such that ΔT is too small to produce a resistive change greater than can be detected by the system. At currents between zero bias and I_2, only the fast component is present with an amplitude which is linear with current.

This general trend has been observed with 100 ps laser pulses[1] from films with thicknesses ranging from 30 nm to 260 nm, and recently with 5 ps laser pulses[2] from films with thicknesses from 47 nm to 200 nm.

1.3. The resistive bolometric response (the slow component)

The resistive bolometric response arises from a change in resistance of the bridge induced by heating from the laser pulse. The sample is biased in the resistive transition, or is biased in a region where the induced voltage transient due to a resistive change is larger then the noise of the system. The resistive bolometric response decays over several nanoseconds, and the amplitude can become very large if biased very far into the resistive transition region.

Figure 3 shows some examples of resistive bolometric signals seen from four films with different thicknesses.[1] It is very apparent in Fig. 3 that the thickest film (260 nm) has the longest decay time and the thinnest film (30 nm) has the shortest. These decay times are consistent with thermal escape times from the film determined by the thermal boundary resistance between the film and the substrate. This makes the thermal escape time proportional to the thickness and the heat capacity of the film. For example, typical thermal escape times near 77 K would be 20 ns for a 200 nm film, 13 ns for a 130 nm film, and only 3 ns for a 30 nm film.

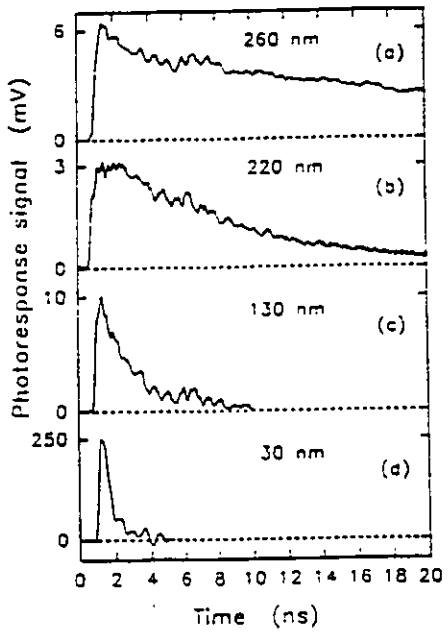

FIG. 3. Examples of resistive bolometric photoresponse signals from films with thicknesses of (a) 260 nm, (b) 220 nm, (c) 130 nm, and (d) 30 nm.

1.4. The kinetic inductive bolometric response (the fast component)

The fast photoresponse using 100 ps laser pulses can be explained by a kinetic inductive bolometric model.[1] A large portion of the 20 ps wide voltage transients seen using 5 ps laser pulses is also due to a kinetic inductive bolometric response.[2] Figure 4 describes the kinetic inductive bolometric mechanism. The lattice temperature T of the film is quickly raised by heating from the incident laser pulse and the superfluid density n_{SC}, which depends on temperature, suddenly decreases. The kinetic inductance L_{KIN} of the bridge, which is inversely proportional to the superfluid density,[1] then increases quickly. This sudden change in the inductance of the bridge results in a fast positive voltage transient given by $V = I\, dL_{KIN}/dt$,[1,4] where I is the bias current. If the thermal escape time is fast enough, then it is possible to see a negative voltage transient as the superfluid density increases back to its original value. It is important to note that a fast response arising from the kinetic inductive bolometric response depends on the rate at which the film is initially heated by the laser pulse and not on the thermal escape time from the film. This explains why a fast response can be seen from films as thick as 200 nm. The linear dependence of the photoresponse on current, once the slow component has disappeared, supports a kinetic inductance model.

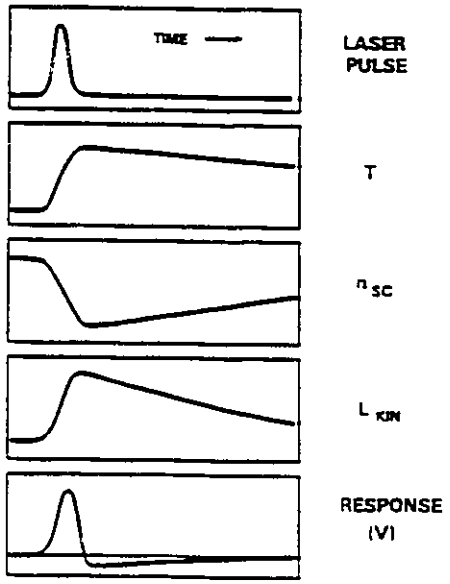

FIG. 4. Description of the kinetic inductive bolometric response.

2. EXPERIMENT

2.1. Processing of the YBCO thin films

The c-axis, epitaxial YBCO films were grown by laser ablation on $LaAlO_3$ substrates and patterned into 50 Ω coplanar transmission line structures using standard photolithographic techniques and a wet chemical etch, as described elsewhere.[1,2] The transmission line was terminated in a bridge 10 μm wide by 100 μm long. The films described here had thicknesses of 135 nm and 200 nm, but 47 nm, 67 nm, and 160 nm films were also studied in the high speed setup. Gold contact pads were evaporated onto the films and then annealed to decrease the contact resistance. After processing, the zero resistance critical temperatures of the films ranged from 86 K to 89 K.

2.2. Laser source

A synchronously pumped dye laser was used to generate 5 ps, 820 nm laser pulses. A pulse selector system was used to reduce the pulse repetition rate from 76 MHz to 38 kHz, which lowered the average laser power incident on the sample to about 70 μW. A lens with a 5 cm focal length produced a 35 μm spot size at the bridge. With an energy per pulse of about 0.1 nJ, the fluence at the sample was about 10 $\mu J/cm^2$.

2.3. High speed photoresponse setup

Figure 5 describes how the photoresponse measurements were made. The YBCO coplanar transmission line sample was connected to a Wiltron "V" connector (DC to 65 GHz) glass bead launcher which coupled the high speed transients to a 15 cm long coaxial cable. A Wiltron bias-tee (0.1 to 60 GHz) connected the other end of the cable to a 50 GHz digital sampling oscilloscope (Tektronix CSA 803 with SD-32 sampling head) and to a current source (0 to 100 mA). Wave forms were acquired at positive and negative bias currents and then

subtracted to eliminate spurious base line effects. A noise level of 0.05 mV was achieved with 512 averages per wave form.

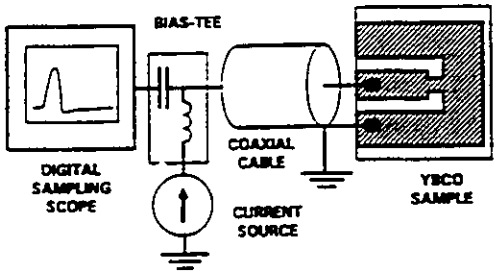

FIG. 5. Schematic of the high speed photoresponse measurement circuit.

A diagram of the sample chamber is shown in Fig. 6. The sample was mounted in vacuum on the end of a cold finger which was cooled by liquid nitrogen. All the photoresponse measurements discussed here, therefore, were taken at liquid nitrogen temperature (77.4 K). The glass bead launcher provided a hermetic seal between the sample and the liquid nitrogen reservoir. This allowed the coaxial cable to be immersed directly in the liquid nitrogen, which greatly reduced heat conduction through the short cable to the sample. Quartz windows on the base of the chamber provided optical access. The entire chamber was designed to be compact and portable to see if it could be used as a practical high speed YBCO photodetector operating at 77 K.

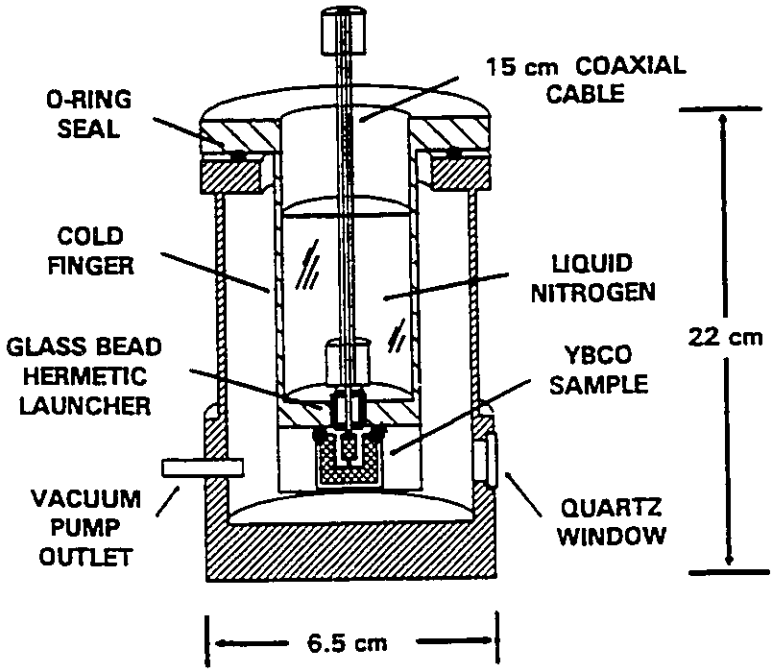

FIG. 6. Cut-away view of the sample chamber.

3. RESULTS AND DISCUSSION

3.1. Fast photoresponse signals and linear current dependence

Examples of photoresponse signals from the 135 nm film are shown in Fig. 7. At a bias of 15 mA, as in Fig. 7(a), a fast component is seen which is followed by a slow component. In Fig. 7(b), the current has been reduced to 11 mA and the slow component has almost disappeared. At lower currents, the slow component has vanished and only the fast component remains with a width of about 20 ps, as shown in Fig. 7(c) for a bias of 6.5 mA. The amplitude of the photoresponse signal as a function of current is shown in Fig. 8. The straight line is a least squares fit to the data below 8 mA, and shows the linear dependence of the fast photoresponse with current. The arrow in the upper inset of Fig. 8 marks the current above which the slow component is present. Below that value, only the fast component remains which varies linearly with current. The lower inset shows the 15 mA waveform from Fig. 7(a) on a longer time scale. This wave form, with a fast component superimposed on top of a slow component, is similar to wave forms that have been seen by other groups.[3,4,5,8]

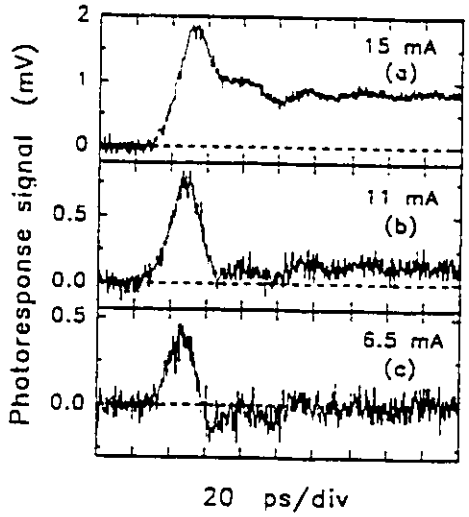

FIG. 7. Photoresponse signals seen from the 135 nm film at a bias of (a) 15 mA, (b) 11 mA, and (c) 6.5 mA.

3.2. Comparison of the observed photoresponse to the kinetic inductive bolometric model

Figure 9 shows the photoresponse from the 200 nm film at a bias of 75 mA which was in the linear current dependence regime for this film.[2] The full width at half maximum (FWHM) of the signal is 16 ps. Also shown in Fig. 9 is the photoresponse expected assuming a kinetic inductive bolometric model as outlined in Ref. 1 with a zero resistance critical temperature of 89 K, initial temperature of 77.4 K, and a $1 - (T/T_c)^2$ dependence of the superfluid density with temperature. The transient temperature induced by the 5 ps wide laser pulse is 0.40 K, which produces a voltage transient shown in Fig. 9 about 1.38 mV high and 5 ps wide. This is close to the observed amplitude of about 1 mV when one considers that bandwidth limitations will broaden and attenuate the voltage pulse generated at the bridge. Similarly for the 135 nm film, the simulation and observed photoresponse peak values are 0.41 mV and 0.40 mV, respectively, at a bias of 6.5 mA (Fig. 7(c)). The reasonable agreement of the simulation results to the observed amplitudes strongly suggests that a large portion of the observed photoresponse must be due to a kinetic inductive bolometric mechanism.

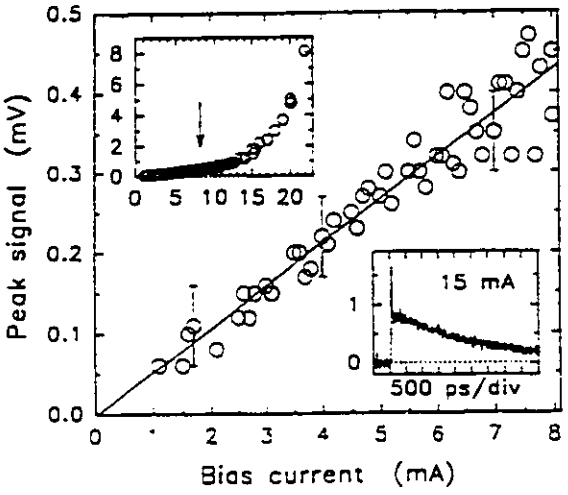

FIG. 8. Amplitude of the photoresponse signal as a function of current for the 135 nm film. The lower inset shows the wave form at a bias of 15 mA.

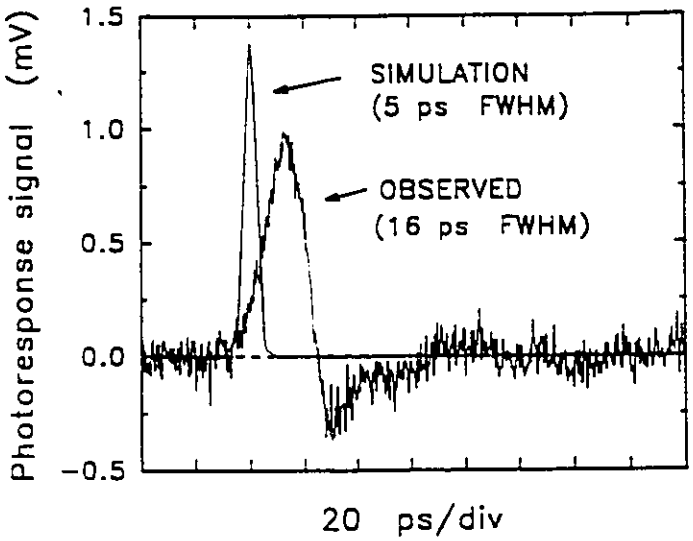

FIG. 9. Comparison of the observed photoresponse from the 200 nm film at a bias of 75 mA to a simulation based on the kinetic inductive bolometric response model.

3.3. Possibility of nonbolometric effects

The kinetic inductive bolometric response is based on a simple model which assumes that the electron and lattice temperatures are in equilibrium as the laser pulse heats the film, and that the local superfluid density is determined by the instantaneous lattice temperature of the film. For 100 ps laser pulses, this may be a reasonable assumption if quasiparticle relaxation times in YBCO determined from microwave experiments[10,11] are less than 1 ps above 60 K. For 5 ps laser pulses, deviations from a simple kinetic inductive bolometric model might be indicative of nonbolometric or nonequilibrium effects in the photoresponse. With potential sources of

error in the simulation results such as estimates of the fluence, it is difficult to look for small deviations from a simple kinetic inductive bolometric model. However, the simulation results shown in Fig. 9 give a negative response due to the slow thermal escape from the sample of only -0.002 mV whereas a much larger negative response with a decay of about 30 ps is observed. In fact, a negative transient with a 30 ps decay time was observed in all the films that were studied from 47 nm to 200 nm.

A fast negative transient in the observed photoresponse, as seen in Fig. 7(c) and Fig. 9, may be interpreted as evidence for recombination of nonequilibrium quasiparticles (which were in excess of the instantaneous local thermal equilibrium value from heating by the laser pulse) back into Cooper pairs.[3,4] Quasiparticle recombination times of about 3 ps at 80 K have been reported from pump-probe experiments on YBCO samples.[12] However, the negative signal may arise from the system response or from the coplanar transmission line characteristics, and caution in the interpretation of the negative photoresponse must be taken. Measuring the temperature dependence of the negative component may help clarify the origin of this response.

4. CONCLUSIONS

We have studied the photoresponse of epitaxial YBCO thin films at 77 K using picosecond laser pulses and a high speed measurement setup. A general trend is observed in the photoresponse data which contains both fast and slow components. The slow component is due to a resistive bolometric response and the fast component is primarily due to a kinetic inductive bolometric response. The fast response has been seen in films with thicknesses from 30 nm to 260 nm. Transients as fast as 16 ps wide have been observed from a 200 nm film. There may be some evidence for a nonbolometric contribution to the photoresponse due to nonequilibrium quasiparticle recombination, but more work is needed to clarify the origin of the negative response.

5. ACKNOWLEDGEMENTS

This work was supported by the Ontario Centre for Materials Research and the Natural Sciences and Engineering Research Council of Canada, and made use of the facilities of the Centre for Electrophotonic Materials and Devices.

5. REFERENCES

1. F.A. Hegmann, J.S. Preston, "Origin of the fast photoresponse of epitaxial $YBa_2Cu_3O_{7-\delta}$ thin films", *Phys. Rev. B* **48**, 16023-16039 (1993).

2. F.A. Hegmann, R.A. Hughes, J.S. Preston, "Picosecond photoresponse of epitaxial $YBa_2Cu_3O_{7-\delta}$ thin films", submitted to *Appl. Phys. Lett.*

3. A. Ghis, S. Pfister, J.C. Villegier, M. Nail, J.P. Maneval, "Ultrafast nonbolometric photoresponse of $YBa_2Cu_3O_{7-x}$ thin films", *IEEE Trans. Appl. Superconductivity* 3, 2136-2139 (1993).

4. N. Bluzer, "Temporal relaxation of nonequilibrium in Y-Ba-Cu-O measured from transient photoimpedance response", *Phys. Rev. B* **44**, 10222-10233 (1991). N. Bluzer, "Temporal relaxation measurements of photoinduced nonequilibrium in superconductors", *J. Appl. Phys.* **71**, 1336-1348 (1992). N. Bluzer, "Biexponential decay and delay artifact in the photoresponse of superconductors", *IEEE Trans. Appl. Superconductivity* 3, 2869-2872 (1993).

5. A.D. Semenov, G.N. Gol'tsman, I. G. Goghidze, A.V. Sergeev, E.M. Gershenzon, P.T. Lang, K.F.

Renk, "Subnanosecond photoresponse of a YBaCuO thin film to infrared and visible radiation by quasiparticle induced suppression of superconductivity", *Appl. Phys. Lett.* **60**, 903-905 (1992). A.D. Semenov, I. G. Goghidze, G.N. Gol'tsman, A.V. Sergeev, E.M. Gershenzon, "Evidence for the spectral dependence of nonequilibrium picosecond photoresponse of YBaCuO thin films", *Appl. Phys. Lett.* **63**, 681-683 (1993).

6. L. Shi, G. L. Huang, C. Lehane, D. Kim, H. S. Kwok, J. Swiatkiewicz, G. C. Xu, P. N. Prasad, "Picosecond photoresponse in Y-Ba-Cu-O ultrathin films", *Phys. Rev. B* **48**, 6550-6555 (1993).

7. A. Frenkel, M. A. Saifi, T. Venkatesan, P. England, X.D. Wu, A. Inam, "Optical response of nongranular high-T_C $Y_1Ba_2Cu_{7-x}$ superconducting thin films", *J. Appl. Phys.* **67**, 3054-3068 (1990). A. Frenkel, "Mechanism of nonequilibrium optical response of high-temperature superconductors", *Phys. Rev. B* **48**, 9717-9725 (1993).

8. M. Johnson, "Nonbolmetric photoresponse of $YBa_2Cu_3O_{7-\delta}$ films", *Appl. Phys. Lett.* **59**, 1371-1373 (1991).

9. A.M. Kadin, M. Leung, A.D. Smith, J.M. Murdoch, "Photofluxonic detection: A new mechanism for infrared detection in superconducting thin films", *Appl. Phys. Lett.* **57**, 2847-2849 (1990).

10. D.A. Bonn, R. Liang, T.M. Riseman, D.J. Baar, D.C. Morgan, K. Zhang, P. Dosanjh, T.L. Duty, A. MacFarlane, G.D. Morris, J.H. Brewer, W.N. Hardy, C. Kallin, A.J. Berlinsky, "Microwave determination of the quasiparticle scattering time in $YBa_2Cu_3O_{6.95}$", *Phys. Rev. B* **47**, 11314-11328 (1993).

11. F. Gao, J.W. Kruse, C.E. Platt, M. Feng, M.V. Klein, "Microwave surface impedance at 10 GHz and quasiparticle scattering in $YBa_2Cu_3O_7$ films", *Appl. Phys. Lett.* **63**, 2274-2276 (1993).

12. S. G. Han, Z. V. Vardeny, K. S. Wong, O. G. Symko, G. Koren, "Femtosecond optical detection of quasiparticle dynamics in high-T_C $YBa_2Cu_3O_{7-\delta}$ superconducting thin films", *Phys. Rev. Lett.* **65**, 2708-2711 (1990). S. G. Han, Z. V. Vardeny, O. G. Symko, G. Koren, "Femtosecond dynamics of quasiparticles in $YBa_2Cu_3O_{7-\delta}$ superconductor films", *IEEE Trans. Magn.* **2**, 1548 (1991).

Paper D

"Picosecond photoresponse of epitaxial $YBa_2Cu_3O_{7-\delta}$ thin films"

F. A. Hegmann, R. A. Hughes, and J. S. Preston, Appl. Phys. Lett. 64, 3172-3174 (1994).

Summary:

Paper D describes the photoresponse data taken with 5 ps laser pulses. The 16 ps wide voltage transient observed from a 200 nm film is shown in this paper and compared to the KIB model. The 50 GHz bandwidth limitation of the oscilloscope was also considered when the expected amplitude of the photoresponse signal was estimated. As of September, 1994, the 16 ps wide transient reported in Paper D is still the fastest voltage transient observed to date from a YBCO film. The fact that the KIB model could account for a large portion of the amplitude of the observed response suggested that nonequilibrium heating was not significant over the time scale of the 5 ps laser pulse.

Picosecond photoresponse of epitaxial $YBa_2Cu_3O_{7-\delta}$ thin films

F. A. Hegmann[a] and R. A. Hughes
Department of Physics and Astronomy, McMaster University, Hamilton, Ontario, Canada L8S 4M1

J. S. Preston
Department of Engineering Physics, McMaster University, Hamilton, Ontario, Canada L8S 4L7

(Received 21 December 1993; accepted for publication 22 March 1994)

Photoresponse signals as fast as 16 ps (full width at half-maximum) have been observed from current-biased bridge structures of epitaxial $YBa_2Cu_3O_{7-\delta}$ thin films on $LaAlO_3$ using 5 ps, 820 nm laser pulses. Operating at liquid-nitrogen temperature (77.4 K), the amplitude of the fast response was found to be linear with current at low bias currents. At higher bias currents, a slow component appeared in the signal with a decay over several nanoseconds which could be attributed to a resistive bolometric response. Fast transients about 20 ps wide have been observed in films with thicknesses ranging from 47 to 200 nm. We believe the fast response is primarily due to a kinetic inductive bolometric mechanism associated with heating of the film by the laser pulse. There is some evidence of a nonbolometric contribution but it is not yet conclusive.

Several groups[1–7] have reported fast photoresponse signals from current-biased epitaxial $YBa_2Cu_3O_{7-\delta}$ (YBCO) thin films below the transition temperature using short laser pulses. Transients as fast as 30 ps wide have been observed from 30 nm films,[1] which were followed by a slow component with a decay over several nanoseconds. One of the motivations behind these studies has been to understand the origin of this fast response, since it cannot be explained in most cases by a resistive bolometric response where the laser pulse simply heats the film in the resistive transition region. Several nonbolometric (or nonthermal) mechanisms have been proposed based on nonequilibrium phenomena which result in optically induced gap suppression[2–5] or changes in the sample's kinetic inductance.[1,5] Photoactivated flux flow has also been suggested[4] as one possible mechanism.

We have already studied the photoresponse of YBCO thin films using 100 ps laser pulses[7] and concluded that the fast response could be adequately explained by a kinetic inductive bolometric mechanism. In this mechanism, heating of the film by the laser pulse rapidly decreases the superfluid density which increases the kinetic inductance of the bridge resulting in a fast voltage transient. The mechanism is bolometric because the kinetic inductance is determined by the local temperature of the film. In the work described here, we have tried to look for evidence of nonbolometric effects in the photoresponse over much shorter time scales. To our knowledge, the 16-ps-wide transients described in this letter (with no slow component afterwards) are the fastest observed so far from YBCO thin films. The photoresponse is due to kinetic inductance effects, but it is unclear if nonbolometric mechanisms are present.

The photoresponse measurements described here were taken primarily from a c-axis oriented, epitaxial $YBa_2Cu_3O_{7-\delta}$ thin film with a thickness of 200 nm deposited by laser ablation on $LaAlO_3$ at 780 °C in 250 mTorr of oxygen. Standard photolithographic techniques and a wet chemical etch were used to pattern the film into a 2-mm-long coplanar transmission line structure terminated by a 10-μm-wide and 100-μm-long bridge, as shown schematically in Fig. 1. The width of the transmission line was 130 μm, and the gap to the ground planes was 336 μm. A substrate thickness of 500 μm and dielectric constant of 23.5 gave a transmission line impedance of 50 Ω. Gold pads were also deposited onto the YBCO sample to allow four-point probe measurements of the resistance of the bridge. The gold pads were annealed at 500 °C for 30 min to reduce the total contact resistance to about 0.5 Ω and improve the adhesion of the gold to the film. After processing, the zero resistance critical temperature was about 89 K, the resistivity at 100 K was 124 $\mu\Omega$ cm (62 Ω), and the critical current density J_c at 77 K using a 10 μV/cm criteria across the bridge was about 1.5×10^6 A/cm^2 (29 mA).

Figure 1 is a schematic of the experimental setup. Wiltron "V" connectors (dc to 65 GHz) were used to launch the fast voltage transients from the YBCO transmission line structure to a coaxial cable 15 cm long. The sample was mounted in vacuum on the tip of a copper cold finger cooled by liquid nitrogen. This limited the photoresponse measurements to liquid-nitrogen temperature (77.4 K). The launcher provided a hermetic seal between the sample and the coaxial cable, which allowed the cable to be directly cooled by the liquid-nitrogen contained in the cold finger. This greatly reduced heat conduction through the short cable length to the sample. A current source (0–100 mA) provided dc bias to the

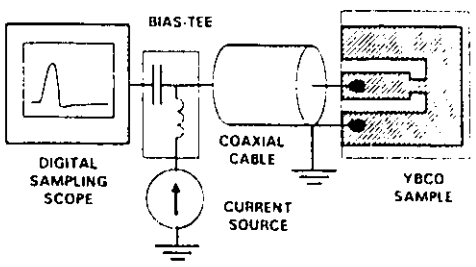

FIG. 1. Schematic of the experimental setup.

[a]Author to whom all correspondence should be addressed.

 0003-6951/94/64(23)/3172/3/$6.00

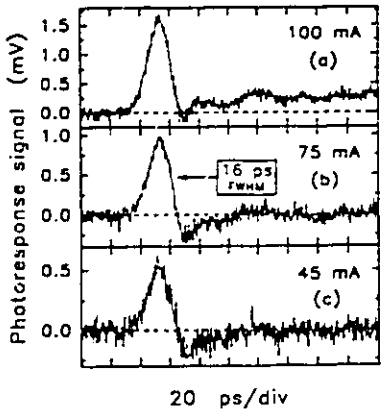

FIG. 2. Photoresponse signals from a 10 μm×100 μm×200 nm bridge at a bias current of (a) 100, (b) 75, and (c) 45 mA. The full width at half-maximum of the fast pulse in (b) is 16 ps.

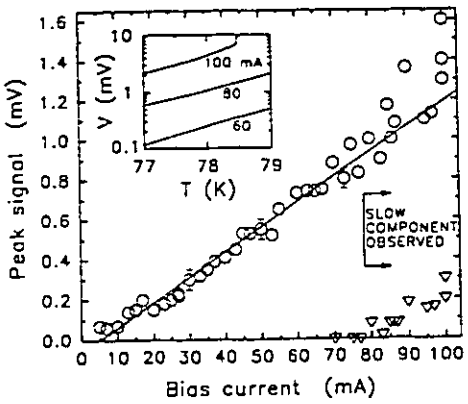

FIG. 3. Peak amplitude of the photoresponse signal (open circles) as a function of bias current for the 200 nm film. The solid line is a least-squares fit to he data below 80 mA. Above 80 mA, a slow component (amplitude denoted by open inverted triangles) is observed in the photoresponse. The inset shows the steady-state voltage across the 100 μm bridge as a function of temperature near 77 K for bias currents of 100, 80, and 60 mA.

sample through a Wiltron bias-tee (0.1–60 GHz). A 50 GHz digital sampling oscilloscope (Tektronix CSA 803 with SD-32 sampling head) was also connected to the bias-tee, and wave forms were acquired at positive and negative bias currents and then subtracted to eliminate base line effects. After 512 averages for each wave form, a voltage resolution of about 0.05 mV was obtained. The bandwidth of the setup was measured by a network analyzer to be greater than 40 GHz, which would give a theoretical rise time of about 8.8 ps. The sample chamber, with a height of only 22 cm and diameter of 6.5 cm, was designed to be compact and portable in order to investigate the viability of a practical high-speed, high-T_c photodetector operating at 77 K.

A synchronously pumped dye laser generating 5 ps, 820 nm pulses was focused by a 5 cm lens to a 35 μm spot size on the sample. A pulse selector system operating at a pulse repetition rate of 38 kHz was used to reduce the average power at the sample to about 70 μW. Each selected pulse had an energy of about 0.1 nJ, resulting in a fluence at the bridge of about 10 μJ/cm^2.

Figure 2(a) shows the photoresponse from the 200 nm film at a bias of 100 mA. A fast transient less than 20 ps wide is followed by a slow component which decays over several nanoseconds. As the bias current is lowered to 75 mA, as shown in Fig. 2(b), the slow component disappears and only the fast component remains with a full width at half-maximum (FWHM) of 16 ps. The fast component persists at even lower currents with decreased amplitude as shown in Fig. 2(c) for a bias of 45 mA. The amplitude of the response from the 200 nm film as a function of bias current can be seen in Fig. 3. Below 80 mA, the slow component disappears and the amplitude of the fast response becomes linear with bias current.

The same trend is observed in the photoresponse from a 135 nm film with a 10-μm-wide bridge as shown in Fig. 4. The upper inset in Fig. 4 shows a photoresponse that rapidly increases with current above 8 mA. This is the region where the slow component appears and becomes very large. An example of a wave form from this region is shown in the lower inset of Fig. 4 for a bias current of 15 mA where the fast component is superimposed on top of the slow component. Below 8 mA, only the fast component is present with an amplitude which is linear with bias current. Similar trends have been observed in the photoresponse from 47, 67, and 160 nm films.

It can be shown that the slow component is a resistive bolometric response. The inset in Fig. 3 shows the steady-state voltage across the 100-μm-long bridge as a function of temperature and bias current as measured in a separate setup by a four-point probe measurement. The estimated temperature transient[7] induced in the 200 nm film by the laser pulse is about 0.40 K. If the initial temperature of the sample is 77.4 K, then the change in voltage across the bridge to a final temperature of 77.8 K is 0.98, 0.21, and 0.056 mV for bias currents of 100, 80, and 60 mA, respectively. Since the spot size is only 35 μm, the laser pulse illuminates only a 35-μm-long section of the 100-μm-long bridge. The voltage tran-

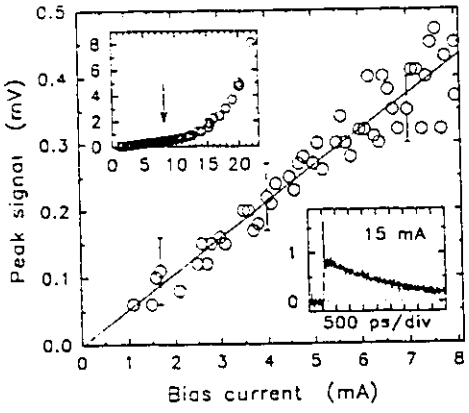

FIG. 4. Peak amplitude of the photoresponse signal as a function of bias current for a 10 μm×100 μm×135 nm bridge. The solid line is a least-squares fit to the data below 8 mA. Above 8 mA, as indicated by the arrow in the upper inset, a slow component is observed in the photoresponse and the amplitude increases sharply. The lower inset shows an example of a wave form with a slow component taken at a bias current of 15 mA.

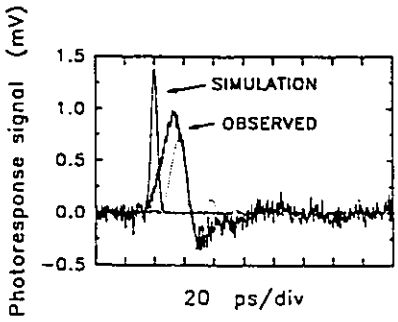

FIG. 5. Comparison of the observed photoresponse to a simulation based on a kinetic inductive bolometric model for the 200 nm film. The dashed curve represents the simulation pulse limited to the 50 GHz bandwidth of the sampling head. The width of the simulation transient is 5 ps, the observed response taken at 75 mA is 16 ps wide, and the width of the broadened simulation pulse is 11 ps.

sient expected from a resistive bolometric response would then be 35/100 of the above voltage changes, or 0.34, 0.07, and 0.02 mV. As seen in Fig. 2(a), the amplitude of the slow component observed at a bias of 100 mA is about 0.3 mV, which agrees quite well with the predicted change of 0.34 mV from the steady-state measurements shown in the inset of Fig. 3. In Fig. 2(b), the disappearance of the slow component at 75 mA also agrees with a predicted 0.07 mV amplitude for the slow component at 80 mA since the noise level of the system is 0.05 mV. The decay of the slow component, which depends on the thermal escape time from the sample,[7] should be about 20 ns for the 200 nm sample at 77 K or about 13 ns for the 135 nm film. The lower inset in Fig. 4, however, shows a decay for the slow component from the 135 nm film of only 3 ns. This decay for the slow component, which is faster than expected, can be explained by the lower cutoff frequency of the bias-tee (Fig. 1) of 0.1 GHz which would give a calculated fall time of 3.5 ns. Qualitatively similar wave forms to the one shown in the lower inset of Fig. 4 have been observed by other groups.[1,2,5,6]

The origin of the 20-ps-wide fast photoresponse seen in all of our films is accounted for by kinetic inductance changes induced by the laser pulse in the current-biased bridge. The voltage expected from such a response is given by[5,7] $V=IdL_{KIN}/dt$, where I is the bias current and L_{KIN} is the kinetic inductance of the bridge. The observed linear current dependence of the photoresponse agrees with a kinetic inductive mechanism. However, it is not certain whether the fast response provides clear evidence for nonequilibrium mechanisms over a 20 ps time scale.

Figure 5 compares simulation results assuming a kinetic inductive bolometric response[7] to the observed response at 75 mA for the 200 nm film from Fig. 2(b). The kinetic inductive bolometric model gives a 1.38 mV peak value and a 5-ps-wide signal which is the same width as the incident laser pulse. The dashed curve in Fig. 5 shows the simulation pulse broadened to a width of 11 ps due to the 50 GHz bandwidth limitation of the sampling head. Dispersion effects in the coplanar transmission line[9] and a time jitter of about 5 ps associated with the wave form acquisition on the oscilloscope will also contribute to broadening, but have not been included in the broadened simulation pulse shown in Fig. 5. The amplitude of the broadened pulse is about 0.69 mV, which is close to the observed peak photoresponse of about 1 mV. The fast response, therefore, must have a large component arising from the kinetic inductive bolometric mechanism.

However, the fast photoresponse signals from all the films we studied show a negative transient with a decay time of about 30 ps as seen in Figs. 2 and 5. Negative transients have also been seen by other groups, and have been interpreted as evidence for nonequilibrium recombination of photoexcited quasiparticles back into Cooper pairs.[1,5] Pump-probe experiments on YBCO samples[8] have reported quasiparticle recombination times of the order of 3 ps. The kinetic inductive bolometric model[7] shown in Fig. 5 predicts a negative response of only -0.002 mV. The broadened simulation pulse shows negative going oscillations, but none with a decay time of 30 ps. The dispersion effects in the coplanar transmission line must be studied further before any conclusions can be made regarding the origin of the negative-going transient.

In summary, we have observed 16-ps-wide photoresponse transients from YBCO thin films with thicknesses up to 200 nm. We believe the response is due to kinetic inductance effects and that a large portion of the response is due to a kinetic inductive bolometric mechanism from heating of the film by the laser pulse. It is still not clear at this point whether nonequilibrium mechanisms are present in the photoresponse data over this time scale and at a temperature of 77 K, even though the observed negative transients might suggest nonequilibrium recombination of quasiparticles into Cooper pairs. Performing the same experiments as a function of temperature may help reveal more information on the origin of the negative photoresponse signal.

This work was supported by the Ontario Centre for Materials Research and the Natural Sciences and Engineering Research Council of Canada, and made use of the facilities of the Centre for Electrophotonic Materials and Devices.

[1] A. Ghis, S. Pfister, J. C. Villegier, M. Nail, and J. P. Maneval, IEEE Trans. Appl. Supercond. 3, 2136 (1993).
[2] A. D. Semenov, I. G. Goghidze, G. N. Gol'tsman, A. V. Sergeev, and E. M. Gershenzon, Appl. Phys. Lett. 63, 681 (1993).
[3] L. Shi, G. L. Huang, C. Lehane, D. Kim, H. S. Kwok, J. Swiatkiewicz, G. C. Xu, and P. N. Prasad, Phys. Rev. B 48, 6550 (1993).
[4] A. Frenkel, M. A. Saifi, T. Venkatesan, P. England, X. D. Wu, and A. Inam, J. Appl. Phys. 67, 3054 (1990); A. Frenkel, Phys. Rev. B 48, 9717 (1993).
[5] N. Bluzer, Phys. Rev. B 44, 10222 (1991); N. Bluzer, J. Appl. Phys. 71, 1336 (1992); N. Bluzer, IEEE Trans. Appl. Supercond. 3, 2869 (1993).
[6] M. Johnson, Appl. Phys. Lett. 59, 1371 (1991).
[7] F. A. Hegmann and J. S. Preston, Phys. Rev. B 48, 16023 (1993).
[8] S. G. Han, Z. V. Vardeny, K. S. Wong, O. G. Symko, and G. Koren, Phys. Rev. Lett. 65, 2708 (1990); S. G. Han, Z. V. Vardeny, O. G. Symko, and G. Koren, IEEE Trans. Magn. 2, 1548 (1991).
[9] M. C. Nuss, P. M. Mankiewich, R. E. Howard, B. L. Straughn, T. E. Harvey, C. D. Brandle, G. W. Berkstresser, K. W. Goossen, and P. R. Smith, Appl. Phys. Lett. 54, 2265 (1989).